Intradermal delivery of nanoparticulate vaccines using coated and hollow microneedles
Du, G.

Citation

Version:	Not Applicable (or Unknown)
License:	[Licence agreement concerning inclusion of doctoral thesis in the Institutional Repository of the University of Leiden](https://hdl.handle.net/1887/66514)
Downloaded from:	https://hdl.handle.net/1887/66514

Cover Page

Universiteit Leiden

The handle

Author: Du, G.
Title: Intradermal delivery of nanoparticulate vaccines using coated and hollow microneedles
Issue Date: 2018-10-30

Intradermal delivery of nanoparticulate vaccines using coated and hollow microneedles

Guangsheng Du

杜广盛

Intradermal delivery of nanoparticulate vaccines using coated and hollow microneedles

PhD thesis with summary in Dutch

Intradermal delivery of nanoparticulate vaccines using coated and hollow microneedles

PROEFSCHRIFT

ter verkrijging van

de graad van Doctor aan de Universiteit Leiden,

op gezag van de Rector Magnificus prof.mr. C.J.J.M. Stolker,

volgens besluit van het College voor Promoties

te verdedigen op dinsdag 30 Oktober 2018

klokke 15.00 uur

door

Guangsheng Du

Geboren te Linyi, China

in 1988

Promotoren:

Prof. Dr. J.A. Bouwstra

Prof. Dr. W. Jiskoot

Promotiecommissie:

Prof. Dr. H. Irth, LACDR, Chair

Prof. Dr. A.P. Ijzerman, LACDR, Secretary

Prof. Dr. J. Kuiper, LACDR

Prof. Dr. H.W. Frijlink, Universiteit Groningen

Prof. Dr. V. Préat, Universite catholique de Louvain

Dr. E. Mastrobattista, Universiteit Utrecht

Table of Contents

Chapter 1

General introduction, aim and outline of this thesis

Chapter 1

General introduction

Vaccination is the most effective tool to fight against infectious diseases [1]. With vaccination smallpox was eradicated in 1979, which had killed millions of people in 20th century and before [2]. The incidence of other devastating diseases such as polio, tuberculosis and tetanus has substantially declined owing to the routine vaccination programs [3]. However, there is still a need for new and better vaccines against infectious diseases [4]. Nowadays, in addition vaccination gains increasing attention for therapeutic use against established diseases, such as cancer and chronic auto-immune disorders [5].

Traditional vaccines are derived from attenuated organisms or inactivated pathogens. These vaccines can induce potent immune responses, but safety issues including the administration of potentially harmful components and reversion to virulent forms have restricted their application. Nowadays, subunit antigens containing only antigenic parts of a pathogen are being extensively investigated because of their better safety. However, they are generally less immunogenic than traditional vaccines. In order to improve their immunogenicity, immune modulators and nanoparticle delivery systems can be used [6-9].

Microneedle technology for vaccine delivery

Most vaccines are administered by intramuscular or subcutaneous injection, but these methods can cause pain and stress due to the fear of injection [10]. Furthermore, there is a risk of infection due to the reuse of needles especially in developing countries [11]. Lastly, the delivery of vaccines to antigen presenting cells may be inefficient as these delivery sites are not rich of antigen presenting cells.

As an alternative, intradermal delivery has gained attention because of its potential for needle-free administration. Additionally, the skin is easy to access and contains a large number of antigen presenting cells, such as Langerhans cells in epidermis and dendritic cells in dermis, making the skin an attractive site for vaccination [12]. However, the stratum corneum, the uppermost layer of the skin, forms the main barrier and prevents most foreign substances from entering our body. To effectively overcome the skin barrier, microneedles have been developed [13]. Microneedles are micro-sized needle structures which can be used to penetrate the skin in a non-invasive and pain-free way, as they only pierce the upper layers of skin without touching the deeper nerves and blood vessels [14].

Microneedles were first used for pretreatment of the skin [15]. After the conduits were made and the microneedles were removed, the vaccine-loaded patch or formulation was applied onto the microneedle-penetrated skin. However, the diffusion of vaccines through the microneedle-made conduits is slow due to the small diameter of the conduits and small surface area of the pretreated skin. As a result, only a small fraction of the antigen is delivered into the skin. Furthermore, the conduits may close soon after the removal of the microneedles, limiting the time available for diffusion [16]. To increase the delivery efficiency of vaccines and avoid the separate application of vaccines after the removal of the microneedles, several types of new microneedle systems have been developed in the past twenty years, including coated, hollow and dissolvable microneedles [13, 14, 17, 18].

In case of coated microneedles, antigens are coated onto the surface of microneedles. After the microneedles are inserted into the skin, the antigen should be quickly released. One disadvantage of using coated microneedles is that the coating amount of antigen is limited due to the small surface area of microneedles. At the same time, there could be a waste of antigen during the coating process, as the coating efficiency is normally much lower than 100%.

Several methods have been reported for the coating of antigen on microneedles. Gill et al. described a dip coating method and found that the surface tension and viscosity of the coating solution had a major influence on the uniformity and thickness of the coating, respectively [19, 20]. Chen et al. proposed a gas jet drying approach to reduce vaccine wastage and produce a thinner coating of antigen [21]. In our group, we developed pH-sensitive microneedles by modifying their silicon surface with pyridine groups. The microneedles can adsorb negatively charged antigens at slightly acidic conditions and release them at neutral pH [22]. Finally, in some studies a layer-by-layer coating approach was used, in which the amount of coated antigen can be tailored by adjusting the number of coating layers [23, 24].

Dissolvable microneedles are made of water soluble polymers or low-molecular-weight sugars and the antigen is loaded inside the solid microneedle matrix [25]. When the microneedles are inserted into the skin, they start to dissolve, thereby releasing the antigen [17, 25]. The advantage of using dissolvable microneedles is that there is no sharp waste after the application of the microneedles. The mostly used method for fabrication of dissolvable microneedles is micromolding [25]. The micromolds are first filled with an aqueous polymer/sugar solution, and through evaporation of the solvent the polymer/sugar will be solidified to form the microneedles [26]. Recently, efforts have been made to load vaccines only in the tips of dissolvable microneedles, aiming to maximize the delivery/release of the loaded antigen during the application of microneedles [27, 28].

Hollow microneedles contain conduits through which the liquid formulation of vaccines can be injected into the skin. The advantage of using hollow microneedles, compared to coated and dissolvable microneedles, is that the injection volume, rate and depth can be precisely controlled [14, 29]. Furthermore, there is no need to optimize the loading process of vaccines in the microneedles and in case of liquid vaccine formulations the formulation buffer does not have to be developed. A disadvantage is that dry vaccine formulations need to be reconstituted in water or buffer before injection [13]. Hollow microneedles can be made from metal, polymer or silicon [13]. Davis et al. reported a laser micromachining method in which nickel was coated onto a polymer mold made by laser drilling. The prepared hollow microneedles were released by etching the polymer mold [30]. In our group a method was developed to prepare hollow microneedles by etching fused silica capillaries with hydrofluoric acid [31].

Microneedles can be penetrated into skin manually or by using an applicator. As the elastic skin will stretch and deform when being pressed, the manual application may result in a low and variable penetration efficiency of microneedles [32]. By using an applicator, the microneedles can be applied with a fast, controlled rate with the penetration force precisely controlled. However, the disadvantage is that a sophisticated and expensive applicator needs to be developed.

Nanoparticles for vaccine delivery

Nanoparticle delivery systems have been extensively studied for vaccination, as they are able to enhance the immunogenicity of antigens by protecting them from degradation, increasing their uptake by antigen presenting cells and co-delivering them with adjuvants [8]. Furthermore, the immune responses can be potentially modified by tuning the properties of nanoparticles such as size, surface charge, loading and release of antigens [33]. Different types of nanoparticles have been studied for vaccination, such as polymeric nanoparticles, liposomes, inorganic nanoparticles and emulsions [7, 8, 33-38].

Polymeric nanoparticles are prepared from synthetic or natural polymers such as poly(lactic-co-glycolic) (PLG), poly(lactic-co-glycolic acid) PLGA, chitosan and gelatin [39]. The most often studied polymeric nanoparticles are PLGA nanoparticles and the antigens are normally encapsulated inside the PLGA matrix. The antigens will be released from the nanoparticles during the PLGA degradation process. Liposomes are made of lipids and the antigens can be adsorbed on the surface of liposomes, loaded in the core or incorporated in between the lipid bilayers. Polymeric nanoparticles and liposomes have been extensively investigated for vaccine delivery because of their excellent biocompatibility and biodegradability. Inorganic nanoparticles have been studied for the delivery of vaccines because of their rigid structure and excellent thermo stability. Recently, mesoporous silica nanoparticles (MSNs) have gained increasing attention for vaccine delivery because of their excellent biocompatibility and multiple options for surface functionalization. Additionally, the large pores and surface area of MSNs allow for efficient loading of relatively large amounts of antigens [40, 41].

Studies have shown that the physicochemical characteristics of nanoparticles such as size, surface charge and release property of antigens have an important influence on the immunogenicity of the encapsulated antigens. Nanoparticles with a size below 200 nm have been shown to be more efficiently taken up by dendritic cells [33, 42]. Nanoparticulate vaccines with a positive zeta potential have been reported to enhance the activation of antigen presenting cells and the subsequent immune responses [43]. Besides, the sustained release of antigen together with the depot effect of nanoparticles on cell surface could allow longer interaction of antigen with the antigen presenting cells [6, 44].

An increasing number of studies focuses on the use of nanoparticles for co-delivery of antigen and Toll-like receptor (TLR) ligands [46-54]. These ligands can function as pathogen-associated molecular patterns and selectively bind to the TLRs of antigen-presenting cells, thereby enhancing the immune responses. Among different types of TLR ligands, poly(I:C) and CpG, which are ligands for TLR3 and TLR9 respectively, have been extensively investigated. Both of these adjuvants are capable of enhancing $Th1/CD8^+$ T cell responses [9]. Recent reported studies have shown that antigen and poly(I:C)/CpG co-encapsulated nanoparticles elicited superior $Th1/CD8^+$ T cell responses compared to mixture of antigen and adjuvant solution [46, 48-54]. The co-delivery of antigen and immune modulator to the same antigen presenting cells is likely responsible for this [47, 52].

Combination of microneedles and nanoparticles for intradermal delivery of vaccines

The intradermal delivery of nanoparticulate vaccines was first studied by using traditional hypodermic needles [46, 48, 50, 53-56]. Some studies have shown that the intradermal injection of these vaccines induce stronger IgG2a [54] or $CD8^+$ T cell responses than subcutaneous injection [56]. Other studies further have shown that the antigen and adjuvant co-encapsulated nanoparticles induce higher IgG2a titers [46, 53] and $CD8^+$ T cell responses [50] compared to antigen and adjuvant solution after the intradermal delivery by hypodermic needles.

Nowadays, researchers are trying to combine the utilization of microneedles and nanoparticles for intradermal delivery of vaccines. Initially, microneedles were used for pretreatment of skin and the nanoparticles were applied onto the pretreated skin after removal of the microneedles. Microneedle-assisted administration of nanoparticle vaccines has been shown to induce stronger immune responses than antigen solution [57, 58]. However, the reported results were conflicting. Another study showed that antigen-loaded liposomes did not enhance immune responses compared to antigen solution in microneedle pretreated mice, most likely

because the transport of the nanoparticles in the conduits made by microneedles was limited [59].

To improve the delivery efficiency of nanoparticulate vaccines, coated, hollow and dissolvable microneedles were used [24, 49, 60, 61]. For coated microneedles, the processes of the encapsulation of antigen into nanoparticles and the coating process of nanoparticles onto microneedles need to be optimized, in order to reach a sufficient antigen dose coated on the microneedles. Demuth et al. described the coating of antigen-loaded lipid nanocapsules onto PLGA based microneedles by using a layer-by-layer coating approach [24]. The coated multilayers were rapidly released into the skin after the application of microneedles into the skin, resulting in a balanced response of multiple IgG isotypes, whereas the immunization with soluble antigen only induced a weak IgG1-biased immune response. In case of dissolvable microneedles, it is important to study whether the loading of nanoparticles in the microneedles does not affect the properties of dissolvable microneedles, such as the mechanical strength or dissolution rate of microneedles in the skin. It has been reported that antigen-loaded PLGA nanoparticles were successfully encapsulated into methylvinylether and maleic anhydride (PMVE/MA) based dissolvable microneedles [60, 61]. The prepared microneedles were able to penetrate the skin and dissolve quickly within 15 min. The dissolvable microneedles loaded with antigen encapsulated PLGA nanoparticles induced higher Th1/CD8$^+$ responses than antigen solution [60, 61]. In case of hollow microneedles, a suspension of nanoparticulate vaccine can be directly injected into the skin. Siddhapura et al. reported the use of hollow microneedles for intradermal injection of tetanus toxoid -loaded chitosan nanoparticles into mice. This was found to induce a higher IgG2a response and stronger expression of Th1 cytokines than a commercial vaccine delivered intradermally [62].

From the above it can be concluded that microneedle-mediated intradermal delivery of nanoparticulate vaccines is a promising approach for effective intradermal vaccination. However, there are no systematic studies reported yet focusing on 1) optimization of microneedle-based systems for the delivery of nanoparticulate vaccines, 2) the effect of physicochemical characteristics of nanoparticles on the immunogenicity of encapsulated antigens after microneedle-mediated intradermal vaccination.

As described above, coated microneedle arrays with pyridine modified pH-sensitive surface and hollow microneedles prepared from fused silica capillaries have been developed in our lab and used successfully for intradermal delivery of various protein antigens [14]. The results of the immunization studies have shown that the microneedle mediated immunization groups induced comparable immune responses as compared to subcutaneous or intramuscular group [22-23, 31, 63-65]. Therefore it is attractive to combine these microneedle approach with nanoparticles to improve ithe immunogenicity of the antigens.

Aim and outline of this thesis

The aim of this thesis is to determine whether a combination of microneedles and nanoparticles can be used to elicit potent immune responses after intradermal administration and whether the immune response can be tailored by the choice of the nanoparticles. For these purposes, two types of microneedles, namely coated and hollow microneedles, and several types of nanoparticles, covering a broad range of physicochemical parameters, were used.

In Chapter 2, the development of a new type of MSNs for the encapsulation of ovalbumin (OVA) is described. Additionally, the coating of OVA-loaded MSNs onto pH-sensitive microneedle arrays was investigated. In Chapter 3, another type of nanoparticles, namely PLGA nanoparticles, are used for the encapsulation of OVA and an adjuvant (poly(I:C)). T

cell responses induced by these nanoparticles after hollow microneedle-mediated intradermal immunization in mice were studied. In Chapter 4, hollow microneedles are used to study the effect of nano-encapsulation of OVA and poly(I:C) on humoral and cellular immune responses. In this study, four types of nanoparticles, namely MSNs, PLGA nanoparticles, liposomes and gelatin nanoparticles, were compared. In Chapter 5, hollow microneedles are used to examine the effect of encapsulation manner of diphtheria toxoid (DT) and poly(I:C) in liposomes on the antibody responses in mice. In Chapter 6, the antibody responses of DT-loaded MSNs after coated and hollow microneedle-mediated intradermal vaccination are compared. In Chapter 7, the main findings of the studies described in this thesis are summarized and discussed. The future prospects of using microneedles for intradermal delivery of nanoparticulate vaccines are briefly discussed.

References:
[1] B. Pulendran, R. Ahmed, Immunological mechanisms of vaccination, Nat Immunol, 12 (2011) 509-517.
[2] A.M. Behbehani, The Smallpox Story - Life and Death of an Old Disease, Microbiol Rev, 47 (1983) 455-509.
[3] B. Greenwood, The contribution of vaccination to global health: past, present and future, Philosophical transactions of the Royal Society of London. Series B, Biological sciences, 369 (2014) 20130433.
[4] R. Rappuoli, M. Pizza, G. Del Giudice, E. De Gregorio, Vaccines, new opportunities for a new society, Proceedings of the National Academy of Sciences of the United States of America, 111 (2014) 12288-12293.
[5] C.J. Melief, T. van Hall, R. Arens, F. Ossendorp, S.H. van der Burg, Therapeutic cancer vaccines, The Journal of clinical investigation, 125 (2015) 3401-3412.
[6] Y. Fan, J.J. Moon, Nanoparticle Drug Delivery Systems Designed to Improve Cancer Vaccines and Immunotherapy, Vaccines, 3 (2015) 662-685.
[7] M.L. De Temmerman, J. Rejman, J. Demeester, D.J. Irvine, B. Gander, S.C. De Smedt, Particulate vaccines: on the quest for optimal delivery and immune response, Drug Discov Today, 16 (2011) 569-582.
[8] L. Zhao, A. Seth, N. Wibowo, C.X. Zhao, N. Mitter, C.Z. Yu, A.P.J. Middelberg, Nanoparticle vaccines, Vaccine, 32 (2014) 327-337.
[9] S.G. Reed, M.T. Orr, C.B. Fox, Key roles of adjuvants in modern vaccines, Nat Med, 19 (2013) 1597-1608.
[10] I. Preza, S. Subaiya, J.B. Harris, D.C. Ehlman, K. Wannemuehler, A.S. Wallace, S. Huseynov, T.B. Hyde, E. Nelaj, S. Bino, L.M. Hampton, Acceptance of the Administration of Multiple Injectable Vaccines in a Single Immunization Visit in Albania, J Infect Dis, 216 (2017) S146-S151.
[11] M. Kermode, Unsafe injections in low-income country health settings: need for injection safety promotion to prevent the spread of blood-borne viruses, Health Promot Int, 19 (2004) 95-103.
[12] N. Li, L.H. Peng, X. Chen, S. Nakagawa, J.Q. Gao, Transcutaneous vaccines: novel advances in technology and delivery for overcoming the barriers, Vaccine, 29 (2011) 6179-6190.
[13] Y.C. Kim, J.H. Park, M.R. Prausnitz, Microneedles for drug and vaccine delivery, Adv Drug Deliver Rev, 64 (2012) 1547-1568.
[14] K. van der Maaden, W. Jiskoot, J. Bouwstra, Microneedle technologies for (trans)dermal drug and vaccine delivery, Journal of Controlled Release, 161 (2012) 645-655.
[15] S. Henry, D.V. McAllister, M.G. Allen, M.R. Prausnitz, Microfabricated microneedles: a novel approach to transdermal drug delivery, J Pharm Sci, 87 (1998) 922-925.
[16] S. Bal, A.C. Kruithof, H. Liebl, M. Tomerius, J. Bouwstra, J. Lademann, M. Meinke, In vivo visualization of microneedle conduits in human skin using laser scanning microscopy, Laser Physics Letters, 7 (2010) 242-246.
[17] E. Larraneta, M.T.C. McCrudden, A.J. Courtenay, R.F. Donnelly, Microneedles: A New Frontier in Nanomedicine Delivery, Pharm Res-Dordr, 33 (2016) 1055-1073.
[18] M.R. Prausnitz, Microneedles for transdermal drug delivery, Adv Drug Deliver Rev, 56 (2004) 581-587.
[19] H.S. Gill, M.R. Prausnitz, Coated microneedles for transdermal delivery, Journal of controlled release : official journal of the Controlled Release Society, 117 (2007) 227-237.
[20] H.S. Gill, M.R. Prausnitz, Coating formulations for microneedles, Pharm Res, 24 (2007) 1369-1380.

[21] X. Chen, T.W. Prow, M.L. Crichton, D.W. Jenkins, M.S. Roberts, I.H. Frazer, G.J. Fernando, M.A. Kendall, Dry-coated microprojection array patches for targeted delivery of immunotherapeutics to the skin, Journal of controlled release : official journal of the Controlled Release Society, 139 (2009) 212-220.
[22] K. van der Maaden, H.X. Yu, K. Sliedregt, R. Zwier, R. Leboux, M. Oguri, A. Kros, W. Jiskoot, J.A. Bouwstra, Nanolayered chemical modification of silicon surfaces with ionizable surface groups for pH-triggered protein adsorption and release: application to microneedles, Journal of Materials Chemistry B, 1 (2013) 4466-4477.
[23] K. van der Maaden, E. Sekerdag, P. Schipper, G. Kersten, W. Jiskoot, J. Bouwstra, Layer-by-Layer Assembly of Inactivated Poliovirus and N-Trimethyl Chitosan on pH-Sensitive Microneedles for Dermal Vaccination, Langmuir, 31 (2015) 8654-8660.
[24] P.C. DeMuth, J.J. Moon, H. Suh, P.T. Hammond, D.J. Irvine, Releasable layer-by-layer assembly of stabilized lipid nanocapsules on microneedles for enhanced transcutaneous vaccine delivery, ACS nano, 6 (2012) 8041-8051.
[25] M. Leone, J. Monkare, J. Bouwstra, G. Kersten, Dissolving Microneedle Patches for Dermal Vaccination, Pharm Res-Dordr, 34 (2017) 2223-2240.
[26] J. Monkare, M. Reza Nejadnik, K. Baccouche, S. Romeijn, W. Jiskoot, J.A. Bouwstra, IgG-loaded hyaluronan-based dissolving microneedles for intradermal protein delivery, Journal of controlled release : official journal of the Controlled Release Society, 218 (2015) 53-62.
[27] E. Korkmaz, E.E. Friedrich, M.H. Ramadan, G. Erdos, A.R. Mathers, O.B. Ozdoganlar, N.R. Washburn, L.D. Falo, Jr., Tip-Loaded Dissolvable Microneedle Arrays Effectively Deliver Polymer-Conjugated Antibody Inhibitors of Tumor-Necrosis-Factor-Alpha Into Human Skin, J Pharm Sci-Us, 105 3453-3457.
[28] J.Y. Kim, M.R. Han, Y.H. Kim, S.W. Shin, S.Y. Nam, J.H. Park, Tip-loaded dissolving microneedles for transdermal delivery of donepezil hydrochloride for treatment of Alzheimer's disease, European journal of pharmaceutics and biopharmaceutics : official journal of Arbeitsgemeinschaft fur Pharmazeutische Verfahrenstechnik e.V, 105 (2016) 148-155.
[29] T.M. Tuan-Mahmood, M.T.C. McCrudden, B.M. Torrisi, E. McAlister, M.J. Garland, T.R.R. Singh, R.F. Donnelly, Microneedles for intradermal and transdermal drug delivery, Eur J Pharm Sci, 50 (2013) 623-637.
[30] S.P. Davis, W. Martanto, M.G. Allen, M.R. Prausnitz, Hollow metal microneedles for insulin delivery to diabetic rats, Ieee T Bio-Med Eng, 52 (2005) 909-915.
[31] K. van der Maaden, S.J. Trietsch, H. Kraan, E.M. Varypataki, S. Romeijn, R. Zwier, H.J. van der Linden, G. Kersten, T. Hankemeier, W. Jiskoot, J. Bouwstra, Novel Hollow Microneedle Technology for Depth-Controlled Microinjection-Mediated Dermal Vaccination: A Study with Polio Vaccine in Rats, Pharm Res-Dordr, 31 (2014) 1846-1854.
[32] F.J. Verbaan, S.M. Bal, D.J. van den Berg, J.A. Dijksman, M. van Hecke, H. Verpoorten, A. van den Berg, R. Luttge, J.A. Bouwstra, Improved piercing of microneedle arrays in dermatomed human skin by an impact insertion method, Journal of Controlled Release, 128 (2008) 80-88.
[33] N. Benne, J. van Duijn, J. Kuiper, W. Jiskoot, B. Slutter, Orchestrating immune responses: How size, shape and rigidity affect the immunogenicity of particulate vaccines, Journal of Controlled Release, 234 (2016) 124-134.
[34] T. Akagi, M. Baba, M. Akashi, Biodegradable Nanoparticles as Vaccine Adjuvants and Delivery Systems: Regulation of Immune Responses by Nanoparticle-Based Vaccine, in: S. Kunugi, T. Yamaoka (Eds.) Polymers in Nanomedicine, 2012, pp. 31-64.
[35] D. Christensen, K.S. Korsholm, P. Andersen, E.M. Agger, Cationic liposomes as vaccine adjuvants, Expert Rev Vaccines, 10 (2011) 513-521.

[36] K.T. Mody, A. Popat, D. Mahony, A.S. Cavallaro, C.Z. Yu, N. Mitter, Mesoporous silica nanoparticles as antigen carriers and adjuvants for vaccine delivery, Nanoscale, 5 (2013) 5167-5179.

[37] L.J. Peek, C.R. Middaugh, C. Berkland, Nanotechnology in vaccine delivery, Adv Drug Deliv Rev, 60 (2008) 915-928.

[38] N. Sahoo, R.K. Sahoo, N. Biswas, A. Guha, K. Kuotsu, Recent advancement of gelatin nanoparticles in drug and vaccine delivery, International Journal of Biological Macromolecules, 81 (2015) 317-331.

[39] A. Gutjahr, C. Phelip, A.L. Coolen, C. Monge, A.S. Boisgard, S. Paul, B. Verrier, Biodegradable Polymeric Nanoparticles-Based Vaccine Adjuvants for Lymph Nodes Targeting, Vaccines, 4 (2016).

[40] D. Mahony, A.S. Cavallaro, F. Stahr, T.J. Mahony, S.Z. Qiao, N. Mitter, Mesoporous silica nanoparticles act as a self-adjuvant for ovalbumin model antigen in mice, Small, 9 (2013) 3138-3146.

[41] K.T. Mody, D. Mahony, J. Zhang, A.S. Cavallaro, B. Zhang, A. Popat, T.J. Mahony, C. Yu, N. Mitter, Silica vesicles as nanocarriers and adjuvants for generating both antibody and T-cell mediated immune resposes to Bovine Viral Diarrhoea Virus E2 protein, Biomaterials, 35 (2014) 9972-9983.

[42] M.O. Oyewumi, A. Kumar, Z.R. Cui, Nano-microparticles as immune adjuvants: correlating particle sizes and the resultant immune responses, Expert Rev Vaccines, 9 (2010) 1095-1107.

[43] Y. Ma, Y. Zhuang, X. Xie, C. Wang, F. Wang, D. Zhou, J. Zeng, L. Cai, The role of surface charge density in cationic liposome-promoted dendritic cell maturation and vaccine-induced immune responses, Nanoscale, 3 (2011) 2307-2314.

[44] A.L. Silva, R.A. Rosalia, A. Sazak, M.G. Carstens, F. Ossendorp, J. Oostendorp, W. Jiskoot, Optimization of encapsulation of a synthetic long peptide in PLGA nanoparticles: low-burst release is crucial for efficient CD8(+) T cell activation, European journal of pharmaceutics and biopharmaceutics : official journal of Arbeitsgemeinschaft fur Pharmazeutische Verfahrenstechnik e.V, 83 (2013) 338-345.

[45] S. Hamdy, O. Molavi, Z.S. Ma, A. Haddadi, A. Alshamsan, Z. Gobti, S. Elhasi, J. Samuel, A. Lavasanifar, Co-delivery of cancer-associated antigen and Toll-like receptor 4 ligand in PLGA nanoparticles induces potent CD8(+) T cell-mediated anti-tumor immunity, Vaccine, 26 (2008) 5046-5057.

[46] S.M. Bal, S. Hortensius, Z. Ding, W. Jiskoot, J.A. Bouwstra, Co-encapsulation of antigen and Toll-like receptor ligand in cationic liposomes affects the quality of the immune response in mice after intradermal vaccination, Vaccine, 29 (2011) 1045-1052.

[47] E. Schlosser, M. Mueller, S. Fischer, S. Basta, D.H. Busch, B. Gander, M. Groettrup, TLR ligands and antigen need to be coencapsulated into the same biodegradable microsphere for the generation of potent cytotoxic T lymphocyte responses, Vaccine, 26 (2008) 1626-1637.

[48] M.A. Boks, S.C.M. Bruijns, M. Ambrosini, H. Kalay, L. van Bloois, G. Storm, T. de Gruijl, Y. van Kooyk, In situ Delivery of Tumor Antigen- and Adjuvant-Loaded Liposomes Boosts Antigen-Specific T-Cell Responses by Human Dermal Dendritic Cells, Journal of Investigative Dermatology, 135 (2015) 2697-2704.

[49] L. Guo, J.M. Chen, Y.Q. Qiu, S.H. Zhang, B. Xu, Y.H. Gao, Enhanced transcutaneous immunization via dissolving microneedle array loaded with liposome encapsulated antigen and adjuvant, International Journal of Pharmaceutics, 447 (2013) 22-30.

[50] E.M. Varypataki, K. van der Maaden, J. Bouwstra, F. Ossendorp, W. Jiskoot, Cationic liposomes loaded with a synthetic long peptide and poly(I:C): a defined adjuvanted vaccine for induction of antigen-specific T cell cytotoxicity, AAPS J, 17 (2015) 216-226.

[51] E.M. Varypataki, A.L. Silva, C. Barnier-Quer, N. Collin, F. Ossendorp, W. Jiskoot, Synthetic long peptide-based vaccine formulations for induction of cell mediated immunity: A comparative study of cationic liposomes and PLGA nanoparticles, Journal of Controlled Release, 226 (2016) 98-106.

[52] A.M. Hafner, B. Corthesy, H.P. Merkle, Particulate formulations for the delivery of poly(I:C) as vaccine adjuvant, Adv Drug Deliv Rev, 65 (2013) 1386-1399.

[53] B. Slutter, S.M. Bal, Z. Ding, W. Jiskoot, J.A. Bouwstra, Adjuvant effect of cationic liposomes and CpG depends on administration route, Journal of controlled release : official journal of the Controlled Release Society, 154 (2011) 123-130.

[54] D. Mohanan, B. Slutter, M. Henriksen-Lacey, W. Jiskoot, J.A. Bouwstra, Y. Perrie, T.M. Kundig, B. Gander, P. Johansen, Administration routes affect the quality of immune responses: A cross-sectional evaluation of particulate antigen-delivery systems, Journal of controlled release : official journal of the Controlled Release Society, 147 (2010) 342-349.

[55] S.M. Bal, B. Slutter, E. van Riet, A.C. Kruithof, Z. Ding, G.F.A. Kersten, W. Jiskoot, J.A. Bouwstra, Efficient induction of immune responses through intradermal vaccination with N-trimethyl chitosan containing antigen formulations, Journal of Controlled Release, 142 (2010) 374-383.

[56] C. Liard, S. Munier, M. Arias, A. Joulin-Giet, O. Bonduelle, D. Duffy, R.J. Shattock, B. Verrier, B. Combadiere, Targeting of HIV-p24 particle-based vaccine into differential skin layers induces distinct arms of the immune responses, Vaccine, 29 (2011) 6379-6391.

[57] A. Kumar, P. Wonganan, M.A. Sandoval, X.R. Li, S.J. Zhu, Z.R. Cui, Microneedle-mediated transcutaneous immunization with plasmid DNA coated on cationic PLGA nanoparticles, Journal of Controlled Release, 163 (2012) 230-239.

[58] A. Kumar, X. Li, M.A. Sandoval, B.L. Rodriguez, B.R. Sloat, Z. Cui, Permeation of antigen protein-conjugated nanoparticles and live bacteria through microneedle-treated mouse skin, International journal of nanomedicine, 6 (2011) 1253-1264.

[59] Z. Ding, S.M. Bal, S. Romeijn, G.F. Kersten, W. Jiskoot, J.A. Bouwstra, Transcutaneous immunization studies in mice using diphtheria toxoid-loaded vesicle formulations and a microneedle array, Pharm Res, 28 (2011) 145-158.

[60] M. Zaric, O. Lyubomska, C. Poux, M.L. Hanna, M.T. McCrudden, B. Malissen, R.J. Ingram, U.F. Power, C.J. Scott, R.F. Donnelly, A. Kissenpfennig, Dissolving Microneedle Delivery of Nanoparticle-Encapsulated Antigen Elicits Efficient Cross-Priming and Th1 Immune Responses by Murine Langerhans Cells, Journal of Investigative Dermatology, 135 (2015) 425-434.

[61] M. Zaric, O. Lyubomska, O. Touzelet, C. Poux, S. Al-Zahrani, F. Fay, L. Wallace, D. Terhorst, B. Malissen, S. Henri, U.F. Power, C.J. Scott, R.F. Donnelly, A. Kissenpfennig, Skin dendritic cell targeting via microneedle arrays laden with antigen-encapsulated poly-D,L-lactide-co-glycolide nanoparticles induces efficient antitumor and antiviral immune responses, ACS nano, 7 (2013) 2042-2055.

[62] K. Siddhapura, H. Harde, S. Jain, Immunostimulatory effect of tetanus toxoid loaded chitosan nanoparticles following microneedles assisted immunization, Nanomedicine : nanotechnology, biology, and medicine, 12 (2016) 213-222.

[63] K. van der Maaden, E.M. Varypataki, S. Romeijn, F. Ossendorp, W. Jiskoot, J. Bouwstra, Ovalbumin-coated pH-sensitive microneedle arrays effectively induce ovalbumin-specific antibody and T-cell responses in mice, European journal of pharmaceutics and biopharmaceutics : official journal of Arbeitsgemeinschaft fur Pharmazeutische Verfahrenstechnik e.V, 88 (2014) 310-315.

[64] P. Schipper, K. van der Maaden, V. Groeneveld, M. Ruigrok, S. Romeijn, S. Uleman, C. Oomens, G. Kersten, W. Jiskoot, J. Bouwstra, Diphtheria toxoid and N-trimethyl chitosan layer-by-layer coated pH-sensitive microneedles induce potent immune responses upon

dermal vaccination in mice, Journal of controlled release : official journal of the Controlled Release Society, 262 (2017) 28-36.

[65] P. Schipper, K. van der Maaden, S. Romeijn, C. Oomens, G. Kersten, W. Jiskoot, J. Bouwstra, Repeated fractional intradermal dosing of an inactivated polio vaccine by a single hollow microneedle leads to superior immune responses, Journal of controlled release : official journal of the Controlled Release Society, 242 (2016) 141-147.

Chapter 1

Chapter 2

Mesoporous silica nanoparticle-coated microneedle arrays for intradermal antigen delivery

Guangsheng Du [1,†] · Jing Tu [2,†] · M. Reza Nejadnik [1] · Juha Mönkäre [1] · Koen van der Maaden [1] · Paul H. H. Bomans [3] · Nico A. J. M. Sommerdijk [3] · Bram Slütter [1] · Wim Jiskoot [1] · Joke A. Bouwstra [1,*] · Alexander Kros [2,*]

[1] Division of BioTherapeutics, Leiden Academic Centre for Drug Research (LACDR), Leiden University, Leiden, 2300 RA, The Netherlands

[2] Department of Supramolecular & Biomaterials Chemistry, Leiden Institute of Chemistry (LIC), Leiden University, Leiden, 2300 RA, The Netherlands

[3] Laboratory of Materials and Interface Chemistry & Center of Multiscale Electron Microscopy, Department of Chemical Engineering and Chemistry, and Institute for Complex Molecular Systems, Eindhoven University of Technology, Eindhoven, 5600 MB, The Netherlands

[†] These authors contributed equally.

ABSTRACT

Purpose To develop a new intradermal antigen delivery system by coating microneedle arrays with lipid bilayer-coated, antigen-loaded mesoporous silica nanoparticles (LB-MSN-OVA).

Methods Synthesis of MSNs with 10-nm pores was performed and the nanoparticles were loaded with the model antigen ovalbumin (OVA), and coated with a lipid bilayer (LB-MSN-OVA). The uptake of LB-MSN-OVA by bone marrow-derived dendritic cells (BDMCs) was studied by flow cytometry. The designed LB-MSN-OVA were coated onto pH-sensitive pyridine-modified microneedle arrays and the delivery of LB-MSN-OVA into *ex vivo* human skin was studied.

Results The synthesized MSNs demonstrated efficient loading of OVA with a maximum loading capacity of about 34% and the lipid bilayer enhanced the colloidal stability of the MSNs. Uptake of OVA loaded in LB-MSN-OVA by BMDCs was higher than that of free OVA, suggesting effective targeting of LB-MSN-OVA to antigen-presenting cells. Microneedles were readily coated with LB-MSN-OVA at pH 5.8, yielding 1.5 µg of encapsulated OVA per microneedle array. Finally, as a result of the pyridine modification, LB-MSN-OVA were effectively released from the microneedles upon piercing the skin.

Conclusion Microneedle arrays coated with LB-MSN-OVA were successfully developed and shown to be suitable for intradermal delivery of the encapsulated protein antigen.

Keywords Intradermal antigen delivery · lipid bilayer · mesoporous silica nanoparticles · pH-sensitive microneedle arrays

INTRODUCTION

Vaccination is regarded as one of the most promising strategies for reducing mortality and improving human health [1, 2]. Most of the current vaccines are delivered by intramuscular or subcutaneous injection, which have inherent limitations, such as the risk of infections induced by reusing needles and syringes and the needle fear of children and patients. Therefore, new needle-free, easy to use and effective vaccination methods are urgently needed. One of these potential methods is microneedle-mediated intradermal vaccination [3].

Intradermal vaccination is attractive because the skin is easily accessible and harbors a large number of immune cells, such as dendritic cells (DCs) [1, 4]. Microneedles are micron-sized structures with a length of less than 1 mm which can be used to overcome the skin barrier located in the top layer of the skin. As these needles do not penetrate to the depths where nerve endings reside, coating of antigens on microneedles enables minimally-invasive and pain-free delivery of vaccines into skin [5-7]. A major challenge however, is the limited dose that can be delivered with coated microneedles. In an effort to improve coating efficiency, our lab designed pH-sensitive pyridine-modified microneedles with a surface pK_a below physiological pH, which allows the adsorption of negatively-charged proteins at slightly acidic conditions (pH 5.8) and their release at neutral pH (pH 7.4). In our previous study, intradermal immunization using pH-sensitive microneedles coated with 5.7 µg OVA were compared to conventional subcutaneous or intradermal immunization [8, 9]. Microneedle-mediated immunization led to comparable T-cell responses but 10-fold lower IgG responses when compared to conventional subcutaneous or intradermal immunization. Possible strategies to further improve the immunogenicity of vaccines by the intradermal route could be adding an adjuvant or using nanoparticles to deliver the antigens [2, 6, 10-13].

The adjuvanticity of nanoparticles is attributed to their capability of protecting antigens from degradation, forming a depot at the site of injection, and facilitating antigen uptake by DCs [14]. A variety of nanosized vaccine delivery systems have been developed, such as polymeric nanoparticles [15], emulsions [16], and lipid-based nanoparticles [15, 17]. Recently mesoporous silica nanoparticles (MSNs) have gained significant attention as drug delivery vehicles because of their controlled size and mesostructure, excellent *in vivo* biocompatibility, and their large surface area and pore volume, enabling the efficient loading of active small molecules or proteins [2, 18-21].

Herein, we report a new intradermal delivery system, which synergistically integrates the advantages of nanoparticles and microneedles by coating pH-sensitive microneedles with antigen-loaded, lipid bilayer-covered MSNs. As a model antigen, OVA was used. This protein is negatively charged (pI of 4.9) [22] at pH 7.4. For the delivery of OVA, a novel type of ultrafine MSNs with large pores (~10 nm in diameter) was synthesized with a positive surface charge (AEP-MSNs), resulting in efficient loading of OVA in the AEP-MSN pores. To enhance the colloidal stability of OVA-loaded AEP-MSNs and generate a negative surface charge, a negatively charged lipid bilayer (LB) was assembled at the AEP-MSN surface and the lipid-coated and OVA-loaded AEP-MSNs are referred to as LB-MSN-OVA [23-25]. This method synergistically combines features of liposomes and MSNs and has been reported to address the multiple challenges including stability, targeting and multicomponent delivery [24, 25]. The designed LB-MSN-OVA were coated onto pH-sensitive pyridine-modified silicon microneedles by electrostatic interactions between the pyridine groups and the LB-MSN-OVA at low ionic strength. Piercing the LB-MSN-OVA coated microneedles into *ex vivo* human skin resulted in the successful release of the nanoparticles due to a shift in pH from 5.8 to 7.4 (Scheme 1).
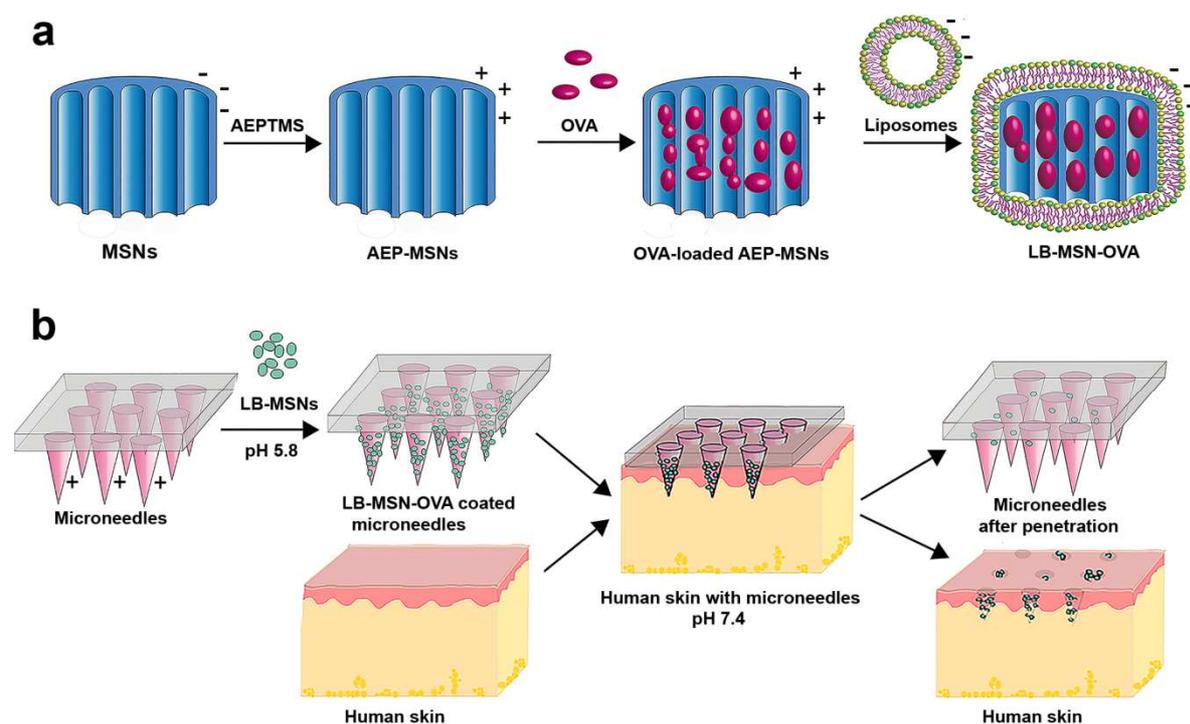
Scheme 1. Preparation and application of pH-sensitive microneedle arrays coated with LB-MSN-OVA. (a) Encapsulation of OVA into AEP-MSNs, followed by fusion of liposomes (composed of DOPC/DOPS/cholesterol), resulting in LB-MSN-OVA. (b) Adsorption of LB-MSN-OVA onto pH-sensitive microneedles and penetration of microneedles into human skin, resulting in a pH shift and delivery of LB-MSN-OVA into the viable epidermis and dermis.

MATERIALS AND METHODS

Materials

Tetraethyl orthosilicate (TEOS, 98%), sulfuric acid (96-98%), hydrochloric acid (36%-38%), (3-aminopropyl)triethoxysilane (APTES, 99%), 4-pyridinecarboxaldehyde (97%), sodium cyanoborohydride (95%), 3-[2-(2-aminoethylamino)ethylamino] propyltrimethoxysilane (AEPTMS, technical grade), Ovalbumin (OVA, ≥98%), 1,3,5-trimethylbenzene (TMB, 97%), Pluronic P123 ($EO_{20}PO_{70}EO_{20}$, Mn ~ 5800 g/mol), and cholesterol (≥99%) were purchased from Sigma-Aldrich (Zwijndrecht, the Netherlands). Fluorocarbon surfactant FC-4 was purchased from Yick-Vic Chemicals & Pharmaceuticals (HK) Ltd. 1,2-dioleoyl-sn-glycero-3-phosphocholine (DOPC), 1,2-dioleoyl-sn-glycero-3-[phospho-L-serine](sodium salt) (DOPS), and 1,2-dioleoyl-sn-glycero-3-phosphoethanolamine-N-(lissamine rhodamine B sulfonyl) (ammonium salt) (DOPE-LR) were purchased from Avanti Polar Lipids Inc (Alabaster, AL). Hydrogen peroxide (30%) and ethylenediaminetetraacetic acid (EDTA) were purchased from Fluka (Steinheim, Germany). Toluene (≥99.7%) was purchased from Biosolve (Valkenswaard, the Netherlands). Alexa Fluor®488 ovalbumin conjugates (OVA-AF488), anti-CD40-FITC, anti-CD80-PE and anti-CD86-APC were purchased from Thermo Fisher Scientific (Waltham, MA). Sterile phosphate buffered saline (PBS, 163.9 mM Na^+, 140.3 mM Cl^-, 8.7 mM HPO_4^{2-}, 1.8 mM $H_2PO_4^-$, pH 7.4) was obtained from Braun (Oss, the Netherlands). All the other chemicals used are of analytical grade and used without further purification. Milli-Q water (18.2 MΩ/cm, Millipore Co., USA) was used for the preparation of solutions. 1 mM phosphate buffer (PB) with a pH of 7.4 was prepared in the lab. Silicon microneedle arrays

with 576 microneedles per array on a back plate of 5×5 mm^2 and a length of 200 µm per microneedle were kindly provided by Robert Bosch GmbH (Stuttgart, Germany).

Synthesis of MSNs and Amino-functionalized MSNs (AEP-MSNs)

Mesoporous silica nanoparticles were synthesized according to a published procedure with modifications [26]. Briefly, surfactant Pluronic P123 (0.5 g) and FC-4 (1.4 g) were dissolved in HCl (80 mL, 0.02 M), followed by the introduction of TMB (0.48 mL). After stirring for 6 h, TEOS (2.14 mL) was added dropwise. The resulting mixture was stirred at 30 °C for 24 h and transferred to an autoclave at 120 °C for 2 days. Finally, the solid product was isolated by centrifugation, and washed with ethanol and Milli-Q water. The organic template was completely removed by calcination at 550 °C for 5 h.

To prepare cationic MSNs, AEPTMS in absolute ethanol (4 mL, 20 wt%) was incubated with MSNs (100 mg) overnight at room temperature. The desired AEP-MSNs were collected by centrifugation and washed with ethanol to remove unreacted AEPTMS.

Characterization of MSNs and AEP-MSNs

Morphology of MSNs and AEP-MSNs was visualized by transmission electron microscopy (TEM) using a JEOL 1010 instrument (JEOL Ltd, Peabody, MA) with an accelerating voltage of 70 kV. To prepare the samples, several droplets of nanoparticle suspension (1 mg/ml) were put on a copper grid, dried overnight and coated with carbon.

Nitrogen adsorption-desorption isotherms of samples were obtained with a TriStar II 3020 surface area analyzer (Micromeritics, Norcross, GA). Before each measurement, MSNs were outgassed in the vacuum (below 0.15 mbar) at 300 °C for 16 h, while AEP-MSNs were outgassed at room temperature. The specific surface areas were calculated from the adsorption data in the low pressure range using the Brunauer-Emmett-Teller (BET) model [27]. The pore size distribution was determined following the Barrett-Joyner-Halenda (BJH) model. Thermogravimetric analysis (TGA) with a Perkin Elmer TGA7 (Waltham, MA) was used to measure the amount of amine-containing groups on the surface of AEP-MSNs. All the samples were tested under an air atmosphere from 25 °C to 800 °C at a heating rate of 10 °C/min.

Encapsulation of OVA in AEP-MSNs

For loading of OVA into AEP-MSNs, OVA (0.5 mL, 0.5 mg/mL 1mM PB) and AEP-MSNs (0.5 mL, 2 mg/mL, 1mM PB) were mixed and incubated in Eppendorf mixer (400 rpm, 25 °C, Nijmegen, the Netherlands) for different time periods (0, 0.5, 1, 2, 4, 8 and 24 h). After incubation, the suspensions were centrifuged and the encapsulation efficiency (EE%) of OVA was determined by measuring the difference in its intrinsic fluorescence intensity with a plate reader (Tecan M1000, Männedorf, Switzerland) (excitation wavelength = 280 nm and emission wavelength = 320 nm) in the supernatant before and after the encapsulation.

To determine the maximum loading capacity (LC%) of OVA in AEP-MSNs, the AEP-MSNs (2 mg/mL) were mixed with different initial concentrations of OVA (ranging from 0.25, 0.5, 1, 1.5, 2 to 3 mg/mL) and incubated in an Eppendorf mixer (400 rpm, 25 °C) for 0.5 h. Next, the suspensions were centrifuged at 9000 g for 5 min. The EE% of OVA was determined by measuring the difference in their intrinsic fluorescence intensity in the supernatant before and after the encapsulation with a plate reader (Tecan M1000).

The EE% and LC% were calculated as below:

$$EE \% = \frac{t_{ova} - f_{ova}}{t_{ova}} \times 100 \% \hspace{2cm} (1)$$

$$LC \% = \frac{t_{ova} - f_{ova}}{OVA \ loaded \ AEP\text{-}MSNs} \times 100 \% \hspace{1.5cm} (2)$$

Where t_{ova} represents the total content of OVA, and f_{ova} is the content of free OVA (OVA in the supernatant).

Preparation of Liposomes

Liposomes were prepared by dispensing stock solutions of DOPC, DOPS and cholesterol in a molar ratio of 7/1/2 into scintillation vials. All lipids were dissolved in chloroform. A lipid film was generated by slow evaporation of chloroform in the vial under a nitrogen flow and dried under vacuum overnight. The lipid film was rehydrated by the addition of PB (1 mL, 1 mM, pH 7.4) and the mixture was vortexed for 10 s to form a cloudy lipid suspension. The obtained suspension was sonicated in a water bath for 10 min. The resulting clear liposomes dispersions were stored at 4 °C. To obtain fluorescent liposomes, a fluorescently labeled lipid (DOPE-LR) was incorporated into the liposomes by adding the lipids at 1 wt% DOPE-LR to the lipid solution prior to liposome formation.

Preparation of LB-MSN-OVA

To prepare LB-MSN-OVA, OVA (0.5 mL, 0.25 mg/mL) solution in PB (1 mM, pH 7.4) was first transferred into a 2-mL Eppendorf tube, followed by the addition of AEP-MSNs (0.5 mL, 1 mg/mL) in PB (1 mM, pH 7.4) and liposome (0.5 mL, 2 mg/mL) in PB (1 mM, pH 7.4). The resulting mixture was incubated in the Eppendorf mixer for 1.5 h (400 rpm, 25 °C). The particles were collected and excess liposomes and OVA were removed by centrifugation (9000 g, 5 min). The encapsulation efficiency of OVA was determined by measuring the difference in their intrinsic fluorescence intensity in the supernatant before and after the encapsulation on a Tecan M1000 plate reader. All experiments were performed in triplicate. For the uptake study of LB-MSN-OVA in dendritic cells, OVA-AF488 was used to prepare LB-MSN-OVA.

Characterization of LB-MSN-OVA

The hydrodynamic size distribution was measured with dynamic light scattering (DLS) using a Malvern Nano-zs instrument (Worcestershire, UK). Samples were diluted with 1 mM PB (pH 7.4) and measured 3 times each with 10 runs at 25 °C. The zeta potential was measured by laser Doppler velocimetry using the same instrument. Samples were diluted with 1 mM PB (pH 7.4) and measured 3 times with 20 runs.

The size distribution was also measured by NanoSight LM20 (NanoSight Ltd., Amesbury, UK). Samples were injected into chamber by an automatic pump (Harvard Apparatus, catalog no. 98-4362, Holliston MA). The samples were diluted to 5 µg/ml with 1 mM PB (pH 7.4) and measured at 25 °C. A 90-s video was captured with the shutter set at 1495 and the gain at 680. The data was analyzed by NTA 2.0 Build 127 software.

Imaging of LB-MSN-OVA was performed by using a CryoTitan (FEI Corp, Hillsboro, OR) operating at 300 kV and equipped with a field emission gun (FEG). Cryo-samples were prepared from a 3 µL droplet of sample solution placed on the grid inside the Vitrobot™ chamber at 100% relative humidity and 20 °C. Prior to use the TEM grids were glow discharged by a Cressington 208 carbon coater to render them hydrophilic. The samples were

blotted to remove excess solution and vitrified by using an automated vitrification robot (Vitrobot™ Mark III, FEI Corp).

OVA Release Studies from AEP-MSNs and LB-MSN-OVA

To study the influence of ionic strength on the release of OVA from AEP-MSNs, phosphate buffer (PB, 1 mM Na_2HPO_4 and 1 mM NaH_2PO_4 were mixed at molar ratio of 5:2, pH 7.4) with various concentrations of NaCl (0, 0.9, 1.8, 3.6, 7.2, 14.4 and 28.8%, m/v) were prepared. AEP-MSNs loaded with OVA (1 mg, based on the mass of AEP-MSNs) were dispersed in one of the buffers (1 mL) mentioned above. The suspensions were kept in the Eppendorf mixer for 0.5 h (400 rpm, 37 °C), followed by centrifugation (9000 g, 5 min) to collect the supernatant. The amount of released OVA in the buffer was quantified by measuring the intrinsic fluorescence intensity of OVA with a Tecan M1000 plate reader. The released OVA in PB with 0.9, 1.8 and 3.6% NaCl was also tested by high pressure size-exclusion chromatography (HP-SEC). Far-UV circular dichroism (CD) spectra of OVA before and after release were measured by using a Jasco J-815 spectropolarimeter (Tokyo, Japan). Spectra were collected from 260–190 nm, at 25 °C.

To compare the *in vitro* release of OVA from AEP-MSNs and LB-MSN-OVA, OVA-loaded AEP-MSNs and LB-MSN-OVA were dispersed in PBS (pH 7.4) and incubated in the Eppendorf mixer (400 rpm, 37 °C). At various time points, the suspensions were centrifuged and the supernatants were replaced with fresh PBS. The amount of OVA released into the supernatant was determined by measuring the intrinsic fluorescence intensity of OVA on a Tecan M1000 plate reader.

Interaction of LB-MSN-OVA with Bone marrow-derived dendritic cells (BMDCs)

Dendritic cells were cultured from BALB/c donor mice as previously described [28]. The study was carried out under the guidelines compiled by the animal ethic committee of the Netherlands, and approved by the ethical committee on animal experiments of Leiden University. Briefly, cell suspensions of bone marrow were obtained by flushing the femurs and tibia of adult BALB/c mice with culture medium. The cells (6×10^6 cells/well) were cultured for 10 days in Iscove's Modified Dulbecco's Medium (IMDM) supplemented with 10% (v/v) fetal bovine serum, penicillin and streptomycin (100 units/ml), 20 μM beta-mercaptoethanol and 20 ng/ml GM-CSF. The cells were cultured at 37 °C with 5% CO_2. The medium was refreshed every 2 days.

To study the uptake of nanoparticles, BMDCs (2.5×10^5 cells/ml) were cultured with LB-MSN-OVA containing 6 μg/ml, 0.6 μg/ml or 0 μg/ml (culture medium) OVA-AF488 for 4 h at either 4°C or 37 °C. Free OVA-AF488 solution with the same concentrations was used as a control. After 4 h, the uptake of OVA-AF488 was measured using flow cytometry (FACSCanto II, Becton Dickinson, NJ). To quench the external AF488 signal, 0.02% trypan blue was added 5 min before FACS analysis. The uptake of OVA-AF488 was expressed as the mean fluorescence intensity (MFI, fluorescence intensity of each cell in average) in the AF488 channel.

To study the activation of BMDCs by the nanoparticles, BMDCs (5×10^5 cells/ml) were cultured with LB-MSN-OVA containing 6 μg/ml, 0.6 μg/ml or 0 μg/ml (culture medium) OVA-AF488 for 4 h at 37 °C. OVA-AF488 solution with the same concentrations and LPS (1 μg/ml) were used as controls. The cells were stained for 30 min with a mixture of 300 × diluted anti-CD40-FITC, anti-CD80-PE, and anti-CD86-APC. The cells were washed and the expression of CD40, CD80 and CD86 were quantified by flow cytometry.

Modification of Silicon Microneedle Arrays to Obtain a pH-sensitive Surface

To coat negatively charged particles onto silicon microneedle arrays, the microneedles were chemically modified to obtain a pH-sensitive surface (positively charged at pH 5.8) by using pyridine groups, as described previously [6]. The surface of silicon was first cleaned by acetone and methanol. Next the surfaces were hydroxylated by a fresh piranha mixture consisting of 30% (v/v) H_2O_2 and 70 % (v/v) H_2SO_4. Then the surface was incubated with 2% (v/v) APTES in toluene overnight at room temperature to obtain the amine-modified silicon surface.

The amine-modified surface was modified with 4-pyridinecarboxaldehyde (100 mM) in anhydrous isopropanol with acetic acid (1%, v/v) at room temperature. The obtained imine bonds on pyridine-modified surface were reduced to a secondary amine by incubating in $NaBH_3CN$ (50 mM) in isopropanol for 2 h. Finally the modified surface was cleaned with isopropanol and methanol and dried in a vacuum oven at 50 $^{\circ}$C for 0.5 h.

Coating of LB-MSN-OVA on pH-sensitive Microneedle Arrays

To determine the level of binding of LB-MSN-OVA on the microneedle arrays, DOPE-LR was added to the lipids when the LB-MSN-OVA were prepared. The top of the microneedle arrays was incubated with LB-MSN-OVA (50 µl) with a concentration of 0.1, 0.5 and 1 mg/mL in EDTA buffer (1 mM, pH 5.8) for 2 h at room temperature. The microneedles were then washed with coating buffer (450 µl) and the solution was kept for measurement. The binding efficiency of LB-MSN-OVA was determined by comparing the DOPE-LR concentration in the coating solution before and after coating by using a Tecan M1000 plate reader (Excitation wavelength = 575 nm and Emission wavelength = 590 nm). The structure, geometry and the surface morphology of the LB-MSN-OVA coated pH-sensitive microneedle arrays were examined by scanning electron microscopy (SEM) in a FEI NOVA nanoSEM 200 (Hillsboro, OR). The LB-MSN-OVA coated on microneedle arrays were also visualized by Nikon D-Eclipse C1 confocal laser scanning microscope (CLSM, Tokyo, Japan) with a depth resolution of 5 µm/step, equipped with a 10 × Plan Apo objective. The x and y resolution was 2.5 µm. An argon laser (488 nm) was used to visualize OVA-AF488 with a 530/55 emission filter and a diode-pumped solid-state laser (561 nm) with a 590/55 emission filter was used to visualize DOPE-LR.

Delivery of LB-MSN-OVA from Microneedles into *ex vivo* Human Skin

After coated with LB-MSN-OVA, the pH-sensitive microneedles were pierced into human skin from the abdomen, which was used within 24 h after cosmetic surgery from a local hospital. The study was conducted in accordance to Helsinki principles and written informed patient consent was obtained. The microneedles were applied into the skin by an impact-insertion applicator with a velocity of 54.8 cm/s as described previously [6]. After 1 s, the applicator was removed and the microneedles were kept inside the skin for 30 min. Then the microneedles were removed and visualized by scanning electron microscopy (SEM) in a FEI NOVA nanoSEM 200 (Hillsboro, OR). The skin was visualized by Nikon D-Eclipse C1 CLSM (Tokyo, Japan) with a depth resolution of 5 µm/step, equipped with a 4 × Plan Apo objective. The x and y resolution was 6.3 µm. An argon laser (488 nm) was used to visualize OVA-AF488 with a 530/55 emission filter and a diode-pumped solid-state laser (561 nm) with a 590/55 emission filter was used to visualize DOPE-LR.

Statistical Analysis

All data shown are mean corrected values ± SD of at least three experiments. The results of cell experiments are analyzed by Two-way ANOVA with Bonferroni posttests.

## RESULTS

Characterization of MSNs and AEP-MSNs

The MSNs were synthesized from the silica precursor tetraethoxy silane (TEOS) by using a mixture of a nonionic triblock copolymer (Pluronic P-123) and the cationic fluorocarbon surfactant (FC-4) as organic templates. Furthermore the swelling agent TMB was added to induce the formation of large-pore MSNs [29]. The obtained pristine MSNs were modified with AEPTMS in order to generate a positively charged surface (AEP-MSNs). Inspection with TEM revealed that the negatively charged MSNs were rectangular in shape with mesochannels along the short axis (Fig. 1a). Modification with AEPTMS did not alter the morphology or mesostructure (Fig. 1b), as compared to pristine MSNs. Furthermore, characterization with N_2 adsorption-desorption isotherms of both MSNs and AEP-MSNs showed that these nanoparticles have typical IV isotherms according to International Union of Pure and Applied Chemistry (IUPAC) classification (Fig. 1c) [30]. The existence of channel-type mesopores was confirmed by the existence of a type-H_1 hysteresis loop (Fig. 1c) [31]. The values for BET specific surface area (S_{BET}), the total pore volume (V_t), BJH pore diameter (W_{BJH}) and surface charge of MSNs and AEP-MSNs are summarized in Table 1. It can be seen that after modification with AEPTMS, S_{BET}, V_t and W_{BJH} were slightly reduced because of the attachment of the functionalized silanes on the pore surface. The pore diameter of the AEP-MSNs was 1-2 nm smaller than that of MSNs (Fig. 1d), but still sufficiently large to accommodate OVA ($4 \times 5 \times 7$ nm) [78]. Dynamic light scattering (DLS) measurements showed that the hydrodynamic diameter of MSNs and AEP-MSNs was 146.3 ± 0.3 nm and 213.7 ± 0.8 nm, respectively. The observed increase in Z-average size for AEP-MSNs may be attributed to some particle aggregation, which is probably due to the decreased charge repulsion among AEP-MSNs compared to MSNs (Table 1).

Table 1 Physical characteristics of nanoparticles (n=3)

Sample	BET surface area (m²/g)	Pore volume (cm³/g)	Pore diameter (nm)[a]	Size (nm)	PDI	Zeta-potential (mV)[b]
MSNs	506	1.01	10 ± 1	146.3 ± 0.3	0.154 ± 0.035	-27.8 ± 0.4
AEP-MSNs	318	0.71	9 ± 1	213.7 ± 0.8	0.170 ± 0.062	10.9 ± 0.5
AEP-MSN-OVA	-	-	-	1842 ± 126	0.373 ± 0.056	-8.1 ± 1.3
LB-MSN-OVA	-	-	-	190.7 ± 2.7	0.125 ± 0.029	-24.0 ± 0.7

[a]Calculated from desorption branch of the N_2 sorption isotherms based on the BJH method.
[b]Zeta-potential was measured in 1 mM PB at pH 7.4.
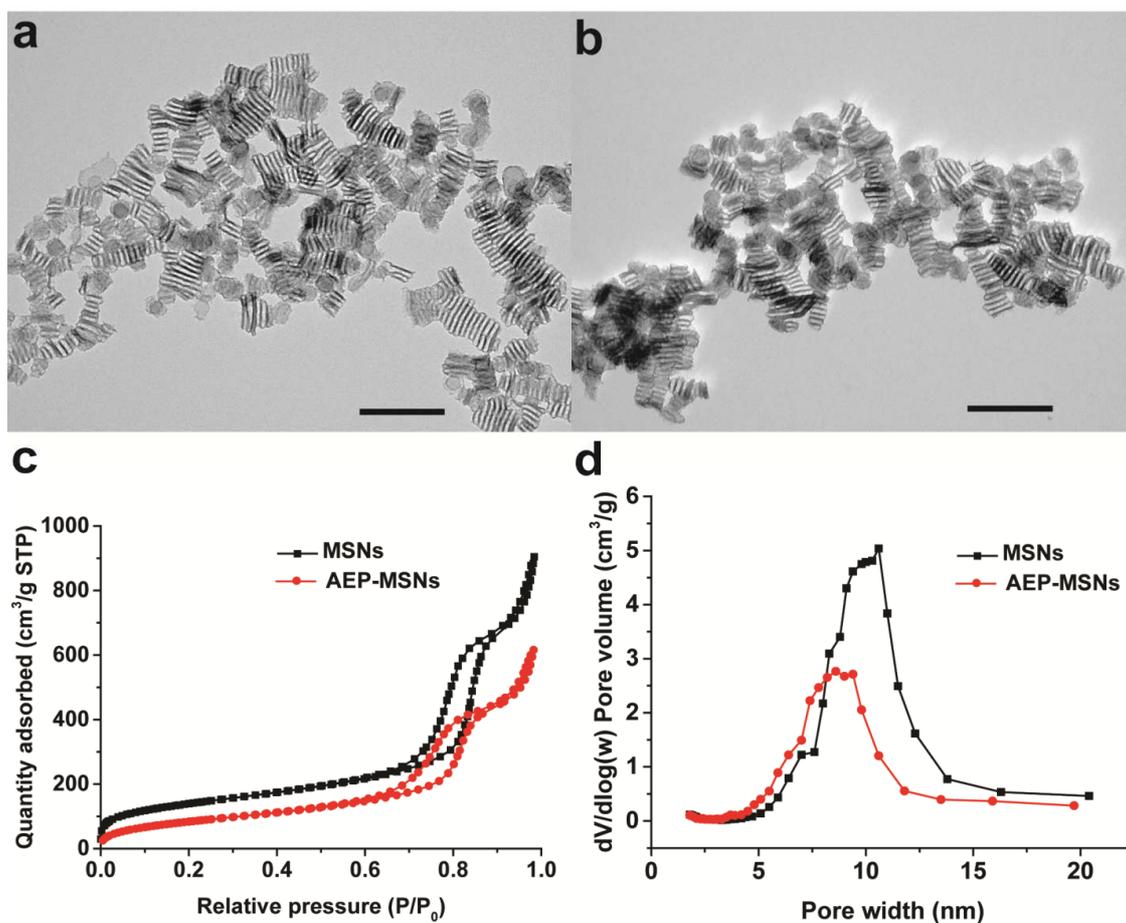
Fig. 1 Characterization of the MSNs and AEP-MSNs. TEM images of (a) MSNs and (b) AEP-MSNs. Scale bar = 200 nm. (c) Nitrogen adsorption-desorption isotherms and (d) plots of pore diameter vs. pore volume (inset), calculated from the desorption isotherms using BJH model, show that the MSNs and AEP-MSNs have an average pore diameter of 10 nm and 9 nm, respectively.

Encapsulation and Release of OVA from AEP-MSNs

The percentage of grafted amine-containing groups on the surface of AEP-MSNs was 6.9%, as determined by thermogravimetric analysis (TGA, see Fig. 2a). The encapsulation efficiency (EE%), defined as the percentage of OVA which is adsorbed in the MSNs or AEP-MSNs was determined as a function of incubation time (Fig. 2b). The calibration curve used to calculate the concentration of OVA is shown in supplementary Fig. 1a. This study revealed that the OVA encapsulation within AEP-MSNs was very efficient, as $95 \pm 0.4\%$ (mean $\pm$ SD, n = 3) of the protein was encapsulated in the AEP-MSNs. Furthermore, equilibrium of OVA encapsulation was reached in less than 5 min. In comparison, only $12 \pm 2\%$ (mean $\pm$ SD, n = 3) of OVA was encapsulated in negatively charged MSNs after 24 h. The loading capacity (LC%) of OVA was calculated from the amount of OVA encapsulated in AEP-MSNs and expressed as the percentage of the total weight of OVA-loaded AEP-MSNs. The LC% of OVA in AEP-MSNs was dependent on the initial concentration of OVA (Fig. 2c). The maximum LC% was $34 \pm 4\%$ (mean $\pm$ SD, n = 3) and was achieved by increasing the initial concentration of OVA, indicating a diffusion-driven encapsulation process [32].

To examine the influence of ionic strength of the medium on the release profile of OVA from the AEP-MSNs, the concentration of NaCl in the buffer was varied. The calibration curve used to calculate the concentration of OVA is shown in supplementary Fig. 1b. The release percentage of OVA (defined as the percentage of OVA released from total encapsulated OVA in AEP-MSNs) increased from $0.6 \pm 0.2\%$ (mean $\pm$ SD, n=3) in NaCl-free buffer to $82 \pm 2\%$ (mean $\pm$ SD, n = 3) in buffer containing 7.2% NaCl (Fig. 2d). These results demonstrate that the ionic strength of the medium plays an important role in the release of OVA, indicating that the interaction between OVA and AEP-MSNs is mainly electrostatic in nature. The structural integrity of the released OVA was examined by HP-SEC, showing that the released OVA was mainly monomeric (Fig. 2e), and far-UV CD spectroscopy, indicating that the secondary structure of released protein was similar to that of native OVA (supplementary Fig. 2). These results strongly indicate that encapsulation and release have no adverse effect on the protein structure.

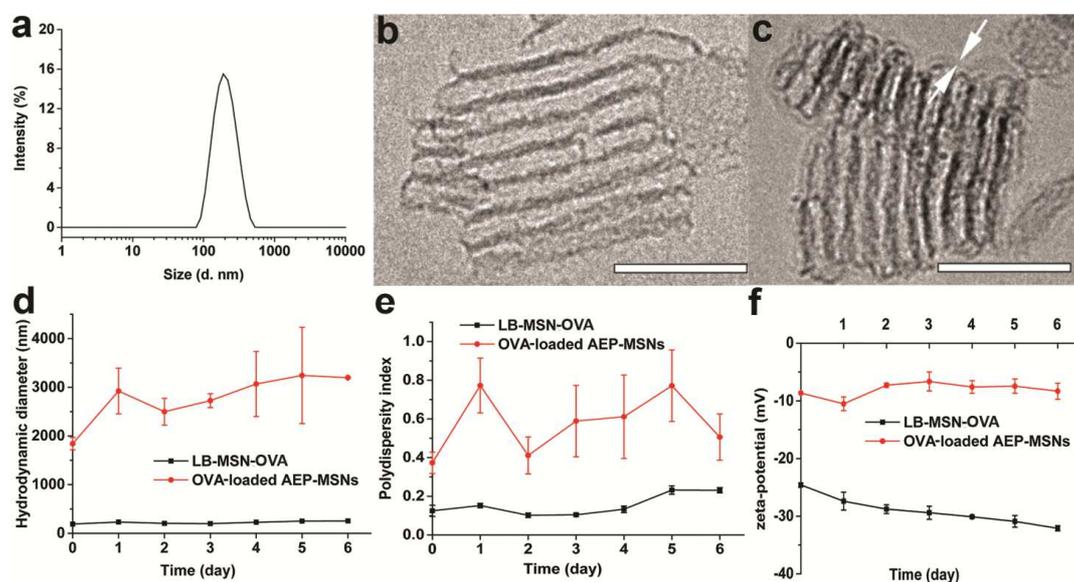## Preparation and Characterization of LB-MSN-OVA

The OVA-loaded AEP-MSNs had the tendency to precipitate and form large aggregates (Table 1), probably due to the decreased surface charge upon protein encapsulation (-8.1 $\pm$ 1.3 mV, mean $\pm$ SD, n = 3). In order to increase the colloidal stability, the OVA-loaded AEP-MSNs were stabilized with a lipid bilayer composed of DOPC, DOPS and cholesterol. For this, liposomes and OVA-loaded AEP-MSNs were mixed and equilibrated for 1.5 h and afterwards the excess lipids were removed by centrifugation. The encapsulation efficiency of OVA in the resulting lipid-coated AEP-MSNs (LB-MSN-OVA) was determined to be 74 $\pm$ 1%, as compared to 99 $\pm$ 1% without lipid (mean $\pm$ SD, n = 3). The obtained LB-MSN-OVA were characterized by DLS, NTA and TEM. The mean number-based hydrodynamic diameter (176 $\pm$ 11 nm, mean $\pm$ SD, n = 3) measured by NTA (supplementary Fig. 3) was close to the Z-average hydrodynamic diameter (190.7 $\pm$ 2.7 nm; PDI = 0.125 $\pm$ 0.029; mean $\pm$ SD, n = 3) found by DLS (Fig. 3a). The existence of a lipid bilayer surrounding the AEP-MSNs was confirmed by cryoTEM (Fig. 3b and 3c). The colloidal stability of the formulation was examined by measuring the hydrodynamic diameter and zeta-potential of LB-MSN-OVA for one week (Fig. 3d-f). It showed that LB-MSN-OVA slightly changed in diameter and zeta-potential, revealing that the lipid bilayer strongly enhanced the colloidal stability. The release of OVA from AEP-MSNs and LB-MSN-OVA was examined in PBS (pH 7.4) for 32 h (Fig. 2f). The burst release of OVA from LB-MSN-OVA was less in comparison to AEP-MSNs, indicating that the lipid bilayer acts as a barrier retaining the OVA for longer inside the AEP-MSNs.

Interaction of LB-MSN-OVA with BMDCs

As proteins in serum may interact with the particles, the colloidal stability of LB-MSN-OVA in cell culture medium was studied. Only limited aggregation of the nanoparticles was observed and a modest amount of OVA (15%) was released after 4 h (supplementary Table 1). To examine whether LB-MSN-OVA facilitate the uptake by BMDCs, the uptake of LB-MSN-OVA was assessed by flow cytometry and compared to that of free OVA solution. As shown in Fig. 4, at 4ºC there was almost no uptake (no significance compared to culture medium only) of LB-MSN-OVA or OVA in BMDCs (Fig. 4a), indicating that the uptake of LB-MSN-OVA and OVA is mediated by an active process. At 37 ºC the fluorescent level of LB-MSN-OVA treated cells was significantly higher (p<0.001) than that for free OVA-AF488 with the OVA concentration of 6 µg/ml (Fig. 4b). There was no significant difference found between LB-MSN-OVA and free OVA at lower concentration. These results indicate that LB-MSN-OVA are capable of promoting antigen uptake by antigen-presenting cells
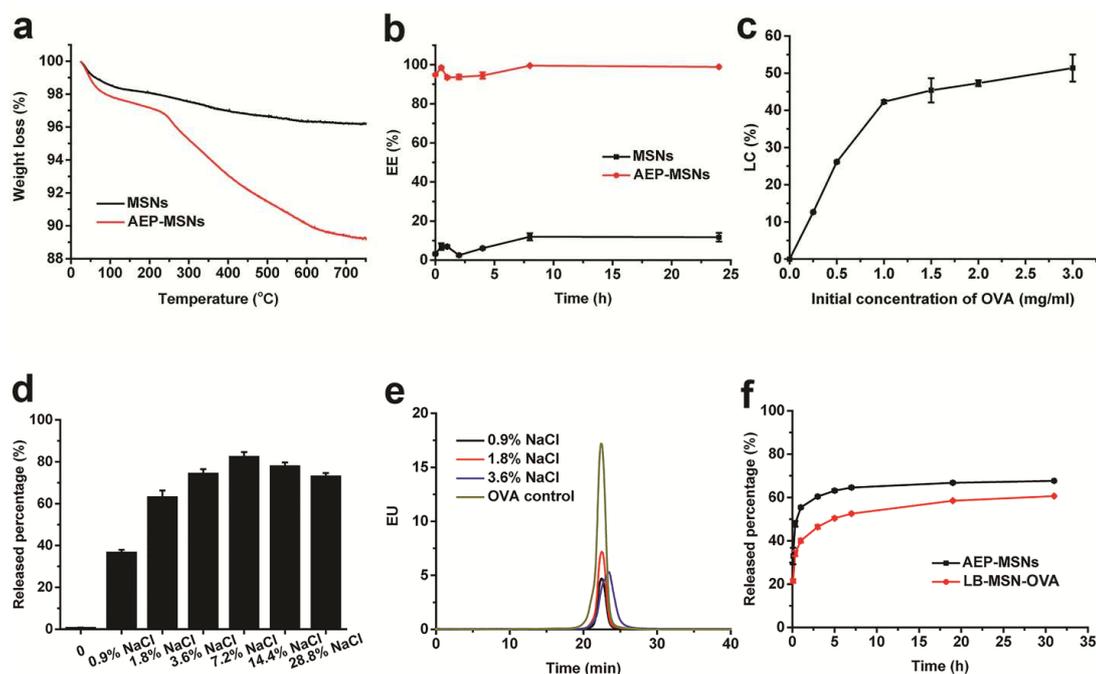
Fig. 2 (a) Thermogravimetric analysis (TGA) curves of MSNs and AEP-MSNs. (b) Encapsulation kinetics of OVA into MSNs and AEP-MSNs (mean ± SD, n = 3), concentration of OVA is 0.5 mg/mL and MSNs (AEP-MSNs) is 2 mg/mL. (c) Loading capacity (LC%) of OVA into AEP-MSNs (mean ± SD, n = 3) at different initial concentration of OVA. (d) Influence of ionic strength on OVA release from AEP-MSNs (mean ± SD, n = 3). (e) HP-SEC chromatograms of the released OVA from AEP-MSNs. (f) Release profiles of OVA from AEP-MSNs and LB-MSN-OVA in PBS (pH 7.4) (mean ± SD, n = 3).

Fig. 3 Characterization of LB-MSN-OVA. (a) Hydrodynamic diameter of LB-MSN-OVA determined by DLS. (b) CryoTEM image of AEP-MSNs, and (c) LB-MSN-OVA, revealing a lipid bilayer thickness of ~4 nm (indicated by white arrows), scale bar = 100 nm. (d-f) colloidal stability of OVA-loaded AEP-MSNs and LB-MSN-OVA over one week (d: hydrodynamic diameter, e: polydispersity index and f: zeta potential).

(BMDCs). In order to study the activation of BMDCs by the nanoparticles, BMDCs were incubated with different formulations for 4 h and the expression of CD40, CD80 and CD86 was measured. Whereas exposure to LPS led to a significant upregulation of these activation markers, LB-MSN-OVA did not induce increased expression of CD40, CD80 or CD86 on dendritic cells compared to free OVA or cell culture medium (Fig. 4c).
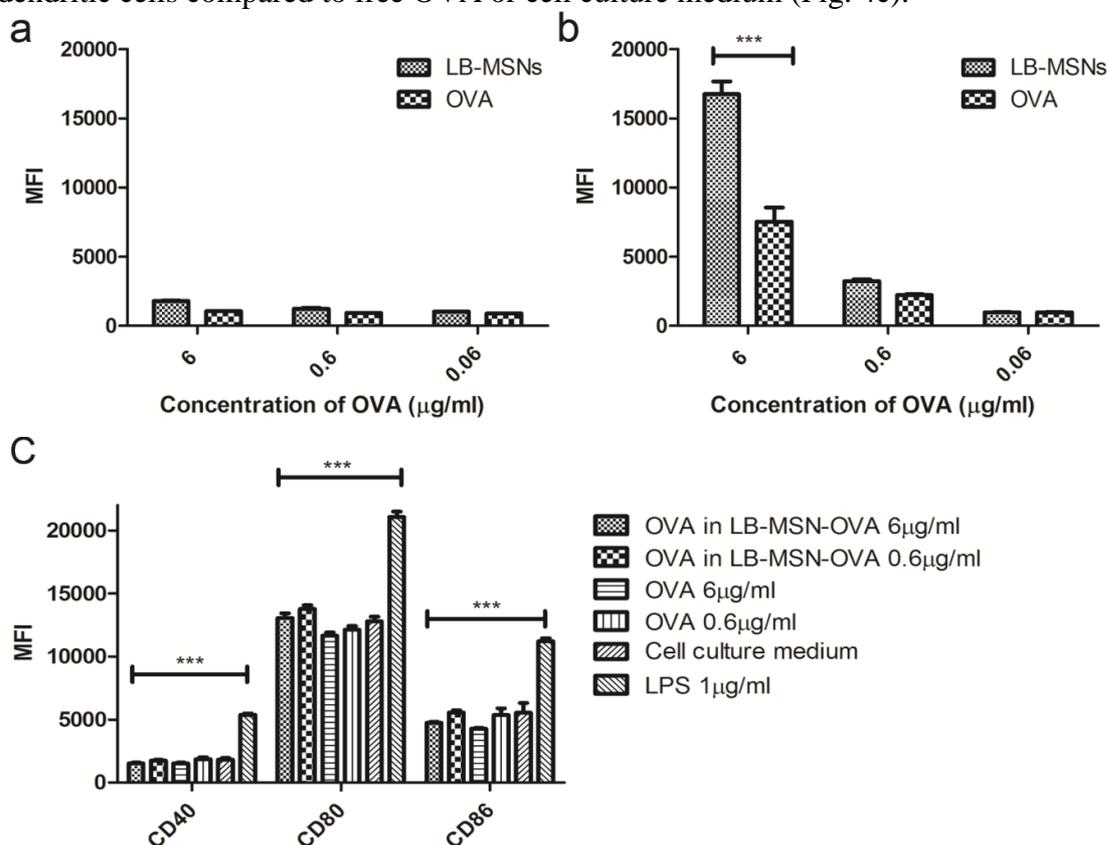
Fig. 4 The uptake of LB-MSN-OVA in BMDCs at 4 ℃ (a) and 37 ℃ (b), and the activation of BMDCs by LB-MSN-OVA (c). Bars represent mean ± SD, n=3. The uptake of OVA-AF488 and expression of CD40, CD80 and CD86 were expressed as the mean fluorescence intensity (MFI). *** P＜0.001.

**Table 2** Coating amount of LB-MSN-OVA and OVA on microneedle arrays

Amount of LB-MSN-OVA[a] (μg)	Coated LB-MSN-OVA (μg)	Coated OVA[b] (μg)	Coating efficiency (%)
5	1.3 ± 0.2	0.24 ± 0.03	27 ± 3
25	5.4 ± 1.7	1.0 ± 0.3	22 ± 7
50	7.9 ± 1.3	1.5 ± 0.2	16 ± 3

[a]The amount of LB-MSN-OVA in coating solution; [b]The amount of coated OVA was calculated from the loading capacity of OVA and the coating amount of LB-MSN-OVA. All the coating amounts are expressed as the amount of AEP-MSNs and are based on one microneedle array which contains 576 needles per array. All the results are based on 3 independent microneedle arrays.

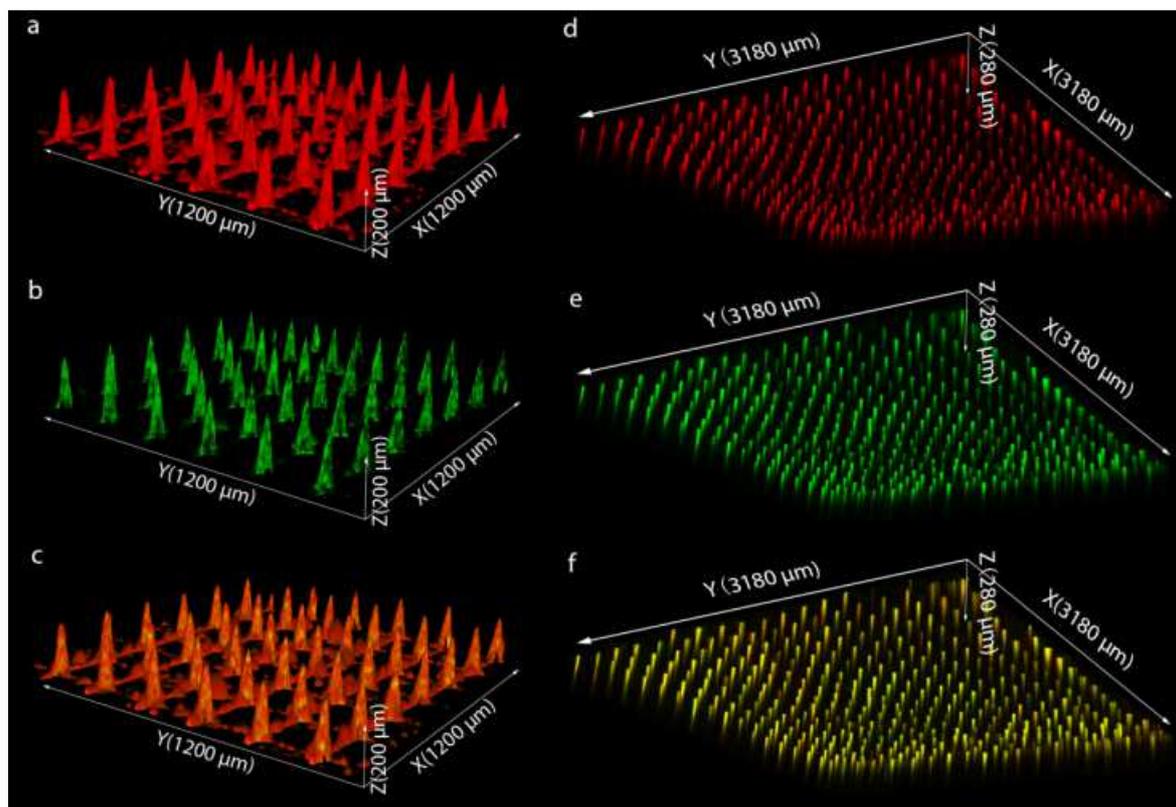**Coating of LB-MSN-OVA on Microneedles**

Next, we investigated whether the LB-MSN-OVA could be adsorbed onto a silicon microneedle array via physical adsorption. First, the pH-sensitive pyridine-modified microneedle arrays were prepared as described previously [6]. The microneedle arrays were coated with LB-MSN-OVA at pH 5.8 in an EDTA buffer (1 mM). To determine the optimal concentration of LB-MSN-OVA for the coating process, the nanoparticle concentration was varied in the buffered coating solution. Increasing the LB-MSN-OVA concentration resulted in increased amounts of LB-MSN-OVA coated onto the microneedle array surfaces. However, the coating efficiency is reduced (Table 2). The lowest coating efficiency obtained was $16 \pm 2.7\%$ (mean $\pm$ SD, n = 3), corresponding to 7.9 ± 1.3 µg (mean $\pm$ SD, n = 3) and 1.5 ± 0.24 µg (mean $\pm$ SD, n = 3) of LB-MSN-OVA and OVA, respectively coated on the microneedle array. Considering the surface area of the microneedles accounts for 40% of the total surface area of microneedle arrays, 3.2 ± 0.5 µg (mean $\pm$ SD, n = 3) of nanoparticles and 0.58 ± 0.10 µg (mean $\pm$ SD, n = 3) of OVA were coated onto the microneedle surface of one array.
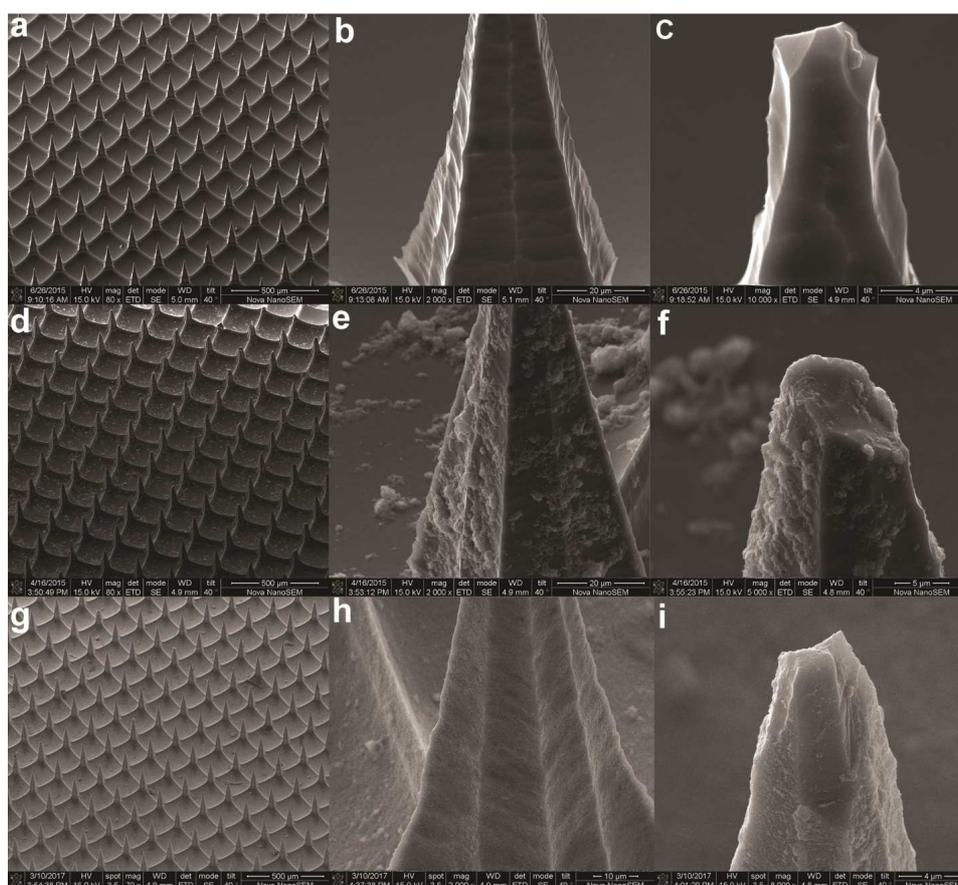
Fig. 5 SEM images of pyridine-modified microneedle arrays before the adsorption of LB-MSN-OVA with different magnifications (a: 80 ×; b: 2000 ×; c: 5000 ×), after the adsorption of LB-MSN-OVA with different magnifications (d: 80 ×; e: 2000 ×; f: 5000 ×) and after the penetration of human skin (g: 80 ×; h: 2000 ×; i: 5000 ×).

Scanning electron microscopy imaging was used to visualize the presence of the LB-MSN-OVA on the pyridine-modified microneedle arrays (Fig. 5a-f). Compared to untreated pyridine-modified arrays (Fig. 5a-c), a high number of nanoparticles were observed on the surface of the microneedles (Fig. 5d-f) after coating with LB-MSN-OVA. To determine whether the OVA and nanoparticles colocalized on the microneedles, the LB-MSN-OVA coated microneedles were visualized by CLSM. For this experiment, we used OVA-AF488 and DOPE-LR enabling the visualization of both the protein and lipids. Imaging revealed that

the fluorescent labels were both located at the microneedle surfaces indicative of the integrity of the LB-MSN-OVA upon physical adsorption (Fig. 6a-c). This showed us that LB-MSN-OVA could be immobilized onto microneedles via electrostatic interaction.

Fig. 6 CLSM images of LB-MSN-OVA coated microneedles (a-c). Red: DOPE-LR (a); Green: OVA-AF488 (b); Merged (c). The x and y arrows show that the scanning area is 1200 μm × 1200 μm large. The z arrow indicates the scanning depth of 200 μm. CLSM images of human skin after removal of the LB-MSN-OVA coated microneedle arrays (d-f). Red: DOPE-LR (d); Green: OVA-AF488 (e); Merged (f). The x and y arrows show that the scanning area is 3180 μm × 3180 μm large. The z arrow indicates the scanning depth of 280 μm.

Delivery of LB-MSN-OVA into Human Skin

Next, the delivery of LB-MSN-OVA from the surface of microneedles into the skin was studied. For this, the nanoparticle-coated microneedle arrays were applied onto human skin *ex vivo* for 30 min and subsequently withdrawn. Next the intradermal delivery was studied by both SEM and CLSM. Less particles were observed on surface of microneedles after the penetration and withdrawal from human skin (Fig. 5g-i). Colocalization of the fluorescence from both OVA-AF488 and DOPE-LR was observed inside the skin (Fig. 6d-f), illustrating that the microneedles penetrated into the skin and successfully delivered the LB-MSN-OVA.

DISCUSSION

An alarming trend towards decreased vaccine compliance in the western world emphasizes the need to develop effective, but also safe and easily administrable vaccines. In this respect dermal vaccination is interesting as the skin provides an easily accessible (and potentially painless) route of administration and also provides an environment which is very conductive for the initiation of immunological memory. Topical administration of vaccines is often not effective as bulky vaccines do not permeate the skin. Recently, we and other groups have shown that antigens can effectively be delivered into the epidermis and dermis by means of

coated microneedles [3, 4, 10, 33]. However, some major challenges remain, which include the effective dose that can be delivered with coated microneedles and the immunogenicity of the subunit vaccines [4, 6].

Here we introduce a novel carrier system for subunit vaccines with a high loading efficiency that effectively delivers a model antigen into the skin using a complementary charged microneedle array. To our best knowledge, the current study is the first example of a microneedle-mediated intradermal delivery system for mesoporous nanoparticles, which could be a promising tool to deliver a wide range of compounds into the skin. High loading efficiency was achieved by encapsulating the model antigen OVA into surface-modified MSNs with large pores (>10 nm). We chose MSNs because of their advantageous properties, including large surface area, controlled particle size and pore structure as well as ease of surface modification. Moreover, a previous study showed that subcutaneous immunization with 2 µg of OVA-loaded MSNs induced comparable antibody responses as 50 µg OVA adjuvanted with Quil-A [18], demonstrating that antigen-loaded MSNs can elicit an immune response at reduced antigen doses compared to a conventional delivery system. Our results indicate that one of the reasons for the immune enhancing effect on MSNs may be the increased uptake by dendritic cells when OVA is associated with MSNs (Fig. 4). LB-MSN-OVA do not increase the activation of dendritic cells compared to free OVA, which is in line with previous findings [34]. Similar results were reported with OVA-loaded PLGA nanoparticles [35] as OVA-loaded PLGA nanoparticles were found not to increase activation of human monocyte-derived dendritic cells (MHC II, CD83 and CD86). This suggests that the addition of adjuvants capable of inducing DC maturation, may further increase the immunogenicity of LB-MSN-OVA.

For an efficient dermal delivery of nanoparticulate vaccines, MSNs are required that are small in size. In addition, they should have large pores (inner diameter > 5 nm) in order to encapsulate large amounts of proteins. Most nanosized MSNs do not fit these criteria, although recently some examples have emerged, mainly for the delivery of DNA/RNA [24, 36-39]. MSNs with a large pore size of about 10 nm, recently developed in our lab [26], were used in the current study to accommodate the relatively large OVA molecules ($4 \times 5 \times 7$ nm). The encapsulation study showed that the synthesized MSNs can accommodate a large amount of OVA within 5 min after mixing AEP-MSNs with OVA. It has been reported that MSNs with a pore size of 3.6 and 2.3 nm had a maximum OVA LC% of 21.8% [1] and 7.2% [18], respectively. The even higher maximum LC% of OVA in our study of 33.9% may be due to the larger pore size.

To coat nanoparticles onto the pyridine-modified microneedles, the nanoparticles should have a negative surface charge allowing for adsorption based on electrostatic interactions, and a good colloidal stability allowing uniform and reproducible coating. In our study, negative liposomes were used to fuse to the surface of the positively charged AEP-MSNs, to achieve a negative surface charge. This fusion method was previously used for coating fluorophore [40], photosensitizers [41] and DNA loaded MSNs [23] and was reported to be based on the electrostatic interaction between the lipids and surface of MSNs [23]. The fusion of lipid bilayer on MSN surface has been shown to be able to modify the charge, improve the stability of MSNs and contain the drug inside the pores of MSNs. In order to prepare the liposomes, DOPC and cholesterol were used because in a previous study liposomes containing DOPC and cholesterol were shown to be able to stabilize drug-, small interfering RNA- and toxin-loaded MSNs [25]. DOPS was used to give the liposomes a negative charge, which is needed to coat the nanoparticles onto the positively charged microneedles. Our results show that the colloidal stability of OVA-loaded MSNs was improved after liposome fusion and the lipid

bilayer generated a negatively charged surface on LB-MSN-OVA. The LB-MSN-OVA were coated onto microneedles at pH 5.8 where more than 90% of the pyridine groups are positively charged [6]. Combined with the low ionic strength of the buffer, this allows for the binding of the negatively charged LB-MSN-OVA via electrostatic interactions. The presence of the lipid bilayer on the surface of MSNs was confirmed by cryoTEM and indicated by the change of surface charge (from +11 mV to -24.0 mV at pH7.4). The encapsulation efficiency of OVA was decreased by about 25% after the fusion of liposomes, which may be because the negatively charged lipid bilayer and OVA were competing with each other for the binding on the MSN surface and some of the OVA coated on the AEP-MSN surface may be replaced by the lipid bilayer. The release study showed that the coated lipid bilayer functioned as a gate and prolonged the release of the antigen, which could be important for the nanoparticles to remain their adjuvant effect [35].

The binding of LB-MSN-OVA on microneedles was visualized by both SEM and CLSM. The SEM images showed that after coating the microneedles with LB-MSN-OVA, the surface of the microneedles became rougher, but the sharpness of the microneedles was not affected. One major disadvantage of coated microneedles is the limited amount of materials that can be coated on microneedles because of the small surface area. The amount of LB-MSN-OVA coated on one microneedle array was 7.9 µg and was higher than that of inactivated polio virus (IPV) in a previous study (100 ng) [33]. Thus next to improving the immunogenicity of antigens, LB-MSN-OVA could also provide an effective way of increasing the antigen dose coated on microneedles. This may be because LB-MSN-OVA have a lower zeta potential than IPV under similar conditions (-16.8 mV vs -7.8 mV in 1 mM EDTA at pH 5.8). In our study the coated OVA loaded in LB-MSN-OVA is 1.5 µg on one microneedle array and is much higher than the amount of coated IPV [33] in a previous study. Other possibilities to increase the delivered amount of antigen are increasing the number of microneedle arrays used or increasing the number of needles on one array.

To effectively deliver antigens into the skin, next to efficient coating of the antigen on the microneedles, rapid dissolution from the microneedles once inserted into the skin, is critical. The pH-sensitive microneedles used in the present study were developed in our lab for the intradermal delivery of vaccines by coating antigens at slightly acidic pH and releasing them at physiological pH. CLSM images showed that the LB-MSN-OVA were successfully released into the holes made by the microneedles. The fluorescence from lipids and OVA was found to still co-localize with each other in the holes made by microneedles, indicating that the LB-MSN-OVA may be still intact after the release. This would be important for LB-MSN-OVA to remain their adjuvant effect [25].

Thus, the developed system combines the advantages of microneedles and nanoparticles. Microneedles allow non-invasive delivery of vaccines into skin and antigen-loaded nanoparticles have the potential to increase and modify the immune response against the antigen. In addition, by coating the nanoparticles onto the pH-sensitive pyridine-modified microneedles, the separate application of antigen after microneedle penetration is avoided. An important concern is the bio-distribution of MSNs after intradermal delivery. Studies have shown that intravenously injected MSNs were mainly excreted out of mice through urine and feces, indicating that MSNs are biodegradable [42] and other studies showed that MSNs can undergo hydrolysis to form non-toxic silica acid [43]. However, as deposition in the skin may alter the biodistribution and clearance of the MSNs, systematic studies need to be performed in order to assess the safety of these nanoparticles in animals and humans.

CONCLUSION

In conclusion, the LB-MSN-OVA coated microneedle arrays represent a novel intradermal antigen delivery system. The large pores of MSNs enabled the rapid encapsulation of OVA with a high loading capacity. The introduction of lipid bilayers significantly improved the colloidal stability of OVA-loaded AEP-MSNs and concomitantly reduced the premature release of OVA. In addition, it enabled the coating of the nanoparticles on the surface of pH-sensitive microneedle arrays. Application of LB-MSN-OVA coated microneedle arrays into human skin (*ex vivo*) resulted in the successful delivery of the OVA-loaded nanoparticles into the skin. The method is not restricted to the delivery of antigens, but may also be useful to deliver any compound that can be encapsulated in MSNs like (low-molecular-weight) drugs, RNA, DNA and proteins.

ACKNOWLEDGMENTS

REFERENCES

[1] Y.B. Deng, R. Mathaes, G. Winter, J. Engert, Encapsulation of antigen-loaded silica nanoparticles into microparticles for intradermal powder injection, Eur. J. Pharm. Sci. 63 (2014) 154-166.

[2] K.T. Mody, A. Popat, D. Mahony, A.S. Cavallaro, C. Yu, N. Mitter, Mesoporous silica nanoparticles as antigen carriers and adjuvants for vaccine delivery, Nanoscale 5 (2013) 5167-5179.

[3] Y.Z. Ma, W.Q. Tao, S.J. Krebs, W.F. Sutton, N.L. Haigwood, H.S. Gill, Vaccine delivery to the oral cavity using coated microneedles induces systemic and mucosal immunity, Pharm. Res. 31 (2014) 2393-2403.

[4] K. van der Maaden, W. Jiskoot, J. Bouwstra, Microneedle technologies for (trans)dermal drug and vaccine delivery, J. Control. Release 161 (2012) 645-655.

[5] S.M. Bal, B. Slutter, E. van Riet, A.C. Kruithof, Z. Ding, G.F.A. Kersten, W. Jiskoot, J.A. Bouwstra, Efficient induction of immune responses through intradermal vaccination with N-trimethyl chitosan containing antigen formulations, J. Control. Release 142 (2010) 374-383.

[6] K. van der Maaden, H. Yu, K. Sliedregt, R. Zwier, R. Leboux, M. Oguri, A. Kros, W. Jiskoot, J.A. Bouwstra, Nanolayered chemical modification of silicon surfaces with ionizable surface groups for pH-triggered protein adsorption and release: application to microneedles, J. Mater. Chem. B 1 (2013) 4466-4477.

[7] E. Larraneta, M.T.C. McCrudden, A.J. Courtenay, R.F. Donnelly, Microneedles: A new frontier in nanomedicine delivery, Pharm. Res. 33 (2016) 1055-1073.

[8] K. van der Maaden, K. Sliedregt, A. Kros, W. Jiskoot, J. Bouwstra, Fluorescent nanoparticle adhesion assay: a novel method for surface pK(a) determination of self-assembled monolayers on silicon surfaces, Langmuir 28 (2012) 3403-3411.

[9] K. van der Maaden, E.M. Varypataki, S. Romeijn, F. Ossendorp, W. Jiskoot, J. Bouwstra, Ovalbumin-coated pH-sensitive microneedle arrays effectively induce ovalbumin-specific antibody and T-cell responses in mice, Eur. J. Pharm. Biopharm. 88 (2014) 310-315.

[10] P.C. DeMuth, X.F. Su, R.E. Samuel, P.T. Hammond, D.J. Irvine, Nano-layered microneedles for transcutaneous delivery of polymer nanoparticles and plasmid DNA, Adv. Mater. 22 (2010) 4851-4856.

[11] S.A. Coulman, A. Anstey, C. Gateley, A. Morrissey, P. McLoughlin, C. Allender, J.C. Birchall, Microneedle mediated delivery of nanoparticles into human skin, Int. J. Pharm. 366 (2009) 190-200.

[12] M. Zaric, O. Lyubomska, C. Poux, M.L. Hanna, M.T. McCrudden, B. Malissen, R.J. Ingram, U.F. Power, C.J. Scott, R.F. Donnelly, A. Kissenpfennig, Dissolving microneedle delivery of nanoparticle-encapsulated antigen elicits efficient cross-priming and Th1 immune responses by murine langerhans cells, J. Invest. Dermatol. 135 (2015) 425-434.

[13] M. Zaric, O. Lyubomska, O. Touzelet, C. Poux, S. Al-Zahrani, F. Fay, L. Wallace, D. Terhorst, B. Malissen, S. Henri, U.F. Power, C.J. Scott, R.F. Donnelly, A. Kissenpfennig, Skin dendritic cell targeting via microneedle arrays laden with antigen-encapsulated poly-D,L-lactide-co-glycolide nanoparticles induces efficient antitumor and antiviral immune responses, ACS Nano 7 (2013) 2042-2055.

[14] P. Sahdev, L.J. Ochyl, J.J. Moon, Biomaterials for nanoparticle vaccine delivery systems, Pharm. Res. 31 (2014) 2563-2582.

[15] R. De Rose, A.N. Zelikin, A.P.R. Johnston, A. Sexton, S.F. Chong, C. Cortez, W. Mulholland, F. Caruso, S.J. Kent, Binding, internalization, and antigen presentation of vaccine-loaded nanoengineered capsules in blood, Adv. Mater. 20 (2008) 4698-4703.

[16] J.C. Aguilar, E.G. Rodriguez, Vaccine adjuvants revisited, Vaccine 25 (2007) 3752-3762.

[17] R.A. Rosalia, L.J. Cruz, S. van Duikeren, A.T. Tromp, A.L. Silva, W. Jiskoot, T. de Gruijl, C. Lowik, J. Oostendorp, S.H. van der Burg, F. Ossendorp, CD40-targeted dendritic cell delivery of PLGA-nanoparticle vaccines induce potent anti-tumor responses, Biomaterials 40 (2015) 88-97.

[18] D. Mahony, A.S. Cavallaro, F. Stahr, T.J. Mahony, S.Z. Qiao, N. Mitter, Mesoporous silica nanoparticles act as a self-adjuvant for ovalbumin model antigen in mice, Small 9 (2013) 3138-3146.

[19] F. Porta, G.E.M. Lamers, J. Morrhayim, A. Chatzopoulou, M. Schaaf, H. den Dulk, C. Backendorf, J.I. Zink, A. Kros, Folic acid-modified mesoporous silica nanoparticles for cellular and nuclear targeted drug delivery, Adv. Healthc. Mater. 2 (2013) 281-286.

[20] J. Tu, T. Wang, W. Shi, G. Wu, X. Tian, Y. Wang, D. Ge, L. Ren, Multifunctional ZnPc-loaded mesoporous silica nanoparticles for enhancement of photodynamic therapy efficacy by endolysosomal escape, Biomaterials 33 (2012) 7903-7914.

[21] S.R. Bhattarai, E. Muthuswamy, A. Wani, M. Brichacek, A.L. Castaneda, S.L. Brock, D. Oupicky, Enhanced gene and siRNA delivery by polycation-modified mesoporous silica nanoparticles loaded with chloroquine, Pharm. Res. 27 (2010) 2556-2568.

[22] S. Hudson, J. Cooney, E. Magner, Proteins in mesoporous silicates, Angew. Chem. Int. Ed. 47 (2008) 8582-8594.

[23] E.C. Dengler, J.W. Liu, A. Kerwin, S. Torres, C.M. Olcott, B.N. Bowman, L. Armijo, K. Gentry, J. Wilkerson, J. Wallace, X.M. Jiang, E.C. Carnes, C.J. Brinker, E.D. Milligan, Mesoporous silica-supported lipid bilayers (protocells) for DNA cargo delivery to the spinal cord, J. Control. Release 168 (2013) 209-224.

[24] K. Epler, D. Padilla, G. Phillips, P. Crowder, R. Castillo, D. Wilkinson, B. Wilkinson, C. Burgard, R. Kalinich, J. Townson, B. Chackerian, C. Willman, D. Peabody, W. Wharton, C.J. Brinker, C. Ashley, E. Carnes, Delivery of ricin toxin a-chain by peptide-targeted mesoporous silica nanoparticle-supported lipid bilayers, Adv. Healthc. Mater. 1 (2012) 348-353.

[25] C.E. Ashley, E.C. Carnes, G.K. Phillips, D. Padilla, P.N. Durfee, P.A. Brown, T.N. Hanna, J. Liu, B. Phillips, M.B. Carter, N.J. Carroll, X. Jiang, D.R. Dunphy, C.L. Willman, D.N. Petsev, D.G. Evans, A.N. Parikh, B. Chackerian, W. Wharton, D.S. Peabody, C.J. Brinker, The targeted delivery of multicomponent cargos to cancer cells by nanoporous particle-supported lipid bilayers, Nat. Mater. 10 (2011) 389-397.

[26] J. Tu, A.L. Boyle, H. Friedrich, P.H.H. Bomans, J. Bussmann, N.A.J.M. Sommerdijk, W. Jiskoot, A. Kros, Mesoporous silica nanoparticles with large pores for the encapsulation and release of proteins, ACS Appl. Mater. Interfaces 8 (2016) 32211-32219.

[27] S. Brunauer, P.H. Emmett, E. Teller, Adsorption of gases in multimolecular layers, J. Am. Chem. Soc. 60 (1938) 309-319.

[28] C. Keijzer, B. Slutter, R. van der Zee, W. Jiskoot, W. van Eden, F. Broere, PLGA, PLGA-TMC and TMC-TPP nanoparticles differentially modulate the outcome of nasal vaccination by inducing tolerance or enhancing humoral immunity, Plos One 6 (2011).

[29] Y. Han, J.Y. Ying, Generalized fluorocarbon-surfactant-mediated synthesis of nanoparticles with various mesoporous structures, Angew. Chem. Int. Ed. 44 (2005) 288-292.

[30] B.L. Zhang, Z. Luo, J.J. Liu, X.W. Ding, J.H. Li, K.Y. Cai, Cytochrome c end-capped mesoporous silica nanoparticles as redox-responsive drug delivery vehicles for liver tumor-targeted triplex therapy in vitro and in vivo, J. Control. Release 192 (2014) 192-201.

[31] J. Sun, H. Zhang, R. Tian, D. Ma, X. Bao, D.S. Su, H. Zou, Ultrafast enzyme immobilization over large-pore nanoscale mesoporous silica particles, Chem. Commun. 12 (2006) 1322-1324.

[32] I.I. Slowing, B.G. Trewyn, V.S.Y. Lin, Mesoporous silica nanoparticles for intracellular delivery of membrane-impermeable proteins, J. Am. Chem. Soc. 129 (2007) 8845-8849.

[33] K. van der Maaden, E. Sekerdag, P. Schipper, G. Kersten, W. Jiskoot, J. Bouwstra, Layer-by-layer assembly of inactivated poliovirus and N-trimethyl chitosan on pH-sensitive microneedles for dermal vaccination, Langmuir 31 (2015) 8654-8660.

[34] H. Vallhov, S. Gabrielsson, M. Stromme, A. Scheynius, A.E. Garcia-Bennett, Mesoporous silica particles induce size dependent effects on human dendritic cells, Nano. Lett.7 (2007) 3576-3582.

[35] B. Slutter, S. Bal, C. Keijzer, R. Mallants, N. Hagenaars, I. Que, E. Kaijzel, W. van Eden, P. Augustijns, C. Lowik, J. Bouwstra, F. Broere, W. Jiskoot, Nasal vaccination with N-trimethyl chitosan and PLGA based nanoparticles: nanoparticle characteristics determine quality and strength of the antibody response in mice against the encapsulated antigen, Vaccine 28 (2010) 6282-6291.

[36] N.Z. Knezevic, J.-O. Durand, Large pore mesoporous silica nanomaterials for application in delivery of biomolecules, Nanoscale 7 (2015) 2199-2209.

[37] H.K. Na, M.H. Kim, K. Park, S.R. Ryoo, K.E. Lee, H. Jeon, R. Ryoo, C. Hyeon, D.H. Min, Efficient functional delivery of siRNA using mesoporous silica nanoparticles with ultralarge pores, Small 8 (2012) 1752-1761.

[38] S.B. Hartono, N.T. Phuoc, M.H. Yu, Z.F. Jia, M.J. Monteiro, S.H. Qiao, C.Z. Yu, Functionalized large pore mesoporous silica nanoparticles for gene delivery featuring controlled release and co-delivery, J. Mater. Chem. B 2 (2014) 718-726.

[39] D.S. Lin, Q. Cheng, Q. Jiang, Y.Y. Huang, Z. Yang, S.C. Han, Y.N. Zhao, S.T. Guo, Z.C. Liang, A.J. Dong, Intracellular cleavable poly(2-dimethylaminoethyl methacrylate) functionalized mesoporous silica nanoparticles for efficient siRNA delivery in vitro and in vivo, Nanoscale 5 (2013) 4291-4301.

[40] J. Liu, X. Jiang, C. Ashley, C.J. Brinker, Electrostatically mediated liposome fusion and lipid exchange with a nanoparticle-supported bilayer for control of surface charge, drug containment, and delivery, J. Am. Chem. Soc. 131 (2009) 7567-7569.

[41] Y. Yang, W. Song, A. Wang, P. Zhu, J. Fei, J. Li, Lipid coated mesoporous silica nanoparticles as photosensitive drug carriers, Phys. Chem. Chem. Phys. 12 (2010) 4418-4422.

[42] J. Lu, M. Liong, Z. Li, J.I. Zink, F. Tamanoi, Biocompatibility,biodistribution, and drug-delivery efficiency of mesoporous silica nanoparticles for cancer therapy in animals, Small 6 (2010):1794-1805.

[43] Y. Chen, H. Chen, J. Shi, In vivo bio-safety evaluations and diagnostic/therapeutic applications of chemically designed mesoporous silica nanoparticles, Adv. Mater. 25 (2013) 3144-3176.

Supplementary Information
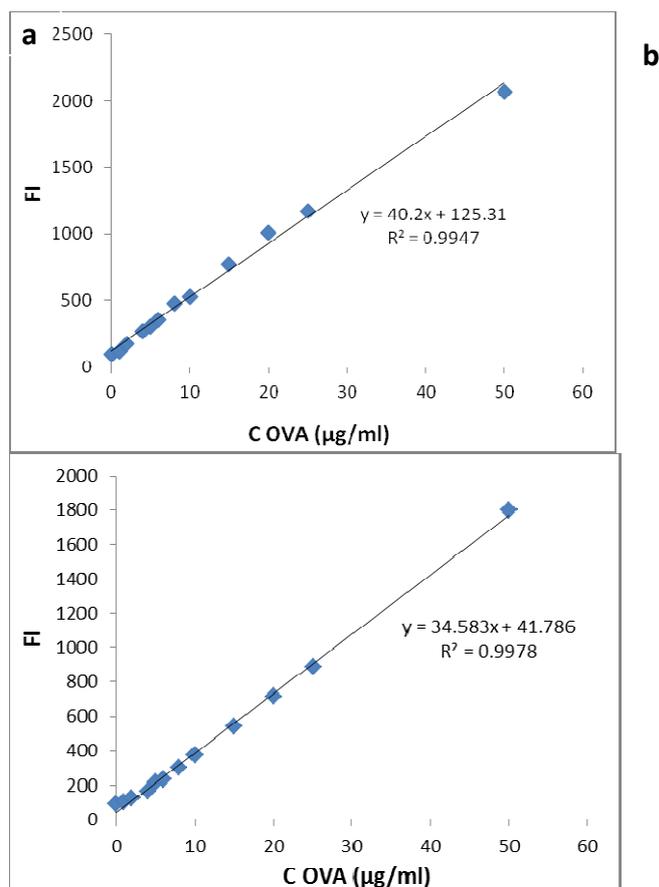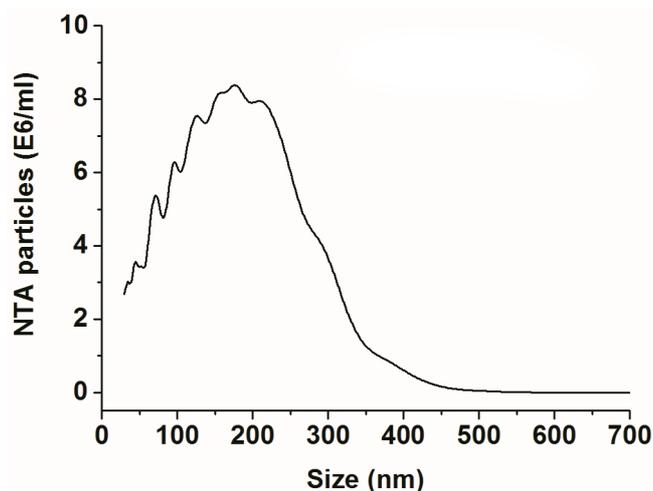

Supplementary Fig. 1 Calibration curves for quantification of OVA in 1 mM PB with a pH of 7.4 (a) and PBS with a pH of 7.4 (b). The intrinsic fluorescence intensity (FI) of OVA was measured with an excitation wavelength of 280 nm and an emission wavelength of 320 nm.
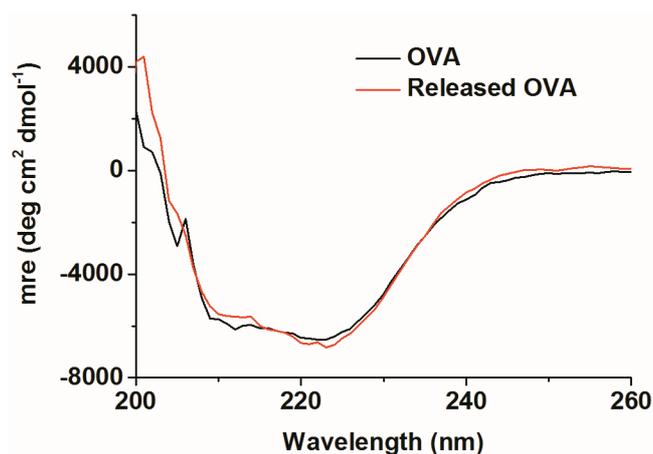
Supplementary Fig. 2 Far-UV CD spectra of free OVA and OVA released from AEP-MSNs in PBS, pH 7.4, 25 °C.

Supplementary Fig. 3 Size distribution of the LB-MSN-OVA determined by nanoparticle tracking analysis (NTA).

Supplementary Table 1. Stability of LB-MSN-OVA in cell culture medium (n=3).

Time (h)	Size (nm)	PDI	Zeta Potential (mv)	Released OVA (%)
0	632.5 ± 13.9	0.528 ± 0.031	-10.8 ± 0.6	
1	575.0 ± 18.3	0.535 ± 0.051	-11.7 ± 0.4	
2	536.5 ± 19.6	0.584 ± 0.057	-12.8 ± 0.5	
4	566.1 ± 64.5	0.485 ± 0.158	-13.3 ± 0.2	15.2 ± 0.6

Chapter 2

Chapter 3

Hollow microneedle-mediated intradermal delivery of model vaccine antigen-loaded PLGA nanoparticles elicits protective T cell-mediated immunity to an intracellular bacterium

Guangsheng Du [1±], Anne Marit de Groot [2±], Juha Mönkäre[1], Anouk C.M. Platteel[2], Femke Broere[2], Joke A. Bouwstra[1], Alice J.A.M. Sijts[2]*

[1]Division of BioTherapeutics, Leiden Academic Centre for Drug Research, Leiden University, Leiden, The Netherlands

[2]Department of Infectious Diseases and Immunology, Faculty of Veterinary Medicine, Utrecht University, Utrecht, The Netherlands

[±] equal contributions

Abstract

The skin is an attractive organ for immunization due to the presence of a large number of epidermal and dermal antigen-presenting cells. Hollow microneedles allow for precise and non-invasive intradermal delivery of vaccines. In this study, ovalbumin (OVA)-loaded poly(lactic-co-glycolic acid) (PLGA) nanoparticles with and without TLR3 agonist poly(I:C) were prepared and administered intradermally by hollow microneedles. The capacity of the PLGA nanoparticles to induce a cytotoxic T cell response, contributing to protection against intracellular pathogens, was examined. We show that a single injection of OVA-loaded PLGA nanoparticles, compared to soluble OVA, primed both adoptively transferred antigen-specific naïve transgenic $CD8^+$ and $CD4^+$ T cells with markedly high efficiency. Applying a triple immunization protocol, PLGA nanoparticles primed also endogenous OVA-specific $CD8^+$ T cells. Immune response, following immunization with in particular anionic PLGA nanoparticles co-encapsulated with OVA and poly(I:C), provided protection against a recombinant strain of the intracellular bacterium *Listeria monocytogenes*, secreting OVA. Taken together, we show that PLGA nanoparticle formulation is an excellent delivery system for protein antigen into the skin and that protective cellular immune responses can be induced using hollow microneedles for intradermal immunizations.

Keywords: protein vaccine, hollow microneedles, intradermal immunization, PLGA nanoparticles, cytotoxic T cell response

Hollow microneedle-mediated intradermal delivery of model vaccine antigen-loaded PLGA nanoparticles elicits protective T cell-mediated immunity to an intracellular bacterium

1. Introduction

The skin is an organ with many immune cells and is considered a potent organ for immunizations [1]. However, the challenge is to deliver high-molecular-weight antigens across the stratum corneum, which is the outermost layer of the skin and acts as an effective natural barrier for penetration of pathogens and allergens into the skin. One of the methods to circumvent the skin barrier is the use of microneedles. Microneedles are miniaturized needles that provide the possibility of minimally invasive vaccination in the dermis and epidermis of the skin. There are other benefits in using microneedles compared to traditional hypodermic needles, like possible painless vaccination, the requirement of less trained personnel and reduced contamination risk [2]. Nowadays a wide variety of these microneedles exist, including solid, coated, dissolving and hollow microneedles [3, 4].

Hollow microneedles have multiple benefits, for instance they can be used to inject a wide variety of fluids into the skin at different pressure-driven flow rates [3, 5, 6] and offer the highest precision in dose delivery among all microneedle types. Furthermore, they offer the possibility to screen formulations without time-consuming design and preparation of microneedles, as in case of coated and dissolving microneedles. Recently, hollow microneedles and an applicator for them were developed in our laboratory to inject formulations in precise manner into the skin. These microneedles were successfully used for formulations with inactivated polio virus vaccine in rats resulting in effective humoral immune responses [7-9]. However, whether hollow microneedle-mediated delivery may also induce T cell responses towards vaccine antigens is presently unclear.

Cytotoxic CD8$^+$ T cells play an important role in cellular immune protection against intracellular pathogens or tumor growth. To induce such CD8$^+$ T cell responses, an antigen needs to be processed in the cell and presented by MHC-I molecules on professional antigen-presenting cells (pAPC) to the immune system. Delivery of vaccine protein antigens over the cellular membrane can be achieved using delivery systems and over the past decades different types of them, such as polymeric nanoparticles, emulsions and lipid-based nanoparticles have been developed [10-12]. Nano-encapsulation of antigens has several advantages, such as stabilization of antigens *in vivo*, enhancement of the uptake by pAPC and also reduction of antigen release into systemic circulation [4, 13]. The immune outcome can be potentially shaped by using nanoparticles with difference size [14] and surface charge [15], and by co-encapsulating antigen and adjuvant into the nanoparticles [16, 17].

For the production of polymeric nanoparticles, poly(lactic-*co*-glycolic acid) (PLGA) is the most commonly used polymer, because of its superior biocompatibility and biodegradability [18-20]. Previous studies have shown that model antigen- and adjuvant-loaded PLGA nanoparticles used for vaccination were able to improve the induction of cell-mediated immune response in mice [17, 21-23]. However, relatively little is known about how encapsulation in PLGA nanoparticles modifies T cell responses to antigen/adjuvant combinations that are delivered intradermally by microneedles. One recent study reported that PLGA nanoparticles, delivered intradermally using dissolving microneedles arrays [24], induced cellular immune responses and protection against viral infection and tumor growth.

In this study, nanoparticles were prepared and characterized in terms of size, surface charge and antigen/adjuvant release profiles. We investigated the ability of hollow microneedle-delivered protein antigens, encapsulated in either anionic or cationic PLGA nanoparticles with and without co-encapsulated TLR3 agonist poly(I:C) to induce a protective cellular immune response towards an intracellular pathogen in a mouse model.

2. Materials and Methods

2.1. Materials

PLGA (acid terminated, lactide glycolide 50:50, Mw 24.000 - 38.000), polyethylenimine (PEI, linear, average M_n 10,000), Roswell Park Memorial Institute medium (RPMI) and Fetal bovine serum (FBS) were purchased from Sigma-Aldrich (Zwijndrecht, The Netherlands). PVA 4-88 (31 kDa) was obtained from Fluka (Steinheim, Germany). Endotoxin-free ovalbumin (OVA), polyinosinic-polycytidylic acid (poly(I:C)) (low molecular weight) and its rhodamine-labelled version were obtained from Invivogen (Toulouse, France). Alexa647 labelled OVA (OVA-Alexa647) was ordered from Thermo-Fischer Scientific (Waltham, MA). Dimethylsulfoxide (DMSO) was obtained from Biosolve BV (Valkenswaard, The Netherlands). Sodium dodecyl sulfate (SDS) was obtained from Merck Millipore (Hohenbrunn, Germany). Ammonium-Chloride-Potassium (ACK) lysis buffer (150 mM NH_4CL, 1 mM $NaHCO_3$; pH 7.40) and 1 mM phosphate buffer (PB; pH 7.4) were prepared in the lab. Milli-Q water (18.2 MΩ/cm, Millipore Co., USA) was used for the preparation of solutions. Sterile phosphate buffered saline (PBS) was obtained from Braun (Oss, The Netherlands). All other chemicals used are of analytical grade.

Purification antibodies used for DynaBeads® selection were all made in house and included the following antibody clones: αCD11b (clone M1/70), αMHC-II (M5/114), αB220 (RA3-6B2), αCD4 (GK1.4), αCD8 (YTS169) and αCD25 (PC61). Purification antibodies for sorting via flow cytometry were αCD8-APC (53-6.7; eBioscience), CD44-FITC (IM7; eBioscience) and CD62L-PE (MEL-14; BD Bioscience) using a BD influx (BD Biosciences). For the detection of the adoptively transferred T cells the antibodies αCD45.2-PerCPCy5.5 (104; eBioscience), αCD4-PE (GK1.5; eBioscience) and αCD8-APC (53-6.7; BD Bioscience) were used. Detection of the endogenous T cells was measured using the antibodies αCD8-APC (53-6.7; eBioscience), αCD4-eFluor450 (GK1.5; eBioscience), αCD62L-Horizon B510, αCD44-FITC (IM7; eBioscience), αCD16/CD32-unstained (2.4G2; made in house) and αIFN-γ-PE (XMG1.2; eBioscience).

2.2. Preparation of PLGA nanoparticles

OVA-loaded PLGA nanoparticles were prepared by double emulsion with solvent evaporation method as previously reported with modifications [25]. Briefly, 75 µl OVA (20 mg/ml) in PBS was dispersed in 1 ml PLGA (25 mg/ml) in ethyl acetate by a Branson sonifier 250 (Danbury, USA) for 15 s with a power of 20 W. To prepare anionic OVA-loaded PLGA nanoparticles (anPLGA-OVA), the obtained water-in-oil emulsion was emulsified with 2 ml 2% (w/v) PVA with the sonifier (15 s, 20 W) to get a water-in-oil-in-water double emulsion. In case of cationic OVA-loaded PLGA nanoparticles (catPLGA-OVA), the single emulsion was emulsified with 2 ml 2% (w/v) PVA and 4% (w/v) PEI solution. The double emulsion was added dropwise into 25 ml 0.3% (w/v) PVA (40 °C) under stirring. The ethyl acetate was evaporated by a rotary evaporator (Buchi rotavapor R210, Switzerland) for 3 h (150 mbar, 40 °C). The nanoparticle suspension was centrifugated (Avanti™ J-20XP centrifuge, Beckman Coulter, Brea, CA) at 35000 g for 10 min, washed twice with 1 mM PB to remove the excess OVA and PVA, and dried in a Alpha1-2 freeze dryer (Osterode, Germany, -49 °C, 90 mbar) overnight. To prepare OVA and poly(I:C) co-encapsulated PLGA nanoparticles (anPLGA-OVA-PIC), 18.75 µl OVA (40 mg/ml) and 75 µl poly(I:C) (46.7 mg/ml, including 0.03% fluorescently labelled equivalent) were emulsified with 1 ml PLGA (25 mg/ml) in ethyl acetate to obtain the water-in-oil emulsion. The remaining of the procedure was identical to that of anPLGA-OVA. The obtained nanoparticles were stored at 4 °C for analysis

Hollow microneedle-mediated intradermal delivery of model vaccine antigen-loaded PLGA nanoparticles elicits protective T cell-mediated immunity to an intracellular bacterium

and further use. To prepare the PLGA nanoparticles for release study, 10% OVA-Alexa647 was used during the preparation.

2.3. Characterization of PLGA nanoparticles

The size and polydispersity index (PDI) of nanoparticles were measured by dynamic light scattering and the zeta potential of nanoparticles was measured by laser doppler velocimetry using a Nano ZS® zetasizer (Malvern Instruments, Worcestershire, U.K.). The samples were diluted with 1 mM PB buffer to a nanoparticle concentration of 25 µg/ml before each measurement. To determine the loading efficiency of OVA and poly(I:C) in PLGA nanoparticles, approximately 1 mg of nanoparticles were dissolved in a mixture of 15% (v/v) DMSO and 85% (v/v) 0.05 M NaOH and 0.5% SDS. The amount of OVA was determined by MicroBCA method following the manufacturer's instructions. The amount of poly(I:C) was quantified by the fluorescence intensity of rhodamine labelled poly(I:C) (λ_{ex} 545 nm/ λ_{em} 576 nm). The encapsulation efficiency (EE) and loading capacity (LC) of OVA and poly(I:C) in the nanoparticles were calculated as below:

$$ EE \% = \frac{M_{loaded\ OVA\ /poly(I:C)}}{M_{totoal\ ova\ /poly(I:C)}} \times 100 \% \qquad (1) $$

$$ LC \% = \frac{M_{loaded\ OVA\ /\ poly(I:C)}}{M_{nanoparticles}} \times 100 \% \qquad (2) $$

Where $M_{loaded\ OVA/poly(I:C)}$ represents the mass of loaded OVA or poly(I:C), $M_{total\ OVA/poly\ (I:C)}$ is the total amount of OVA or poly(I:C) added to the formulation and $M_{nanoparticles}$ is the weight of nanoparticles.

2.4. Release of OVA and poly(I:C) from PLGA nanoparticles

Nanoparticles were prepared in triplicate as described above. To study the release of OVA and poly(I:C) from PLGA nanoparticles, 3 mg anPLGA-OVA, catPLGA-OVA or anPLGA-OVA-PIC were dispered into 1 ml RPMI supplemented with 10% FBS and incubated at 37 °C with a shaking speed of 350 rpm. At different time points, the suspensions were centrifuged (9000 g, 5 min) with Sigma 1-15 centrifuge (Osterode, Germany). A release sample of 600 µl of the supernatant was collected and replaced by fresh medium. The released amount of OVA and poly(I:C) was determined by fluoresence intensity of OVA-Alexa647 (λ_{ex} 647 nm/λ_{em} 671 nm) and rhodamine labelled poly(I:C) (λ_{ex} 545 nm/λ_{em} 576 nm), respectively.

2.5. Mice and intradermal immunizations

8-18 week old male B6.SJL/ptprcaPep3b/BoyCrl (B6.SJL) wild type mice and 8-30 week old transgenic (tg) mice that express pOVA$_{323-339}$-specific T cell receptor (OT-II mice) or pOVA$_{257-264}$-specific T cell receptor (OT-I mice) were initially obtained from Charles River and were bred in house. Abdomen of mice were shaved prior to immunization on both flanks and intradermal immunization was done using a single hollow microneedle as reported previously [8, 9]. The hollow microneedle was inserted into the abdomen of mice using an applicator controlling precisely the depth, volume and rate of the injections. The injections were performed at a depth of 120 µm, a volume of 40 µl in 3 injections (2 on right flank, 1 on left flank) and with a rate of 10 µl/min. In several mice, the depth was increased up to 200 µm if leakage was observed in the beginning of injection. In all experiments a total of 5 µg OVA or 50 µg OVA peptides was injected per immunization. In case of anPLGA-OVA-PIC, the dose of poly(I:C) was also 5 µg. Ethical approval was given by the Animal Ethics Committee from Utrecht University, The Netherlands.

2.6. Adoptive transfer of OVA specific tg T Cells

OVA-specific T cell transferred mice were obtained by injecting OT-I CD8$^+$ and OT-II CD4$^+$ T cells into wildtype B6.SJL mice. In order to obtain OT-I and OT-II cells, spleens were isolated from OT-I and OT-II mice and erythrocyte-depleted splenocytes were obtained as follows. Single cell suspensions were prepared by passage over a 70 µM cell strainer after homogenizing the spleens with a syringe plunger, in RPMI 1640 GlutaMAX supplemented with 8.5% fetal calf serum (Bodinco), 30 µM 2-mercaptoethanol and penicillin/streptomycin (complete RPMI medium). The erythrocytes were depleted by lysis with ACK lysis buffer. Transgenic naïve CD4$^+$ (OT-II) cells and transgenic CD8$^+$ (OT-I) cells were isolated from splenocytes by negative selection using Magnetic DynaBeads® (Thermo Fisher Scientific, Waltham, MA). Antibodies used were αCD11b, αMHC-II, αB220 and either αCD4 for CD8 (OT-I) T cell purification or αCD8 and αCD25 for naïve CD4$^+$ (OT-II) T cell purification. After negative selection by magnetic beads, a purity around 70% was achieved for naïve tg CD4$^+$ (OT-II) T cells. An additional sorting was necessary to separate naïve from non-naïve tg CD8$^+$ (OT-I) T cells. After selection on CD8$^+$, CD44^{low} and CD62L^{high} using a BD influx, 100% purity of naïve tg CD8$^+$ (OT-I) T cells was obtained. Naïve tg CD4$^+$ (OT-II) T cells were stained with carboxy-fluorescein succinimidyl ester (CFSE; 0.5 µM, Invitrogen) and naïve tg CD8$^+$ (OT-I) T cells were stained with Cell trace violet (CTV; 5 µM, Invitrogen) for 10 min at 37°C. A total of 2×10^6 CFSE-labelled naïve tg CD4$^+$ T cells and 1×10^6 CTV-labelled naïve tg CD8$^+$ cells were injected into the tail vein of recipient mice, one day before immunization to obtain OVA-specific T cell transferred mice.

2.7. *In vivo* proliferation of adoptively transferred T cells

OVA-specific T cell transferred mice were immunized with OVA, anPLGA-OVA and catPLGA-OVA at day 0. PBS and OVA peptide immunizations were used as negative and positive control, respectively. Proliferation of tg T cells was studied at day 3, 5 and 7. 2.5×10^6 erythrocyte depleted splenocytes or draining (inguinal) lymph node cells were stained with αCD45.2, αCD4 and αCD8 and transferred cells were measured as a percentage of CD45.2$^+$ and either CD8$^+$ or CD4$^+$ cells of total cells using a FACSCanto II (BD Biosciences) and FlowJo (TriStar) analysis software. Percentages of fully *proliferated* (> 6 division) transferred cells were measured by similar antibody staining, but as CD45.2$^+$ and either CTV$^-$ CD4$^+$ and CFSE^{low} or as CFSE$^-$CD8$^+$ and CTV^{low}, all after gating on live cells on FSC-A/SSC-A and single cells in FSC-A/FSC-H.

2.8. Endogenous CD4$^+$ and CD8$^+$ T cell responses

B6.SJL mice were immunized with OVA, OVA+poly(I:C) (OVA+PIC), anPLGA-OVA, catPLGA-OVA or anPLGA-OVA-PIC at day 0, 3, 6 and T cell responses were analyzed at day 13. The endogenous CD4$^+$ T cell response was measured by ^{3}H thymidine incorporation. For this 0.2×10^6 erythrocyte-depleted splenocytes or inguinal lymph node cells were plated in complete RPMI medium in a 96 well round bottom plate for 72 h with or without 10 µg/mL OVA Endo-Fit (Worthigton) or ConA, at 37 °C in a humidified incubator. After 72 h, ^{3}H-Thymidine (0.4 µCi/well; Amersham Biosciences Europe GmbH) was added for an additional 18 h and incorporation into DNA was measured by liquid scintillation counting (Microbeta, Perkin-Elmer Inc.).

CD8$^+$ T cell activation was measured using intracellular IFN-γ staining as described previously [26]. In short, 2.5×10^6 erythrocyte-depleted splenocytes were incubated in complete RPMI medium with 1 µg/ml pOVA$_{257-264}$ (Genscript) or complete RPMI medium with 10 µM monensin (eBioscience) for 6 h at 37 °C in 6% humidified incubator. Cells were

stained with either αCD8, αCD4, αCD62L or αCD44 in the presence of αCD16/CD32 to block Fc-receptors. Next they were fixed with 2% paraformaldehyde and stained with αIFN-γ antibody in the presence of 0.05% saponin. Samples were measured on a FACSCanto II (BD Biosciences) and analyzed using FlowJo software (Tree Star).

2.9. CFU counts in bacterial challenge study

B6.SJL mice were immunized with OVA, OVA+PIC, anPLGA-OVA, catPLGA-OVA or anPLGA-OVA-PIC at day 0, 3 and 6. Mice were challenged with recombinant *Listeria monocytogenes* secreting OVA (rLM-OVA) 21 days after final immunization. rLM-OVA [27, 28] were cultured in Brain Hart Infusion broth (BHI; Sigma-Aldrich) with 5 µg/mL erythromycin and to challenge the mice 100.000 CFU bacteria from a LOG-phase culture were injected in 200 µl/mouse in the tail vein. Mice immunized with 10.000 CFU rLM-OVA at day 6 were used as positive control and unimmunized mice served as negative control. To study the elimination of bacteria, three days after challenge spleens were isolated and single cell suspensions were made in RPMI medium. Serial dilutions were plated on BHI agar plates and CFU counts were determined after approximately 36 h in a 37 °C incubator. The remaining mice were sacrificed 5 days after the challenge to study the $CD4^+$ and $CD8^+$ T cell responses. The specific T cell response was determined in spleen using intracellular IFN-γ staining method as described in section 2.8.. To determine the memory phenotype of the $CD8^+$ T cells, CD62L and CD44 antibodies were used. Firstly, in the gate of the total $CD8^+$ T cells, three different populations were gated (**Supplement Figure 1B;** solid lines). $CD44^-$ were considered naïve T cells, $CD44^+CD62L^+$ are T central memory cells and $CD44^+CD62L^-$ are T effector and T effector memory cells. Secondly, in order to determine the antigen specific memory phenotype, the gates that were set on all $CD8^+$ T cells were copied in the $CD8^+IFN-γ^+$ population.

2.10. Statistics

Statistical significance was determined using Krukis-Wallis and multiple comparison/post hoc analysis was done with Dunns correction, *=p<0.05, **=p<0.01, ***=p<0.001.

3. Results

3.1. Preparation and characterization of PLGA nanoparticles

The physicochemical characteristics of PLGA nanoparticles are shown in **Table 1.** All types of PLGA nanoparticles had a size of approximately 150 nm with a low PDI ranging from 0.032 to 0.100. AnPLGA-OVA had a negative surface charge with a zeta potential of approximately -18 mV and catPLGA-OVA possessed a positive surface charge with an opposite zeta potential around +10 mV. The EE% of OVA was around 50% in both anPLGA-OVA and anPLGA-OVA-PIC, and catPLGA-OVA showed a significantly higher EE% of 87%. CatPLGA-OVA had also a higher LC% (10.4%) of OVA than anPLGA-OVA (6.6%) and anPLGA-OVA-PIC (2.8%). The ratio between the initial amount of OVA and poly(I:C) in the formulations during the preparation procedure was adjusted in order to prepare anPLGA-OVA-PIC with similar LC% of OVA (2.8%) and poly(I:C) (2.7%).

**Table 1: Physicochemical characteristics of PLGA nanoparticles**

Nanoparticles	Size (nm)	PDI	ZP (mV)	EE%		LC%	
				OVA	Poly(I:C)	OVA	Poly(I:C)
anPLGA-OVA	155.0±6.2	0.064±0.010	-18.2±1.7	54.8±1.0	-	6.6±0.1	-
catPLGA-OVA	147.3±2.1	0.100±0.029	9.9±0.5	87.0±4.8	-	10.4±0.6	-
anPLGA-OVA-PIC	148.4±8.4	0.032±0.007	-17.4±0.8	47.2±16.2	9.6±2.8	2.8±1.0	2.7±0.8

The formulations are characterized in terms of size (diameter) and polydisperse index (PDI), zeta potential (ZP), encapsulation efficiency (EE) and loading capacity (LC) of OVA and poly(I:C). The EE% of OVA or poly(I:C) was defined as the percentage of encapsulated amount of OVA or poly(I:C) compared to the added amount of OVA or poly(I:C). The LC% of OVA or poly(I:C) was defined as the percentage of encapsulated amount of OVA or poly(I:C) compared to the amount of nanoparticles. AnPLGA-OVA: anionic OVA-loaded PLGA nanoparticles. CatPLGA-OVA: catonic OVA-loaded PLGA nanoparticles. AnPLGA-OVA-PIC: OVA and poly(I:C) co-encapsulated anionic PLGA nanoparticles.

3.2. Release of OVA and poly(I:C) from PLGA nanoparticles

Release of OVA and poly(I:C) from PLGA nanoparticles was measured *in vitro* in culture medium containing serum (**Fig. 1**). The developed nanoparticles showed a burst release of OVA within the first day, followed by a slow release. At day 30 around 49%, 22% and 26% OVA were released from anPLGA-OVA, catPLGA-OVA and anPLGA-OVA-PIC, respectively. The release of poly(I:C) followed the trend of OVA in anPLGA-OVA-PIC. At day 30, around 42% poly(I:C) was released. Thus, all of the PLGA nanoparticles released at most half of their content within one month.

Hollow microneedle-mediated intradermal delivery of model vaccine antigen-loaded PLGA nanoparticles elicits protective T cell-mediated immunity to an intracellular bacterium
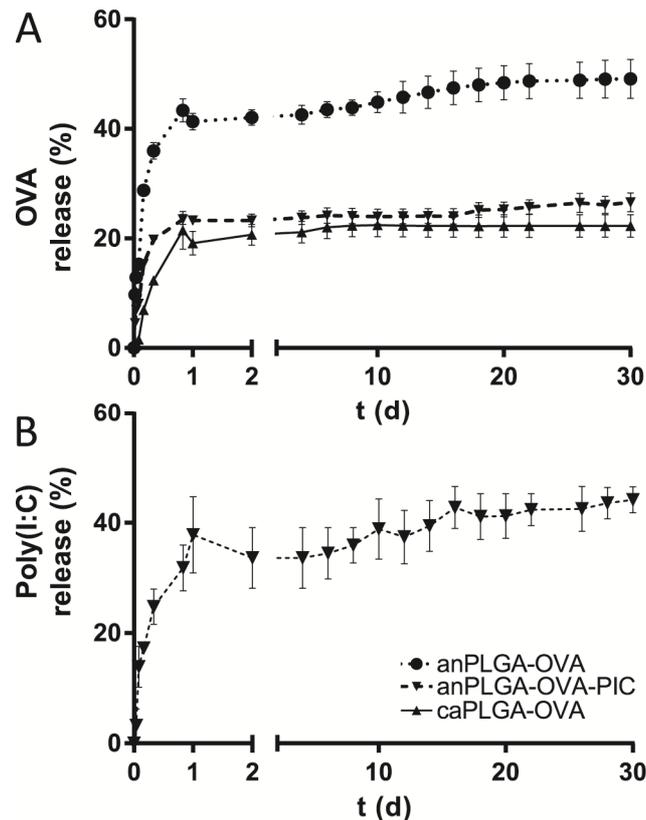

Figure 1. Release of OVA and poly(I:C) from PLGA nanoparticles**.** PLGA nanoparticles were dispersed into culture medium containing serum and incubated at 37 ℃. At different time points, the release sample was collected to determine the release amount of OVA (A) and poly(I:C) (B). Per time point 3 independent measurements were performed (mean ± SEM, n=3)

3.3. OVA-loaded PLGA nanoparticles enhanced antigen-induced activation of tg T helper cells and enabled priming of tg cytotoxic T cells after intradermal immunization using a hollow microneedle

To determine the induction of a cellular immune response towards a protein antigen that is delivered via hollow microneedles, we first examined the ability of a protein antigen to activate transgenic (tg) T cells that were adoptively transferred (**Fig. 2A**). Naïve OVA specific $CD4^+$ and $CD8^+$ T cells were isolated from spleens of OT-II and OT-I mice, expressing a tg T Cell Receptor specific for the $CD4^+$ and $CD8^+$ T cell epitopes ($OVA_{323-339}$ and $OVA_{257-264}$) of the model antigen OVA, respectively [29, 30]. After staining with cell trace dyes, these cells were mixed and transferred into congenic recipient mice, allowing the distinction between host and donor T cells in flow cytometry, based on expression of the congenic marker (**Fig. 2A**). One day later the recipient mice were immunized intradermally, using a hollow microneedle, with full length OVA protein or with the OVA epitopes (pOVA). These epitopes do not require any antigen processing in order to activate tg T cells and served as a positive control. We first determined if $CD4^+$ T helper cells were activated in the present study. Tg $CD4^+$ T cells were detected in flow cytometry as $CD4^+$ $CD45.2^+$ T cells within the lymphocyte gate in either draining inguinal lymph nodes (dLN) or in the spleens. In OVA protein-immunized mice, a small increase in numbers of tg $CD4^+$ T cells compared to PBS group was found in the dLN after immunization (**Fig. 2B**). Minimal systemic responses were measured in the spleen (**Fig. 2C**). Besides, minimal numbers of transferred $CD4^+$ T cells activated by OVA protein were fully proliferated (**Fig. 2D-F**; depicted by more than 6 dilutions of cell trace dye). Numbers of tg $CD4^+$ T cells were higher than PBS group in both

dLN and spleen in mice immunized with peptides (**Fig. 2B**). OVA peptides showed a high proliferation rate of the tg CD4$^+$ T cells at day 5, while at day 7 the numbers of fully proliferated cells dropped (**Fig. 2E-F**).
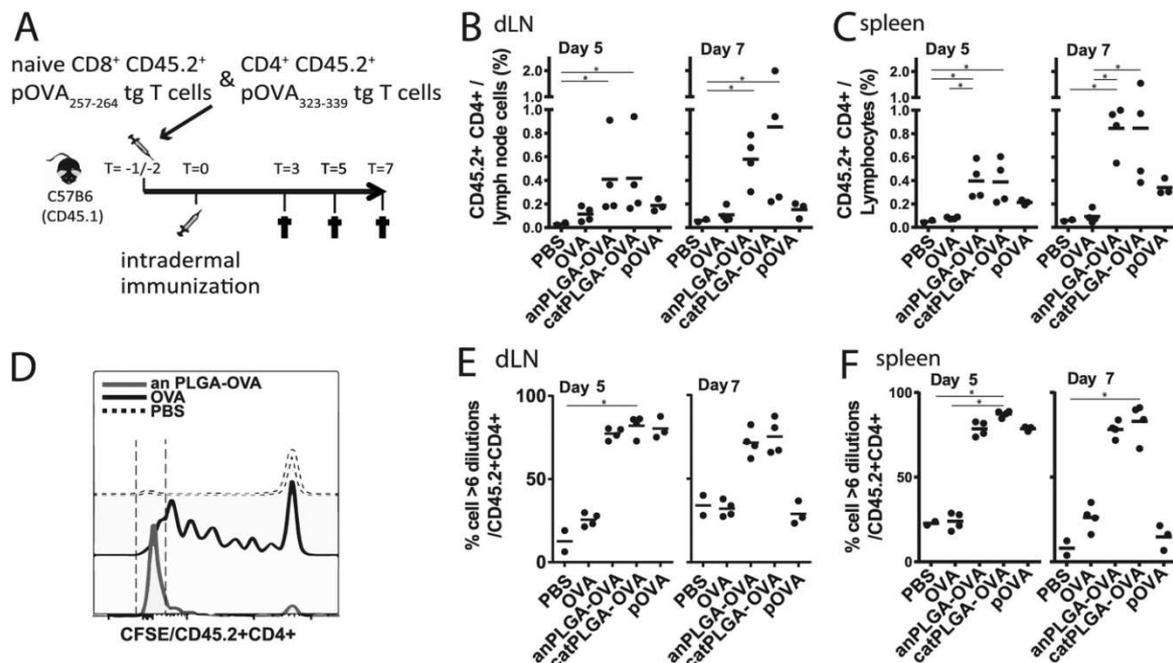
Figure 2. Encapsulation of OVA by PLGA nanoparticles enhances activation of tg CD4$^+$ T cells after intradermal immunization using hollow microneedle.
(A) Experimental design; naïve CD8$^+$ tg T cells specific for OVA$_{257-264}$ were isolated from spleens of OT-I mice and stained with Cell Trace Violet. CD4$^+$ tg T cells specific for OVA$_{323-339}$ were isolated from spleens of OT-II mice and stained with Carboxyfluorescein succinimidyl ester (CFSE). From both cell types 1×10^6 cells were injected in tail vein of B6.SJL mice 1 or 2 days before intradermal immunization. T cell responses were analyzed on day 3, 5 and 7. (B-F) CD4$^+$ T cell response of tg transferred T cells. (B-C) Amount of transferred tg T cells as a percentage of CD45.2$^+$CD4$^+$ cells in either dLN cells (B) or lymphocyte gate of splenocytes (C). (D) Indication of fully proliferated (>6 dilutions) cells in the CFSE window of CTV$^-$ / CD45.2$^+$CD4$^+$ / lymphocyte gate. (E-F) Percentage of cells that are CD45.2$^+$CD4$^+$ and divided more than 6 times as measured by CFSE intensity on day 5 or 7 in either dLN (E) or spleen (F) after intradermal immunization via hollow microneedles with the formulations indicated on X-axes. Graphs are representative for 1 of total 2 independent experiments. Per experiment the number of mice used is n=4 for OVA, anPLGA-OVA and catPLGA immunization groups, n=3 for pOVA immunization groups, and n=2 for PBS immunization group (as depicted by the amount of dots in the graph). Statistical significance was determined using Krukis-Wallis and multiple comparison/post hoc analysis was done comparing immunization strategies versus PBS or OVA immunization with Dunns correction, *=p<0.05.

We then determined whether OVA encapsulation in PLGA nanoparticles could enhance OVA-specific tg CD4$^+$ T cell responses. When mice were immunized with OVA-loaded anPLGA-OVA and catPLGA-OVA, we detected higher numbers of OVA-specific tg CD4$^+$ T cells than OVA group in dLN and spleen, both at day 5 and 7 post-immunization (**Fig. 2B-C**). Total numbers of tg CD4$^+$ T cells retrieved from PLGA-OVA nanoparticle immunized mice were also much higher than that in mice immunized with OVA peptides (**Fig. 2B-C**). Over 95% of these cells were fully proliferated in anPLGA-OVA and catPLGA-OVA groups, while OVA induced only slightly more fully proliferated cells than PBS locally on day 5 (**Fig. 2E**)

and systemically (**Fig. 2F**) on day 7. No differences were observed between responses detected against anPLGA-OVA and catPLGA-OVA. Taken together, we show that encapsulation in PLGA nanoparticles enhanced the activation of tg T helper cells by OVA after intradermal immunization using hollow microneedles.

Next, it was determined if the followed immunization strategy also induced a cytotoxic cellular immune response. Activation and proliferation of CD8^{+} tg T cells was measured in the experimental setup as shown in **Fig. 2A**. As expected, no increase in the numbers of tg CD8^{+} T cells was detected in either dLN or spleen at day 3, 5 or 7 after immunization with soluble OVA protein (**Fig. 3A-B**). On day 3, immunization with OVA had induced some T cell proliferation, as shown by dilution of cell trace dye (**Fig. 3C-D**), although this proliferation did not lead to a significant increase in tg CD8^{+} T cell numbers (**Fig. 3A-B**) as compared to PBS group. In contrast, immunization with OVA-loaded PLGA nanoparticles induced a marked increase in tg CD8^{+} T cell numbers in both dLN and spleen, as detected at both days 5 and 7 (**Fig. 3A-B**). Most of these cells were fully proliferated and there was no difference observed between responses induced by anPLGA-OVA and catPLGA-OVA (**Fig. 3C-D**). Immunization with OVA peptides induced a strong systemic tg CD8^{+} T cell response at day 5, but in contrast to nanoparticle-immunization, this response decreased significantly at day 7 (**Fig. 3A-B**). This was probably due to differing kinetics of T cell responses triggered by precise T cell epitopes, compared to full length OVA, which requires prior antigen processing. In conclusion, our data indicate that encapsulation of OVA in PLGA nanoparticles enables OVA to trigger CD8^{+} tg T cell responses upon hollow microneedle-mediated intradermal delivery.
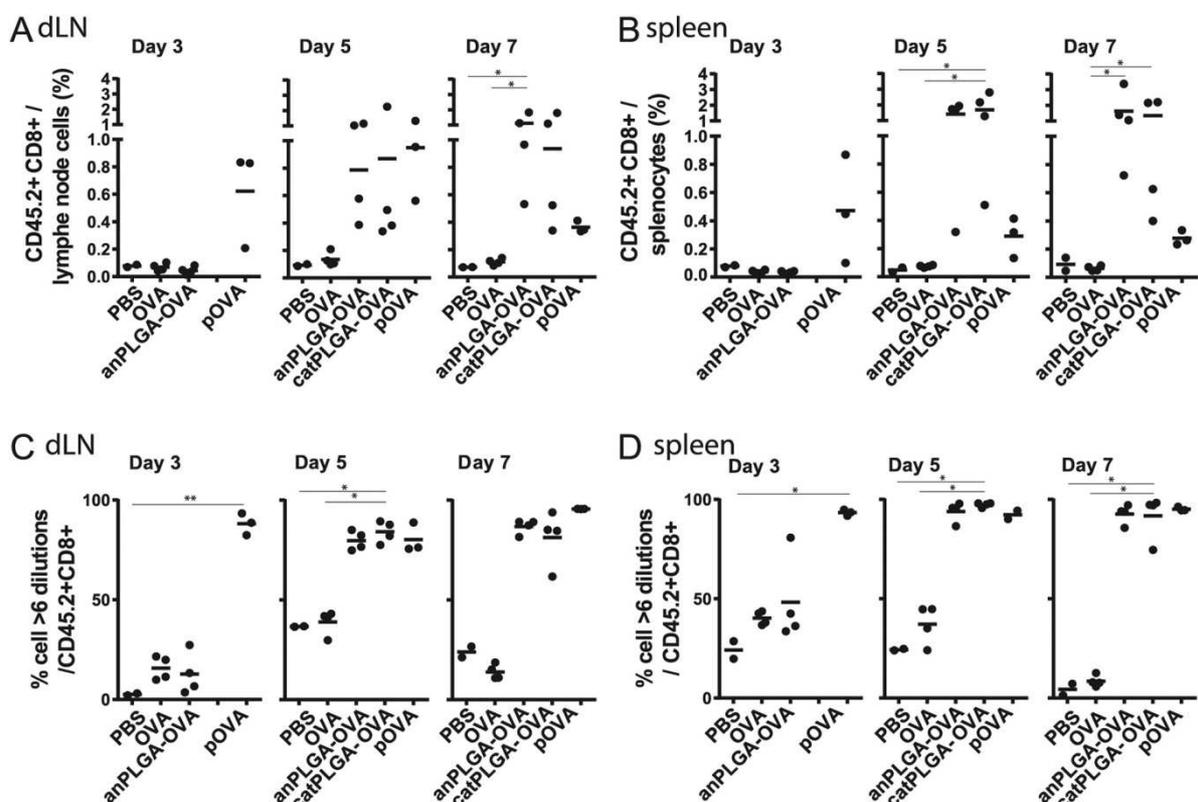

Figure 3. Encapsulation of OVA by PLGA nanoparticles enabled activation of tg CD8^{+} T cells after intradermal immunization using hollow microneedle. CD8^{+} T cell response of tg transferred T cells. (A-B) Amount of transferred tg T cells as a percentage of

CD45.2$^+$CD8$^+$ cells in either dLN cells (A) or lymphocyte gate of splenocytes (B). (C-D) Percentage of cells that are CD45.2$^+$CD8$^+$ and divided more than 6 times as measured by Cell Trace Violet intensity on day 3, 5 or 7 in either dLN (C) or spleen (D) after intradermal immunization via hollow microneedles with the formulations indicated on X-axes. Graphs are representative for 1 of total 2 independent experiments. Per experiment the number of mice used is n=4 for OVA, anPLGA-OVA and catPLGA immunization groups, n=3 for pOVA immunization groups and n=2 for PBS immunization group (as depicted by the amount of dots in the graph). Statistical significance was determined using Krukis-Wallis and multiple comparison/post hoc analysis was done comparing immunization strategies versus PBS immunization with Dunns correction, *=p<0.05.

3.4. OVA primed both endogenous CD4$^+$ and CD8$^+$ T cell responses in immunized hosts when particulated in PLGA nanoparticles or adjuvanted with TLR3 agonist

Having shown that hollow microneedle-mediated immunization with OVA-loaded PLGA nanoparticles activates adoptively transferred tg T cells (**Fig. 2-3**), we next examined whether this strategy also primes endogenous T cell responses in immunized hosts. To this end, wild type mice were immunized at day 0, 3 and 6 with OVA, OVA+PIC, anPLGA-OVA, catPLGA-OVA or anPLGA-OVA-PIC (**Table 1; Fig. 4A**).
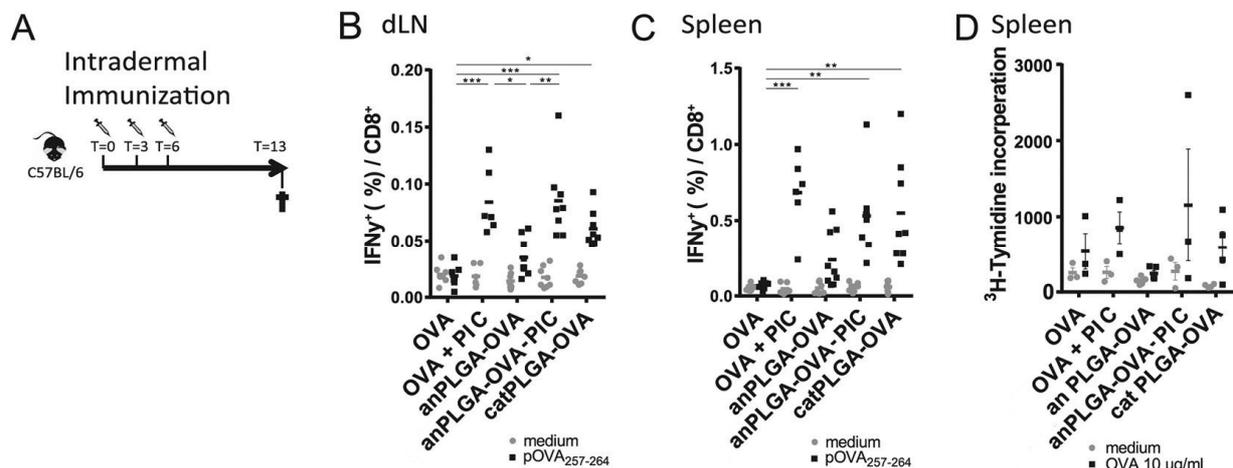
Figure 4. Specific endogenous T cell responses induced by OVA when particulated in anionic, cationic PLGA nanoparticles or when adjuvanted with TLR3 agonist.
(A) Schematic overview of immunization strategy of measuring wild type T cell responses. Intradermal immunization on day 0, 3 and 6 and responses measured 7 days after final immunization (day 13). (B-C) Percentage of IFN-y$^+$ cells in CD8$^+$ gate within the lymphocyte gate on FSC/SSC of dLN (B) or spleen (C). IFN-γ^+ cells upon stimulation with medium is considered background and shown in gray. Results were pooled of 2 experiments with a total of 6-9 mice/group. (D) CD4$^+$ T cell response was measured by proliferation of splenocytes upon stimulation of OVA protein. Each data point represents the results of one animal. Incorporation of ^{3}H-thymdine in DNA was measured liquid scintillation counting as CCTM. Statistical significance was determined using Krukis-Wallis and multiple comparison/post hoc analysis was done comparing all immunization groups with Dunns correction, *=p<0.05, **=p<0.01, ***=p<0.001.

At day 13, antigen-specific CD8$^+$ T cell responses were detected by intracellular IFN-γ cytokine staining (**Supplement Fig. 1A**). Background levels of IFN-γ produced by CD8$^+$ T cells was low in all mice, as depicted by restimulation of cells with medium (**Fig. 4B-C**). As expected, no OVA$_{257-264}$-specific CD8$^+$ T cell response was detected in mice immunized with

soluble OVA (**Fig. 4B-C**)**.** In contrast, responses to this epitope were clearly detectable in dLN (**Fig. 4B**) and the spleen (**Fig. 4C**) of mice immunized with OVA+PIC, anPLGA-OVA or catPLGA-OVA. Responses in the anPLGA-OVA group tended to be lower than that in the catPLGA-OVA group. The addition of poly(I:C) enhanced the $CD8^+$ response, either when mixed with OVA solution or co-encapsulated with OVA in PLGA nanoparticles (anPLGA-OVA-PIC) (**Fig. 4B-C**)**.** Thus, following hollow microneedle-mediated delivery, a specific recipient $CD8^+$ T cell response is induced by OVA when encapsulated in PLGA nanoparticles or when adjuvanted with TLR3 agonist (either mixed or co-encapsulated with OVA in PLGA nanoparticles). Furthermore, induction of OVA-specific $CD4^+$ T cell responses in the immunized mice was determined by measuring ^{3}H-thymidine incorporation in 72 h splenocyte cultures incubated with OVA protein. Some OVA-specific proliferation was detected in mice immunized with OVA+PIC, catPLGA-OVA, and anPLGA-OVA-PIC (**Fig. 4D**), although no significant differences between groups were observed.

Thus, hollow microneedle-mediated intradermal immunization with OVA loaded PLGA nanoparticle with or without poly(I:C) induces clearly detectable $OVA_{257-264}$-specific $CD8^+$ T cell responses and minor OVA-specific $CD4^+$ T cell responses in mice.

3.5. Protective immune response towards recombinant rLM-OVA after intradermal immunization using hollow microneedles

$CD8^+$ T cells play an essential role in clearance of the intracellular bacterium *Listeria monocytogenes* [31]. Next, we determined whether hollow microneedle-mediated vaccination with PLGA nanoparticles induces protective immunity against rLM-OVA. Mice were immunized with OVA, OVA+PIC, anPLGA-OVA, catPLGA-OVA or anPLGA-OVA-PIC at day 0, 3 and 6 and challenged with the bacterium 21 days after final immunizations (**Fig. 5A**). Unimmunized mice served as a negative control and mice immunized with rLM-OVA at day 6 served as a positive control, as these mice are typically able to completely clear the bacterium within 3 days after challenge. Determination of CFU counts in the spleens at day 30 showed that mice immunized with rLM-OVA indeed completely cleared the challenge dose, while spleens of non-immunized mice contained in average approximately 100.000 bacteria (**Fig. 5B**). While immunization with soluble OVA, OVA+PIC and anPLGA-OVA failed to protect (**Fig. 5B**), protection was observed in at least one mouse immunized with catPLGA-OVA. Moreover, anPLGA-OVA-PIC induced full protection, resulting in zero bacteria count in the spleen, similar to mice immunized with rLM-OVA (**Fig. 5B**). This indicates that immunization with anPLGA-OVA-PIC, and to some degree catPLGA-OVA, via the intradermal route using hollow microneedles, elicited a protective cellular immune response.
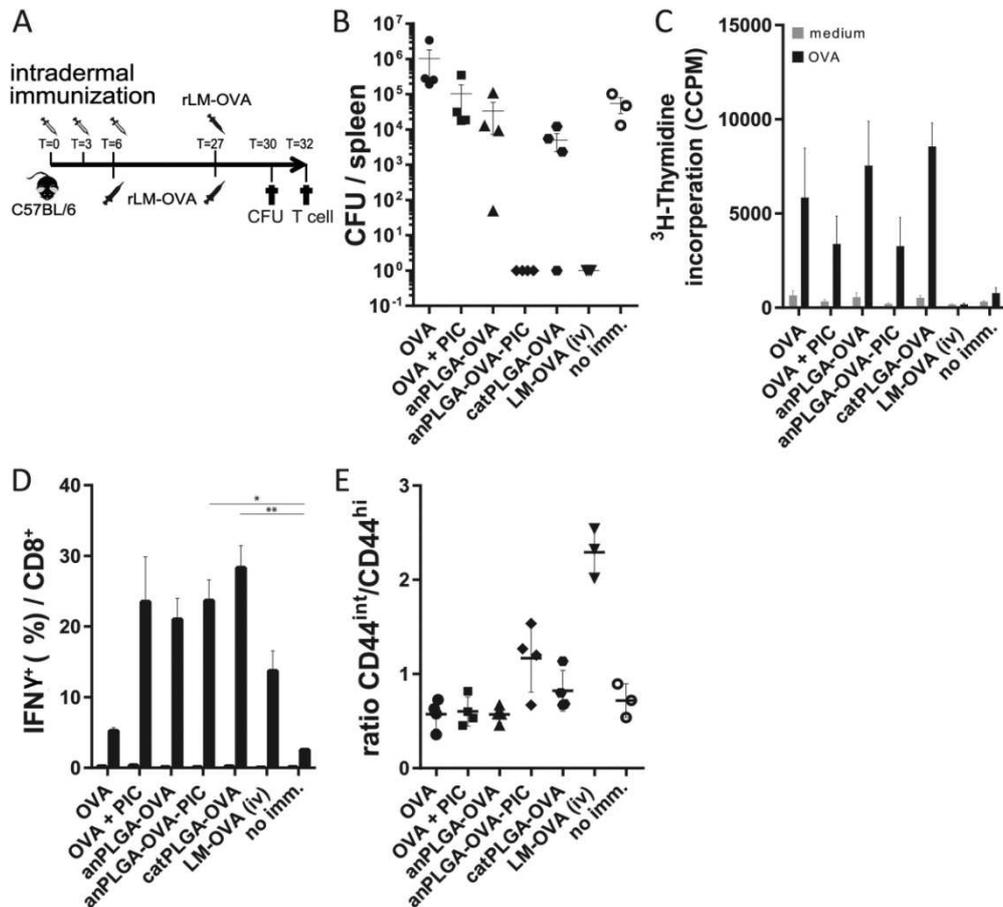
Figure 5. Protective immune response towards rLM-OVA after hollow microneedle mediated intradermal immunization. (A) Schematic overview of challenge study in which the mice received an i.v. challenge of 100.000 recombinant Listeria monocytogenes-OVA (rLM-OVA) 21 days after 3 immunizations with different formulations. CFU count of rLM-OVA in spleen was determined 3 days after challenge and T cell activation was measured 5 days after challenge. (B) Spleens were isolated and serial dilutions were plated on BHI agar plates and CFU's were counted 36 h after incubation at 37°C. (C-D) CD4$^+$ T cell and CD8$^+$ T cell responses were measured by using a procedure identical to that used for T cell responses showed in **Fig. 4B-D**. Gentamycin was added to culture medium to prevent further growth of potential rLM-OVA. Per experiment n=4 for OVA, anPLGA-OVA and catPLGA-OVA immunization groups, n=3 for pOVA immunization groups and n=2 for PBS immunization group (as depicted by the amount of dots in the graph). Statistical significance was determined using Krukis-Wallis and multiple comparison/post hoc analysis was done with Dunns correction, *=p<0.05.

To study the possible relation between T cell response and the capacity to clear the pathogen, the T cell response in the spleen of the challenged mice was measured. Results of T cell responses 5 days after challenge with rLM-OVA showed that all immunization regimens triggered OVA-specific CD4$^+$ T cell responses, and that the addition of poly(I:C) did not further increase these responses **(Fig. 5C).** In all immunized groups except OVA-immunized mice a particularly robust activation of antigen-specific CD8$^+$ T cells was detected (**Fig. 5D**). Remarkably, the activated CD8$^+$ T cells in OVA-immunized mice consisted of 40% central memory T cells (Tcm; CD62L$^+$CD44$^+$) and 60% effector T cells and effector memory T cells (Teff/Tem ;CD62L$^-$CD44$^+$). In contrast, in the other immunization groups the Tcm populations were much smaller and the Teff/Tem cell population much larger (**Sup Fig. 1B-D; solid line**). While Tcm:Teff/Tem cell ratio failed to correlate with immune protection,

cells within the CD62L⁻CD44⁺ gate were further analyzed (**Sup. Fig. 1B-D; dotted line**). We found higher CD44^{int}:CD44^{hi} cell ratios in mice that had received anPLGA-OVA-PIC, catPLGA-OVA and rLM-OVA, i.e. the immunization regimens that led to reduced CFU counts following bacterial challenge (**Fig. 5E**). Thus, the presence of antigen-specific CD44^{int} CD8$^+$ T cells seems favorable for immune protection to rLM-OVA infection.

4. Discussion

Nowadays, most of the vaccines under investigation are based on recombinant proteins or subunits of pathogens, because of improved safety and lower production cost compared to live or attenuated vaccines [32]. However, in general such vaccines are poorly immunogenic and fail to elicit robust cell-mediated immunity against intracellular pathogens. In this respect, nanoparticle-based delivery of antigens may be an attractive tool, because it can improve immune response induction to encapsulated antigens [33]. In this study, OVA was used as a model antigen and encapsulated into PLGA nanoparticles with or without the adjuvant poly(I:C). The capacity of the nanoparticle formulations to stimulate cell-mediated immunity was investigated by intradermal immunization using hollow microneedles. We show that intradermal delivery using hollow microneedles can elicit a protective cellular immune response when the antigen is encapsulated in cationic PLGA nanoparticles or when the antigen and adjuvant are co-encapsulated in anionic PLGA nanoparticles. These data expand on previous studies using hollow microneedles where humoral immune responses were detected [7-9], which illustrate the attractiveness of the intradermal route for the delivery of vaccines.

Nanocarriers used for delivery of proteins or subunit vaccines enhance antigen uptake by antigen presenting cells and contribute to a prolonged presentation of the vaccine antigen at the cell surface [34, 35]. This leads to activation of a cellular immune response, which was exemplified in previous studies showing that PLGA nanoparticle-encapsulated antigens, with or without adjuvant, may induce strong T helper type 1 and cytotoxic T cell immune response (Th1/CTL) when delivered systemically or subcutaneously [15, 17, 36]. However, relatively little is known about the immune responses elicited by nanoparticle vaccines when administered intradermally using microneedles. Some previous studies showed that coated and dissolvable microneedle delivered protein antigen induced CD8$^+$ T cell responses [39-41]. In these studies none of the vaccine antigens were encapsulated in nanoparticles. Our results showed that the encapsulation of antigen in nanoparticles with and without adjuvant can enhance the T cell responses. These results are in line with a previous study, in which dissolving microneedles loaded with PLGA nanoparticle encapsulated antigens were used for intradermal vaccination, and shown to induce a robust antigen-specific protective cellular immune response in mice [24].

Our data show that hollow microneedle-delivered particulated OVA not only activated transferred tg T cells, but also primed endogenous protective CD8$^+$ T cell responses in immunized mice. In mice adoptively transferred with tg T cells, an endogenous T cell response could not be detected (data not shown). This may be explained by the single injection immunization regimen in these studies, which may be sufficient to prime adoptively transferred tg CD8$^+$ T cells, but not the naïve antigen-specific T cell repertoire. Alternatively, interference of the relatively easily activated tg T cells with priming of naïve T cells of recipient mice, for example by cytotoxicity towards antigen presenting pAPC as part of an immune homeostasis feedback loop, may explain this observation. For this reason, to examine whether hollow microneedle-mediated immunization with PLGA nanoparticles encapsulated OVA may prime OVA-specific endogenous CD8$^+$ T cells in mice, a priming procedure

consisting of three immunizations delivered over a time period of 6 days was used. This protocol had been shown to induce cellular immune responses following dermal DNA tattoo immunization [26, 42], but not yet when using hollow microneedles [7]. We report here that this prime boost protocol indeed elicits vigorous CD8$^+$ T cell responses in mice immunized with PLGA nanoparticles encapsulated with antigen, when using hollow microneedles as delivery method.

A variety of dendritic cells in the dermis and epidermis have been shown to contribute to immune activation following dermal immunization [43, 44], and they all express diverse pathogen recognition receptors, such as Toll-like receptors (TLRs). In agreement with this observation, multiple intradermal immunization studies have shown added effects of different Toll-like receptor (TLR) agonists based adjuvants [16, 45]. In our study, co-delivery of OVA and the TLR3 agonist poly(I:C) in PLGA nanoparticles, led to protective cellular immune responses to rLM-OVA. Possibly, the nanoparticles act as a depot system and stimulate the immune system by controlling the release of OVA and poly(I:C), resulting in prolonged OVA presentation and enhanced immunogenicity [23].

Cationic PLGA nanoparticles are considered to be more immunogenic than anionic PLGA nanoparticle, as their positive surface charge facilitate the interaction with anionic cell membranes, enhancing uptake of these nanoparticles by phagocytic cells [46]. However, this enhanced interaction can also lead to increased cell cytotoxicity [10], contributing to the challenges faced for therapeutic use in humans. In our adoptive transfer studies anPLGA-OVA and catPLGA-OVA seemed to perform equally well. However, catPLGA-OVA primed the endogenous cellular immune responses efficiently, while anPLGA-OVA did not show significant increase of response compared to OVA solution. Besides, although one mouse showed full protection from subsequent infection with rLM-OVA after immunization with catPLGA-OVA, no statistical difference in degree of immune protection induced by plain cationic compared to anPLGA-OVA was detected. Our results show that inclusion of poly(I:C) in the anionic nanoparticles was needed to fully protect immunized mice from infection.

Remarkably, although immune protection differed between mice immunized with OVA particulated in cationic or anionic PLGA without or with poly(I:C), vigorous OVA-specific CD8$^+$ T cell responses were detected in all groups except for mice immunized with soluble OVA. Further analysis of CD8$^+$ T cell phenotype showed that there was no difference within percentage of Tcm and Tem/Teff cells between the different PLGA nanoparticle immunized groups, but an enhanced ratio of CD8$^+$ T cells with CD44^{int} phenotype was detected in mice immune to rLM-OVA challenge. Difference in antigen release can have a role in shaping the memory phenotype [47], however we found similar release profiles of OVA in the different nanoparticle formulations. Thus, although no clear definition of CD44^{int}CD62L^{neg} is available [48-50], we show a correlation between their presence and intradermal immunization-induced protective immunity to challenge with rLM-OVA.

Taken together, we show that hollow microneedles are an excellent tool for intradermal vaccination, leading to the induction of minor CD4$^+$ T cell and vigorous CD8$^+$ T cell responses to PLGA nanoparticle encapsulated with antigens. Evoked CD8$^+$ T cell responses provided full protection against an intracellular bacterium if poly(I:C) was co-encapsulated with the OVA antigen in PLGA nanoparticles. Future studies may show whether other adjuvants have similar effects or whether specific adjuvants may induce protection to specific categories of intracellular pathogens.

Hollow microneedle-mediated intradermal delivery of model vaccine antigen-loaded PLGA nanoparticles elicits protective T cell-mediated immunity to an intracellular bacterium

Acknowledgements

Chapter 3

References

[1] Levin C, Perrin H, Combadiere B. Tailored immunity by skin antigen-presenting cells, Hum. Vaccin. Immunother. 11 (2015) 27-36.

[2] van der Maaden K, Jiskoot W, Bouwstra J. Microneedle technologies for (trans)dermal drug and vaccine delivery, J. Control. Release 161 (2012) 645-655.

[3] Kim Y, Park J, Prausnitz M. Microneedles for drug and vaccine delivery, Adv. Drug Deliv. Rev. 64 (2012):1547-1568.

[4] Larraneta E, McCrudden MTC, Courtenay A, Donnelly R, Larrañeta E. Microneedles: A new frontier in nanomedicine delivery, Pharm. Res. 33 (2016) 1055-1073.

[5] Prausnitz M. Microneedles for transdermal drug delivery, Adv. Drug Deliv. Rev. 56 (2004) 581-587.

[6] Quinn H, Kearney M, Courtenay A, McCrudden MTC, Donnelly R. The role of microneedles for drug and vaccine delivery, Expert Opin. Drug Deliv. 11 (2014) 1769-1780.

[7] Van Der Maaden K, Trietsch SJ, Kraan H, Varypataki EM, Romeijn S, Zwier R, et al. Novel hollow microneedle technology for depth-controlled microinjection-mediated dermal vaccination: A study with polio vaccine in rats, Pharm. Res. 31 (2014) 1846-1854.

[8] Schipper P, van der Maaden K, Romeijn S, Oomens C, Kersten G, Bouwstra J, et al. Determination of depth-dependent intradermal immunogenicity of adjuvanted inactivated polio vaccine delivered by microinjections via hollow microneedles, Pharm. Res. 33 (2016) 2269-2279.

[9] Schipper P, van der Maaden K, Romeijn S, Oomens C, Kersten G, Jiskoot W, et al. Repeated fractional intradermal dosing of an inactivated polio vaccine by a single hollow microneedle leads to superior immune responses, J. Control. Release 242 (2016) 141-147.

[10] Zhao L, Seth A, Wibowo N, Zhao C, Mitter N, Yu C. Nanoparticle vaccines, Vaccine 32 (2014) 327-337.

[11] Kundig T, Storni T, Kündig T, Senti G, Johansen P. Immunity in response to particulate antigen-delivery systems, Adv. Drug Deliv. Rev. 57 (2005) 333-355.

[12] Parveen S, Misra R, Sahoo S. Nanoparticles: a boon to drug delivery, therapeutics, diagnostics and imaging, Nanomedicine 8 (2012) 147-166.

[13] De Geest B, Willart M, Hammad H, Lambrecht B, Pollard C, Bogaert P, et al. Polymeric multilayer capsule-mediated vaccination induces protective immunity against cancer and viral infection, ACS Nano 6 (2012) 2136-49.

[14] Manolova V, Flace A, Bauer M, Schwarz K, Saudan P, Bachmann M. Nanoparticles target distinct dendritic cell populations according to their size, Eur. J. Immunol. 38 (2008) 1404-1413.

[15] Varypataki E, Silva A, Barnier Quer C, Collin N, Ossendorp F, Jiskoot W. Synthetic long peptide-based vaccine formulations for induction of cell mediated immunity: A comparative study of cationic liposomes and PLGA nanoparticles, J. Control. Release 226 (2016) 98-106.

[16] Varypataki E, van der Maaden K, Bouwstra J, Ossendorp F, Jiskoot W. Cationic liposomes loaded with a synthetic long peptide and poly(I:C): a defined adjuvanted vaccine for induction of antigen-specific T cell cytotoxicity, AAPS J. 17 (2015) 216-226.

[17] Hamdy S, Molavi O, Ma Z, Haddadi A, Alshamsan A, Gobti Z, et al. Co-delivery of cancer-associated antigen and Toll-like receptor 4 ligand in PLGA nanoparticles induces potent CD8+ T cell-mediated anti-tumor immunity, Vaccine 26 (2008) 5046-5057.

[18] Danhier F, Ansorena E, Silva J, Le Breton A, Coco R, Préat V. PLGA-based nanoparticles: an overview of biomedical applications, J. Control. Release 161 (2012) 505-522.

[19] Panyam J, Labhasetwar V. Biodegradable nanoparticles for drug and gene delivery to cells and tissue, Adv. Drug Deliv. Rev. 55 (2003) 329-347.

54

[20] Panyam J, Labhasetwar V. Biodegradable nanoparticles for drug and gene delivery to cells and tissue, Adv. Drug Deliv. Rev. 64 (2012) 61-71.

[21] Chong C. Enhancement of T helper type 1 immune responses against hepatitis B virus core antigen by PLGA nanoparticle vaccine delivery, J. Control. Release 102 (2005) 85-99.

[22] Schlosser E, Mueller M, Fischer S, Basta S, Busch D, Gander B, et al. TLR ligands and antigen need to be coencapsulated into the same biodegradable microsphere for the generation of potent cytotoxic T lymphocyte responses, Vaccine 26 (2008) 1626-1637.

[23] Akagi T, Baba M, Akashi M, Kunugi S, Yamaoka T. Biodegradable nanoparticles as vaccine adjuvants and delivery systems: regulation of immune responses by nanoparticle-based vaccine, In: BERLIN: Springer Berlin Heidelberg; 2012. p. 31-64.

[24] Zaric M, Lyubomska O, Touzelet O, Poux C, Al Zahrani S, Fay F, et al. Skin dendritic cell targeting via microneedle arrays laden with antigen-encapsulated poly-D,L-lactide-co-glycolide nanoparticles induces efficient antitumor and antiviral immune responses, ACS Nano 7 (2013) 2042-2055.

[25] Slutter B, Plapied L, Fievez V, Alonso Sande M, des Rieux A, Slütter B, et al. Mechanistic study of the adjuvant effect of biodegradable nanoparticles in mucosal vaccination, J. Control. Release 138 (2009) 113-121.

[26] Platteel AC, de Groot AM, Keller C, Andersen P, Ovaa H, Kloetzel P, et al. Strategies to enhance immunogenicity of cDNA vaccine encoded antigens by modulation of antigen processing, Vaccine 34 (2016) 5132-5140.

[27] Shen H, Matloubian M, Ahmad R, Slifka MK, Jensen ER, Miller JF. Recombinant Listeria monocytogenes as a live vaccine vehicle for the induction of protective anti-viral cell-mediated immunity, Proc. Natl. Acad. Sci. U S A. 92 (1995) 3987-3991.

[28] Pope C, Kim SK, Marzo A, Masopust D, Williams K, Jiang J, et al. Organ-specific regulation of the CD8 T cell response to Listeria monocytogenes infection, J. Immunol. 166 (2001) 3402-3409.

[29] Kelly JM, Sterry SJ, Cose S, Turner SJ, Fecondo J, Rodda S, et al. Identification of conserved T cell receptor CDR3 residues contacting known exposed peptide side chains from a major histocompatibility complex class I-bound determinant, Eur. J. Immunol. 23 (1993) 3318-3326.

[30] Barnden MJ, Allison J, Heath WR, Carbone FR. Defective TCR expression in transgenic mice constructed using cDNA-based alpha- and beta-chain genes under the control of heterologous regulatory elements, Immunol. Cell Biol. 76 (1998) 34-40.

[31] McGregor DD, Koster FT, Mackaness GB. Biological sciences: The short lived small lymphocyte as a mediator of cellular immunity, Nature 228 (1970) 855-856.

[32] Perrie Y, Mohammed A, Kirby D, McNeil S, Bramwell V. Vaccine adjuvant systems: enhancing the efficacy of sub-unit protein antigens, Int. J. Pharm. 364 (2008) 272-280.

[33] Silva J, Videira M, Preat V, Florindo H, Gaspar R, Préat V. Immune system targeting by biodegradable nanoparticles for cancer vaccines, J. Control. Release 168 (2013) 179-199.

[34] Shen H, Ackerman A, Cody V, Giodini A, Hinson E, Cresswell P, et al. Enhanced and prolonged cross-presentation following endosomal escape of exogenous antigens encapsulated in biodegradable nanoparticles, Immunology 117 (2006) 78-88.

[35] Waeckerle Men Y, Allmen EU, Gander B, Scandella E, Schlosser E, Schmidtke G, et al. Encapsulation of proteins and peptides into biodegradable poly(D,L-lactide-co-glycolide) microspheres prolongs and enhances antigen presentation by human dendritic cells, Vaccine 24 (2006) 1847-1857.

[36] Waeckerle Men Y, Groettrup M. PLGA microspheres for improved antigen delivery to dendritic cells as cellular vaccines, Adv. Drug Deliv. Rev. 57 (2005) 475-482.

[37] Bal S, Slutter B, Jiskoot W, Bouwstra J, Slütter B. Small is beautiful: N-trimethyl chitosan-ovalbumin conjugates for microneedle-based transcutaneous immunisation, Vaccine 29 (2011) 4025-4032.

[38] Kumar A, Wonganan P, Sandoval M, Li X, Zhu S, Cui Z. Microneedle-mediated transcutaneous immunization with plasmid DNA coated on cationic PLGA nanoparticles, J. Control. Release 163 (2012) 230-239.

[39] Ng H, Fernando GJP, Kendall MAF. Induction of potent CD8^{+} T cell responses through the delivery of subunit protein vaccines to skin antigen-presenting cells using densely packed microprojection arrays, J. Control. Release 162 (2012) 477-484.

[40] Van Der Maaden K, Varypataki EM, Romeijn S, Ossendorp F, Jiskoot W, Bouwstra J. Ovalbumin-coated pH-sensitive microneedle arrays effectively induce ovalbumin-specific antibody and T-cell responses in mice, Eur. J. Pharm. Biopharm. 88 (2014) 310-315.

[41] Van Der Maaden K, Varypataki EM, Yu H, Romeijn S, Jiskoot W, Bouwstra J. Parameter optimization toward optimal microneedle-based dermal vaccination. Eur. J. Pharm. Sci. 64 (2014) 18-25.

[42] Bins AD, Jorritsma A, Wolkers MC, Hung CF, Wu TC, Schumacher TNM, et al. A rapid and potent DNA vaccination strategy defined by in vivo monitoring of antigen expression, Nat. Med. 11 (2005) 899-904.

[43] Fehres C, Garcia Vallejo J, Unger WWJ, van Kooyk Y. Skin-resident antigen-presenting cells: instruction manual for vaccine development, Front Immunol. 4 (2013) 157.

[44] Zaric M, Lyubomska O, Poux C, Hanna ML, McCrudden MT, Malissen B, et al. Dissolving microneedle delivery of nanoparticle-encapsulated antigen elicits efficient cross-priming and th1 immune responses by murine langerhans cells, J. Invest. Dermatol. 135 (2015) 425-434.

[45] Weldon W, Zarnitsyn V, Esser ES, Taherbhai M, Koutsonanos D, Vassilieva E, et al. Effect of adjuvants on responses to skin immunization by microneedles coated with influenza subunit vaccine, PLoS ONE 7 (2012) 41501.

[46] Foged C, Brodin B, Frokjaer S, Sundblad A. Particle size and surface charge affect particle uptake by human dendritic cells in an in vitro model, Int. J. Pharm. 298 (2005) 315-322.

[47] Demento S, Cui W, Criscione J, Stern E, Tulipan J, Kaech S, et al. Role of sustained antigen release from nanoparticle vaccines in shaping the T cell memory phenotype, Biomaterials 33(2012) 4957-4964.

[48] Pihlgren M, Arpin C, Walzer T, Tomkowiak M, Thomas A, Marvel J, et al. Memory CD44(int) CD8 T cells show increased proliferative responses and IFN-gamma production following antigenic challenge in vitro, Int. Immunol. 11 (1999) 699-706.

[49] Roberts A, Ely K, Woodland D. Differential contributions of central and effector memory T cells to recall responses, J. Exp. Med. 202 (2005) 123-133.

[50] Opata MM, Stephens R. Early Decision: Effector and effector memory T cell differentiation in chronic infection, Curr. Immunol. Rev. 9 (2013) 190-206.

Supplementary information
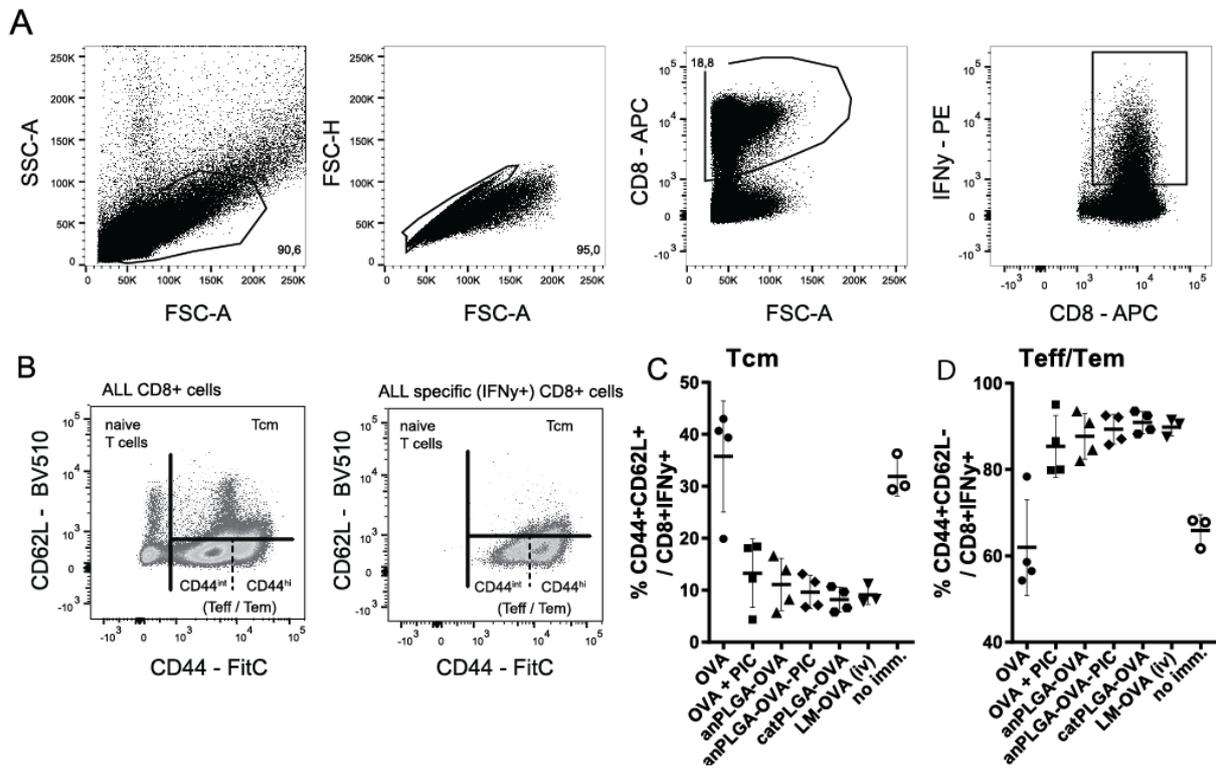
Supplementary Figure 1.
(A) Gating strategy used for determination of CD8^{+} T cell response. After live gate on forward/sideward scatter, double or adhering cells are excluded on FSC-A/FSC-H gate. IFN-γ^+ cells were determined after gating on CD8^{+} cells. (B) All CD8^{+} cells were used to determine different population on CD62L and CD44 surface markers. Memory phenotype was next determined on CD8^{+}IFN-γ^+ population only. (C+D) Percentage of Tcm (CD62L^{+} CD44int/hi) and Teff/Tem (CD62L^{-}CD44int/hi) in the specific T cell population. Statistical significance was determined using Kruskal-Wallis, and multiple comparison/post hoc analysis was done with Dunn's correction, *=p<0.05.

Chapter 3

Chapter 4

Intradermal vaccination with hollow microneedles: a comparative study of various protein antigen and adjuvant encapsulated nanoparticles

Guangsheng Du[1], Rania M. Hathout[1,2], Maha Nasr[1,2], M. Reza Nejadnik[1], Jing Tu[3], Roman I. Koning[4], Abraham J. Koster[4], Bram Slütter[1], Alexander Kros[3], Wim Jiskoot[1], Joke A. Bouwstra[1,*], Juha Mönkäre[1]

[1] Division of BioTherapeutics, Leiden Academic Centre for Drug Research, Leiden University, Leiden, The Netherlands

[2] Department of Pharmaceutics and Industrial Pharmacy, Faculty of Pharmacy, Ain Shams University, Cairo, Egypt

[3] Department of Supramolecular & Biomaterials Chemistry, Leiden Institute of Chemistry, Leiden University, Leiden, The Netherlands

[4] Department of Molecular Cell Biology, Section Electron Microscopy, Leiden University Medical Center, Leiden University, Leiden, The Netherlands

Abstract

In this study, we investigated the potential of intradermal delivery of nanoparticulate vaccines to modulate the immune response of protein antigen using hollow microneedles. Four types of nanoparticles covering a broad range of physiochemical parameters, namely poly (lactic-co-glycolic) (PLGA) nanoparticles, liposomes, mesoporous silica nanoparticles (MSNs) and gelatin nanoparticles (GNPs) were compared. The developed nanoparticles were loaded with a model antigen (ovalbumin (OVA)) with and without an adjuvant (poly(I:C)), followed by the characterization of size, zeta potential, morphology, and loading and release of antigen and adjuvant. An in-house developed hollow-microneedle applicator was used to inject nanoparticle suspensions precisely into murine skin at a depth of about 120 µm. OVA/poly(I:C)-loaded nanoparticles and OVA/poly(I:C) solution elicited similarly strong total IgG and IgG1 responses. However, the co-encapsulation of OVA and poly(I:C) in nanoparticles significantly increased the IgG2a response compared to OVA/poly(I:C) solution. PLGA nanoparticles and liposomes induced stronger IgG2a responses than MSNs and GNPs, correlating with sustained release of the antigen and adjuvant and a smaller nanoparticle size. When examining cellular responses, the highest $CD8^+$ and $CD4^+$ T cell responses were induced by OVA/poly(I:C)-loaded liposomes. In conclusion, the applicator controlled hollow microneedle delivery is an excellent method for intradermal injection of nanoparticle vaccines, allowing selection of optimal nanoparticle formulations for humoral and cellular immune responses.

Key words: Intradermal vaccination, hollow microneedles, nanoparticles, antigen, adjuvant

Intradermal vaccination with hollow microneedles: a comparative study of various protein antigen and adjuvant encapsulated nanoparticles

1. Introduction

Skin is an attractive administration site for immunization and may act as an excellent alternative for traditional intramuscular or subcutaneous vaccination. Furthermore, intradermal vaccination may enable dose sparing, since the skin has a rich network of immune cells compared to muscle or subcutaneous tissue [1]. However, the uppermost layer of the skin, the stratum corneum, is the main barrier that prevents the transport of vaccines (>500 Da) across the skin. Therefore, novel delivery methods need to be developed. Among various methods developed for antigen delivery via the skin, especially microneedle-based approaches have recently attracted increasing attention [2]. The major advantage of microneedles is their ability to pierce the skin in a minimally invasive manner and subsequently deliver their payload in the superficial skin layers potentially without pain, owing to the limited penetration depth of microneedles (typically <500 µm) [3].

Several microneedle types have been developed for vaccine delivery, such as coated or dissolving microneedles which can release the dry antigen into the epidermis and dermis after the piercing of the skin [2]. In contrast, hollow microneedles can be used to deliver antigens or particulate formulations as solutions or suspensions into the skin. To this end, in our group a hollow microneedle device has been developed that allows precise and controlled injections into the epidermis and dermis by using etched fused-silica capillary-based microneedles [4-6]. The advantage of the hollow microneedles compared to dissolving or coated microneedles is that little time is required for modifying the dose, formulation or administration depth. This is particularly advantageous when studying optimization of formulations or parameters for the immunization (e.g. penetration depth or vaccine dose). Furthermore, if required a higher dose can be injected into the skin compared to dissolving and coated microneedles.

Subunit antigens are based on purified antigens and are regarded safer than traditional whole bacterium- or virus-based vaccines [7]. However, these antigens have often lower immunogenicity and therefore adjuvants, such as toll-like receptor (TLR) ligands or toxoids, are needed to increase the immune response [8]. Recently, nanoparticles have gained growing attention for the delivery of subunit vaccines because of their capability of protecting antigens from degradation, forming a depot at the site of injection, and facilitating antigen uptake by dendritic cells (DCs) [9-11]. Studies have additionally shown that co-formulation of antigen and adjuvant into a nanoparticle might be crucial to improve immune responses against subunit vaccines [12-15]. However, it is not well understood how the physicochemical properties such as size, material, surface charge or release behavior of antigen/adjuvant influence the immune response. Previously, it has been proposed that positively charged nanoparticles with a size smaller than about 200 nm might be optimal for the interaction with antigen-presenting cells [9, 16-18]. Moreover, sustained release of antigen and adjuvant from nanoparticles and a depot effect of nanoparticles on the cell surface could allow the co-delivery of antigen and adjuvant to antigen-presenting cells [17, 19]. However, most vaccination studies have been performed by intramuscular or subcutaneous injection and no studies have directly compared different nanoparticles for intradermal vaccine delivery.

The aim of this study was to assess the potential of antigen loaded nanoparticles, with or without co-encapsulated adjuvant, to induce humoral and cellular immune responses after hollow microneedle-mediated intradermal immunization. To this end, we prepared four different nanoparticulate delivery systems with varying physicochemical properties, namely poly (lactic-co-glycolic) acid (PLGA) nanoparticles, liposomes, mesoporous silica nanoparticles (MSNs) and gelatin nanoparticles (GNPs). PLGA nanoparticles [10, 20-24] and liposomes [12, 18, 22, 25] have been extensively investigated as biocompatible and

biodegradable nanoparticle vaccine delivery systems. MSNs gain increasing attention for vaccine delivery because of their controlled size and mesostructure, excellent *in vivo* biocompatibility and high loading capacity [26, 27]. Gelatin based nanoparticles have been studied as promising vaccine carriers because of their excellent biocompatibility, stability and aptness for surface modification [28-30].

A model antigen, ovalbumin (OVA), with and without a TLR3 agonist, poly(I:C), was encapsulated into the nanoparticles. First, the physicochemical properties and the *in vitro* release of antigen and adjuvant of the different nanoparticulate formulations were characterized. Next, mice were immunized with the formulations by using a hollow microneedle device followed by the analysis of humoral and cellular immune responses. The results reveal that the immune response depends on encapsulation of antigen/adjuvant and the characteristics of nanoparticles. Furthermore, we demonstrate that the hollow microneedles together with the applicator are excellent tools for intradermal vaccination and screening of nanoparticulate formulations.

2. Materials and methods

2.1. Materials

PLGA (acid terminated, lactide glycolide 50:50, Mw 24 – 38 kDa), gelatin from porcine skin (bloom 300), OVA for *in vitro* studies (albumin from chicken egg white, lyophilized), bovine serum albumin (BSA) ≥96%, gluteraldehyde, glycine, cholamine chloride hydrochloride (2-aminoethyl)-trimethylammoniumchloride hydrochloride, 1-ethyl-3-(3-dimethyl-aminopropyl) carbodiimide hydrochloride (EDC), cholesterol (≥99%) and hydrofluoric acid ≥48% were purchased from Sigma-Aldrich (Zwijndrecht, The Netherlands). Polyvinyl alcohol (PVA) 4-88 (31 kDa) and ethylenediaminetetraacetic acid (EDTA) were purchased from Fluka (Steinheim, Germany). 1-step^{TM} ultra 3,3',5,5'-tetramethylbenzidine (TMB) was obtained from Thermo-Fisher Scientific (Waltham, MA). Endotoxin-free OVA, polyinosinic-polycytidylic acid (poly(I:C)) (low molecular weight) and its rhodamine-labeled version were purchased from Invivogen (Toulouse, France). Egg phosphatidylcholine (EggPC), 1,2-dioleoyl-sn-glycero-3-phosphocholine (DOPC), 1,2-dioleoyl-sn-glycero-3-[phosphor-L-serine](sodium salt) (DOPS), 1,2-dioleoyl-3-trimethylammonium-propane chloride salt (DOTAP) and 1,2-dioleoyl-sn-glycero-3-phosphoethanolamine (DOPE) were ordered from Avanti Polar Lipids (Alabaster, AL). HRP-conjugated goat anti-mouse total IgG, IgG1 and IgG2a were purchased from Southern Biotech (Birmingham, AL). Fluorescently labeled antibodies specific for CD4, CD8 and CD45.1 were ordered from eBioscience (San Diego, The Netherlands). Sulfuric acid (95-98%) was obtained from JT Baker (Deventer, The Netherlands). Ethyl acetate and silicone oil (AK350) were ordered from Boom Chemicals (Meppel, The Netherlands). Dimethylsulfoxide (DMSO) was ordered from Biosolve BV (Valkenswaard, The Netherlands). Sodium dodecyl sulfate (SDS) was purchased from Merck Millipore (Hohenbrunn, Germany). Vivaspin 2 centrifugal concentrators (PES membrane, MWCO 1000 kDa) were obtained from Sartorius Stedim (Nieuwegein, The Netherlands). Sterile phosphate buffered saline (PBS, 163.9 mM Na^+, 140.3 mM Cl^-, 8.7 mM HPO_4^{2-}, 1.8 mM H_2PO^{4-}, pH 7.4) was obtained from Braun (Oss, The Netherlands). Cell culture medium was prepared by mixing Roswell Park Memorial Institute medium (RPMI) with 10% Fetal bovine serum (FBS), 1% L-glutamine and 1% Penicillin-streptamycin. 1 mM phosphate buffer (PB, 0.77 mM Na_2HPO_4, 0.23 mM NaH_2PO_4, pH 7.4), 10 mM PB (7.7 mM Na_2HPO_4, 2.3 mM NaH_2PO_4, pH 7.4), 5 mM 4-(2-hydroxyethyl)piperazine-1-ethanesulfonic acid (HEPES, pH 7.4) buffer, lysis buffer (150 mM ammonium chloride, 10 mM $KHCO_3$, 0.1 mM EDTA, pH 7.2), and FACS buffer (2% FBS in PBS, pH7.4) were prepared in the lab. All the other

chemicals used are of analytical grade and Milli-Q water (18 MΩ/cm, Millipore Co.) was used for the preparation of all solutions.

2.2. Preparation of nanoparticles

2.2.1. Preparation of PLGA nanoparticles

OVA loaded PLGA nanoparticles (PLGA-OVA) were prepared by double emulsion with solvent evaporation method as previously reported with modifications [31]. Briefly, 75 µl OVA (20 mg/ml) in PBS was dispersed in 1 ml ethyl acetate containing 25 mg/ml PLGA by using a Branson sonifier 250 (Danbury, CT) for 15 s with a power of 20 W. The obtained water-in oil-emulsion was emulsified with 2 ml aqueous solution containing 2% (w/v) PVA with the sonifier (15 s, 20 W). The water-in-oil-in-water double emulsion was added dropwisely into 25 ml 0.3% (w/v) PVA (40 °C) under stirring. The ethyl acetate was evaporated by a rotary evaporator (Buchi rotavapor R210, Flawil, Switzerland) for 3 h (150 mbar, 40 °C). The nanoparticles were collected by centrifugation (Avanti^{TM} J-20XP centrifuge, Beckman Coulter, Brea, CA) at 35000 g for 10 min. Finally, they were washed twice with 1 mM PB to remove the excess OVA and PVA and dried in an ice condenser (Alpha 1-2, Osterode, Germany) in freeze vacuum (-49 °C, 90 mbar) overnight for further use and storage.

To prepare OVA and poly(I:C) co-encapsulated PLGA nanoparticles (PLGA-OVA-PIC), 18.75 µl OVA (40 mg/ml) and 75 µl poly(I:C) (46.7 mg/ml, including 0.03% fluorescently labeled equivalent) were emulsified with 1 ml PLGA (25 mg/ml) in ethyl acetate to obtain the water-in-oil emulsion. The rest of the procedure was identical to that of PLGA-OVA.

2.2.2. Preparation of liposomes

Liposomes were prepared by a film hydration method [32]. A thin lipid film of EggPC: DOPE: DOTAP in a molar ratio of 9:1:2.5 was created by evaporating chloroform of lipid stock solutions (25 mg/ml) using a rotary evaporator (Buchi rotavapor R210, Flawil, Switzerland). To prepare OVA loaded liposomes (Lipo-OVA), the lipid film was rehydrated in 10 mM PB (pH 7.4) containing 0.25 mg/ml OVA, and subsequently stabilized at room temperature for 1 h, resulting in final lipid concentration of 12.5 mg/ml. In the case of OVA and poly(I:C) co-encapsulated liposomes (Lipo-OVA-PIC), after lipid film hydration, 250 µl poly(I:C) solution (1.32 mg/ml, containing 0.5% rhodamine-labeled poly(I:C)) was added slowly (2 µl/min) by using a syringe pump to the liposome suspension under stirring. Finally, the liposomes were extruded (LIPEX^{TM} extruder, Northern Lipids, Burnaby, Canada) four times through a carbonate filter with a pore size of 400 nm and another four times through a filter with a pore size of 200 nm (Nucleopore Millipore, Amsterdam, The Netherlands). The obtained suspensions were transferred into VivaSpin 2 centrifuge concentrators (1000 kDa MWCO) and centrifuged (Allegra X-12R, Beckman Coulter, Indianapolis, IN) twice for 7 - 8 h (350 g, 22 °C) to remove the excess OVA and poly(I:C) [18]. The liposome suspensions were collected and stored at 4 °C until further use.

2.2.3. Preparation of MSNs

Large pore MSNs were synthesized and used for the loading of antigen and adjuvant as described earlier [33]. To improve the colloidal stability of antigen loaded MSNs, negatively charged liposomes were fused to the surface of MSNs, as reported previously [34, 35]. For this purpose liposomes were prepared by dispensing stock solutions of DOPC (70 µl, 25 mg/ml), DOPS (20 µl, 12.5 mg/ml) and cholesterol (10 µl, 25 mg/ml) in chloroform into

scintillation vials. A lipid film was created by slow evaporation of chloroform in the vial under a nitrogen flow and dried in vacuum overnight. The lipid film was rehydrated by the addition of 1 ml of 1mM PB (pH 7.4) and the mixture was vortexed for 10 s to form a cloudy lipid suspension. The obtained suspension was sonicated in a water bath for 10 min. The resulting clear liposome dispersions were stored at 4 °C for further use.

To prepare lipid bilayer coated and OVA encapsulated MSNs (LB-MSN-OVA), OVA (0.5 ml, 0.25 mg/ml) in 1 mM PB (pH 7.4) was first transferred into a 2 ml micro-centrifuge tube, followed by the addition of MSNs (0.5 ml, 1 mg/ml) and liposomes (0.5 ml, 2 mg/ml). For OVA and poly(I:C) co-encapsulated and lipid coated MSNs (LB-MSN-OVA-PIC), 0.5 ml solution containing 0.25 mg/ml OVA and 0.094 mg/ml poly(I:C) (containing 1.2% rhodamine-labeled poly(I:C)) were mixed with MSNs and liposomes similarly to LB-MSN-OVA. The resulting mixtures were incubated for 1.5 h under shaking (400 rpm, 25 °C). The nanoparticles were collected and excess liposomes, OVA and poly(I:C) were removed by centrifuging the sample (9000 g, 5 min) with a Sigma 1-15 centrifuge (Osterode, Germany). The obtained nanoparticles were stored at 4 °C before the use.

2.2.4. Preparation of GNPs

GNPs were prepared by using a two-step desolvation method as previously described [36]. First, 1.25 g gelatin (cationic, pI 7-9) was dissolved in 25 ml ultrapure water at 50 °C while stirring at 600 rpm for 30 min. The first desolvation step was carried out by addition of 25 ml acetone. The mixture was left for 1 h until the gelatin precipitated. The supernatant was discarded and the sediment was re-dissolved in 25 ml ultrapure water at 50 °C while stirring at 250 rpm for 30 min. Subsequently, the pH of the solution was adjusted to 2.5 by using concentrated HCl and a second desolvation step was performed by drop-wise (0.1 ml/s) addition of 80 ml acetone at 50 °C while stirring at 1200 rpm. The crosslinking of the GNPs was accomplished by adding 25 (w/w)% glutaraldehyde (GA) solution. The amount of added GA was adjusted such that the molar ratio between the NH_2 groups of gelatin and GA molecules was 1:1. Calculations were performed based on the assumptions that $MW_{gelatin} = 100$ kDa and 1 mol gelatin has 37 mol NH_2 [36]. The resultant suspension was stirred at 600 rpm for 16 h at room temperature. Next, an equal volume of 100 mM glycine solution was added to the suspension to block the unreacted GA and stop the cross-linking reaction. The suspension was stirred for 1 h at room temperature before being centrifuged at 7000 g for 1 h (Avanti[TM] J-20XP centrifuge, Beckman Coulter, Brea, CA) to separate the GNPs from the reaction mixture. The GNPs were rinsed with ultrapure water in three rounds of centrifugation and resuspension. The obtained GNPs were cationized to increase the positive surface charge and consequently enhance the loading of OVA and poly(I:C). Briefly, the pH of GNP suspension was adjusted to 4.5 and the quaternary amine cholamine (10% of the weight of GNPs) was added under constant stirring. After 5 min, EDC (10% of the weight of GNPs) was added to the suspension to activate the carboxylic groups of gelatin which would couple cholamine. The mixture was stirred for 3 h at room temperature. The cationized GNPs were purified by three successive centrifugation steps as described above. Finally, the nanoparticles were resuspended in ultrapure water by using vortexing and probe sonication [37], and stored at 4 °C for further experiments.

To prepare OVA loaded GNPs (GNP-OVA) for the humoral response study, 100 μg OVA in water was added to 2000 μg GNPs in water (total volume 1 ml) and the samples were mixed for 1 h (400 rpm, 25°C). For OVA and poly(I:C) co-loaded GNPs (GNP-OVA-PIC), after shaking OVA and GNPs for 1 h, 100 μg poly(I:C) (containing 1% rhodamine-labeled poly(I:C)) was added to the GNP suspension and the suspension was mixed for another 1 h.

Finally, the loaded nanoparticles were separated by centrifugation at 2800 g for 5 min, followed by re-suspension in de-ionized water. For the cellular response study, a modification of the method was required to allow administration of a higher dose. Instead of water, 4 mM HEPES buffer (pH 7.4) was used for loading to control the pH. For GNP-OVA the added amounts of GNPs and OVA were 6000 µg and 300 µg (in 1.5 ml), respectively, and for GNP-OVA-PIC, the amounts of GNP, OVA and poly(I:C) were 7000 µg, 200 µg and 200 µg (in 1.5 ml), respectively. The modification did not significantly change the characteristics of nanoparticles.

2.3. Characterization of the nanoparticles

2.3.1. Particle size and zeta potential determination

The particle size and polydispersity index (PDI), and zeta potential for all formulations were determined by dynamic light scattering and laser doppler velocimetry, respectively, by using a Nano ZS® zetasizer (Malvern Instruments, Worcestershire, U.K.). Particle size measurements were performed in 10 mM PB (pH 7.4) (PLGA nanoparticles, liposomes and MSNs) or ultrapure water (GNPs), while for zeta potential measurements samples were diluted in 5 mM HEPES buffer (pH 7.4).

2.3.2. Morphological characterization

Morphology of PLGA nanoparticles and GNPs was visualized by using scanning electron microscopy (SEM, Nova NanoSEM, FEI, Eindhoven, The Netherlands) with a voltage of 15 kV. Nanoparticles were first freeze-dried and coated with a thin layer of carbon. MSNs were visualized by transmission electron microscopy (TEM) using a JEOL 1010 instrument (JEOL Ltd, Peabody, MA) with an accelerating voltage of 70 kV. To prepare the samples, several droplets of MSN suspension (1 mg/ml) were added on a copper grid, dried overnight and coated with carbon. Liposomes were visualized by Cryo-EM. The samples were diluted to 5 mg/ml and drops of 3 µl were applied to 300 mesh EM grids with lacey carbon (Ted Pella, USA). Grids were transferred into an electron microscopy grid plunger (EM GP, Leica, Germany) operated at room temperature and 100% humidity. The sample was vitrified by removing excess liquid immediately followed by plunging into liquid ethane and the plunge-frozen grids were stored in liquid nitrogen until further use. Samples were inserted into a Gatan 626 cryo holder (Gatan, Pleasanton, CA). A Tecnai F20 microscope (Thermo-Fisher, Eindhoven, The Netherlands) was operated at 200 kV and the EM images were recorded at defocus values between 1 and 3 micron underfocus on a Gatan 4k x 4k CCD (Gatan, Germany).

2.3.3. Determination of loading efficiency of OVA and poly(I:C)

To determine the loading efficiency of OVA and poly(I:C) in PLGA nanoparticles, the nanoparticles were dissolved in a mixture of 15% (v/v) DMSO and 85% (v/v) 0.05 M NaOH and 0.5% SDS. The amount of OVA was quantified by the microBCA method following the manufacturer's instructions. The amount of poly(I:C) was determined by the fluorescence intensity of rhodamine labeled poly(I:C) (λ_{ex} 545 nm/λ_{em} 576 nm) with a plate reader (Tecan M1000, Männedorf, Switzerland). The loading efficiency of OVA in liposomes, MSNs and GNPs was determined by measuring its intrinsic fluorescence intensity (λ_{ex} 280 nm/λ_{em} 320 nm) with the Tecan M1000 plate reader in the supernatant before and after the encapsulation (MSNs and GNPs) or in the purification filtrates (liposomes). The loading efficiency of poly(I:C) in these nanoparticles was quantified similarly by measuring the fluorescence of its rhodamine labeled equivalent (λ_{ex} 545 nm/λ_{em} 576 nm).

The encapsulation efficiency (EE) and loading capacity (LC) of OVA and poly(I:C) in the nanoparticles were calculated as below:

$$EE \% = \frac{M_{loaded\ OVA/poly(I:C)}}{M_{total\ OVA/poly(I:C)}} \times 100 \% \qquad (1)$$

$$LC \% = \frac{M_{loaded\ OVA/poly(I:C)}}{M_{nanoparticles+OVA+poly(I:C)}} \times 100 \% \qquad (2)$$

Where $M_{loaded\ OVA/poly(I:C)}$ represents the mass of loaded OVA or poly(I:C), $M_{total\ OVA/poly(I:C)}$ is the total amount of OVA or poly(I:C) added to the formulations and $M_{nanoparticles+OVA+poly(I:C)}$ is the total weight of nanoparticles, OVA and poly(I:C).

2.3.4. *In vitro* release studies

To study the release of OVA and poly(I:C), the nanoparticles were dispersed in PBS and shaken by using an Eppendorf thermomixer (Nijmegen, The Netherlands) at 37 $^\circ$C with a speed of 550 rpm. The concentration for PLGA nanoparticles, liposomes, MSNs and GNPs after the suspension was 3 mg/ml, 5 mg/ml (lipid concentration), 1 mg/ml and 1.3 mg/ml, respectively. At predetermined time intervals, the tubes were taken out of the shaker bath and centrifuged at 10000 g for 10 min (PLGA nanoparticles and MSNs) or at 2800 g for 5 min (GNPs). A release sample of 600 µl was taken from the supernatant and replaced by fresh release medium. In the case of liposomes, 300 µl sample was collected to Vivaspin 500 concentrators. After the centrifuging (350 g, 30 min), the filtrate was collected and replaced with fresh medium. The amount of released OVA and poly(I:C) were determined by intrinsic fluorescence of OVA (λ_{ex} 280 nm/λ_{em} 320 nm) and fluorescence of rhodamine labeled poly(I:C) (λ_{ex} 545 nm/λ_{em} 576 nm), respectively, using a Tecan M1000 plate reader. The amount of released OVA in PLGA nanoparticles was determined by the MicroBCA method.

2.4. Hollow microneedles and applicator

Hollow microneedles were prepared as described earlier [38]. Briefly, 4-cm pieces of polyimide-coated fused silica capillaries (Polymicro, Phoenix AZ, 375 µm outer diameter, 50 µm inner diameter) were first filled with silicone oil in a vacuum oven (100 °C) overnight and subsequently etched for 4 h in ≥48% hydrofluoric acid. The polyimide coating was removed from the etched ends of capillaries by dipping them into heated (250 °C) sulfuric acid for 5 min.

A hollow-microneedle applicator was used to control the injection depth and volume as previously reported [5]. A 100-µl syringe with an inner diameter of 1.46 mm was used in conjunction with a syringe pump (NE-300, Prosense, Oosterhout, The Netherlands) and silica capillaries. High-pressure resistant CapTite^{TM} connectors were used to connect the pump, syringe, capillaries and needles.

2.5. Immunization studies

Female BALB/c mice (H2^d) and C57BL/6 mice (H2^b) were used for the antibody response and T-cell response study, respectively. The mice were 7-8 weeks old at the beginning of the experiment. All the mice were purchased from Charles Rivers (Maastricht, The Netherlands) and were housed under standardized conditions in the animal facility of Leiden Academic Centre for Drug Research of Leiden University. Experiments were approved by the ethical committee on animal experiments of Leiden University (Licence number 14176).

2.5.1. Antibody response study

BALB/c mice were anesthetized by intraperitoneal injection of ketamine (60 mg/kg) and xylanize (4 mg/kg), which was followed by the shaving of the injection site. At the same day mice (n = 8/group) were immunized by an intradermal injection of 10 µl nanoparticles loaded with 0.31 µg OVA, with or without approximately 0.31 µg poly(I:C), on the flank of the mouse by using the applicator, as described above. Solutions of 0.31 µg OVA, with or without 0.31 µg poly(I:C), were used as controls. The injection depth was set to about 120 µm. In addition, subcutaneous injection of 0.31 µg OVA (100 µl) was used as another control. Mice were immunized on day 0 (prime), day 21 (1st boost) and day 42 (2nd boost), and sacrificed on day 49. Before each immunization, on the same day, a venous blood sample was collected from the tail to measure the antibody responses. Before the sacrifice, the blood sample was collected from the femoral artery.

2.5.2. T cell response study

OT-I (OVA-specific $CD8^+$) and OT-II (OVA-specific $CD4^+$) T cell transferred C57BL/6 mice were used for the T cell response study. To obtain OT-I and OT-II T cells, spleens of OT-I and OT-II transgenic mice (CD45.1) were isolated and single cell suspensions were obtained by forcing the spleens through a 70 um strainer. After erythrocyte depletion with ammonium chloride, percentage of $CD8^+/Valpha2^+$ or $CD4^+/Valpha2^+$ cells was determined by flow cytometry (BD FACSCanto-II, San Jose, CA). An equivalent of 8000 OT-I and 56000 OT-II cells were intravenously transferred through the tail vein into C57BL/6 mice. Next day, the T cell transferred mice were immunized with nanoparticle formulations. OVA and poly(I:C) solutions were used as controls. Before the immunization, mice were anesthetized by isoflurane inhalation (induction 4-5% and maintenance 1%), which was followed by shaving of the injection site. On the same day, mice (n = 5/group) were immunized by three intradermal injections of 13.3 µl (totally 40 µl) formulation containing 5 µg OVA with or without approximately 5 µg poly(I:C) on the flank of the mouse (two injections on the right side, one injection on the left side) by using the hollow-microneedle applicator as described above. 7 days after the immunization, venous blood sample was collected from the tail to analyze the T cell response.

2.6. Determination of OVA specific IgG antibodies

OVA-specific antibodies were analyzed by a sandwich enzyme-linked immunosorbent assay (ELISA) as described earlier [39]. Briefly, wells of the 96 well-plates were first coated with 500 ng OVA for 1.5 h at 37 °C. The plates were blocked by incubation with 1% (w/v) BSA for 1 h at 37 °C. After the blocking, appropriate three-fold serial dilutions of mouse sera were applied to the plates and incubated for 1.5 h at 37 °C. Then the plates were incubated with horseradish peroxidase-conjugated goat antibodies against IgG, IgG1 and IgG2a (1:5000 dilution) for 1 h at 37 °C. Finally, specific antibodies were detected by TMB. The absorbance was measured at 450 nm (Tecan M1000) and the antibody titer was determined as a log10 value of the mid-point dilution of S-shaped dilution-absorbance curve of the diluted serum level.

2.7. $CD4^+$ and $CD8^+$ T cell responses

The erythrocytes of the blood sample (100 µl) were first lysed by incubating samples with 3 ml lysis buffer for 6 min in ice, followed by addition of 5 ml cell culture medium. After the centrifugation (5 min, 500 g), the supernatant was discarded and the samples were suspended in 5 ml FACS buffer. Next, samples were centrifuged and 200 µl of cell suspension was

added to the 96-well plate after discarding the supernatant. The cell surfaces were stained by incubating the cells with 100 µl diluted (1:800) fluorescently labeled antibodies specific for CD45.1 (eFluor450), CD4 (APC) and CD8α (PerCP) for 30 min (100 µl/well). After 30 min incubation at 4 °C, the excess antibodies were washed by using FACS buffer. The cells were incubated with fixation and permeabilization solution (BD Biosciences) for 10 min at 4 °C. Finally, the cells were washed with FACS buffer and analyzed by flow cytometry (BD FACSCanto-II, San Jose, CA). The data were analyzed by using FlowJo software.

2.8. Statistical analysis

All the data of immunization studies were analyzed by one way ANOVA with Bonferoni's post-test by using GraphPad Prism software (version 5.02). The level of significance was set at $p < 0.05$.

3. Results

3.1. Physicochemical characterization of nanoparticles

Table 1. Physicochemical characteristics of OVA/poly(I:C) loaded nanoparticles.

Nanoparticles	Size[a] (nm)	PDI[b]	ZP[c] (mV)	EE[d] %		LC[e] %	
				OVA	Poly(I:C)	OVA	Poly(I:C)
PLGA-OVA	157±7	0.060±0.028	-18±1	64.7±4.8	-	6.9±0.5	-
PLGA-OVA-PIC	160±1	0.052±0.019	-22±4	76.7±2.0	13.9±4.2	2.7±0.7	3.0±0.9
Lipo-OVA	124±15	0.152±0.026	44±2	97.0±2.4	-	1.6±0.1	-
Lipo-OVA-PIC	171±9	0.270±0.040	41±1	92.1±5.6	98.6±2.3	1.5±0.1	1.6±0.1
LB-MSN-OVA	656±5	0.280±0.018	-33±3	73.8±5.7	-	15.6±1.2	-
LB-MSN-OVA-PIC	603±17	0.318±0.040	-38±3	34.4±3.3	64.9±14.6	7.9±0.8	5.9±1.3
GNP-OVA	507±31	0.131±0.116	21±2	90.9±14.2	-	4.3±0.7	-
GNP-OVA-PIC	757±235	0.320±0.179	8±12	96.8±4.3	95.0±4.4	3.5±0.9	3.4±1.0

Data are average ± SD of at least 3 independent batches.
[a]Size: Z-average in diameter, [b]PDI: poly dispersity index, [c]ZP: zeta potential, [d]EE: encapsulation efficiency, [e]LC: loading capacity.

Four different nanoparticle formulations (PLGA nanoparticles, liposomes, MSNs and GNPs) were developed and characterized in terms of size, zeta potential, surface morphology, and loading and release properties of encapsulated antigen and adjuvant. Physicochemical characteristics of the nanoparticles are summarized in **Table 1**. According to DLS, PLGA nanoparticles and liposomes had an average diameter between 120 nm and 170 nm with a PDI value below 0.1 (PLGA nanoparticles) and 0.3 (liposomes). MSNs and GNPs had a larger diameter, ranging from 500 nm to 760 nm, and PDI values between 0.1 and 0.3. The electron microscopy images revealed a spherical shape of PLGA nanoparticles, liposomes and GNPs, whereas MSNs had a rectangular shape with mesochannels along the short axis (**Fig. 1**). The

estimated size based on electron microscopy images is consistent with the size in **Table 1** for
PLGA nanoparticles and liposomes. MSNs had a smaller particle size in TEM images than in
DLS measurements, indicating the presence of aggregates in these nanoparticle suspensions.
In the case of GNPs, particles are swelling in aqueous medium [40], which may explain the
smaller particle size in SEM images as compared to DLS.

PLGA nanoparticles and MSNs had a negative zeta potential, whereas liposomes and GNPs
possessed a positive zeta potential. In general, co-encapsulation of poly(I:C) did not
substantially affect the size, the PDI and zeta potential of the nanoparticles (**Table 1**).
Moreover, both OVA and poly(I:C) were efficiently encapsulated into the nanoparticles. The
EE% of OVA reached more than 60% for all nanoparticles except LB-MSN-OVA-PIC (34%)
(**Table 1**). Similarly, poly(I:C) had a EE% higher than 60%, except for PLGA nanoparticles
(13.9%). During the development of the preparation process of the nanoparticles, the
introduced amounts of antigen and adjuvant were optimized to obtain similar loading
capacities of OVA and poly(I:C) for each delivery system (**Table 1**).
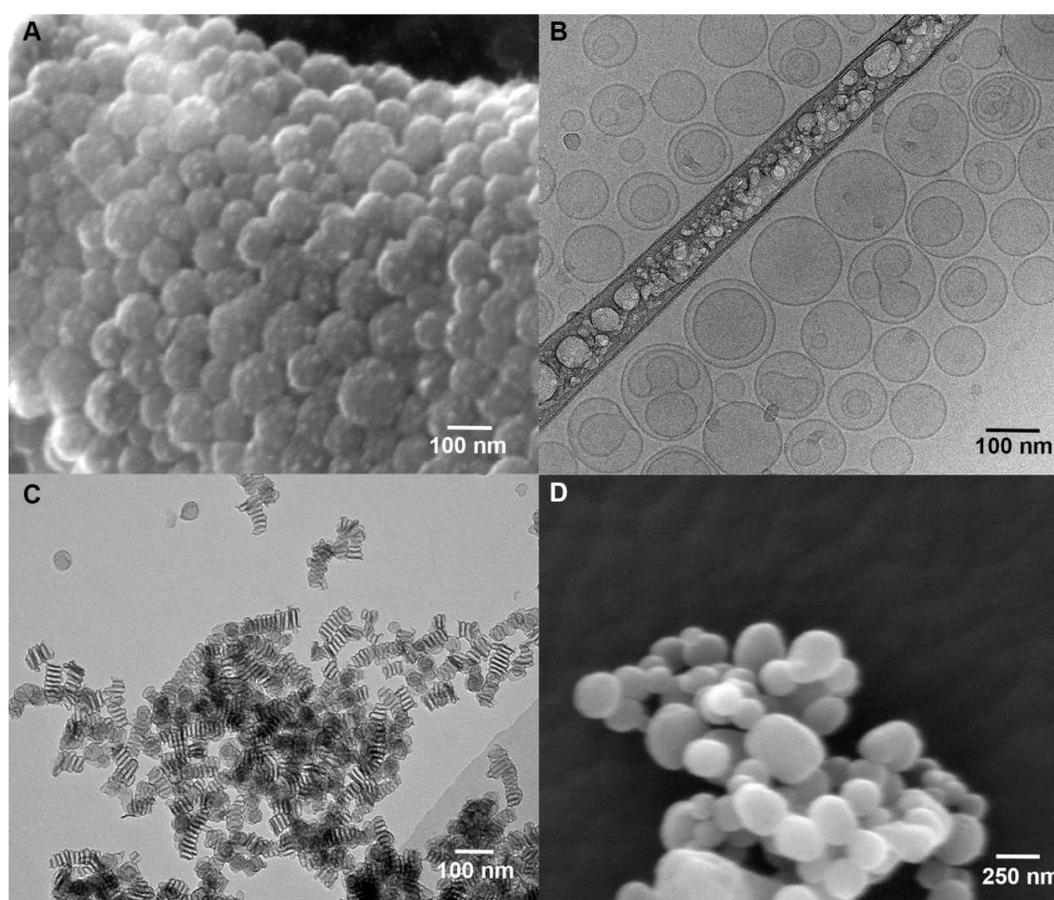
Figure 1. Electron microscope images of nanoparticles. A) Scanning electron microscopy
(SEM) image of PLGA nanoparticles; B) Cryo-EM image of liposomes; C) Transmission
electron microscopy (TEM) image of MSNs; D) SEM image of GNPs.

3.2. *In vitro* release of OVA and poly(I:C) from nanoparticles
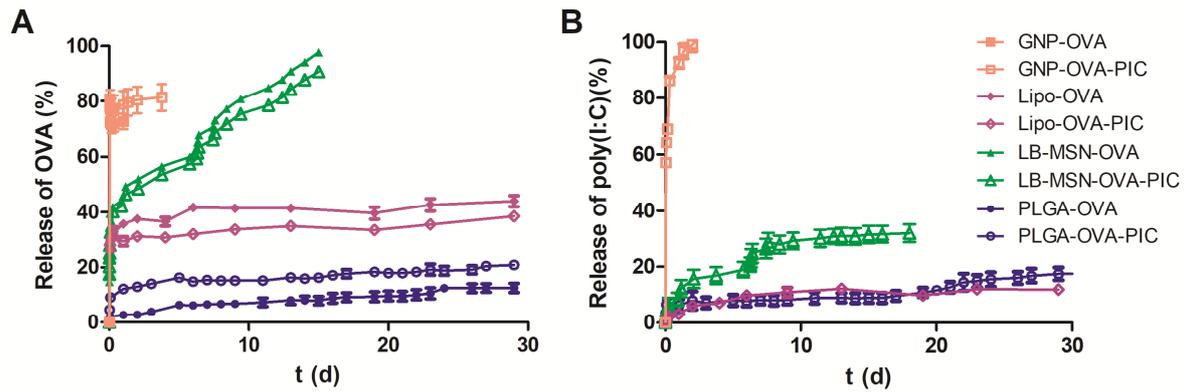
Figure 2. Release profiles of OVA (A) and poly(I:C) (B) from PLGA nanoparticles (blue/spheres), liposomes (purple/diamonds), MSNs (green/triangles) and GNPs (brown/squares) in PBS at 37 ˚C. Open and closed symbols correspond to poly(I:C)-containing and poly(I:C)-free nanoparticles, respectively. Data points represent mean ± SD, n = 3.

To determine the release properties of OVA or poly(I:C) from the nanoparticles, the particles were dispersed in PBS and the released amount of OVA or poly(I:C) was measured at regular time intervals during one month (**Fig. 2**). PLGA nanoparticles slowly released OVA and on day 30, approximately 13% and 20% of the encapsulated OVA were released from PLGA-OVA and PLGA-OVA-PIC, respectively. Poly(I:C) release followed the OVA release and approximately 20% of the encapsulated poly(I:C) was released during one month. Liposomes released about 30% OVA on the first day, followed by a slow release to 40% during one month. Approximately 12% poly(I:C) was slowly released from liposomes during one month. MSNs showed a burst release of approximately 40% OVA within the first 6 h, followed by a slower and linear release phase from 40% to almost 100% in the subsequent two weeks. The release of poly(I:C) was slower and only 30% poly(I:C) was released from LB-MSN-OVA-PIC within 15 days. GNPs showed a burst release of nearly all loaded OVA and poly(I:C) within 2 h, followed by a slow release until 4 days.

3.3. Antibody responses after intradermal immunization
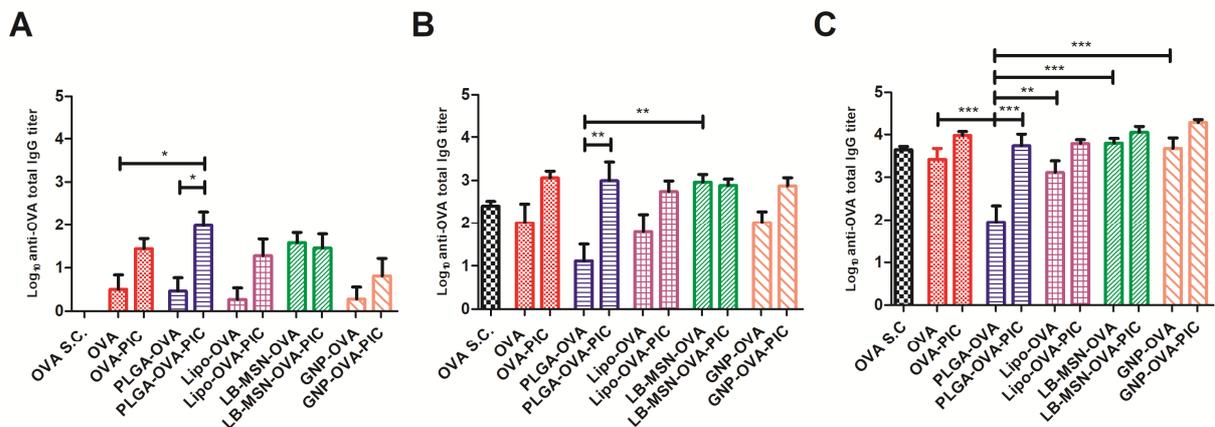
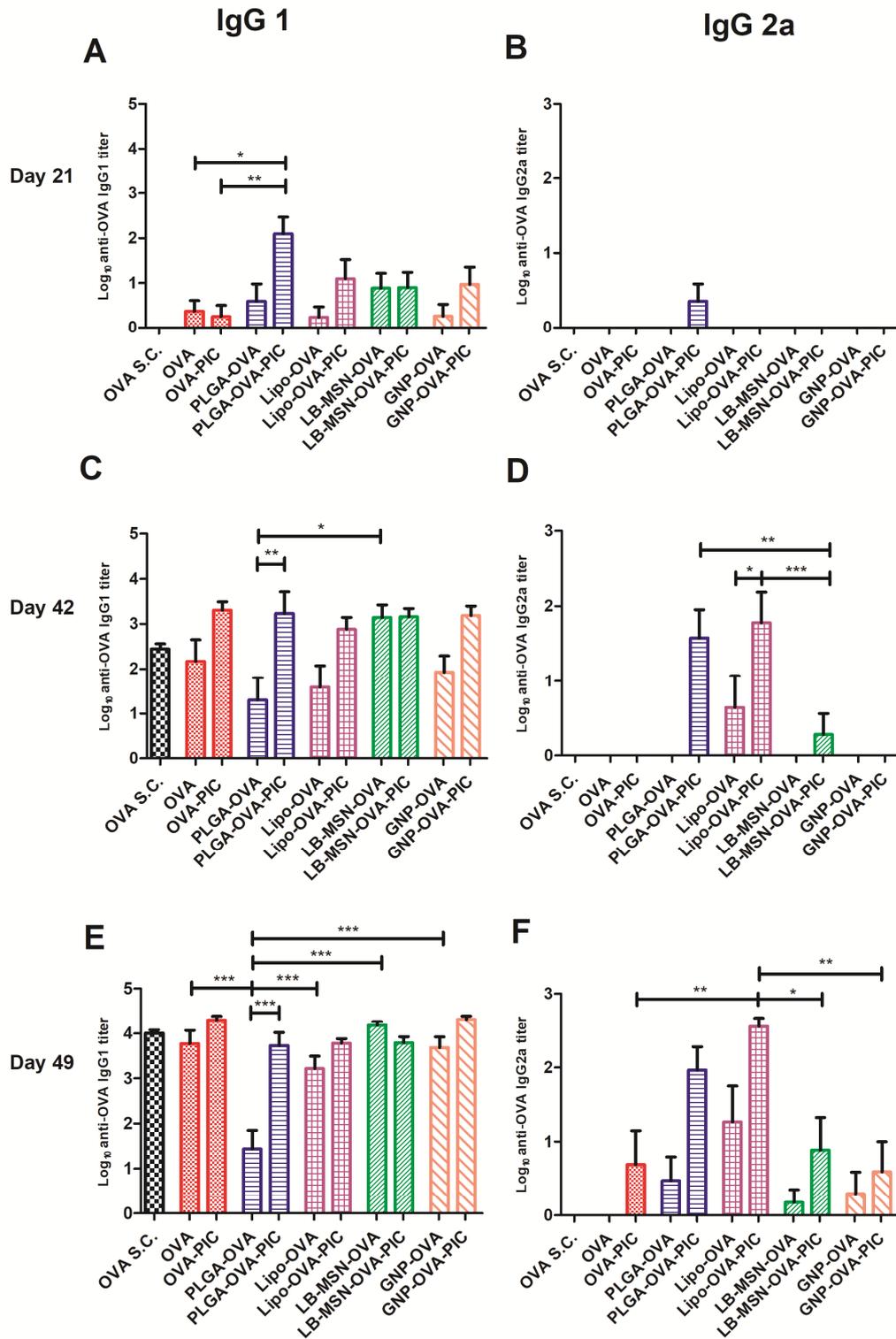

Figure 3. OVA-specific total IgG antibody titers measured in BALB/c mice on day 21 (A), day 42 (B) and day 49 (C). Bars represent mean ± SEM, n = 8. *p < 0.05, **p < 0.01, *** p < 0.001. All the formulations were injected intradermally, except the subcutaneous control of

OVA solution (OVA S.C.). Groups without a bar showed titers below the detection limit of the ELISA.

First, it was examined whether intradermal vaccination with solutions or nanoparticles containing 0.31 µg OVA with or without poly(I:C) (~0.31 µg) (**Table 1**) can induce antigen specific antibodies. The dose of antigen was chosen based on a dose response study (data not shown). As shown in **Fig. 3**, all groups, except the subcutaneous control of OVA solution, showed a detectable total IgG response on day 21, and the highest response was detected for the PLGA-OVA-PIC group (**Fig. 3A**). The total IgG levels increased after the boost on day 21 (**Fig. 3B**) and 42 (**Fig. 3C**). All studied nanoparticle formulations and OVA or OVA-poly(I:C) solutions gave similar total IgG responses, except for PLGA-OVA. These nanoparticles showed significant weaker total IgG responses on day 42 and 49, but co-encapsulation of poly(I:C) in PLGA nanoparticles increased significantly total IgG titers to similar levels observed with the other nanoparticle suspensions. In conclusion, the nano-encapsulation of OVA or co-encapsulation of OVA and poly(I:C) did not lead to enhanced total IgG titers.

Next, the subtype IgG1 and IgG2a titers were determined (**Fig. 4**). The IgG1 titers followed the trend of total IgG titers (**Fig. 4A, C, E**) and similarly the encapsulation of OVA or co-encapsulation of OVA and poly(I:C) did not increase the IgG1 response. However, the encapsulation of OVA, and particularly co-encapsulation of OVA and poly(I:C), strikingly increased the IgG2a response compared to OVA and poly(I:C) solution (**Fig. 4B, D, F**) (except GNP-OVA-PIC). Furthermore, liposomes and PLGA nanoparticles showed higher IgG2a responses than MSNs and GNPs (**Fig. 4F**). Specifically, on day 21 only PLGA-OVA-PIC induced an IgG2a response (**Fig. 4B**). After each boosting on day 21 (**Fig. 4D**) and 42 (**Fig. 4F**), there were more groups having an IgG2a response. On day 42, after prime and one boost, all OVA and poly(I:C) co-encapsulated nanoparticles, except GNP-OVA-PIC, showed an IgG2a response (**Fig. 4D**). After the second boost, on day 49, all the groups, except OVA solution, induced a measurable IgG2a response (**Fig. 4F**). These results illustrate that encapsulation of OVA especially co-encapsulation of OVA and poly(I:C) in nanoparticles is critical for enhancement of IgG2a response but the magnitude of this effect depends on the type of nanoparticles.

The higher IgG2a responses observed with liposomes and PLGA nanoparticles suggested that these formulations may be able to trigger cellular immune responses more effectively. To study the efficacy of the developed nanoparticle formulations to induce T cell mediated immunity *in vivo*, OT-I (OVA specific CD8$^+$ T cells) and OT-II (OVA specific CD4$^+$ T cells) cells were transferred into C57BL/6 mice before intradermal vaccination. Seven days after the immunization T cell responses in blood were analyzed by flow cytometry with gating strategy shown in **Fig. 5A**. Lipo-OVA-PIC evoked significant higher CD8$^+$ T cell responses than OVA and poly(I:C) solution and the other nanoparticle formulations (**Fig. 5B**), suggesting efficient induction of CTL responses by liposomes. In general, nano-encapsulation of OVA or co-encapsulation of OVA and poly(I:C) increased the CD8$^+$ response compared to OVA or OVA-poly(I:C) solution. In the case of CD4$^+$ T cell response, Lipo-OVA-PIC and LB-MSN-OVA-PIC induced the strongest response (**Fig. 5C**). OVA loaded nanoparticles induced similar CD4$^+$ response compared to OVA solution. Poly(I:C) co-encapsulation slightly increased CD4$^+$ responses compared to OVA-loaded nanoparticles but only in the case of liposomes the improvement was significant. Furthermore, the Lipo-OVA-PIC formulation induced a significantly higher CD4$^+$ response than OVA and poly(I:C) solution.

Figure 4. OVA-specific IgG1 (A, C, E) and IgG2a (B, D, F) antibody titers measured in BALB/c mice on day 21 (A, B), 42 (C, D) and 49 (E, F). Bars represent mean ± SEM, n = 8. *p < 0.05, **p < 0.01, *** p < 0.001. All the formulations were injected intradermally, except the subcutaneous control of OVA solution (OVA S.C). Groups without a bar showed titers below the detection limit of the ELISA.

3.4. T cell responses after intradermal immunization
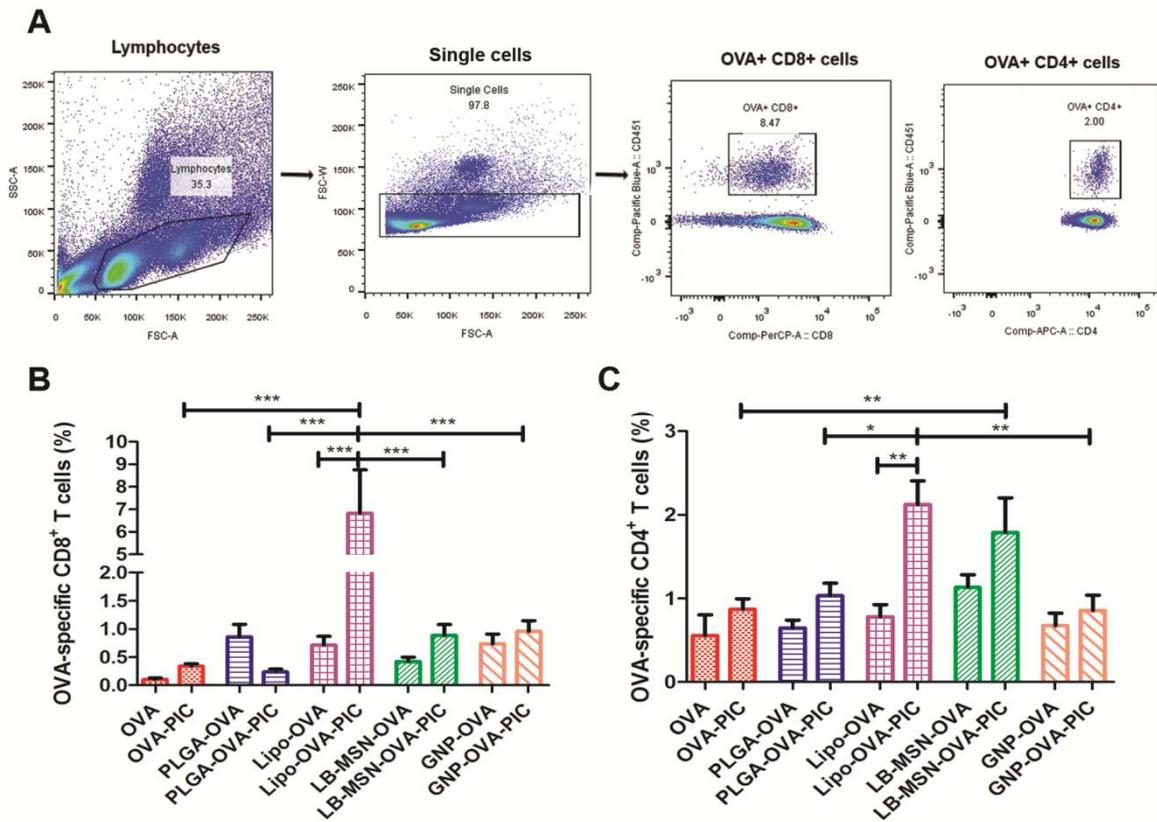
Figure 5. OVA-specific T cell responses. (A) An example of the flow cytometry gating strategy used to determine the T cell responses. Lymphocytes were gated on forward/sideward scatter, followed by the exclusion of double or adhering cells. After pregating on CD4$^+$ or CD8$^+$ T cells, the percentage of respectively OT-II and OT-I were measured by gating on CD45.1$^+$ cells. OVA specific CD8$^+$ (B) and CD4$^+$ (C) responses of transferred OT-I and OT-II cells in mouse blood 7 days after the immunization (mean ± SEM, n = 5). *p < 0.05, **p < 0.01, *** p < 0.001.

4. Discussion

In recent years, nanoparticles have been intensively investigated as vaccine delivery systems because of their advantages, such as protection of antigen from degradation, increased antigen uptake by dendritic cells and the ability to co-deliver antigen and adjuvant [10, 22, 41]. Nanoparticles also offer the possibility to adjust the type of immune response by modifying the nanoparticle characteristics such as size, surface charge and antigen release profile [10]. Numerous studies have indicated that nanoparticles can be used to modulate the immune response [9, 10, 12, 15, 17, 18, 20, 22, 25, 39, 42]. Owing to its high density of antigen-presenting cells, the skin could be an attractive site of administration of nanoparticulate vaccines. However, relatively little is known about the effect of nanoparticulate vaccines after (microneedle-mediated) intradermal vaccination. Therefore, in this study, we used hollow microneedles together with an applicator to examine the effect of nano-encapsulation of antigen and adjuvant on both the humoral and cellular response in mice. Our results showed that antigen and adjuvant loaded nanoparticles were successfully delivered intradermally in mice by using hollow microneedles together with the applicator, leading to an effective nanoparticle-dependent immune response. Furthermore, after co-encapsulation of OVA and poly(I:C) into nanoparticles, the immune response was modulated towards a Th1 direction.

Previously, the in-house developed hollow microneedle/applicator system has been used for immunization with inactivated virus [4-6]. In these studies we used hollow microneedles with a bore diameter of 20 µm. However, the system has not been used with nanoparticles with larger size (>100 nm). Therefore, the injection of nanoparticles through the system was tested *in vitro* (data not shown) prior to the *in vivo* studies presented here. These pilot studies showed that the hollow microneedles could be blocked due to occasional nanoparticle aggregation if the bore diameter was 20 µm. By increasing the bore diameter to 50 µm, this problem could be circumvented since increase of the bore diameter decreases particle obstruction in the CapTite[TM] connectors in the system. Consequently, there was no blockage or leakage of formulation during the immunization studies. The success of intradermal injection was confirmed by the formation of a bleb at the injection site after each injection. Furthermore, no adverse effects, such as erythema or skin induration, were observed at the injection site during the studies.

Intradermally administered OVA/poly(I:C) loaded nanoparticles did not increase the total IgG response compared to administration of antigen/adjuvant alone. These results indicate that the encapsulation of OVA or co-encapulation of OVA and poly(I:C) is not required for a strong IgG response following intradermal administration. This may be caused by the efficient uptake of the free antigen/adjuvant by antigen-presenting cells in epidermis and dermis (Langerhans cells and dendritic cells) and lymph nodes beneath the skin. Additionally, poly(I:C) has been shown to strongly improve CD8 responses rather than IgG responses [43-45]. In case of PLGA nanoparticles, PLGA-OVA showed even a lower total IgG response than OVA alone. This may be due to a change in the tertiary structure of OVA, either during preparation or in the acidic environment of PLGA nanoparticles during the degradation of the polymer after administration [46, 47]. Furthermore, in the current study the OVA dose was much lower (0.31 µg) compared to the dose used in previous studies (e.g. > 5 µg) [27, 42, 48]. The low dose can magnify the detrimental effect of partial OVA degradation in PLGA nanoparticles.

Our results clearly show that co-delivery of the antigen and adjuvant in nanoparticles, increased significantly the IgG2a antibody response compared to OVA/poly(I:C) solution. This indicates that the nanoparticles skewed the immune response of the antigen more towards a Th1 direction [39]. Interestingly, PLGA nanoparticles and liposomes induced higher IgG2a responses than GNPs and MSNs. There are at least two possible underlying factors that may play a role. i) The higher IgG2a response is in line with the slower release of OVA and poly(I:C) from PLGA nanoparticles and liposomes. The sustained release can allow the co-processing of adjuvant and antigen within the same antigen-presenting cell, which is suggested to be crucial for a higher IgG2a response [15, 19, 22]. Differences in release behavior of OVA/poly(I:C) between the nanoparticles may stem from the differences in the location of the antigen and adjuvant in nanoparticles and in the strength of the interaction between antigen/adjuvant and the nanoparticle matrix. On the one hand, in PLGA nanoparticles and liposomes the antigen/adjuvant is mixed with nanoparticle precursors during synthesis, and the antigen/adjuvant is expected to be localized inside the matrix of PLGA nanoparticles or in the aqueous core layer of liposomes. Therefore, it is likely that the antigen/adjuvant is mostly released after the nanoparticles are taken up and processed by antigen-presenting cells or degraded. On the other hand, with GNPs and MSNs the loading of antigen/adjuvant is done post-synthesis through adsorption of the antigen/adjuvant onto the surface of nanoparticles, presumably based on electrostatic interactions. In addition, in MSNs interactions are expected to occur also between OVA/poly(I:C) and the stabilizing lipid bilayer. Antigen and adjuvant loaded in MSNs and GNPs are sensitive to environmental conditions, such as salts and endogenous proteins present in the skin tissue, that can accelerate

the release. As a result, the release of antigen/adjuvant from MSNs and GNPs can be faster than that from PLGA nanoparticles and liposomes, as suggested by the *in vitro* release data. Premature release can consequently lead to separate uptake and processing of antigen and adjuvant by different antigen-presenting cells. ii) The size of PLGA nanoparticles and liposomes (less than 200 nm) is substantially smaller than that of MSNs and GNPs (above 500 nm). Although single MSNs had a size below 200 nm, as shown by TEM images [33], DLS showed a larger diameter, indicating the aggregation of MSNs. Smaller particles with a size below 200 nm are expected to be more efficiently taken up by dendritic cells than bigger particles [16]. Moreover, large nanoparticles (500-2000 nm) have been shown to be mostly associated with dendritic cells at the injection site after intradermal delivery, while small (20-200 nm) nanoparticles are able to drain to lymph nodes and target there the dendritic cells [49]. Therefore, the higher IgG2a response induced by the OVA/poly(I:C) loaded PLGA nanoparticles and liposomes could be due to their better uptake by dendritic cells and faster trafficking to the lymph nodes.

As IgG2a levels merely give an indication of the extent of IFN-γ induced isotype switching, we also directly assessed the capacity of each type of nanoparticulate formulation to induce $CD8^+$ and $CD4^+$ T cell responses in OT cell transferred mice. The number of transferred OT cells were kept low as an excess of transgenic T-cells have previously been shown to alter the T-cell response [50]. Our results showed that the Lipo-OVA-PIC formulation showed an exceptional high capacity to induce both $CD8^+$ and $CD4^+$ T cell responses, in line with the data from previous studies [18, 48]. The DOTAP based cationic liposomes have been shown to be very effective for the induction of CTL responses [9, 12, 18], as the cationic lipids promote the activation and maturation of dendritic cells and subsequently the T cell priming. Moreover, EggPC, the main lipid component of the present liposomes, has been shown to facilitate antigen presentation by enhancing peptide binding to MHC class II molecules [51]. So, the superior immune responses of liposomes may be caused by the properties of the lipids.

As explained above, MSNs and GNPs may not be able to enhance the immune response because of their fast release of OVA/poly(I:C) and large size. In case of PLGA-OVA-PIC group, our data showed that the co-encapsulation of OVA and poly(I:C) did not increase the T cell responses. This is in contrast to previous reports [12-14], which have shown that the co-encapsulation of OVA and poly(I:C) in PLGA nanoparticles can induce a strong CTL response after intramuscular or subcutaneous vaccination. This indicates that vaccine formulations that provide potent immune responses after intramuscular or subcutaneous administration, may be less suitable for intradermal delivery, reemphasizing the need for route-specific optimization of vaccine formulations [12, 18, 42]. Furthermore, targeting of different skin layers may also affect immune responses, as shown in previous studies [52, 53]. Nowadays, there is an increasing need of efficient Th1/CTL immune response, for example, in therapeutic vaccinations for cancer [13, 17, 45] and intracellular pathogens [14, 21]. Our results indicate that cationic liposomes are very promising nano-carriers to induce a superior Th1/CTL immune response compared to the other nanoparticles following hollow microneedle-mediated intradermal administration.

5. Conclusions

OVA and poly(I:C) loaded PLGA nanoparticles, liposomes, MSNs and GNPs were successfully developed and compared for hollow microneedle-mediated intradermal immunization in mice. The encapsulation of OVA and co-encapsulation of OVA and poly(I:C) induced a strikingly higher IgG2a antibody response than OVA/poly(I:C) solution, but the type of nanoparticle has a major effect on response. PLGA nanoparticles and especially

cationic liposomes induced the highest IgG2a, CD8$^+$ T cell and CD4$^+$ T cell responses, suggesting their superiority for intradermal vaccination. Finally, our study demonstrated that the in house developed hollow microneedle/applicator system is an excellent tool for nanoparticle-based intradermal vaccination and to screen different intradermal vaccine formulations.

Acknowledgements

References

[1] N. Li, L.H. Peng, X. Chen, S. Nakagawa, J.Q. Gao, Transcutaneous vaccines: novel advances in technology and delivery for overcoming the barriers, Vaccine, 29 (2011) 6179-6190.

[2] K. van der Maaden, W. Jiskoot, J. Bouwstra, Microneedle technologies for (trans)dermal drug and vaccine delivery, J. Control. Release 161 (2012) 645-655.

[3] F.J. Verbaan, S.M. Bal, D.J. van den Berg, J.A. Dijksman, M. van Hecke, H. Verpoorten, A. van den Berg, R. Luttge, J.A. Bouwstra, Improved piercing of microneedle arrays in dermatomed human skin by an impact insertion method, J. Control. Release 128 (2008) 80-88.

[4] K. van der Maaden, S.J. Trietsch, H. Kraan, E.M. Varypataki, S. Romeijn, R. Zwier, H.J. van der Linden, G. Kersten, T. Hankemeier, W. Jiskoot, J. Bouwstra, Novel hollow microneedle technology for depth-controlled microinjection-mediated dermal vaccination: a study with polio vaccine in rats, Pharm. Res. 31 (2014) 1846-1854.

[5] P. Schipper, K. van der Maaden, S. Romeijn, C. Oomens, G. Kersten, W. Jiskoot, J. Bouwstra, Determination of depth-dependent intradermal immunogenicity of adjuvanted inactivated polio vaccine delivered by microinjections via hollow microneedles, Pharm. Res. 33 (2016) 2269-2279.

[6] P. Schipper, K. van der Maaden, S. Romeijn, C. Oomens, G. Kersten, W. Jiskoot, J. Bouwstra, Repeated fractional intradermal dosing of an inactivated polio vaccine by a single hollow microneedle leads to superior immune responses, J. Control. Release 242 (2016) 141-147.

[7] M.L. De Temmerman, J. Rejman, J. Demeester, D.J. Irvine, B. Gander, S.C. De Smedt, Particulate vaccines: on the quest for optimal delivery and immune response, Drug Discov. Today, 16 (2011) 569-582.

[8] S.G. Reed, M.T. Orr, C.B. Fox, Key roles of adjuvants in modern vaccines, Nat. Med. 19 (2013) 1597-1608.

[9] N. Benne, J. van Duijn, J. Kuiper, W. Jiskoot, B. Slutter, Orchestrating immune responses: How size, shape and rigidity affect the immunogenicity of particulate vaccines, J. Control. Release 234 (2016) 124-134.

[10] T. Akagi, M. Baba, M. Akashi, Biodegradable nanoparticles as vaccine adjuvants and delivery systems: regulation of immune responses by nanoparticle-based vaccine, in: S. Kunugi, T. Yamaoka (Eds.) Polymers in Nanomedicine 2012, pp. 31-64.

[11] L. Zhao, A. Seth, N. Wibowo, C.X. Zhao, N. Mitter, C.Z. Yu, A.P.J. Middelberg, Nanoparticle vaccines, Vaccine 32 (2014) 327-337.

[12] E.M. Varypataki, A.L. Silva, C. Barnier-Quer, N. Collin, F. Ossendorp, W. Jiskoot, Synthetic long peptide-based vaccine formulations for induction of cell mediated immunity: A comparative study of cationic liposomes and PLGA nanoparticles, J. Control. Release 226 (2016) 98-106.

[13] S. Hamdy, O. Molavi, Z.S. Ma, A. Haddadi, A. Alshamsan, Z. Gobti, S. Elhasi, J. Samuel, A. Lavasanifar, Co-delivery of cancer-associated antigen and Toll-like receptor 4 ligand in PLGA nanoparticles induces potent CD8(+) T cell-mediated anti-tumor immunity, Vaccine 26 (2008) 5046-5057.

[14] C.S.W. Chong, M. Cao, W.W. Wong, K.P. Fischer, W.R. Addison, G.S. Kwon, D.L. Tyrrell, J. Samuel, Enhancement of T helper type 1 immune responses against hepatitis B virus core antigen by PLGA nanoparticle vaccine delivery, J. Control. Release 102 (2005) 85-99.

[15] E. Schlosser, M. Mueller, S. Fischer, S. Basta, D.H. Busch, B. Gander, M. Groettrup, TLR ligands and antigen need to be coencapsulated into the same biodegradable microsphere for the generation of potent cytotoxic T lymphocyte responses, Vaccine 26 (2008) 1626-1637.

[16] M.O. Oyewumi, A. Kumar, Z.R. Cui, Nano-microparticles as immune adjuvants: correlating particle sizes and the resultant immune responses, Expert Rev. Vaccines 9 (2010) 1095-1107.

[17] Y. Fan, J.J. Moon, Nanoparticle drug delivery systems designed to improve cancer vaccines and immunotherapy, Vaccines (Basel) 3 (2015) 662-685.

[18] E.M. Varypataki, K. van der Maaden, J. Bouwstra, F. Ossendorp, W. Jiskoot, Cationic liposomes loaded with a synthetic long peptide and poly(I:C): a defined adjuvanted vaccine for induction of antigen-specific T cell cytotoxicity, AAPS J. 17 (2015) 216-226.

[19] A.L. Silva, R.A. Rosalia, A. Sazak, M.G. Carstens, F. Ossendorp, J. Oostendorp, W. Jiskoot, Optimization of encapsulation of a synthetic long peptide in PLGA nanoparticles: low-burst release is crucial for efficient CD8(+) T cell activation, Eur. J. Pharm. Biopharm. 83 (2013) 338-345.

[20] R.A. Rosalia, L.J. Cruz, S. van Duikeren, A.T. Tromp, A.L. Silva, W. Jiskoot, T. de Gruijl, C. Lowik, J. Oostendorp, S.H. van der Burg, F. Ossendorp, CD40-targeted dendritic cell delivery of PLGA-nanoparticle vaccines induce potent anti-tumor responses, Biomaterials 40 (2015) 88-97.

[21] M. Zaric, O. Lyubomska, O. Touzelet, C. Poux, S. Al-Zahrani, F. Fay, L. Wallace, D. Terhorst, B. Malissen, S. Henri, U.F. Power, C.J. Scott, R.F. Donnelly, A. Kissenpfennig, Skin dendritic cell targeting via microneedle arrays laden with antigen-encapsulated poly-D,L-lactide-co-glycolide nanoparticles induces efficient antitumor and antiviral immune responses, ACS Nano 7 (2013) 2042-2055.

[22] A.M. Hafner, B. Corthesy, H.P. Merkle, Particulate formulations for the delivery of poly(I:C) as vaccine adjuvant, Adv. Drug Deliv. Rev. 65 (2013) 1386-1399.

[23] A.L. Silva, R.A. Rosalia, E. Varypataki, S. Sibuea, F. Ossendorp, W. Jiskoot, Poly-(lactic-co-glycolic-acid)-based particulate vaccines: Particle uptake by dendritic cells is a key parameter for immune activation, Vaccine 33 (2015) 847-854.

[24] A.L. Silva, P.C. Soema, B. Slutter, F. Ossendorp, W. Jiskoot, PLGA particulate delivery systems for subunit vaccines: Linking particle properties to immunogenicity, Human vaccines & immunotherapeutics, 12 (2016) 1056-1069.

[25] D. Christensen, K.S. Korsholm, P. Andersen, E.M. Agger, Cationic liposomes as vaccine adjuvants, Expert Rev. Vaccines 10 (2011) 513-521.

[26] K.T. Mody, A. Popat, D. Mahony, A.S. Cavallaro, C.Z. Yu, N. Mitter, Mesoporous silica nanoparticles as antigen carriers and adjuvants for vaccine delivery, Nanoscale 5 (2013) 5167-5179.

[27] D. Mahony, A.S. Cavallaro, F. Stahr, T.J. Mahony, S.Z. Qiao, N. Mitter, Mesoporous silica nanoparticles act as a self-adjuvant for ovalbumin model antigen in mice, Small 9 (2013) 3138-3146.

[28] A.O. Elzoghby, W.M. Samy, N.A. Elgindy, Protein-based nanocarriers as promising drug and gene delivery systems, J. Control. Release 161 (2012) 38-49.

[29] M.S. Sudheesh, S.P. Vyas, D.V. Kohli, Nanoparticle-based immunopotentiation via tetanus toxoid-loaded gelatin and aminated gelatin nanoparticles, Drug. Deliv. 18 (2011) 320-330.

[30] A.O. Elzoghby, Gelatin-based nanoparticles as drug and gene delivery systems: Reviewing three decades of research, J. Control. Release 172 (2013) 1075-1091.

[31] B. Slutter, S.M. Bal, I. Que, E. Kaijzel, C. Lowik, J. Bouwstra, W. Jiskoot, Antigen-adjuvant nanoconjugates for nasal vaccination: an improvement over the use of nanoparticles? Mol. Pharm. 7 (2010) 2207-2215.

[32] A.D. Bangham, M.M. Standish, J.C. Watkins, Diffusion of univalent ions across the lamellae of swollen phospholipids, J. Mol. Biol. 13 (1965) 238-252.

[33] J. Tu, A.L. Boyle, H. Friedrich, P.H. Bomans, J. Bussmann, N.A. Sommerdijk, W. Jiskoot, A. Kros, Mesoporous silica nanoparticles with large pores for the encapsulation and release of proteins, ACS Appl. Mater. Interfaces 8 (2016) 32211-32219.

[34] E.C. Dengler, J. Liu, A. Kerwin, S. Torres, C.M. Olcott, B.N. Bowman, L. Armijo, K. Gentry, J. Wilkerson, J. Wallace, X. Jiang, E.C. Carnes, C.J. Brinker, E.D. Milligan, Mesoporous silica-supported lipid bilayers (protocells) for DNA cargo delivery to the spinal cord, J. Control. Release 168 (2013) 209-224.

[35] J. Tu, G. Du, M. Reza Nejadnik, J. Monkare, K. van der Maaden, P.H.H. Bomans, N. Sommerdijk, B. Slutter, W. Jiskoot, J.A. Bouwstra, A. Kros, Mesoporous silica nanoparticle-coated microneedle arrays for intradermal antigen delivery, Pharm. Res. 34 (2017) 1693-1706.

[36] H. Wang, M.B. Hansen, D.W. Lowik, J.C. van Hest, Y. Li, J.A. Jansen, S.C. Leeuwenburgh, Oppositely charged gelatin nanospheres as building blocks for injectable and biodegradable gels, Adv. Mater. 23 (2011) H119-124.

[37] S. Azarmi, Y. Huang, H. Chen, S. McQuarrie, D. Abrams, W. Roa, W.H. Finlay, G.G. Miller, R. Lobenberg, Optimization of a two-step desolvation method for preparing gelatin nanoparticles and cell uptake studies in 143B osteosarcoma cancer cells, J. Pharm. Pharm. Sci. 9 (2006) 124-132.

[38] K. van der Maaden, S.J. Trietsch, H. Kraan, E.M. Varypataki, S. Romeijn, R. Zwier, H.J. van der Linden, G. Kersten, T. Hankemeier, W. Jiskoot, J. Bouwstra, Novel hollow microneedle technology for depth-controlled microinjection-mediated dermal vaccination: a study with polio vaccine in rats, Pharm. Res. 31 (2014) 1846-1854.

[39] B. Slutter, S.M. Bal, Z. Ding, W. Jiskoot, J.A. Bouwstra, Adjuvant effect of cationic liposomes and CpG depends on administration route, J. Control. Release 154 (2011) 123-130.

[40] A.K. Bajpai, J. Choubey, Design of gelatin nanoparticles as swelling controlled delivery system for chloroquine phosphate, J. Mater. Sci. Mater. Med. 17 (2006) 345-358.

[41] L.J. Peek, C.R. Middaugh, C. Berkland, Nanotechnology in vaccine delivery, Adv. Drug Deliv. Rev. 60 (2008) 915-928.

[42] D. Mohanan, B. Slutter, M. Henriksen-Lacey, W. Jiskoot, J.A. Bouwstra, Y. Perrie, T.M. Kundig, B. Gander, P. Johansen, Administration routes affect the quality of immune responses: A cross-sectional evaluation of particulate antigen-delivery systems, J. Control. Release 147 (2010) 342-349.

[43] H. Mitsui, T. Watanabe, H. Saeki, K. Mori, H. Fujita, Y. Tada, A. Asahina, K. Nakamura, K. Tamaki, Differential expression and function of Toll-like receptors in Langerhans cells: comparison with splenic dendritic cells, J. Invest. Dermatol. 122 (2004) 95-102.

[44] H. Fujita, A. Asahina, H. Mitsui, K. Tamaki, Langerhans cells exhibit low responsiveness to double-stranded RNA, Biochem. Biophys. Res. Commun. 319 (2004) 832-839.

[45] R. Ammi, J. De Waele, Y. Willemen, I. Van Brussel, D.M. Schrijvers, E. Lion, E.L.J. Smits, Poly(I:C) as cancer vaccine adjuvant: Knocking on the door of medical breakthroughs, Pharmacol. Therapeut. 146 (2015) 120-131.

[46] K. Fu, D.W. Pack, A.M. Klibanov, R. Langer, Visual evidence of acidic environment within degrading poly(lactic-co-glycolic acid) (PLGA) microspheres, Pharm. Res. 17 (2000) 100-106.

[47] M. van de Weert, W.E. Hennink, W. Jiskoot, Protein instability in poly(lactic-co-glycolic acid) microparticles, Pharm. Res. 17 (2000) 1159-1167.

[48] S.M. Bal, S. Hortensius, Z. Ding, W. Jiskoot, J.A. Bouwstra, Co-encapsulation of antigen and Toll-like receptor ligand in cationic liposomes affects the quality of the immune response in mice after intradermal vaccination, Vaccine 29 (2011) 1045-1052.

[49] V. Manolova, A. Flace, M. Bauer, K. Schwarz, P. Saudan, M.F. Bachmann, Nanoparticles target distinct dendritic cell populations according to their size, Eur. J. Immunol. 38 (2008) 1404-1413.

[50] V.P. Badovinac, J.S. Haring, J.T. Harty, Initial T cell receptor transgenic cell precursor frequency dictates critical aspects of the CD8(+) T cell response to infection, Immunity 26 (2007) 827-841.

[51] R.W. Roof, I.F. Luescher, E.R. Unanue, Phospholipids enhance the binding of peptides to class II major histocompatibility molecules, Proc. Natl. Acad. Sci. U S A 87 (1990) 1735-1739.

[52] C. Liard, S. Munier, M. Arias, A. Joulin-Giet, O. Bonduelle, D. Duffy, R.J. Shattock, B. Verrier, B. Combadiere, Targeting of HIV-p24 particle-based vaccine into differential skin layers induces distinct arms of the immune responses, Vaccine 29 (2011) 6379-6391.

[53] C. Levin, O. Bonduelle, C. Nuttens, C. Primard, B. Verrier, A. Boissonnas, B. Combadiere, Critical role for skin-derived migratory DCs and langerhans cells in TFH and GC responses after Intradermal immunization, J. Invest. Dermatol. 137 (2017) 1905-1913.

Chapter 5

Immunogenicity of diphtheria toxoid and poly(I:C) loaded cationic liposomes after hollow microneedle-mediated intradermal injection in mice

Guangsheng Du[1], Mara Leone[1], Stefan Romeijn[1], Gideon Kersten[1,2], Wim Jiskoot[1], Joke A. Bouwstra[1]*

[1] Division of BioTherapeutics, Leiden Academic Centre for Drug Research, Leiden University, Leiden, 2300 RA, The Netherlands

[2] Department of Analytical Development and Formulation, Intravacc, Bilthoven, 3720 AL, The Netherlands

Abstract

In this study, we aimed to investigate the immunogenicity of cationic liposomes loaded with diphtheria toxoid (DT) and poly(I:C) after hollow microneedle-mediated intradermal vaccination in mice. The following liposomal formulations were studied: DT loaded liposomes, a mixture of free DT and poly(I:C)-loaded liposomes, a mixture of DT-loaded liposomes and free poly(I:C), and liposomal formulations with DT and poly(I:C) either individually or co-encapsulated in the liposomes. Reference groups were DT solution adjuvanted with or without poly(I:C) (DT/poly(I:C)). The liposomal formulations were characterized in terms of particle size, zeta potential, loading and release of DT and poly(I:C). After intradermal injection of BALB/c mice with the formulations through a hollow microneedle, the immunogenicity was assessed by DT-specific ELISAs. All formulations induced similar total IgG and IgG1 titers. However, all the liposomal groups containing both DT and poly(I:C) showed enhanced IgG2a titers compared to DT/poly(I:C) solution, indicating that the immune response was skewed towards a Th1 direction. This enhancement was similar for all liposomal groups that contain both DT and poly(I:C) in the formulations. Our results reveal that a mixture of DT encapsulated liposomes and poly(I:C) encapsulated liposomes have a similar effect on the antibody responses as DT and poly(I:C) co-encapsulated liposomes. These findings may have implications for future design of liposomal vaccine delivery systems.

Keywords : Immunogenicity, diphtheria toxoid, poly(I:C), liposomes, hollow microneedle, intradermal vaccination

Immunogenicity of diphtheria toxoid and poly(I:C) loaded cationic liposomes after hollow microneedle-mediated intradermal injection in mice

1. Introduction

Vaccination has become the most effective method for preventing infectious diseases, having led to the eradication of smallpox and severe restriction of other devastating diseases such as polio and measles [1, 2]. However, there is still a need for new and better vaccines against emerging infectious diseases [3]. Nowadays, vaccination gains increasing attention also for therapeutic use against established diseases such as cancer and chronic auto-immune disorders [4]. Most vaccines are delivered by intramuscular or subcutaneous injection. However, these injections need special training and can cause pain [5]. To avoid the drawbacks of the hypodermic needles, microneedles have been developed [6]. Microneedles are micro-sized needle structures with a length shorter than 1 mm and can be used to penetrate skin barrier in a non-invasive and pain-free way [7-9]. Owing to the large number of antigen presenting cells in viable dermis and epidermis, dose-sparing may be achieved [10, 11].

Traditional vaccines are derived from attenuated organisms or inactivated pathogens and toxins. Attenuated vaccines have safety concerns as they may revert back to their virulent form [12]. Inactivated vaccines like subunit antigens are safer but they are generally less immunogenic [1, 12]. To enhance and modify the immune response, immune modulators or nanoparticle delivery systems can be used [13]. Nanoparticles are expected to improve the immunogenicity of antigens by protecting the antigens from degradation, increasing their uptake by antigen-presenting cells and co-delivering antigens and immune modulators [14].

Liposomes have been studied frequently because of their excellent biocompatibility and biodegradability [15]. Studies have shown that co-formulating antigen and immune modulators in liposomes can affect the quality of immune response after intradermal vaccination [15-23]. One recent study showed that co-encapsulation of OVA and poly(I:C), a TLR3 ligand, in 1,2-dioleoyl-3-trimethylammonium-propane chloride (DOTAP)-based cationic liposomes significantly increased the IgG2a response (Th1 type) and the CD8$^+$ T cell response compared to OVA and poly(I:C) solutions [17]. Another study in a human skin explant model showed that a melanoma-associated antigen and immune modulator co-encapsulated liposomes induced a higher CD8$^+$ T cell response compared to the co-administration of antigen loaded liposomes and free solution of the immune modulator [21]. These results are noteworthy, as nowadays there is an increasing need for potent cellular immune responses, e.g., for immunotherapy of cancer [14, 24, 25] and intracellular pathogens [26, 27]. However, it is not yet well understood whether the antigen and immune modulator need to be co-encapsulated in liposomes, or they can similarly modulate the immune response when encapsulated individually in liposomes.

In the present study, we aimed to study the immunogenicity of diphtheria toxoid (DT) and poly(I:C) loaded liposomes after intradermal delivery. DT and poly(I:C) were used as a model antigen and immune modulator, respectively. DT and poly(I:C) were individually encapsulated or co-encapsulated into DOTAP-based cationic liposomes. The prepared liposomal formulations were injected into mice by using hollow microneedles. The IgG1 and IgG2a titers, which are indications of a Th2 and a Th1 type immune response, respectively [18], were determined. The results revealed that the liposomal formulations skewed the immune response towards a Th1 direction, no matter whether DT and poly(I:C) were encapsulated individually or co-encapsulated in liposomes, as compared to DT/poly(I:C) solutions.

2. Materials and methods

2.1. Materials

DT (batch 04-44, 1 µg equal to 0.3 Lf) and diphtheria toxin were provided by Intravacc (Bilthoven, The Netherlands). Aluminum phosphate was purchased from Brenntag (Ballerup, Denmark). Egg phosphatidylcholine (EggPC), DOTAP and 1,2-dioleoyl-sn-glycero-3-phosphoethanolamine (DOPE) were ordered from Avanti Polar Lipids (Alabaster, AL). Polyinosinic-polycytidylic acid (poly(I:C)) (low molecular weight) and its rhodamine-labeled version were purchased from Invivogen (Toulouse, France). Foetal bovine serum (FBS), M199 medium (with Hanks' salts and L-glutamin), bovine serum albumin (BSA) and hydrofluoric acid ≥48% were ordered from Sigma-Aldrich (Zwijndrecht, The Netherlands). Glucose solution, L-Glutamine (200 mM), penicillin-streptomycin (10000 U/ml) and 1-step^{TM} ultra 3,3',5,5'-tetramethylbenzidine (TMB) were obtained from Thermo-Fisher Scientific (Waltham, MA). HRP-conjugated goat anti-mouse total IgG, IgG1 and IgG2a were purchased from Southern Biotech (Birmingham, AL). Sulfuric acid (95-98%) was obtained from JT Baker (Deventer, The Netherlands). VivaSpin 2 and 500 centrifugal concentrators (PES membrane, MWCO 1000 kDa) were obtained from Sartorius Stedim (Nieuwegein, The Netherlands). Sterile phosphate buffered saline (PBS, 163.9 mM Na$^+$, 140.3 mM Cl$^-$, 8.7 mM HPO$_4^{2-}$, 1.8 mM H$_2$PO^{4-}, pH 7.4) was obtained from Braun (Oss, The Netherlands). 10 mM PB (7.7 mM Na$_2$HPO$_4$, 2.3 mM NaH$_2$PO$_4$, pH 7.4) was prepared in the laboratory. All the other chemicals used were of analytical grade and Milli-Q water (18 MΩ/cm, Millipore Co.) was used for the preparation of all solutions.

2.2. Preparation of liposomes

Liposomes were prepared by thin-film hydration followed by extrusion, as reported earlier [23]. EggPC (25 mg/ml), DOPE (25 mg/ml) and DOTAP (25 mg/ml) in chloroform were mixed in a molar ratio of 9:1:2.5 in a round bottom flask. The organic solvent was evaporated by using a rotary evaporator (Buchi rotavapor R210, Flawil, Switzerland) for 1 h at 40 °C and 120 rpm. To prepare DT encapsulated liposomes (Lipo-DT), the lipid film was hydrated with 0.25 mg/ml DT dissolved in 10 mM PB (pH 7.4) by vortexing for 10 s, resulting in a 12.5 mg/ml lipid suspension. To prepare poly(I:C) encapsulated liposomes (Lipo-PIC), the lipid film was hydrated with 0.25 mg/ml poly(I:C) solution (containing 0.5% (w/w) rhodamine-labeled poly(I:C)). To prepare DT and poly(I:C) co-encapsulated liposomes (Lipo-DT-PIC), after lipid film hydration with DT solution, 0.25 mg/ml poly(I:C) (containing 0.5% (w/w) rhodamine-labeled poly(I:C)) dissolved in 10 mM PB (pH 7.4) was added slowly (2 µl/min) into the lipid suspension by using a syringe pump (NE-300, Prosense, Oosterhout, The Netherlands). Next, the lipid vesicles were extruded (LIPEX^{TM} extruder, Northern Lipids, Burnaby, Canada) four times through a carbonate filter with a pore size of 400 nm and another four times through a filter with a pore size of 200 nm (Nucleopore Millipore, Amsterdam, The Netherlands). To remove the DT/poly(I:C) not associated with liposomes, the suspension was transferred into VivaSpin 2 centrifugal concentrators (1000 kDa MWCO) and centrifuged (Allegra X-12R, Beckman Coulter, Indianapolis, IN) for 6 h (350 g, 22 °C). Finally, the liposomes were washed with 10 mM PB and kept at 4 °C in the refrigerator prior to use. The filtrates, containing the free DT/poly(I:C), were collected for determination of loading efficiency of DT and poly(I:C).

2.3. Characterization of liposomal formulations

2.3.1. Particle size and zeta potential measurements

The particle size of the liposomes was measured by dynamic light scattering by using a Nano ZS$^®$ zetasizer (Malvern Instruments, Worcestershire, U.K.). The zeta potential of liposomes

was measured by the same instrument by using laser Doppler velocimetry. The liposomes were diluted with 10 mM PB (pH 7.4) to a concentration of 25 µg/ml for the measurements. The samples were measured 3 times with 10 runs for each measurement.

2.3.2. Determination of encapsulation efficiency (EE) and loading capacity (LC) of DT/poly(I:C) in liposomes

To determine the EE and LC of DT and poly(I:C), the intrinsic fluorescence intensity of DT (λ_{ex} 280 nm/ λ_{em} 320 nm) and fluorescence intensity of rhodamine labeled poly(I:C) (λ_{ex} 545 nm/ λ_{em} 576 nm) in the purification filtrates were measured by using a Tecan M1000 plate reader (Männedorf, Switzerland). The EE and LC were calculated by using **Eq. (1)** and **Eq. (2)** as below:

$$EE = \frac{M_{loaded\ DT/poly(I:C)}}{M_{total\ DT/poly(I:C)}} \times 100\ \% \qquad (1)$$

$$LC = \frac{M_{loaded\ DT/poly(I:C)}}{M_{Liposomes+DT+poly(I:C)}} \times 100\ \% \qquad (2)$$

Where $M_{loaded\ DT/poly(I:C)}$ represents the mass of encapsulated DT or poly(I:C), $M_{total\ DT/poly(I:C)}$ is the total amount of DT or poly(I:C) added to the formulations and $M_{liposomes+DT+poly(I:C)}$ is the total weight of liposomes, DT and poly(I:C).

2.3.3 *In vitro* release of DT and poly(I:C) from liposomes

To study the *in vitro* release of DT and poly(I:C) from Lipo-DT, Lipo-PIC and Lipo-DT-PIC, the liposomes (containing about 80 µg/ml DT with or without 80 µg/ml poly(I:C)) were dispersed in PBS and shaken with a speed of 550 rpm at 37 ℃ by using an Eppendorf thermomixer (Nijmegen, The Netherlands). At predetermined time points, 300 µl liposomes were transferred into the VivaSpin 500 concentrators and centrifuged for 30 min with a speed of 350 g. After the centrifugation, fresh PBS with the same volume as the filtrates was added back to the liposomes. The concentration of DT and poly(I:C) in the filtrates was determined by measuring the intrinsic fluorescence intensity of DT (λ_{ex} 280 nm/λ_{em} 320 nm) and fluorescence intensity of rhodamine labeled poly(I:C) (λ_{ex} 545 nm/λ_{em} 576 nm), respectively, by using a Tecan M1000 plate reader.

2.3.4 Adsorption of free DT or poly(I:C) on liposomes loaded with the other active ingredient

To investigate the adsorption of free DT to Lipo-PIC, DT was mixed with Lipo-PIC in PBS, resulting in a concentration of 31 µg/ml for both DT and poly(I:C). The samples were incubated in the Eppendorf thermomixer (Nijmegen, The Netherlands) at 37 °C with a speed of 300 rpm. To investigate the adsorption of free poly(I:C) to Lipo-DT, poly(I:C) was mixed with Lipo-DT in PBS, resulting in a concentration of 31 µg/ml for both DT and poly(I:C). After 4 or 24 h, the samples were transferred to VivaSpin 500 centrifugal concentrators (PES membrane, 1000 kDa MWCO) and centrifuged for 30 min with a speed of 350 g. The DT or poly(I:C) in the filtrates was quantified by measuring the intrinsic fluorescence intensity of DT (λ_{ex} 280 nm/ λ_{em} 320 nm) or fluorescence intensity of rhodamine labeled poly(I:C) (λ_{ex} 545 nm/ λ_{em} 576 nm), respectively. The adsorption efficiency of DT or poly(I:C) was calculated according to **Eq. (3)** as follow:

$$\text{Adsorption efficieny }\% = (1 - \frac{M_{DT/poly(I:C)\ in\ filtrates}}{M_{DT/poly(I:C)\ total}}) \times 100\ \% \qquad (3)$$

where $M_{DT/poly(I:C)\ in\ filtrates}$ represents the mass of DT or poly(I:C) in filtrates after centrifugation, and $M_{DT/poly(I:C)\ total}$ is the total mass of DT or poly(I:C) added.

2.4. Hollow microneedles and applicator

The hollow microneedles were prepared by hydrofluoric acid etching of fused silica capillaries [28, 29]. Briefly, silica capillaries (Polymicro, Phoenix AZ, 375 µm outer diameter, 50 µm inner diameter) were cut into 4-cm pieces and filled with silicone oil in a vacuum oven (100 °C) overnight. The silicone oil-filled capillaries were etched into hollow microneedles by immersing their ends in ≥48% hydrofluoric acid for 4 h at room temperature. Finally, the polyimide coating on the microneedles was removed by dipping the microneedles into hot sulfuric acid (250 °C) for 5 min.

To reproducibly insert hollow microneedles into mouse skin, a hollow microneedle applicator developed in our lab was used [28, 29]. The system consists of a syringe pump (NE-300, Prosense, Oosterhout, The Netherlands) and an injector, which were used to accurately control the injection rate (10 µl/min), the injection volume (10 µl) and the injection depth (120 µm). The pump, injector and hollow microneedles were connected by using high-pressure resistant CapTite™ connectors and silica capillaries.

2.5. Immunization study

Female BALB/c (H2^d) mice were ordered from Charles Rivers (Maastricht, The Netherlands) and accommodated under standardized conditions in the animal facility of Leiden Academic Centre for Drug Research, Leiden University. The immunization study was approved by the ethical committee on animal experiments of Leiden University (Licence number 14166).

The mice were 7-8 weeks old at the beginning of the experiments. The mice were anesthetized by intraperitoneal injection of ketamine (60 mg/kg) and xylanize (4 mg/kg) before shaving of the injection site. The mice were then injected with 10 µl of the formulations, containing 0.31 µg DT with or without 0.31 µg poly(I:C), into abdomen skin by using the hollow microneedle and the applicator, as described above. The following liposomal formulations were used: DT encapsulated liposomes (Lipo-DT), a mixture of DT-encapsulated liposomes and free poly(I:C) (Lipo-DT+PIC), a mixture of free DT and poly(I:C)-encapsulated liposomes (DT+Lipo-PIC), a mixture of DT-encapsulated liposomes and poly(I:C)-encapsulated liposomes (Lipo-DT+Lipo-PIC), and DT and poly(I:C) co-encapsulated liposomes (Lipo-DT-PIC). Control groups were injected with 0.31 µg DT with or without 0.31 µg poly(I:C) solution (DT/poly(I:C)). All formulations were freshly prepared and mixed prior to the immunization study. Subcutaneously injected 5 µg DT and 150 µg aluminum phosphate (DT-Alum) was used as a positive control. The mice were immunized on day 0, 21, 42 and sacrificed on day 56. Serum was withdrawn from the tail vein of mice on day 0, 21 and 42 and the sacrifice serum was taken from the femoral artery on day 56.

2.6. Determination of DT-specific IgG antibody titers

DT-specific antibodies were measured by using a sandwich enzyme-linked immunosorbent assay (ELISA) as described earlier [18]. The wells of 96-well plates were coated with 140 ng DT and incubated overnight at 4 °C. The plates were blocked with 1% BSA at 37 °C for 1 h. After blocking, appropriate three-fold serial dilutions of mouse sera were transferred into the plates and incubated for 2 h at 37 °C. The plates were then incubated with horseradish peroxidase-conjugated goat antibodies against total IgG, IgG1 or IgG2a (1:5000 dilution) for 1.5 h at 37 °C. Subsequently, the plates were incubated with TMB and 2 M sulfuric acid was

used to stop the reaction. The absorbance was measured at 450 nm by using a Tecan M1000 plate reader. The antibody titers were expressed as log10 value of the mid-point of S-shaped dilution-absorbance curve of the diluted serum level.

2.7. Determination of DT-neutralizing antibodies

The functionality of the antibody response was determined by measuring diphtheria toxin-neutralizing antibodies in a Vero cell test [30]. The serum samples were first diluted by M199 medium supplemented with 5% FBS, 0.5% glucose, 0.8% L-glutamine and 1% penicillin-streptomycin. Appropriate two-fold serial dilutions of the serum were applied to 96-well plates. Next, 5×10^{-5} Lf diphtheria toxin was added to each well. Subsequently, 1.25×10^{4} Vero cells were added to each well and incubated for 6 days at 37 °C in 5% CO_2. Finally, the neutralizing antibodies were expressed as the log2 value of the highest serum dilution that protected the Vero cells.

2.8. Statistics analysis

All the data of antibody titers were analyzed by one way ANOVA with Newman-Keuls Multiple post-test by using GraphPad Prism software (version 5.02). The level of significance was set at $p < 0.05$.

3. Results

3.1. Physicochemical characteristics of the liposomes and *in vitro* release of DT and poly(I:C)

Lipo-DT, Lipo-PIC and Lipo-DT-PIC were first characterized in terms of particle size, poly dispersity index (PDI) and zeta potential. As shown in **Table 1**, Lipo-DT and Lipo-PIC had a similar average size below 200 nm with a low PDI, while Lipo-DT-PIC showed a slightly larger size and PDI. All the liposomes had a positive zeta potential above +35 mV. Both DT and poly(I:C) were efficiently encapsulated into the liposomes, with a EE higher than 96%. Furthermore, DT and poly(I:C) had a similar LC% of about 1.7% (**Table 1**).

Table 1. Physicochemical characteristics of DT/poly(I:C) encapsulated liposomes (n=3).

Liposomes	Size[a] (nm)	PDI[b]	ZP[c] (mV)	EE[d] (%)		LC[e] (%)	
				DT	Poly(I:C)	DT	Poly(I:C)
Lipo-DT	182±8	0.195±0.012	+37±1	96.5±2.1	-	1.6±0.1	-
Lipo-PIC	184±6	0.153±0.010	+37±1	-	98.5±0.8	-	1.7±0.0
Lipo-DT-PIC	238±11	0.243±0.003	+35±1	98.0±0.8	98.9±0.5	1.7±0.0	1.7±0.0

Data are average ± SEM of 3 independent batches.
[a]Size: Z-average diameter, [b]PDI: poly dispersity index, [c]ZP: zeta potential, [d]EE: encapsulation efficiency, [e]LC: loading capacity.

To study the *in vitro* release of DT and poly(I:C), the prepared liposomes were incubated in PBS for one month. As shown in **Fig. 1A**, there was a burst release of DT of about 25% from both Lipo-DT and Lipo-DT-PIC within the first day. After 3 days, almost no additional DT was released. On day 30, the total release of DT from Lipo-DT and Lipo-DT-PIC was about 50% and 40%, respectively. Similarly, about 20 % of the poly(I:C) was quickly released from

Lipo-PIC and Lipo-DT-PIC within the first day and after day 3 almost no additional release was detected (**Fig. 1B**). On day 30, about 40% and 25% of the loaded poly(I:C) were released from Lipo-PIC and Lipo-DT-PIC, respectively. In summary, after incubation in PBS for one month, less than half of the loaded DT or poly(I:C) was released from the liposomes.
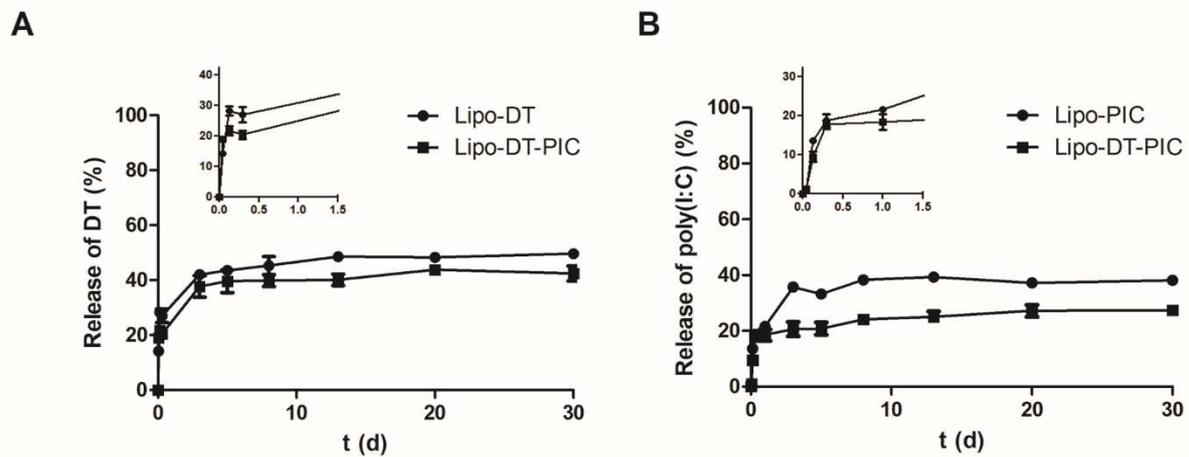
Figure 1. *In vitro* release of DT and poly(I:C) from liposomes. A: Release of DT from Lipo-DT (spheres) and Lipo-DT-PIC (squares). Insertion: release over a period of 1.5 days. B: Release of poly(I:C) from Lipo-PIC (spheres) and Lipo-DT-PIC (squares). Insertion: release over a period of 1.5 days. Bars represent mean $\pm$ SEM, n = 3.
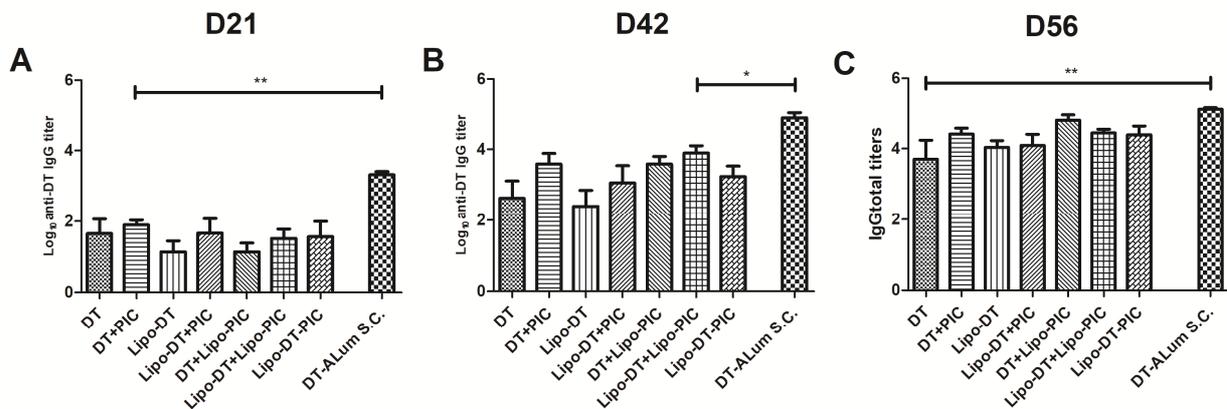
Figure 2. DT-specific total IgG titers on day 21 (A), 42 (B) and 56 (C). Bars represent mean $\pm$ SEM, n = 8. *$p < 0.05$, **$p < 0.01$.

In order to study the interaction between free DT or poly(I:C) and the positively charged liposomes loaded with the other active ingredient after mixing in PBS, the adsorption of DT or poly(I:C) on the liposomes were determined. There were $75.9 \pm 3.8\%$ (mean $\pm$ SEM, n=3) and $77.4 \pm 0.8\%$ (mean $\pm$ SEM, n=3) of DT adsorbing on the surface of Lipo-PIC at 4 h or 24 h after mixing, respectively. In case of poly(I:C), $95.9 \pm 2.7\%$ (mean $\pm$ SEM, n=3) and $95.6 \pm 1.0\%$ (mean $\pm$ SEM, n=3) were adsorbed on the surface of Lipo-DT at 4 or 24 h after mixing, respectively. In summary, most of free DT or poly(I:C) was adsorbed on the surface of liposomes after mixing.

3.2. Intradermal vaccination study

Immunogenicity of diphtheria toxoid and poly(I:C) loaded cationic liposomes after hollow microneedle-mediated intradermal injection in mice

The formulations were intradermally delivered into mice by using hollow microneedles with a DT dose of 0.31 µg with or without 0.31 µg poly(I:C), based on our previous dose response study [31]. Subcutaneously injected DT-Alum with a much higher dose (5 µg DT and 100 µg Alum) was used as a positive control. During the injection, there was no visible leakage and successful injection was indicated by the formation of the bleb on the abdomen area of mouse skin.
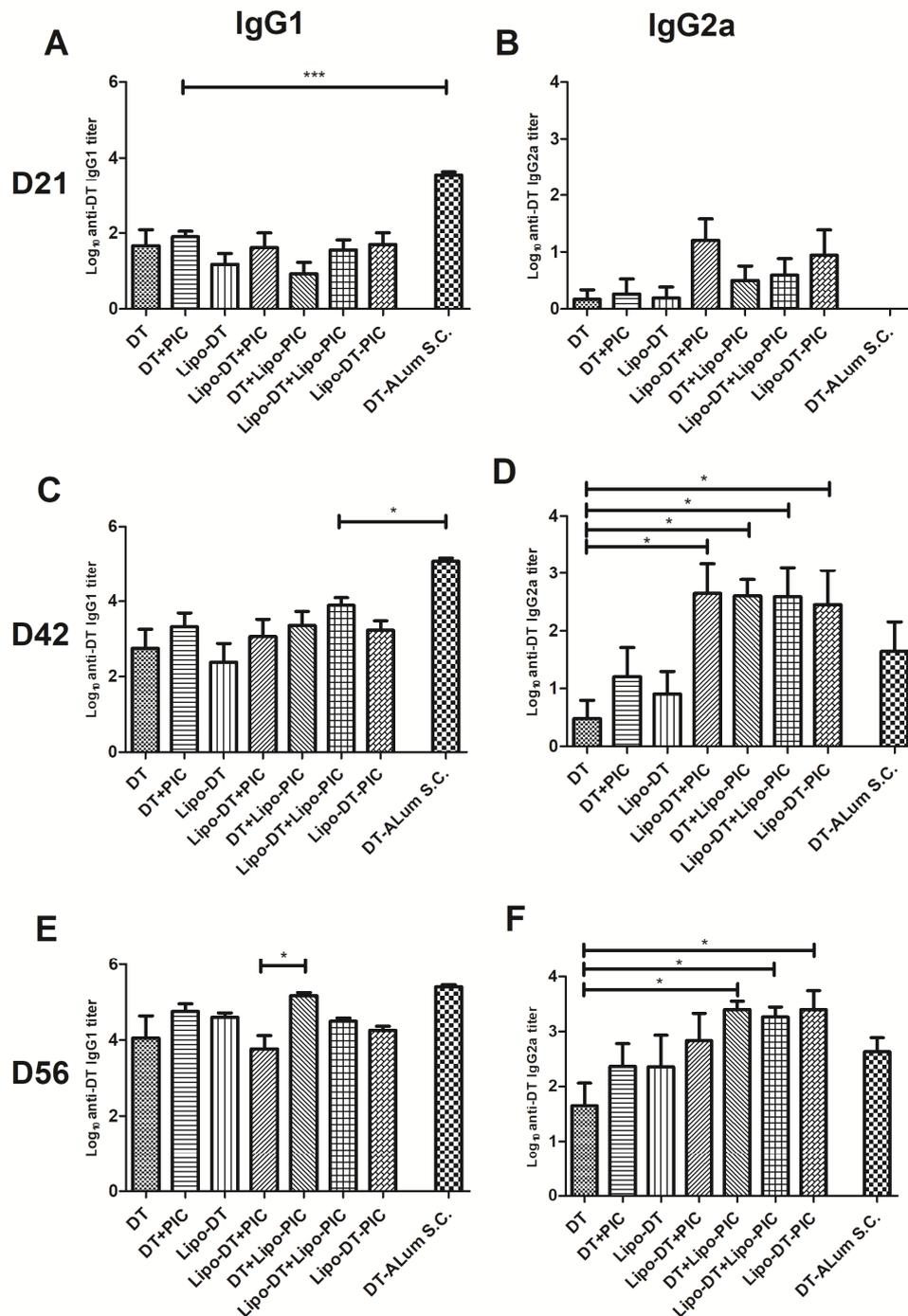
**Figure 3.** DT-specific IgG1 (A, C, E) and IgG2a (B, D, F) titers on day 21 (A, B), 42 (C, D) and 56 (E, F). Bars represent mean ± SEM, n = 8. *p < 0.05, ***p < 0.001.

DT-specific total IgG and subtype titers (IgG1 and IgG2a) are presented in **Fig. 2** and **Fig. 3**, respectively. As shown in **Fig. 2**, total IgG titers increased after each immunization. As expected, DT-Alum induced significantly higher total IgG responses than all other formulations on day 21 and 42 ($p < 0.05$) (**Fig. 2A, B**). However, on day 56 the response of the intradermal groups increased to similar levels to that induced by DT-Alum (except DT), despite the 15-fold lower dose administered (**Fig. 2C**). The encapsulation of DT/poly(I:C) in liposomes did not increase the total IgG response compared to DT/poly(I:C) solutions ($p > 0.05$). Furthermore, the addition of poly(I:C) did not change the total IgG response.

Next, the IgG1 and IgG2a titers were measured. As shown in **Fig. 3**, the IgG1 response followed the total IgG response: liposomal formulation groups induced equally strong IgG1 responses compared to DT/poly(I:C) solutions ($p > 0.05$). However, when focusing on IgG2a response, clear differences were observed among the groups. On day 21 all groups except DT-Alum developed a detectable IgG2a response (**Fig. 3B**). After the 1st boost (day 42), all groups showed an IgG2a response (**Fig. 3D**). Moreover, liposomal groups that contained both DT and poly(I:C), i.e., Lipo-DT+PIC, DT+Lipo-PIC, Lipo-DT+Lipo-PIC and Lipo-DT-PIC, induced a similar IgG2a response that was higher than the response induced by DT solution ($p < 0.05$) and the DT and poly(I:C) mixture (**Fig. 3D**), although compared with the latter the difference is not significant ($p > 0.05$). After the 2nd boost (day 56), the IgG2a response of all groups increased to a higher level, but still the liposomal groups containing both DT and poly(I:C) induced a distinctly higher IgG2a response than DT solution (**Fig. 3F**). In summary, the results showed that the IgG2a response was enhanced when DT/poly(I:C) was loaded in liposomes, no matter whether only one ingredient or both of them were encapsulated in liposomes. Furthermore, DT and poly(I:C) individually encapsulated in liposomes induced a similar IgG2a response compared to DT and poly(I:C) co-encapsulated in liposomes. In contrast, DT encapsulated liposomes (Lipo-DT) did not enhance the IgG2a response compared to DT solution. Additionally, the DT-Alum group did not improve the IgG2a response in spite of a much higher dose.

In order to study functionality of the antibody response, the neutralizing antibody titers in serum on day 56 were determined by a Vero cell assay. The sera of the DT-Alum group contained higher levels of toxin-neutralizing antibodies than all other groups ($p < 0.05$) (**Fig. 4**). The liposomal groups containing both DT and poly(I:C) showed similar neutralizing titers compared to DT/poly(I:C) solutions. The Lipo-DT group seemed to have the lowest titers among the intradermal groups, but the difference is not significant. In summary, the encapsulation of DT/poly(I:C) in liposomes did not improve the protective immunity against diphtheria toxin.
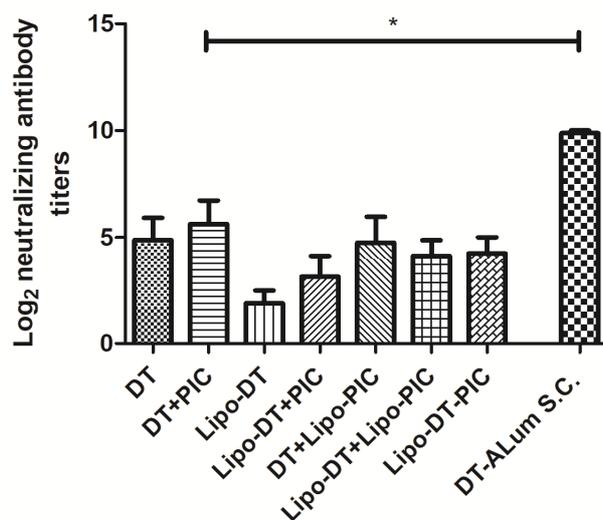
Figure 4. DT-neutralizing antibody titers of mice. Results are shown for serum collected on day 56. Bars represent mean ± SEM, n = 8. *p < 0.05.

4. Discussion

Liposome-based delivery system for vaccination has been extensively investigated [15, 32]. When focusing on intradermal vaccination, several studies have shown that co-encapsulation of antigen and adjuvant in liposomes can increase IgG2a and $CD8^+$ T cell responses [16, 17, 21, 22, 33]. In one of our previous studies, we used hollow microneedles to examine the effect of nano-encapsulation of OVA and poly(I:C) on the immune response in mice after intradermal vaccination. In that study, four types of nanoparticles were compared and the results indicated that OVA- and poly(I:C)-containing cationic liposomes were more potent than the other nanoparticles and significantly increased the IgG2a response compared to OVA and poly(I:C) solutions [17]. In the present study, we used the same liposome composition to study whether co-encapsulation of antigen and immune modulator is the essential factor for increased IgG2a levels. To investigate this, we co-encapsulated DT and poly(I:C) or encapsulated them individually in liposomes and studied the IgG (subtype) response following hollow microneedle-mediated intradermal vaccination. The results showed that liposomal formulations containing both DT and poly(I:C), induced higher IgG2a titers than those induced by DT/poly(I:C) solutions, no matter whether only one ingredient or both of them were encapsulated in liposomes. Furthermore, DT and poly(I:C) that were both individually encapsulated in liposomes induced similar IgG2a titers compared to DT and poly(I:C) co-encapsulated in liposomes.

The results of Lipo-DT-PIC are well in accordance with previously reported results [16, 23], showing that the co-encapsulation of antigen and immune modulator in liposomes can increase IgG2a responses and favor Th1 type immune responses after intradermal delivery by using a hypodermic needle. This may be caused by a liposome induced increase in the uptake of antigen and adjuvant by antigen presenting cells, as the size of liposomes (smaller than 200 nm) is favorable for uptake by dendritic cells [34-36]. Burke et al. additionally showed that liposomes may facilitate the access of poly(I:C) to cellular cytoplasm and up-regulate TLR signalling molecules and NLRP3 inflammasome pathway [37]. Furthermore, cationic liposomes may have a stronger interaction with the negatively charged cell membrane due to the attractive electrostatic interaction compared to negatively charged particles, which allows longer retention time on the cell surface and subsequently sustained release of antigen and adjuvant [15, 38, 39]. Finally, several studies have indicated that the co-processing of antigen

and adjuvant by antigen presenting cells after being taken up may be the reason for a higher IgG2a response [16, 17, 21]. The delivery of antigen and the triggering of TLR in the same dendritic cell may synergistically induce a superior antigen presentation to T cells [21, 40].

The results of Lipo-DT+PIC and DT+Lipo-PIC are in line with our previous study by Varypataki et al, who found that the mixture of antigen-loaded liposomes and free poly(I:C) solution induced a similar IFN-γ-producing CD4$^+$ T cell response (Th1) as antigen and adjuvant co-encapsulated liposomes after hypodermic needle-mediated intradermal delivery [41]. One explanation may be that the negatively charged antigen and adjuvant mixed with the liposome formulation adhered to the surface of positively charged liposomes after intradermal injection due to the electrostatic interaction. As a result, most of the antigen and adjuvant were co-delivered into the antigen presenting cells although they were not co-encapsulated in the liposomes. The adsorption study supported our hypothesis, as most of the DT or poly(I:C) were found to adsorb on the surface of liposomes after mixing in PBS.

In case of the Lipo-DT+Lipo-PIC formulation, we expect that these two liposomes would repel with each other due to their strong surface charge. Indeed, the particle size and zeta potential of Lipo-DT+Lipo-PIC were found to remain the same within 24 h after mixing in PBS (data not shown). Nevertheless, Lipo-DT+Lipo-PIC induced similar IgG2a responses as Lipo-DT-PIC. These results indicate that the individually encapsulated DT and poly(I:C) are as efficient as the DT and poly(I:C) co-encapsulated in the liposomes for activation of immune system when administered intradermally. This may be explained by an efficient uptake of both Lipo-DT and Lipo-PIC by the same antigen presenting cells. One possible approach to further investigate this is to use confocal microscopy to study the fate of fluorescently labeled liposomes and antigen/adjuvant following administration *in vivo*.

In order to produce liposomes loaded with the optimal ratio of antigen/adjuvant with a high loading efficiency, optimization work needs to be done. Our results clearly suggest that co-encapsulation of antigen and adjuvant in liposomes may not be necessary for the use in intradermal delivery. This might simplify the work for the development of formulations. This may even be particularly beneficial for developing formulations that must contain multiple antigens and adjuvants, e.g., for personalized therapies of cancer patients [42]. Such formulations can be prepared by mixing different liposomes loaded with only antigen or only adjuvant. Furthermore, it may be interesting to test whether our current findings also hold true for other nanoparticulate vaccine delivery systems.

Finally, the results of neutralizing antibody assay indicate that high IgG2a titers did not contribute to the immunity against diphtheria, which is in line with a previous study [30]. The high IgG2a titers may be more suitable for anti-viral immune responses where a Th1 response is more desired [43].

5. Conclusion

Our results show that DT and poly(I:C) can be successfully encapsulated into cationic liposomes with a high loading efficiency. After hollow microneedle-mediated intradermal vaccination, the antigen and adjuvant encapsulated liposomes evoked a potent immune response and shifted the IgG1/IgG2a balance more to the IgG2a direction. The combination of DT-encapsulated and poly(I:C)-encapsulated liposomes are able to simulate an equally strong IgG2a response compared to DT and poly(I:C) co-encapsulated liposomes. These findings may have implications for future design of liposomal formulations aiming for modification of immune response after intradermal delivery.

Acknowledgements

References:
[1] L.J. Peek, C.R. Middaugh, C. Berkland, Nanotechnology in vaccine delivery, Adv. Drug Deliv. Rev. 60 (2008) 915-928.
[2] H. Jiang, Q. Wang, X. Sun, Lymph node targeting strategies to improve vaccination efficacy, J. Control. Release 267 (2017) 47-56.
[3] R. Rappuoli, M. Pizza, G. Del Giudice, E. De Gregorio, Vaccines, new opportunities for a new society, Proc. Nati. Acad. USA 111 (2014) 12288-12293.
[4] C.J. Melief, T. van Hall, R. Arens, F. Ossendorp, S.H. van der Burg, Therapeutic cancer vaccines J. Clin. Investi. 125 (2015) 3401-3412.
[5] Y.C. Kim, J.H. Park, M.R. Prausnitz, Microneedles for drug and vaccine delivery, Adv. Drug Deliv. Reviews 64 (2012) 1547-1568.
[6] E. Larraneta, M.T. McCrudden, A.J. Courtenay, R.F. Donnelly, Microneedles: A new frontier in nanomedicine delivery, Pharm. Res. 33 (2016) 1055-1073.
[7] K. van der Maaden, W. Jiskoot, J. Bouwstra, Microneedle technologies for (trans)dermal drug and vaccine delivery, J. Control. Release 161 (2012) 645-655.
[8] J. Tu, G. Du, M. Reza Nejadnik, J. Monkare, K. van der Maaden, P.H.H. Bomans, N. Sommerdijk, B. Slutter, W. Jiskoot, J.A. Bouwstra, A. Kros, Mesoporous silica nanoparticle-coated microneedle arrays for intradermal antigen delivery, Pharm. Res. 34 (2017) 1693-1706.
[9] A.M. de Groot, G. Du, J. Monkare, A.C.M. Platteel, F. Broere, J.A. Bouwstra, A. Sijts, Hollow microneedle-mediated intradermal delivery of model vaccine antigen-loaded PLGA nanoparticles elicits protective T cell-mediated immunity to an intracellular bacterium, J. Control. Release 266 (2017) 27-35.
[10] N. Li, L.H. Peng, X. Chen, S. Nakagawa, J.Q. Gao, Transcutaneous vaccines: novel advances in technology and delivery for overcoming the barriers, Vaccine 29 (2011) 6179-6190.
[11] M. Leone, J. Monkare, J. Bouwstra, G. Kersten, Dissolving microneedle patches for dermal vaccination, Pharm. Res. 34 (2017) 2223-2240.
[12] S.G. Reed, M.T. Orr, C.B. Fox, Key roles of adjuvants in modern vaccines, Nat. Med. 19 (2013) 1597-1608.
[13] L. Zhao, A. Seth, N. Wibowo, C.X. Zhao, N. Mitter, C.Z. Yu, A.P.J. Middelberg, Nanoparticle vaccines, Vaccine 32 (2014) 327-337.
[14] Y. Fan, J.J. Moon, Nanoparticle drug delivery systems designed to improve cancer vaccines and immunotherapy, Vaccines 3 (2015) 662-685.
[15] A.K. Giddam, M. Zaman, M. Skwarczynski, I. Toth, Liposome-based delivery system for vaccine candidates: constructing an effective formulation, Nanomedicine 7 (2012) 1877-1893.
[16] S.M. Bal, S. Hortensius, Z. Ding, W. Jiskoot, J.A. Bouwstra, Co-encapsulation of antigen and Toll-like receptor ligand in cationic liposomes affects the quality of the immune response in mice after intradermal vaccination, Vaccine 29 (2011) 1045-1052.
[17] G. Du, R.M. Hathout, M. Nasr, M.R. Nejadnik, J. Tu, R.I. Koning, A.J. Koster, B. Slutter, A. Kros, W. Jiskoot, J.A. Bouwstra, J. Monkare, Intradermal vaccination with hollow microneedles: A comparative study of various protein antigen and adjuvant encapsulated nanoparticles, J. Control. Release 266 (2017) 109-118.
[18] B. Slutter, S.M. Bal, Z. Ding, W. Jiskoot, J.A. Bouwstra, Adjuvant effect of cationic liposomes and CpG depends on administration route, J. Control. Release 154 (2011) 123-130.
[19] Y.Q. Qiu, L. Guo, S.H. Zhang, B. Xu, Y.H. Gao, Y. Hu, J. Hou, B.K. Bai, H.H. Shen, P.Y. Mao, DNA-based vaccination against hepatitis B virus using dissolving microneedle arrays adjuvanted by cationic liposomes and CpG ODN, Drug Deliv. 23 (2016) 2391-2398.

[20] Y. Suzuki, D. Wakita, K. Chamoto, Y. Narita, T. Tsuji, T. Takeshima, H. Gyobu, Y. Kawarada, S. Kondo, S. Akira, H. Katoh, H. Ikeda, T. Nishimura, Liposome-encapsulated CpG oligodeoxynucleotides as a potent adjuvant for inducing type 1 innate immunity, Cancer Res. 64 (2004) 8754-8760.

[21] M.A. Boks, S.C.M. Bruijns, M. Ambrosini, H. Kalay, L. van Bloois, G. Storm, T. de Gruijl, Y. van Kooyk, In situ delivery of tumor antigen- and adjuvant-loaded liposomes boosts antigen-specific T-Cell responses by human dermal dendritic cells, J. Invest. Dermatol. 135 (2015) 2697-2704.

[22] L. Guo, J.M. Chen, Y.Q. Qiu, S.H. Zhang, B. Xu, Y.H. Gao, Enhanced transcutaneous immunization via dissolving microneedle array loaded with liposome encapsulated antigen and adjuvant, Int. J. Pharmaceut. 447 (2013) 22-30.

[23] E.M. Varypataki, A.L. Silva, C. Barnier-Quer, N. Collin, F. Ossendorp, W. Jiskoot, Synthetic long peptide-based vaccine formulations for induction of cell mediated immunity: A comparative study of cationic liposomes and PLGA nanoparticles, J. Control. Release 226 (2016) 98-106.

[24] S. Hamdy, O. Molavi, Z.S. Ma, A. Haddadi, A. Alshamsan, Z. Gobti, S. Elhasi, J. Samuel, A. Lavasanifar, Co-delivery of cancer-associated antigen and Toll-like receptor 4 ligand in PLGA nanoparticles induces potent CD8(+) T cell-mediated anti-tumor immunity, Vaccine 26 (2008) 5046-5057.

[25] R. Ammi, J. De Waele, Y. Willemen, I. Van Brussel, D.M. Schrijvers, E. Lion, E.L.J. Smits, Poly(I:C) as cancer vaccine adjuvant: Knocking on the door of medical breakthroughs, Pharmacol. Ther. 146 (2015) 120-131.

[26] C.S.W. Chong, M. Cao, W.W. Wong, K.P. Fischer, W.R. Addison, G.S. Kwon, D.L. Tyrrell, J. Samuel, Enhancement of T helper type 1 immune responses against hepatitis B virus core antigen by PLGA nanoparticle vaccine delivery, J. Control. Release 102 (2005) 85-99.

[27] M. Zaric, O. Lyubomska, O. Touzelet, C. Poux, S. Al-Zahrani, F. Fay, L. Wallace, D. Terhorst, B. Malissen, S. Henri, U.F. Power, C.J. Scott, R.F. Donnelly, A. Kissenpfennig, Skin dendritic cell targeting via microneedle arrays laden with antigen-encapsulated poly-D,L-lactide-co-glycolide nanoparticles induces efficient antitumor and antiviral immune responses, ACS Nano 7 (2013) 2042-2055.

[28] K. van der Maaden, S.J. Trietsch, H. Kraan, E.M. Varypataki, S. Romeijn, R. Zwier, H.J. van der Linden, G. Kersten, T. Hankemeier, W. Jiskoot, J. Bouwstra, Novel hollow microneedle technology for depth-controlled microinjection-mediated dermal vaccination: a study with polio vaccine in rats, Pharm. Res. 31 (2014) 1846-1854.

[29] P. Schipper, K. van der Maaden, S. Romeijn, C. Oomens, G. Kersten, W. Jiskoot, J. Bouwstra, Determination of depth-dependent intradermal immunogenicity of adjuvanted inactivated polio vaccine delivered by microinjections via hollow microneedles, Pharm. Res. 33 (2016) 2269-2279.

[30] Z. Ding, E. Van Riet, S. Romeijn, G.F.A. Kersten, W. Jiskoot, J.A. Bouwstra, Immune modulation by adjuvants combined with diphtheria toxoid administered topically in BALB/c mice after microneedle array pretreatment, Pharm. Res. 26 (2009) 1635-1643.

[31] P. Schipper, K. van der Maaden, V. Groeneveld, M. Ruigrok, S. Romeijn, S. Uleman, C. Oomens, G. Kersten, W. Jiskoot, J. Bouwstra, Diphtheria toxoid and N-trimethyl chitosan layer-by-layer coated pH-sensitive microneedles induce potent immune responses upon dermal vaccination in mice, J. Control. Release 262 (2017) 28-36.

[32] Y. Perrie, F. Crofts, A. Devitt, H.R. Griffiths, E. Kastner, V. Nadella, Designing liposomal adjuvants for the next generation of vaccines, Adv. Drug Deliv. Rev. 99 (2016) 85-96.

[33] E.M. Varypataki, K. van der Maaden, J. Bouwstra, F. Ossendorp, W. Jiskoot, Cationic liposomes loaded with a synthetic long peptide and poly(I:C): a defined adjuvanted vaccine for induction of antigen-specific T cell cytotoxicity, AAPS J. 17 (2015) 216-226.
[34] M.O. Oyewumi, A. Kumar, Z.R. Cui, Nano-microparticles as immune adjuvants: correlating particle sizes and the resultant immune responses, Expert Rev. Vaccines 9 (2010) 1095-1107.
[35] V. Manolova, A. Flace, M. Bauer, K. Schwarz, P. Saudan, M.F. Bachmann, Nanoparticles target distinct dendritic cell populations according to their size, Eur. J. Immunol. 38 (2008) 1404-1413.
[36] N. Benne, J. van Duijn, J. Kuiper, W. Jiskoot, B. Slutter, Orchestrating immune responses: How size, shape and rigidity affect the immunogenicity of particulate vaccines, J. Control. Release 234 (2016) 124-134.
[37] M.L. Burke, M. Veer, J. Pleasance, M. Neeland, M. Elhay, P. Harrison, E. Meeusen, Innate immune pathways in afferent lymph following vaccination with poly(I:C)-containing liposomes, Innate immun. 20 (2014) 501-510.
[38] Y.F. Ma, Y. Zhuang, X.F. Xie, C. Wang, F. Wang, D.M. Zhou, J.Q. Zeng, L.T. Cai, The role of surface charge density in cationic liposome-promoted dendritic cell maturation and vaccine-induced immune responses, Nanoscale 3 (2011) 2307-2314.
[39] C. Foged, C. Arigita, A. Sundblad, W. Jiskoot, G. Storm, S. Frokjaer, Interaction of dendritic cells with antigen-containing liposomes: effect of bilayer composition, Vaccine 22 (2004) 1903-1913.
[40] O. Schulz, S.S. Diebold, M. Chen, T.I. Naslund, M.A. Nolte, L. Alexopoulou, Y.T. Azuma, R.A. Flavell, P. Liljestrom, C.R.E. Sousa, Toll-like receptor 3 promotes cross-priming to virus-infected cells, Nature 433 (2005) 887-892.
[41] M. Diwan, M. Tafaghodi, J. Samuel, Enhancement of immune responses by co-delivery of a CpG oligodeoxynucleotide and tetanus toxoid in biodegradable nanospheres, J. Control. Release 85 (2002) 247-262.
[42] S. Grabbe, H. Haas, M. Diken, L.M. Kranz, P. Langguth, U. Sahin, Translating nanoparticulate-personalized cancer vaccines into clinical applications: case study with RNA-lipoplexes for the treatment of melanoma, Nanomedicine-Uk 11 (2016) 2723-2734.
[43] J. Cenna, G.S. Tan, A.B. Papaneri, B. Dietzschold, M.J. Schnell, J.P. McGettigan, Immune modulating effect by a phosphoprotein-deleted rabies virus vaccine vector expressing two copies of the rabies virus glycoprotein gene, Vaccine 26 (2008) 6405-6414.

Chapter 6

Coated and hollow microneedle-mediated intradermal immunization in mice with diphtheria toxoid loaded mesoporous silica nanoparticles

Guangsheng Du[1], Laura Woythe[1], Koen van der Maaden[1], Mara Leone[1], Stefan Romeijn[1], Gideon Kersten[1,2], Wim Jiskoot[1], Joke A. Bouwstra[1,*]

[1]Division of BioTherapeutics, Leiden Academic Centre for Drug Research, Leiden University, Leiden, The Netherlands

[2]Institute for Translational Vaccinology (Intravacc), Bilthoven, The Netherlands

Abstract
The aim of this study was to examine the immunogenicity of diphtheria toxoid (DT) loaded mesoporous silica nanoparticles (MSNs) after coated and hollow microneedle-mediated intradermal immunization in mice. DT was loaded into MSNs and the nanoparticle surface was coated with a lipid bilayer (LB-MSN-DT). To prepare coated microneedles, alternating layers of negatively charged LB-MSN-DT and positively charged N-trimethyl chitosan (TMC) were coated onto pH-sensitive microneedle arrays via a layer-by-layer approach. Microneedle arrays coated with 5 or 3 layers of LB-MSN-DT were used to immunize mice and the elicited antibody responses were compared with those induced by hollow microneedle-injected liquid formulation of LB-MSN-DT. Liquid DT formulation with and without TMC (DT/TMC) injected by a hollow microneedle were used as controls. LB-MSN-DT had an average size of about 670 nm and a zeta potential of -35 mV. The encapsulation efficiency of DT in the nanoparticles was 77%. The amount of nano-encapsulated DT coated onto the microneedle array increased linearly with increasing number of the coating layers. Nano-encapsulated DT induced stronger immune responses than DT solution when delivered intradermally via hollow microneedles, but not when delivered via coated microneedles. In conclusion, both the nano-encapsulation of DT and the type of microneedles affect the immunogenicity of the antigen.
Keywords: Coated microneedles, hollow microneedles, mesoporous silica nanoparticles, diphtheria toxoid, intradermal vaccination

Coated and hollow microneedle-mediated intradermal immunization in mice with diphtheria toxoid loaded mesoporous silica nanoparticles

1. Introduction

Vaccination is one of the most cost-effective tools to prevent infectious diseases in man [1]. Traditional vaccines are based on attenuated or inactivated pathogens. Nowadays, subunit vaccines containing only immunogenic parts of a pathogen are being extensively investigated because they are safer [2]. The disadvantage of subunit vaccines is that they are generally less immunogenic than traditional vaccines. To overcome this, adjuvants such as immune modulators and nanoparticulate delivery systems can be used [3, 4].

Nanoparticles have been extensively studied for the delivery of vaccines, as they can improve the immunogenicity of antigens by enhancing the targeting of antigens to antigen-presenting cells (APCs) [5]. Furthermore, the immune responses can potentially be modified by tuning the properties of nanoparticles such as size, surface charge, and release kinetics of antigens [3, 6, 7]. Among different types of nanoparticles, mesoporous silica nanoparticles (MSNs) have gained increasing attention because of their excellent biocompatibility and stability. Besides, the silica surface can be easily modified and functionalized and the large pores and surface area of MSNs enable efficient loading of antigens with a high loading capacity [8, 9]. Studies have shown that antigen loaded MSNs are able to increase the uptake of antigens by APCs and improve immune responses in mice [9-11].

Vaccines are mostly administered by intramuscular or subcutaneous injection, but these methods have disadvantages such as low acceptance by a considerable number of people and infection risk due to needlestick injuries or reuse of needles [12-14]. Additionally, the delivery of vaccines to APCs may be inefficient as these delivery sites are not rich of APCs [15]. To avoid the drawbacks of hypodermic needles, microneedles have been developed. Microneedles are micrometer-sized needle-like structures and can be used to penetrate skin and deliver the antigen in a minimal invasive and pain-free way [16]. The skin contains a large number of APCs, and therefore microneedle-mediated intradermal delivery of vaccines has potential for effective vaccination [17].

Several types of microneedles are in development, such as coated, dissolvable and hollow microneedles [16]. On the one hand, coated and dissolvable microneedles are used to administer dry-state vaccine formulations [18], which offer the potential advantage of improving antigen stability [16, 19]. Previously, silicon microneedle arrays with a pH-sensitive surface were developed to bind negatively charged vaccines at slightly acidic conditions (pH 5.8) and release the coated material at physiological pH (7.4) [20]. Several studies have shown that the antigen coated microneedles induced a similar immune response as subcutaneously or intramuscularly injected antigen solution [21-23]. On the other hand, hollow microneedles are used to inject liquid formulations and the dose can be precisely controlled. We previously showed that hollow microneedles together with an applicator can be used to deliver antigen-loaded nanoparticles intradermally [24].

In this study, we aimed to examine the immunogenicity of intradermally delivered DT loaded MSNs by using either coated microneedle arrays or a single hollow microneedle. The microneedle arrays were coated with DT loaded in MSNs by using a layer-by-layer coating approach after which the delivered dose into *ex vivo* human skin were examined. In an subsequent immunization study, the antibody response induced by LB-MSN-DT coated microneedles was compared with that obtained after injection of a suspension of LB-MSN-DT by hollow microneedles into mouse skin.

2. Materials and methods

2.1. Materials

DT (batch 04-44, 1 µg equal to 0.3 Lf) and diphtheria toxin were provided by Intravacc (Bilthoven, The Netherlands). (3-aminopropyl)triethoxysilane (APTES, 99%), 4-pyridinecarboxaldehyde (97%), sodium cyanoborohydride (NaBH$_3$CN, 95%), cholesterol (≥99%), fetal bovine serum (FBS), M199 medium (with Hank's salts and L-glutamine) and bovine serum albumin (BSA) were obtained from Sigma-Aldrich (Zwijndrecht, The Netherlands). 1,2-dioleoyl-sn-glycero-3-phosphocholine (DOPC) and 1,2-dioleoyl-sn-glycero-3-[phospho-L-serine](sodium salt) (DOPS) were purchased from Avanti Polar Lipids Inc (Alabaster, AL). Hydrogen peroxide (30%) was purchased from Fluka (Steinheim, Germany). Toluene (≥99.7%) was obtained from Biosolve (Valkenswaard, The Netherlands). N-trimethyl chitosan (TMC) and rhodamine labeled TMC (TMC-Rho) were prepared as reported previously [23, 25]. Glucose solution, L-glutamine (200 nM), penicillin-streptomycin (10000 U/mL) and 1-step^{TM} ultra 3,3',5,5'-tetramethylbenzidine (TMB) were purchased from Thermo-Fisher Scientific (Waltham, MA). IRDye 800CW protein labeling kit (low molecular weight) was ordered from LI-COR (Lincoln, NE). HRP-conjugated goat anti-mouse total IgG, IgG1 and IgG2a were ordered from Southern Biotech (Birmingham, AL). Sulfuric acid (95-98%) was obtained from JT Baker (Deventer, The Netherlands). Sterile phosphate buffered saline (PBS, 163.9 mM Na$^+$, 140.3 mM Cl$^-$, 8.7 mM HPO$_4^{2-}$, 1.8 mM H$_2$PO^{4-}, pH 7.4) was ordered from B. Braun (Oss, The Netherlands). 1 mM phosphate buffer (PB) with a pH of 7.4 or 5.8 was prepared in the lab. Milli-Q water (18 MΩ/cm, Millipore Co.) was used for the preparation of all solutions. All the other chemicals used were of analytical grade.

2.2. Preparation of DT encapsulated and lipid fused MSNs (LB-MSN-DT)

Plain MSNs with a particle size of about 200 nm and large pores (about 10 nm in diameter) were prepared and modified with amino groups to generate a positively charged surface, as described earlier [11, 26]. To improve the colloidal stability of MSNs, liposomes were coated onto the surface of MSNs by using a method as previously described [11]. These liposomes were prepared by lipid film hydration followed by sonication. Briefly, DOPC, DOPS and cholesterol with a molar ratio of 7:1:2 were dissolved in chloroform in a round bottom flask. The organic solvent was evaporated by using a rotary evaporator (Buchi rotavapor R210, Flawil, Switzerland) for 30 min. Subsequently, the lipid film was hydrated with 1 mM PB (pH 7.4) and vortexed for 10 s to form a lipid vesicle suspension. The suspension was sonicated in a Branson 2510 water bath (Danbury, CT) for 10 min. The obtained liposomes were stored at 4 °C in the refrigerator for further use.

To prepare LB-MSN-DT, 0.5 mL MSNs (2 mg/mL) and 0.5 mL DT (0.5 mg/mL) were mixed in 1 mM PB (pH 7.4), followed by addition of 0.5 mL liposomes (2 mg/mL) in 1 mM PB (pH 7.4). To prepare LB-MSN-DT loaded with Alexa488 or IRDye 800CW labeled DT, plain DT was replaced with fluorescently labeled DT according the need of experiments. The mixture was incubated in an Eppendorf thermomixer (Nijmegen, The Netherlands) for 1.5 h at 25 °C with a speed of 300 rpm. To remove the excess DT and liposomes, the suspension was centrifuged by using a Sigma 1-15 centrifuge (Osterode, Germany) for 5 min with a speed of 10,000 g. The resultant pellet was washed and re-dispersed in 1 mM PB (pH 7.4) for further use.

2.3. Characterization of LB-MSN-DT

2.3.1. Measurement of size and zeta potential of LB-MSN-DT

The size and zeta potential of LB-MSN-DT were determined by using dynamic light scattering (DLS) and laser Doppler velocimetry, respectively, with a Nano ZS® zetasizer (Malvern Instruments, Worcestershire, U.K.). The samples were diluted in 1 mM PB (pH 7.4) to a concentration of 25 µg/mL (expressed based on the concentration of MSNs) and measured 3 times with 10 runs for each measurement.

2.3.2. Determination of encapsulation efficiency (EE) and loading capacity (LC) of DT in LB-MSN-DT

The loading efficiency of DT was determined by measuring the intrinsic fluorescence intensity of DT ((λ_{ex} 280 nm/λ_{em} 320 nm) in the supernatant before and after encapsulation by using a Tecan M1000 plate reader (Männedorf, Switzerland). The EE and LC were calculated using the equations below:

$$EE = \frac{M_{loaded\,DT}}{M_{total\,DT}} \times 100\,\%$$

$$LC = \frac{M_{loaded\,DT}}{M_{MSNs}} \times 100\,\%$$

Where $M_{loaded\,DT}$ represents the mass of encapsulated DT, $M_{total\,DT}$ is the total amount of DT added to the formulation and M_{MSNs} is the weight of MSNs.

2.3.3. *In vitro* release of DT from LB-MSN-DT

To study the release of DT, 1 mL nanoparticle suspension with a concentration of 1 mg/mL (expressed based on the concentration of MSNs, corresponding to about 0.2 mg/mL DT) in PBS was incubated for one month at 37 °C by using an Eppendorf thermomixer (Nijmegen, The Netherlands) set at a speed of 550 rpm. At predetermined time points, the samples were centrifuged for 5 min with a speed of 10,000 g. 600 µL sample from the supernatant was collected and the amount of DT was measured by intrinsic fluorescence intensity of DT. Fresh PBS with the same volume of the collected supernatant was added back to the suspension. The release percentage of DT was calculated by dividing the released amount of DT by the total amount of DT initially loaded in LB-MSN-DT.

2.4. Coating of LB-MSN-DT on microneedle arrays and release of LB-MSN-DT in *ex vivo* human skin

2.4.1 Modification of microneedle arrays to achieve a pH-sensitive surface

Silicon microneedle arrays with 576 microneedles per array on a back plate of 5×5 mm^2 with a microneedle length of 200 µm were kindly provided by Robert Bosch GmbH (Stuttgart, Germany). To obtain pH-sensitive microneedles, the surface was modified with pyridine groups as previously reported [20]. In brief, the microneedle surface was first cleaned by piranha solution (70% sulfuric acid and 30% hydrogen peroxide) at 120 °C for 2 h. *Caution: piranha is strongly acidic and oxidizing. Piranha reacts violently with organic compounds, and it should not be stored in closed containers.* Subsequently, the microneedles were extensively washed with MilliQ water followed by washing with acetone and methanol. Next, the microneedles were incubated in 2% APTES in toluene overnight to obtain an amine-modified surface and thereafter incubated with 4-pyridinecarboxaldehyde (100 mM) in anhydrous isopropanol containing 1% acetic acid overnight. Finally, the formed imine bonds were reduced to secondary amines by incubating the microneedles with NaBH₃CN (50 mM) in isopropanol for 2 h. After cleaning the microneedles were stored under vacuum at 50 °C until further use.

2.4.2 Multilayer coating of LB-MSN-DT on the surface of microneedle arrays

LB-MSN-DT and TMC were alternately coated onto the surface of microneedle arrays by using a layer-by-layer approach. The pH-sensitive microneedle arrays were transferred into Greiner Cellstar® 48 well plates. 50 µL negatively charged LB-MSN-DT (0.5 mg/mL) in 1 mM PB (pH 5.8) was added onto the top of each microneedle array and the arrays were incubated for 30 min. The excess nanoparticles were washed by adding 450 µL 1 mM PB (pH 5.8). Next, the microneedle arrays were dried under pressurized nitrogen flow for 10 min. After the first coating layer of LB-MSN-DT, 50 µL positively charged TMC (40 µg/mL) in 1 mM PB (pH 5.8) was added onto the top of each microneedle array and the arrays were incubated with TMC for another 30 min. The concentration of LB-MSN and TMC in the coating solutions based on prior studies [11, 23]. The excess TMC was removed by washing the microneedle arrays with 450 µL 1 mM PB (pH 5.8). Subsequently, the microneedle arrays were dried under nitrogen flow as described above. This procedure was repeated until the desired number of coating layers of LB-MSN-DT was reached. After the last layer of LB-MSN-DT, no more TMC was coated onto the microneedle surface. In order to study the dose effect of DT using coated microneedles, the microneedle arrays were coated with either 5 or 3 layers of LB-MSN-DT and 4 or 2 alternate layers of TMC, respectively.

To determine the coating efficiency of DT on microneedles, the amount of nano-encapsulated DT in the supernatant after washing was determined by measuring the intrinsic fluorescence of DT. The coating efficiency was calculated by dividing the amount of coated DT by the total amount of DT initially added to the coating solution.

2.4.3 Insertion of microneedle arrays into *ex vivo* human skin

 Ex vivo human skin was obtained from a local hospital according to Helsinki principles. A written informed patient consent was obtained. To reproducibly insert the microneedles into the skin, an in-house developed impact-insertion injector together with a uPRAX applicator controller (Delft, The Netherlands) was used by using either a single insertion mode or multiple insertion mode [27, 28]. In case of a single insertion, the microneedle arrays were inserted into the skin with an average velocity of 0.5 m/s and kept in the skin for 30 min by applying a force of 5 N on top of the microneedle array. In case of multiple insertion mode, the microneedle arrays were 10 times inserted into the skin within 10 s with an average velocity of 0.5 m/s. After the last penetration, the microneedles were removed from the skin.

2.4.4 Visualization of the coated microneedles before and after penetration of *ex vivo* human skin by scanning electronic microscopy (SEM)

The 5-layer LB-MSN-DT coated microneedles were visualized with a Nova NanoSEM (Eindhoven, The Netherlands) operated with a voltage of 15 kV before and after removal from the skin. To increase the surface conductivity, the microneedle arrays were coated with a layer of platina/palladium before visualization.

2.4.5 Release of LB-MSN-DT from microneedle arrays into *ex vivo* human skin

To visualize the release of LB-MSN-DT from microneedle arrays into the skin, the 5-layer LB-MSN-DT coated microneedle arrays and the released nanoparticles in the skin were visualized by using a Nikon D-Eclipse C1 CLSM (Tokyo, Japan). For this purpose, DT-Alexa488 and TMC-Rho were used. The coated microneedles and the skin area penetrated by coated microneedles were scanned with a depth resolution of 5 µm/step by using a 10 × and 4 × Plan Apo objective, respectively. An argon laser (488 nm) with a 530/55 emission filter and

a diode-pumped solid-state laser (561 nm) with a 590/55 emission filter were used for visualization of DT-Alexa488 and TMC-Rho, respectively.

The released amount of DT in the *ex vivo* human skin was quantified by using a Perkin-Elmer IVIS Lumina Series III *in vivo* imaging system (Waltham, MA, USA). For this purpose, DT was labeled with IRDye 800 CW (DT-IRDye800) by using a IRDye 800CW protein labeling kit (low molecular weight) according to the manufacturer's instruction. The LB-MSN-DT-IRDye800 coated microneedles were inserted into human skin by using either the single or multiple insertion mode as described above. A calibration curve was prepared by injecting different amounts of LB-MSN-DT-IRDye800 in the skin by using a hollow microneedle (see below). To determine the amount of DT released from the coated microneedles, the fluorescence intensity of DT-IRDye800 in the skin was measured by using the *in vivo* imaging system with a 745 nm excitation wavelength and an ICG emission filter. By using the calibration curve the amount of delivered DT was calculated.

2.5. Hollow microneedles and applicator

The hollow microneedles were prepared by etching of fused silica capillaries with hydrofluoric acid, as previously described [29]. In brief, silica capillaries (375 µm outer diameter, 50 µm inner diameter) were cut into 4-cm pieces and filled with silicone oil in a vacuum oven (100 °C) overnight. The tips of capillaries were etched in ≥48% hydrofluoric acid for 4 h. Subsequently, the polyimide coating was removed by dipping the microneedle tips into hot sulfuric acid (250 °C) for 5 min. The applicator for hollow microneedles consists of a syringe pump and an injector for precise control of injection depth, rate and volume. The hollow microneedles, injector and pump were connected by silica capillaries and high-pressure resistant CapTite[TM] connectors [24].

2.6. Immunization studies in mice

Female BALB/c mice of 7-8 weeks old (Charles River, Maastricht, The Netherlands) at the start of the experiments were used for the immunization study. The animals were housed under standardized conditions in the animal facility of Leiden Academic Centre for Drug Research. The study was approved by the ethical committee on animal experiments of Leiden University (Licence number 14166).

Mice were first anesthetized by intraperitoneal injection of ketamine (60 mg/kg) and xylanize (4 mg/kg) before shaving the abdomen area. In case of coated microneedles, the LB-MSN-DT coated microneedle arrays were inserted into the abdomen of mice by using the multiple insertion mode as described above for the studies in *ex vivo* human skin. Each mouse was immunized with one microneedle array coated with either 5 or 3 layers of LB-MSN-DT. In case of hollow microneedles the following groups were included: a) 10 µL suspension of LB-MSN-DT, b) 10 µL DT solution and c) 10 µL DT and TMC solution. All formulations of hollow microneedle groups contained 0.31 µg DT. The same amount of TMC was included in the DT and TMC group. The formulation was injected into the skin of the abdomen of mice with a rate of 10 µL/min at a depth of 120 µm. Subcutaneously injected 5 µg DT formulated with 150 µg colloidal aluminum phosphate (DT-Alum) in PBS with a volume of 100 µL was used as a positive control. The mice were immunized on day 0 (prime), 21 (1st boost), 42 (2nd boost) and sacrificed on day 56. The serum was withdrawn from the tail veins of the mice on day 0, 21 and 42 prior to the immunization. On day 56 the serum was collected from thoracic vein and the mice were sacrificed by cervical dislocation.

2.7. Measurement of DT-specific antibody titers

The total IgG and subtype IgG1 and IgG2a titers in the serum were measured by using ELISA as previously reported [30]. Briefly, the wells of 96-well plates were first coated with 140 ng DT overnight at 4 °C. Next, the plates were blocked with 1% BSA and appropriate 3-fold serial diluted serum samples were applied to the plates and incubated for 2 h at 37 °C. Subsequently, HRP-conjugated goat anti-mouse total IgG, IgG1 and IgG2a were added into the wells and incubated for 1.5 h. Finally, TMB was added to the plates and 2 M sulfuric acid was added to stop the reaction. The absorbance was measured at 450 nm by using a Tecan M1000 plate reader. The antibody titers were expressed as the ^{10}log value where the corresponding absorbance is located in the middle of the S-shaped dilution-absorbance curve.

2.8. Measurement of DT-neutralizing antibody titers

To check the functionality of the antibodies, diphtheria toxin neutralizing antibody titers in the serum of the mice at day 56 were checked by using a Vero-cell assay [31]. Briefly, appropriate 2-fold serial diluted serum was first applied to 96-well plates. 5×10^{-5} Lf diphtheria toxin was added to each well and incubated for 2 h at 37°C in a stove with 5% CO_2. Subsequently, 1.25×10^4 Vero cells were added to each well and incubated for 6 days at 37°C in the stove with 5% CO_2. Finally, the neutralizing antibodies were shown as the ^{2}log value of the highest dilution times of serum that protected the Vero cells.

2.9. Statistics analysis

All the data of antibody titers were analyzed by one way ANOVA with Newman-Keuls Multiple post-test by using GraphPad Prism software (version 5.02). The level of significance was set at $*p < 0.05$, $**p < 0.01$, $***p < 0.001$.

3. Results

3.1. Physicochemical characteristics of LB-MSN-DT

The physicochemical characteristics of LB-MSN-DT are shown in **Table 1**. The size of LB-MSN-DT was approximately 700 nm with a polydispersity index (PDI) slightly larger than 0.3. The nanoparticles showed a high negative zeta potential. DT was efficiently encapsulated into the nanoparticles with a high EE and LC.

Table 1. Physicochemical characteristics of LB-MSN-DT (n=3).

Nanoparticles	Size[a] (nm)	PDI[b]	ZP[c] (mV)	EE%[d]	LC%[e]
LB-MSN-DT	676 ± 7	0.322 ± 0.016	-35 ± 1	77.1 ± 6.4	19.3 ± 1.6

Data are average ± SEM of 3 independent batches.
[a]Size: Z-average in diameter, [b]PDI: polydispersity index, [c]ZP: zeta potential, [d]EE: encapsulation efficiency, [e]LC: loading capacity.

3.2. *In vitro* release of DT from LB-MSN-DT

The *in vitro* release of DT was investigated by suspending LB-MSN-DT in PBS for one month. As shown in **Fig. 1**, there was a moderate burst release of DT of about 20% within the first day, followed by a sustained release, reaching a total release percentage of about 70% on day 30. These results indicate that the LB-MSN-DT may serve as a reservoir and allow the sustained release of DT, but at the same time retain sufficient DT for a prolonged period of time to deliver it as nanoparticulate antigen to APCs.
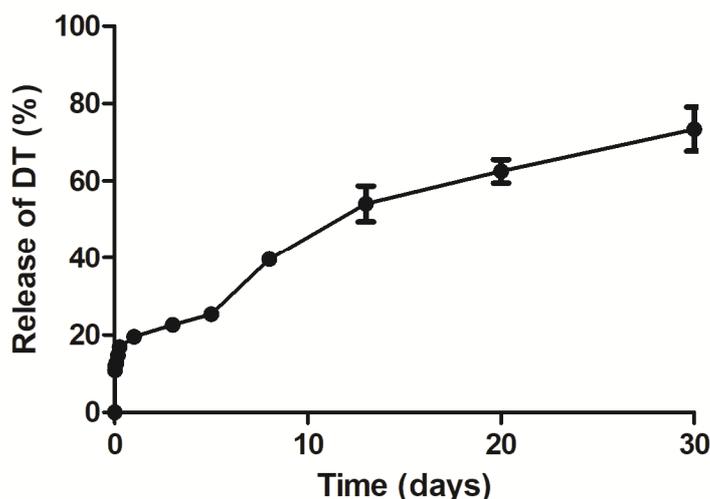
Figure 1. *In vitro* release of DT from LB-MSN-DT in PBS at 37 ˚C as a function of time. Bars represent mean ± SEM, n = 3.

3.3. Coating of LB-MSN-DT on microneedle arrays and release of LB-MSN-DT in *ex vivo* human skin

3.3.1 Quantification of coated amount of nano-encapsulated DT on microneedle arrays

As shown in **Fig. 2A**, the amount of nano-encapsulated DT that was coated onto the microneedles increased linearly with increasing number of layer coatings. About 0.4 µg DT was coated onto the microneedles of one microneedle array per layer. The coating efficiency was similar for each layer and was about 20-26% (**Fig. 2B**). As shown in **Table 2**, the cumulative amount of nano-encapsulated DT coated on the microneedle surfaces of one microneedle array was about 1.9 µg and 1.1 µg, corresponding to 9.7 µg and 5.7 µg LB-MSN-DT (based on the mass of MSNs) for a 5-layer and 3-layer coating, respectively.
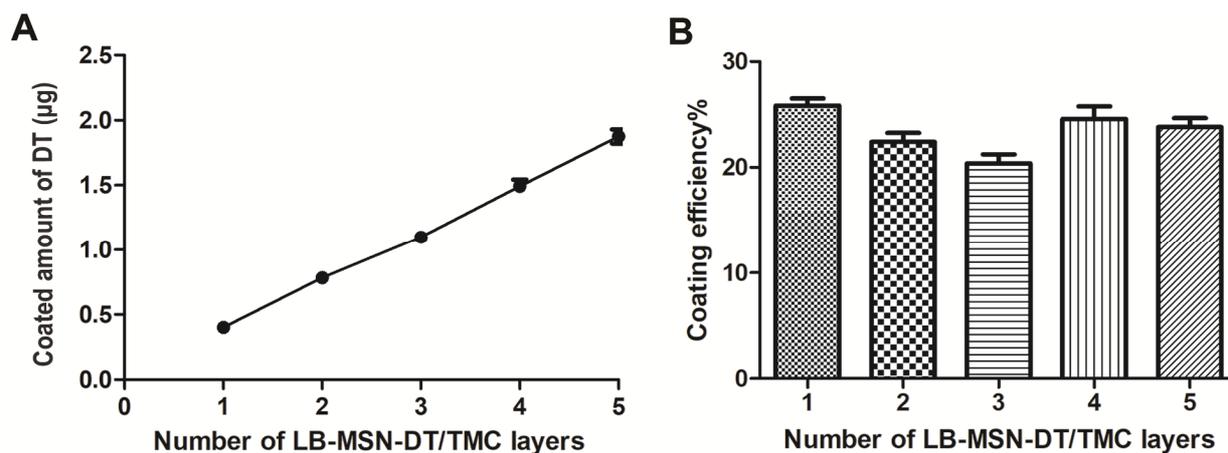
Figure 2. Cumulative amount of nano-encapsulated DT (A) that was coated on the microneedles of one microneedle array and coating efficiency (B) as a function of the number of layers. Data is represented as average ± SEM of 3 independent microneedle arrays.

Table 2. Coated and released amount of DT/LB-MSN-DT from the microneedles of a single 1microneedle array (n=3).

Microneedles	Coated DT (µg)	[a] Coated LB-MSN-DT (µg)	[b] Delivered DT (µg)		[c] Delivered percentage (%)	
			Multiple insertion mode	Single insertion mode	Multiple insertion mode	Single insertion mode
5-layer coated	1.9±0.1	9.7±0.2	0.814±0.008	0.341±0.083	42.8±0.1%	17.9±0.8%
3-layer coated	1.1±0.1	5.7±0.2	0.256±0.001	-	23.2±0.0%	-

Data are average ± SEM of 3 independent microneedle arrays.
[a] The coated amount of LB-MSN-DT is expressed as the mass of MSNs and was calculated by using the coated amount of DT and loading capacity of DT in LB-MSN-DT.
[b] The delivered dose of DT was measured in *ex vivo* human skin.
[c] Delivered percentage was calculated by dividing the delivered amount of DT in *ex vivo* human skin by the coated amount of DT on the microneedles.

3.3.2 Visualization of coated microneedles before and after penetrating *ex vivo* human skin by SEM

The 5-layer LB-MSN-DT coated microneedles were visualized by SEM. The uncoated pH-sensitive microneedles showed a smooth surface (**Fig. 3A, B1-B2**). On the surface of LB-MSN-DT coated microneedles (**Fig. 3C1-C2**), single nanoparticles or clusters of nanoparticles were observed. After insertion of the microneedles into and removal from the skin, the nanoparticle density was reduced on the microneedle surface (**Fig. 3D1-D2**).

3.3.3 Visualization of the released LB-MSN-DT in *ex vivo* human skin

After observation of the reduction of the number of nanoparticles on the microneedle surface after penetration in and withdrawal from human skin, CLSM was used to visualize the released LB-MSN-DT in the skin. To this end, the 5-layer LB-MSN-DT coated microneedles before penetration of the skin were first visualized (**Fig. 4**). The green color from DT-Alexa488 (**Fig. 4A**) and red color from TMC-Rho (**Fig. 4B**) were observed and they colocalized on the surface of the microneedles (**Fig. 4C**). These results support the SEM images of LB-MSN-DT coated microneedles (**Fig. 3C1-C2**), further revealing that LB-MSN-DT were successfully coated onto the surface of the microneedles.

Next, the released LB-MSN-DT in the skin was visualized by CLSM. After a single insertion, the fluorescence of the released DT-Alexa488 and TMC-Rho were clearly observed (**Fig. 4D-F**). The green color from DT-Alexa488 (**Fig. 4D**) and red color from TMC-Rho (**Fig. 4E**) co-localized in the micro-channels induced by the microneedles (**Fig. 4F**). After the microneedles were inserted in and withdrawn from the skin by using the multiple insertion mode, clearly more micro-channels were observed as indicated by the fluorescence of DT-Alexa488 and TMC-Rho (**Fig. 4G-I**). These results together with the SEM images of the coated microneedles after penetration of the skin indicate that LB-MSN-DT were successfully released into skin.
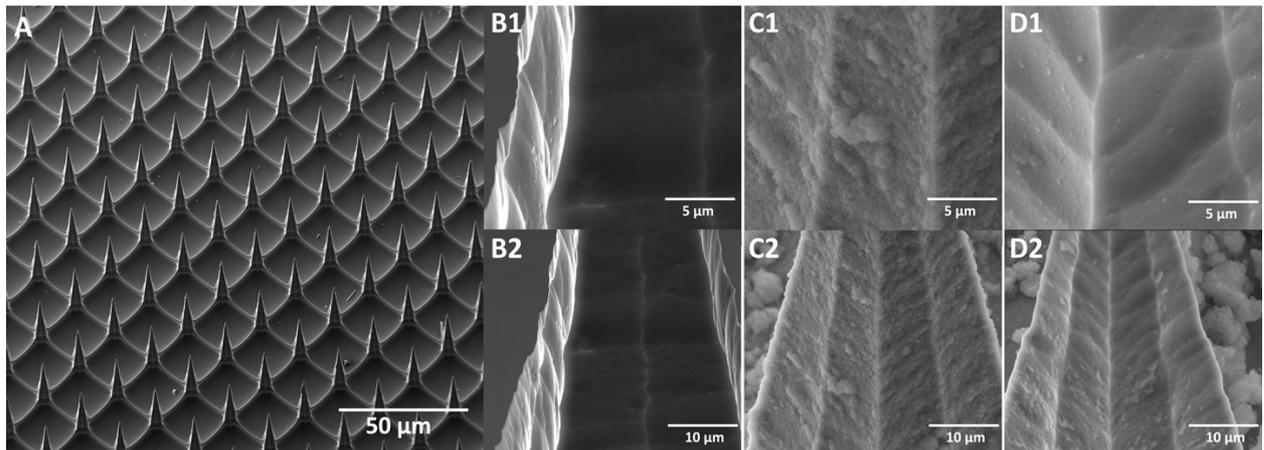
Figure 3. Scanning electron microscopy (SEM) images of uncoated pH-sensitive microneedles (A, B1-B2), microneedles coated with 5 layers of LB-MSN-DT/TMC (C1-C2), and the microneedles after insertion into and removal (multiple insertion mode) from *ex vivo* human skin (D1-D2).
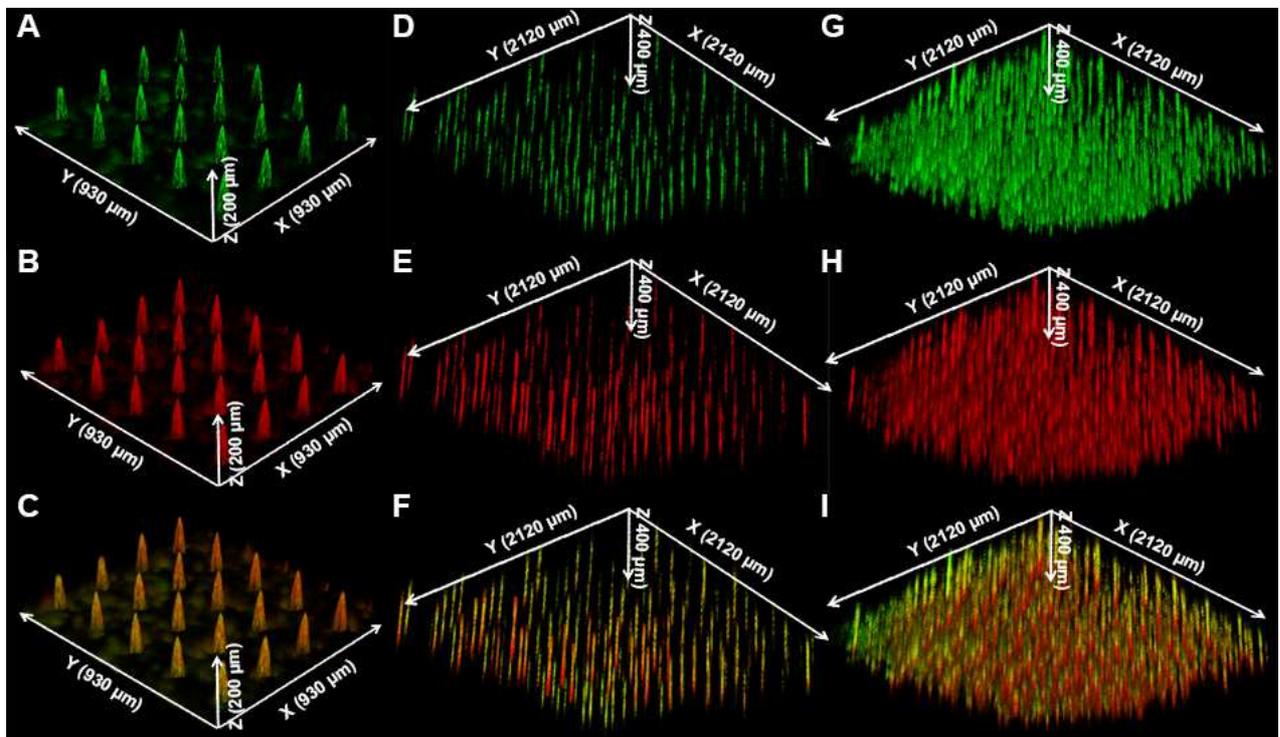
Figure 4. Confocal laser scanning microscopy (CLSM) images of 5-layer LB-MSN-DT coated microneedles (A: DT-Alexa488; B: TMC-Rho; C: merged), and *ex vivo* human skin after insertion and removal of microneedle arrays (5-layer coated) by using single (D: DT-Alexa488; E: TMC-Rho; F: merged) or multiple insertion mode (G: DT-Alexa488; H: TMC-Rho; I: merged).

3.3.4 Quantification of the released amount of DT from microneedles into *ex vivo* human skin

As shown in **Table 2**, after insertion of the 5-layer coated microneedle arrays into *ex vivo* human skin, the delivery efficiency from the microneedles by using the multiple insertion mode (42.8%) was more than twice as high compared to that in single insertion mode (17.9%). Based on this observation, the multiple insertion mode was chosen for subsequent penetration

studies. Next, the released amounts of DT from microneedles coated with 5 and 3 layers of LB-MSN-DT were compared. The amount of delivered DT in the skin from one 5-layer coated microneedle array (0.814 µg) was about 3-fold higher than that from a 3-layer coated microneedle array (0.256 µg) (**Table 2**).

3.4. IgG antibody titers after intradermal vaccination
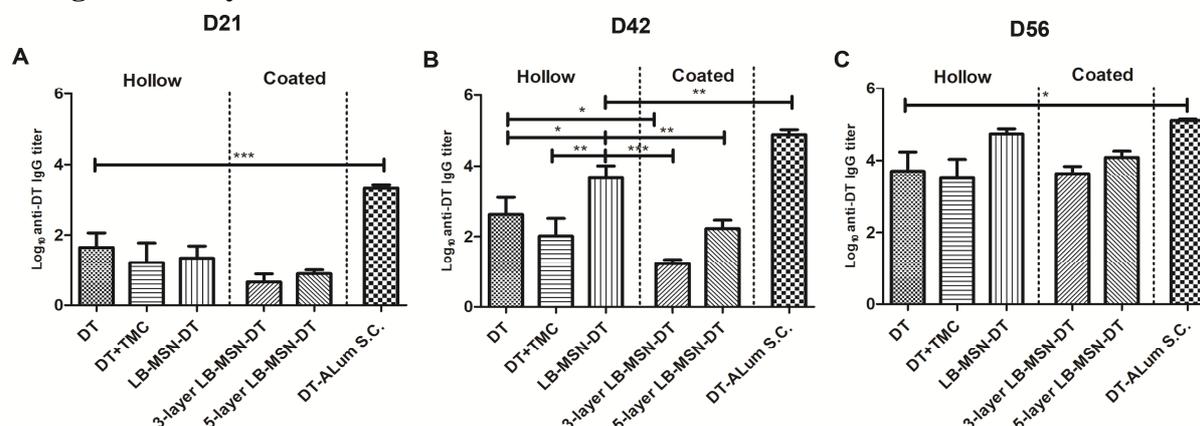
Figure 5. DT-specific total IgG antibody titers on day 21 (A), 42 (B) and 56 (C). Bars represent mean ± SEM, n = 8. *p < 0.05, **p < 0.01, ***p < 0.001.

Total IgG titers are shown in **Fig. 5**. On day 21 all groups showed detectable total IgG titers (**Fig. 5A**). On day 42, the responses of all groups increased compared to those on day 21. Responses of hollow microneedle injected LB-MSN-DT were significantly higher than those induced by DT/TMC solution and LB-MSN-DT coated microneedle groups (**Fig. 5B**) (p<0.05). On day 21 and 42, DT-Alum induced higher total IgG responses than other groups, probably due to the much higher dose used (p<0.01). On day 56, the responses of hollow microneedle injected LB-MSN-DT and 5-layer LB-MSN-DT coated microneedles increased to similar IgG levels as those induced by DT-Alum, despite the ca. 15-fold lower dose, while DT/TMC solution elicited significantly lower levels than DT-Alum.

In all these three immunizations, the addition of TMC did not improve the total IgG response. Additionally, 5-layer LB-MSN-DT coated microneedles seemed to induce a stronger total IgG response than 3-layer coated microneedles, although the difference was not significant (p>0.05). In summary, LB-MSN-DT delivered by both coated and hollow microneedles successfully induced DT-specific total IgG responses. LB-MSN-DT induced superior total IgG responses as compared to DT/TMC solution when administered by hollow microneedles (after 1st boost), but not when using coated microneedles.
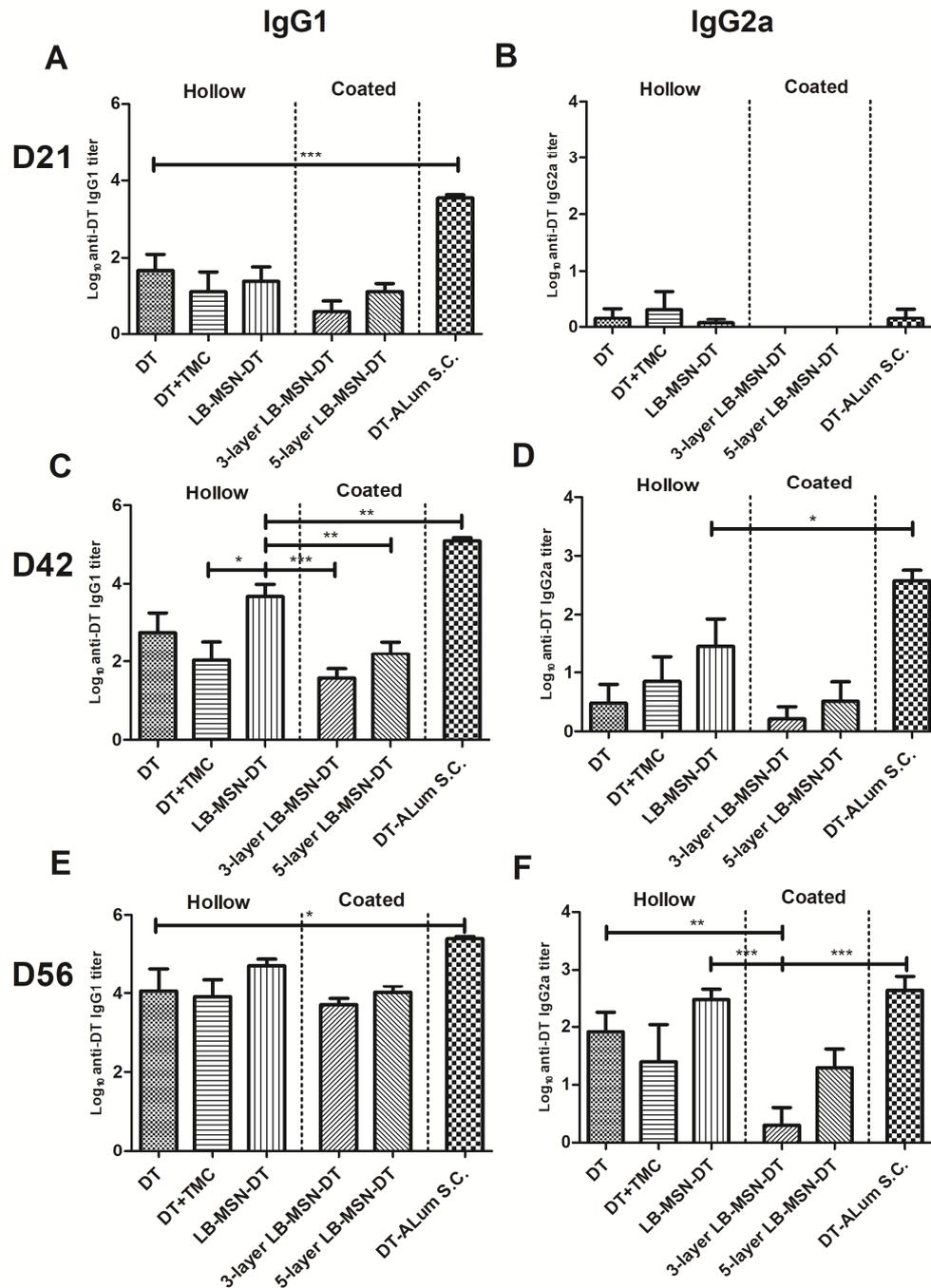
Figure 6. DT-specific IgG1 (A, C, E) and IgG2a (B, D, F) antibody titers on day 21 (A, B), 42 (C, D) and 56 (E, F). Bars represent mean ± SEM, n = 8. *p < 0.05, **p < 0.01, *** p < 0.001.

Besides total IgG, we measured the subtype IgG1 and IgG2a titers. As shown in **Fig. 6**, IgG1 followed the trend of total IgG (**Fig. 6A, C, E**). Hollow microneedle injected LB-MSN-DT induced stronger responses than DT/TMC solution (after 1st boost). However, this advantage of using LB-MSN-DT disappeared when LB-MSN-DT were delivered by coated microneedles. In case of IgG2a titers, on day 21 all groups except coated microneedles induced detectable IgG2a titers (**Fig. 6B**). On day 42, DT-Alum induced significantly higher titers than other groups (**Fig. 6D**) (p<0.05). Although not significant, hollow microneedle

injected LB-MSN-DT seemed to induce a higher IgG2a response compared to DT solution (p=0.10) and coated microneedles (p=0.12). On day 56, hollow microneedle injected LB-MSN-DT and DT solution showed significantly higher IgG2a titers than 3-layer LB-MSN-DT coated microneedle group (p<0.01), but this was not significant compared to 5-layer LB-MSN-DT coated microneedles (**Fig. 6F**) (p=0.15). Furthermore, the IgG2a titers induced by hollow microneedle injected LB-MSN-DT reached a level similar to those induced by DT-Alum. In summary, hollow microneedle injected LB-MSN-DT induced stronger IgG1 and IgG2a titers than LB-MSN-DT coated microneedles.

The functionality of the antibody response was determined by measuring the DT-neutralizing antibodies from serum taken on day 56. As expected, the subcutaneously injected DT-Alum with a high dose induced high neutralizing antibody titers (**Fig. 7**). Hollow microneedle-injected LB-MSN-DT showed a significant higher neutralizing response than a mixture of DT and TMC solution and coated microneedle groups.
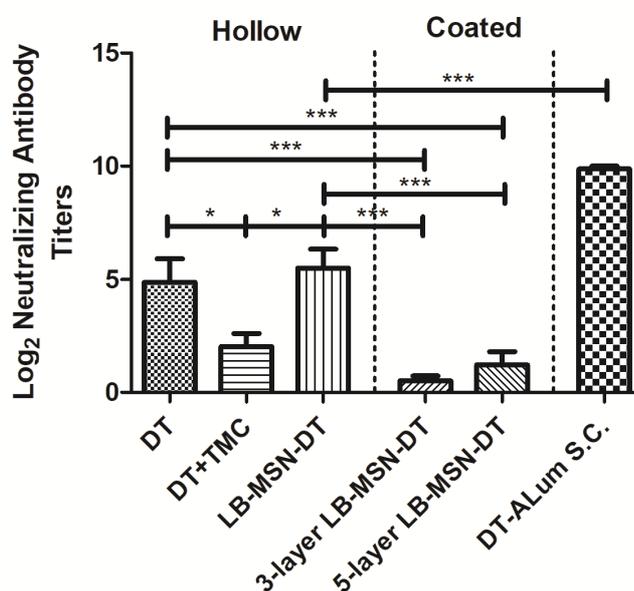
Figure 7. DT-neutralizing antibody titers of mice. Results are shown for serum collected on day 56. Bars represent mean ± SEM, n = 8. *p < 0.05, *** p < 0.001.

4. Discussion

Microneedle technologies for the intradermal delivery of drugs, including vaccines, have been extensively investigated during the past twenty years [32]. As the skin contains a large number of APCs, such as epidermal Langerhans cells and dermal dendritic cells, microneedles have gained particular attention as attractive delivery systems for intradermal vaccination [33]. In this study, we investigated the immunogenicity of DT encapsulated MSNs after coated microneedle- and hollow microneedle-mediated intradermal immunization in mice. We showed that LB-MSN-DT delivered by both coated and hollow microneedles induced DT-specific antibody titers. Both the nano-encapsulation of DT and the type of microneedles were found to affect the immune responses.

Nanoparticulate vaccines have been reported to enhance the immunogenicity of antigens by increasing their uptake by APCs [3, 34]. In this study, MSNs were chosen for the loading of DT as they have large pores which allow for efficient loading of antigen [11]. In a previous study it was shown that ovalbumin (OVA) loaded MSNs were able to elicit antibody

responses with a reduced antigen dose compared to OVA solution adjuvanted with QuilA [9]. In another study, MSNs loaded with a virus related antigen induced 10-fold higher antibody responses than the mixture of the antigen and an immune modulator [10]. Our findings are in line with these results, as we showed that hollow microneedle injected LB-MSN-DT induced distinctly higher total IgG and IgG1 titers as compared to a solution of plain DT.

When coating LB-MSN-DT onto the microneedle arrays, the coated amount of DT per layer on one microneedle array (about 500 ng) was higher than that reported in a previous study (about 300 ng) where plain DT was coated onto the same type of microneedle arrays [23]. The high loading capacity of DT in LB-MSN-DT together with the high surface charge of LB-MSN-DT may synergistically lead to this higher coating amount. Additionally, the multilayer coating approach used in the current study can further increase the coated amount of antigen by increasing the number of coating layers. By adjusting the number of coating layers, the coated amount of nanoparticles/antigen can be tailored.

Besides the successful coating of antigen on microneedles, it is important to have a fast release of the coating after the microneedles were penetrated into skin. Here we showed that by using a multiple insertion mode (10 penetrations within 10 s), the released amount of antigen was increased by 2.5-fold as compared to a single insertion mode. The amount of DT released into the skin was also increased compared to that released from the 5 layer coatings of plain DT using a single penetration [23]. Therefore, the combination of multiple insertions with nanoparticle coatings may require less coating layers, which will facilitate the production process of coated microneedles. When using multiple insertions, the application time was much shorter than that used in single penetration mode. The improvement of release efficiency may be due to the friction force between the microneedles and the skin tissue when the microneedles were inserted in and removed from the skin. The short wearing time of microneedles by using the multiple insertion mode might help improving the acceptance by vaccinees.

While hollow microneedle injected LB-MSN-DT induced a stronger immune response as compared to plain DT, LB-MSN-DT delivered by coated microneedles induced a comparable response as DT/TMC solution. The results of coated microneedles are in contrast with those reported in a recent study, which showed that nanoparticulate vaccine coated microneedles induced superior immune responses as compared to antigen solution intradermally delivered by a hypodermic needle [35]. One explanation is that the dose delivered by coated microneedles may be lower than that delivered by hollow microneedles. However, there are at least two arguments against this hypothesis. Firstly, the coated microneedles delivered a two-fold higher (5-layer coated) or comparable (3-layer coated) dose in *ex vivo* human skin, respectively, compared to that delivered by hollow microneedles. Secondly, a previous study showed that the delivery amount of antigen from coated microneedles into *ex vivo* human skin was similar as that delivered in *ex vivo* mouse skin [23]. Therefore, the lower than expected responses of coated microneedle delivered LB-MSN-DT was not likely caused by lower dose of DT delivered.

Although the LB-MSN-DT coated microneedles induced similar total IgG and IgG1 responses as compared to hollow microneedle injected LB-MSN-DT on day 56 (p>0.05), they induced distinctly lower IgG2a responses. At the same time, it has been reported that nano-encapsulation of antigen can increase IgG2a responses [24, 36]. These results suggest that the advantage of using nanoparticles is abrogated when they are delivered by coated microneedles. One possible explanation for the lower response induced by coated microneedles is that the nanoparticles were not released from the nanoparticle/TMC layers after their deposition in the

skin. As a result, the nanoparticles may be not efficiently taken up by APCs or drained to lymph nodes. In the hollow microneedle groups, the addition of TMC did not improve the immune responses either. An adjuvant effect of TMC has been reported for hypodermic needle-mediated intradermal vaccination [37]. This inconsistency may be caused by the much lower dose of TMC used in our study.

Previous studies have shown that IgG1 titers may be mainly responsible for the neutralizing titers against diphtheria toxin [31]. However, our results showed that although hollow microneedle and coated microneedle groups induced IgG1 responses close to those induced by DT-Alum, they still induced much lower neutralizing antibodies. These results indicate that the IgG1 titers may need to reach a certain threshold in order to achieve protection against diphtheria toxin.

5. Conclusion
In this study, we showed that DT loaded MSNs can be successfully delivered into mice by using coated and hollow microneedles, and evoke DT specific antibody responses. When inserting coated microneedles into skin, the multiple insertion mode of the applicator significantly increased the release efficiency of the coating compared to the single insertion mode. DT encapsulated in MSNs induced a stronger antibody response than antigen solution when delivered by hollow microneedles (after 1st boost), but not by coated microneedles. Our results revealed that both the nano-encapsulation of DT and the type of microneedles affect the immunogenicity of the antigen.

References

[1] B. Greenwood, The contribution of vaccination to global health: past, present and future, Philos. Trans. R. Soc. Lond. B Biol. Sci. 369 (2014) 20130433.

[2] P.M. Moyle, I. Toth, Modern subunit vaccines: development, components, and research opportunities, ChemMedChem 8 (2013) 360-376.

[3] L. Zhao, A. Seth, N. Wibowo, C.X. Zhao, N. Mitter, C.Z. Yu, A.P.J. Middelberg, Nanoparticle vaccines, Vaccine 32 (2014) 327-337.

[4] S.G. Reed, M.T. Orr, C.B. Fox, Key roles of adjuvants in modern vaccines, Nat. Med. 19 (2013) 1597-1608.

[5] M.L. De Temmerman, J. Rejman, J. Demeester, D.J. Irvine, B. Gander, S.C. De Smedt, Particulate vaccines: on the quest for optimal delivery and immune response, Drug Discov. Today 16 (2011) 569-582.

[6] Y. Fan, J.J. Moon, Nanoparticle drug delivery systems designed to improve cancer vaccines and immunotherapy, Vaccines 3 (2015) 662-685.

[7] N. Benne, J. van Duijn, J. Kuiper, W. Jiskoot, B. Slutter, Orchestrating immune responses: How size, shape and rigidity affect the immunogenicity of particulate vaccines, J. Control. Release 234 (2016) 124-134.

[8] K.T. Mody, A. Popat, D. Mahony, A.S. Cavallaro, C.Z. Yu, N. Mitter, Mesoporous silica nanoparticles as antigen carriers and adjuvants for vaccine delivery, Nanoscale 5 (2013) 5167-5179.

[9] D. Mahony, A.S. Cavallaro, F. Stahr, T.J. Mahony, S.Z. Qiao, N. Mitter, Mesoporous silica nanoparticles act as a self-adjuvant for ovalbumin model antigen in mice, Small 9 (2013) 3138-3146.

[10] K.T. Mody, D. Mahony, J. Zhang, A.S. Cavallaro, B. Zhang, A. Popat, T.J. Mahony, C. Yu, N. Mitter, Silica vesicles as nanocarriers and adjuvants for generating both antibody and T-cell mediated immune resposes to Bovine Viral Diarrhoea Virus E2 protein, Biomaterials 35 (2014) 9972-9983.

[11] J. Tu, G. Du, M. Reza Nejadnik, J. Monkare, K. van der Maaden, P.H.H. Bomans, N. Sommerdijk, B. Slutter, W. Jiskoot, J.A. Bouwstra, A. Kros, Mesoporous silica nanoparticle-coated microneedle arrays for intradermal antigen delivery, Pharm. Res. 34 (2017) 1693-1706.

[12] I. Preza, S. Subaiya, J.B. Harris, D.C. Ehlman, K. Wannemuehler, A.S. Wallace, S. Huseynov, T.B. Hyde, E. Nelaj, S. Bino, L.M. Hampton, Acceptance of the administration of multiple injectable vaccines in a single immunization visit in albania, J. Infect. Dis. 216 (2017) S146-S151.

[13] M.H. Danchin, J. Costa-Pinto, K. Attwell, H. Willaby, K. Wiley, M. Hoq, J. Leask, K.P. Perrett, J. O'Keefe, M.L. Giles, H. Marshall, Vaccine decision-making begins in pregnancy: Correlation between vaccine concerns, intentions and maternal vaccination with subsequent childhood vaccine uptake, Vaccine,17 (2017).

[14] T. Grimmond, L. Good, Exposure Survey of Trends in Occupational Practice (EXPO-S.T.O.P.) 2015: A national survey of sharps injuries and mucocutaneous blood exposures among health care workers in US hospitals, Am. J. Infect. Control 45 (2017) 1218-1223.

[15] J.R. Weiser, W.M. Saltzman, Controlled release for local delivery of drugs: barriers and models, J. Control. Release 190 (2014) 664-673.

[16] K. van der Maaden, W. Jiskoot, J. Bouwstra, Microneedle technologies for (trans)dermal drug and vaccine delivery, J. Control. Release 161 (2012) 645-655.

[17] Y.C. Kim, J.H. Park, M.R. Prausnitz, Microneedles for drug and vaccine delivery, Adv. Drug Deliv. Reviews 64 (2012) 1547-1568.

[18] M. Leone, J. Monkare, J. Bouwstra, G. Kersten, Dissolving microneedle patches for dermal vaccination, Pharm. Res. 34 (2017) 2223-2240.

[19] D.G. Koutsonanos, M. del Pilar Martin, V.G. Zarnitsyn, S.P. Sullivan, R.W. Compans, M.R. Prausnitz, I. Skountzou, Transdermal influenza immunization with vaccine-coated microneedle arrays, PloS One 4 (2009) e4773.

[20] K. van der Maaden, H.X. Yu, K. Sliedregt, R. Zwier, R. Leboux, M. Oguri, A. Kros, W. Jiskoot, J.A. Bouwstra, Nanolayered chemical modification of silicon surfaces with ionizable surface groups for pH-triggered protein adsorption and release: application to microneedles, J. Mater. Chem. B 1 (2013) 4466-4477.

[21] K. van der Maaden, E.M. Varypataki, S. Romeijn, F. Ossendorp, W. Jiskoot, J. Bouwstra, Ovalbumin-coated pH-sensitive microneedle arrays effectively induce ovalbumin-specific antibody and T-cell responses in mice, Eur. J. Pharm. Biopharm. 88 (2014) 310-315.

[22] K. van der Maaden, E. Sekerdag, P. Schipper, G. Kersten, W. Jiskoot, J. Bouwstra, Layer-by-layer assembly of inactivated poliovirus and N-trimethyl chitosan on pH-sensitive microneedles for dermal vaccination, Langmuir 31 (2015) 8654-8660.

[23] P. Schipper, K. van der Maaden, V. Groeneveld, M. Ruigrok, S. Romeijn, S. Uleman, C. Oomens, G. Kersten, W. Jiskoot, J. Bouwstra, Diphtheria toxoid and N-trimethyl chitosan layer-by-layer coated pH-sensitive microneedles induce potent immune responses upon dermal vaccination in mice, J. Control. Release 262 (2017) 28-36.

[24] G. Du, R.M. Hathout, M. Nasr, M.R. Nejadnik, J. Tu, R.I. Koning, A.J. Koster, B. Slutter, A. Kros, W. Jiskoot, J.A. Bouwstra, J. Monkare, Intradermal vaccination with hollow microneedles: A comparative study of various protein antigen and adjuvant encapsulated nanoparticles, J. Control. Release 266 (2017) 109-118.

[25] S.M. Bal, B. Slutter, E. van Riet, A.C. Kruithof, Z. Ding, G.F.A. Kersten, W. Jiskoot, J.A. Bouwstra, Efficient induction of immune responses through intradermal vaccination with N-trimethyl chitosan containing antigen formulations, J. Control. Release 142 (2010) 374-383.

[26] J. Tu, A.L. Boyle, H. Friedrich, P.H. Bomans, J. Bussmann, N.A. Sommerdijk, W. Jiskoot, A. Kros, Mesoporous silica nanoparticles with large pores for the encapsulation and release of proteins, ACS Appl. Mater. Interfaces 8 (2016) 32211-32219.

[27] K. van der Maaden, E. Sekerdag, W. Jiskoot, J. Bouwstra, Impact-insertion applicator improves reliability of skin penetration by solid microneedle arrays, AAPS J. 16 (2014) 681-684.

[28] K. van der Maaden, J. Heuts, M. Camps, M. Pontier, A. Terwisscha van Scheltinga, W. Jiskoot, F. Ossendorp, J. Bouwstra, Hollow microneedle-mediated micro-injections of a liposomal HPV E743-63 synthetic long peptide vaccine for efficient induction of cytotoxic and T-helper responses, J. Control. Release 269 (2018) 347-354.

[29] K. van der Maaden, S.J. Trietsch, H. Kraan, E.M. Varypataki, S. Romeijn, R. Zwier, H.J. van der Linden, G. Kersten, T. Hankemeier, W. Jiskoot, J. Bouwstra, Novel hollow microneedle technology for depth-controlled microinjection-mediated dermal vaccination: a study with polio vaccine in rats, Pharm. Res. 31 (2014) 1846-1854.

[30] M. Amidi, H.C. Pellikaan, H. Hirschberg, A.H. de Boerd, D.J.A. Crommelin, W.E. Hennink, G. Kersten, W. Jiskoot, Diphtheria toxoid-containing microparticulate powder formulations for pulmonary vaccination: Preparation, characterization and evaluation in guinea pigs, Vaccine 25 (2007) 6818-6829.

[31] Z. Ding, E. Van Riet, S. Romeijn, G.F.A. Kersten, W. Jiskoot, J.A. Bouwstra, Immune modulation by adjuvants combined with diphtheria toxoid administered topically in BALB/c mice after microneedle array pretreatment, Pharm. Res. 26 (2009) 1635-1643.

[32] E. Larraneta, M.T.C. McCrudden, A.J. Courtenay, R.F. Donnelly, Microneedles: a new frontier in nanomedicine delivery, Pharm. Res. 33 (2016) 1055-1073.

[33] N. Li, L.H. Peng, X. Chen, S. Nakagawa, J.Q. Gao, Transcutaneous vaccines: novel advances in technology and delivery for overcoming the barriers, Vaccine 29 (2011) 6179-6190.

[34] L.J. Peek, C.R. Middaugh, C. Berkland, Nanotechnology in vaccine delivery, Adv. Drug Deliv. Rev. 60 (2008) 915-928.

[35] P.C. DeMuth, J.J. Moon, H. Suh, P.T. Hammond, D.J. Irvine, Releasable layer-by-layer assembly of stabilized lipid nanocapsules on microneedles for enhanced transcutaneous vaccine delivery, ACS Nano 6 (2012) 8041-8051.

[36] B. Slutter, S.M. Bal, Z. Ding, W. Jiskoot, J.A. Bouwstra, Adjuvant effect of cationic liposomes and CpG depends on administration route, J. Control. Release 154 (2011) 123-130.

[37] S.M. Bal, Z. Ding, G.F.A. Kersten, W. Jiskoot, J.A. Bouwstra, Microneedle-based transcutaneous immunisation in mice with N-trimethyl chitosan adjuvanted diphtheria toxoid formulations, Pharm. Res. 27 (2010) 1837-1847.

Chapter 6

Chapter 7

Summarizing discussion and prospects

Introduction

Microneedles have been extensively investigated for intradermal delivery of vaccines during the last two decades. They are, as the name suggests, needle-like structures with a length shorter than 1 mm. The microneedles can be used to effectively pierce stratum corneum, which is the upper-most layer and the main barrier of skin, thereby facilitating the delivery of vaccines into the skin [1, 2]. As the microneedles do not reach nerves and blood vessels, the application of microneedles is minimally invasive and pain free. This will minimize the stress caused by traditional hypodermic needles and thus may improve the compliance of vaccinees. Furthermore, as the skin contains a large number of antigen-presenting cells (APCs), such as epidermal Langerhans cells and dermal dendritic cells, microneede-mediated intradermal delivery of vaccines has high potential for effective vaccination [3].

Different types of microneedles have been developed for vaccine delivery. Initially, solid microneedles were used to pierce the skin, after which vaccine formulations were applied topically onto the penetrated skin after removal of the microneedles [4]. However, an important drawback of this method is that the delivery efficiency of vaccines is low as the diffusion through the conduits is limited because of the small diameter of the conduits. To increase the delivery efficiency, coated, dissolvable and hollow microneedles are now being investigated. Coated microneedles are prepared from solid microneedle arrays by coating the microneedle surface with vaccines. After the microneedle arrays are inserted, the coating is deposited in the skin. Dissolvable microneedles are made of soluble polymers, biodegradable polymers or sugars and the vaccines are loaded in the matrix of microneedles. After insertion of microneedles in the skin, the matrix starts to dissolve or degrade, thereby releasing the vaccine. Hollow microneedles contain a conduit through which the vaccine formulation can be injected into the skin. The preparation methods of these different types of microneedles have been extensively reviewed [1-3, 5].

Nanoparticulate vaccines are antigen loaded nanoparticles with a diameter less than 1000 nm [6]. Nanoparticles are capable of protecting the antigen from degradation and increasing the uptake of antigen by APCs. Additionally, nanoparticles allow the co-delivery of antigen and adjuvant, which has been reported to be crucial for improving immune responses [7, 8]. Besides, it has been reported that the immune responses can be modified or enhanced by tuning the physicochemical characteristics of nanoparticulate vaccines, such as size, surface charge and release kinetics of antigen and adjuvant [9, 10]. Various types of nanoparticles have been investigated as vaccine delivery systems, such as polymeric nanoparticles, liposomes, inorganic nanoparticles, et al [6].

Nowadays, an increasing number of studies are focusing on the use of microneedles for intradermal delivery of nanoparticulate vaccines, aiming to combine the advantages of both microneedles and nanoparticulate vaccines. A previous study showed that microneedles coated with antigen loaded lipid nanocapsules resulted in a higher IgG2a response than plain antigen coated microneedles [11]. Other studies showed that dissolvable microneedles loaded with antigen containing PLGA nanoparticles induced stronger Th1/CD8$^+$ responses than antigen solution [12, 13]. Besides, hollow microneedle injected toxoid-loaded chitosan nanoparticles induced a higher IgG2a response and stronger expression of Th1 cytokines than a commercial vaccine of tetanus toxoid [14]. All of these studies showed the advantages of using microneedles for intradermal delivery of nanoparticulate vaccines.

The aim of this thesis was to determine 1) whether microneedles can be used and optimized to effectively deliver nanoparticulate vaccines intradermally and 2) whether the physicochemical characteristics of nanoparticulate vaccines have an effect on the immunogenicity of antigens

after microneedle-mediated intradermal vaccination. In this thesis, we focused on the use of coated and hollow microneedles for the delivery of nanoparticulate vaccines. In case of coated microneedles, silicon microneedle arrays were modified with pyridine groups to obtain a pH-sensitive surface. These microneedles are capable of binding negatively charged antigens at acidic conditions and releasing the coating at neutral pH [15, 16]. In case of hollow microneedles, the microneedles were prepared by etching fused silica capillaries with hydrofluoric acid [17]. These microneedles can be used to inject liquid formulations intradermally into the skin. Microscopy images of the microneedle array and hollow microneedle are shown in **Fig. 1**.

In the studies described in this thesis, the coated and hollow microneedles were developed and combined with nanoparticles with various physicochemical characteristics. The efficacy of these antigen loaded nanoparticles with and without co-encapsulation of an immune modulator on improving or modulating the immune responses was investigated.
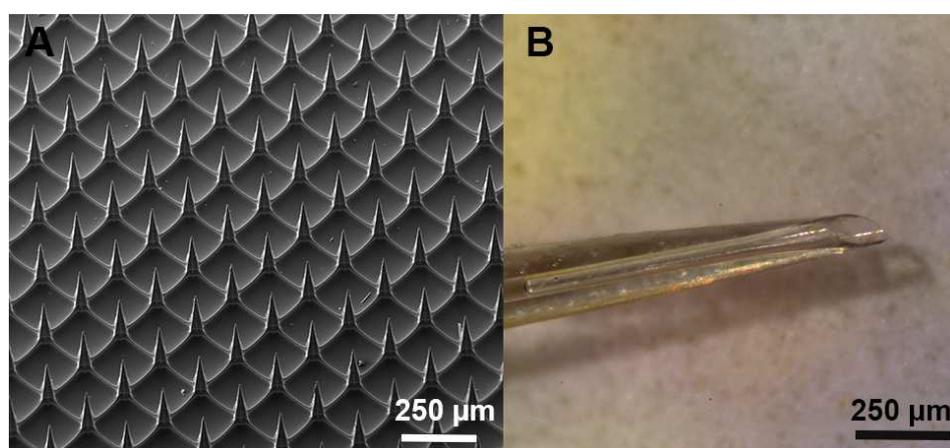
Figure 1. Microscopy images of microneedles. A: scanning electron microscopy (SEM) image of a pH-sensitive microneedle array, B: bright-field microscopy image of a hollow microneedle.

Summary of the results

In Chapter 1, a short introduction to the use of microneedles and nanoparticles for vaccine delivery via the skin is given. Next, the progress of using microneedles for intradermal delivery of nanoparticulate vaccines is briefly described. Finally, the aim and the outline of the thesis are provided.

In Chapter 2, a study is described in which a new type of mesoporous silica nanoparticles (MSNs) with large pores (about 10 nm) was successfully developed. The synthesized nanoparticles showed an efficient loading of ovalbumin (OVA) with a maximum loading capacity of about 34%. The colloidal stability of the MSNs was enhanced by coating the surface of antigen loaded MSNs with a negatively charged lipid bilayer (LB-MSN-OVA). To examine whether the MSNs could enhance antigen uptake by dendritic cells, the uptake of OVA loaded in LB-MSN-OVA by bone marrow derived dendritic cells (BMDCs) was examined. Indeed, LB-MSN-OVA showed a higher uptake than free OVA. In the next step, nanoparticles were coated onto pyridine-modified microneedle arrays. The coating process was based on the electrostatic interaction between the positively charged microneedles and the negatively charged nanoparticles. Scanning electron microscopy (SEM) and confocal laser scanning microscopy (CLSM) showed that LB-MSN-OVA were successfully coated onto the microneedle surface. About 1.5 µg of encapsulated OVA was coated onto one microneedle

array. Finally, a release study showed that LB-MSN-OVA were successfully released from the microneedles upon piercing *ex vivo* human skin.

The studies described in Chapter 3 focus on poly(lactic-co-glycolic acid) (PLGA) nanoparticles. OVA loaded PLGA nanoparticles with a positive or negative zeta potential and OVA and poly(I:C) co-encapsulated PLGA nanoparticles (with a negative zeta potential) were prepared The effect of encapsulation of OVA with or without poly(I:C) on T cell responses was investigated after hollow microneedle mediated intradermal immunization in mice. Firstly, the capacity of OVA-loaded PLGA nanoparticles to induce T cell responses in OVA-specific T cell (OT-I and OT-II cells) transferred mice was studied. It was shown that OVA-loaded PLGA nanoparticles with a positive or negative zeta potential induced similar proliferations of the adoptively transferred OVA-specific CD8$^+$ and CD4$^+$ T cells, which were both significantly higher than those induced by OVA solution. Next, the capacity of PLGA nanoparticles loaded with OVA with and without poly(I:C) to induce endogenous T cell responses in wild type mice was studied. The OVA-loaded PLGA nanoparticles (both cationic and anionic), and OVA and poly(I:C) co-encapsulated nanoparticles were found to be able to induce endogenous OVA-specific CD8$^+$ T cell responses in the wild type mice. The addition of poly(I:C) (either mixed with OVA solution or co-encapsulated with OVA in PLGA nanoparticles) enhanced CD8$^+$ T cell responses. Furthermore, OVA loaded PLGA nanoparticles with a positive zeta potential induced stronger endogenous CD8$^+$ T cell responses than anionic PLGA nanoparticles. Finally, it was studied whether the elicited endogenous T cell responses were able to protect the wild type mice from infection with OVA-secreting intracellular bacterium *Listeria monocytogenes*. It was shown that OVA and poly(I:C) co-encapsulated PLGA nanoparticles provided a full protection against the bacterium. In summary, in this study it was shown that PLGA nanoparticle formulations are excellent systems for delivery of protein antigen into the skin to induce protective cellular immune responses by using hollow microneedles for intradermal immunization.

The results of Chapter 2 and 3 demonstrate the advantages of using nanoparticulate vaccines for improving the immunogenicity of antigen. In Chapter 4, studies are reported in which hollow microneedles were used to further investigate the effect of nano-encapsulation of antigen and adjuvant on the immune responses. OVA and poly(I:C) loaded PLGA nanoparticles, liposomes, MSNs and gelatin nanoparticles (GNPs), covering a broad range of physicochemical particle characteristics, were compared. PLGA nanoparticles and liposomes showed a smaller particle size (below 200 nm) and slower release of OVA/poly(I:C) than MSNs and GNPs (mean particle size of both particles was about 500-700 nm). The vaccination studies revealed that the encapsulation of OVA and co-encapsulation of OVA and poly(I:C) in the various types of nanoparticles induced similar total IgG and IgG1 responses, but higher IgG2a antibody responses as compared to OVA/poly(I:C) solution. The type of nanoparticles had a major effect on the IgG2a response: PLGA nanoparticles and cationic liposomes induced higher responses than MSNs and GNPs, correlating with a smaller nanoparticle size and a slower release of antigen and adjuvant. When studying cell mediated immune responses, the antigen and adjuvant loaded cationic liposomes induced the strongest proliferation of adoptively transferred CD8$^+$ and CD4$^+$ T cells, suggesting their superiority for intradermal vaccination over the other nanoparticles. The studies described in this chapter demonstrate that the in-house developed hollow microneedles can be used to screen different nanoparticulate vaccine formulations for intradermal vaccination.

After the observation of the superior immune responses of antigen and adjuvant co-encapsulated liposomes as compared to other nanoparticles, the aim of the next series of studies was to examine whether the co-encapsulation of antigen and adjuvant in liposomes is

a crucial factor for the higher IgG2a responses. These studies have been described in Chapter 5, using the same type of cationic liposomes as in the studies reported in Chapter 4. Diphtheria toxoid (DT) and poly(I:C) were used as a model antigen and adjuvant, respectively. DT and poly(I:C) were either individually encapsulated or co-encapsulated in the liposomes with high loading efficiencies of more than 90%. After hollow microneedle-mediated intradermal immunization, the antigen- and adjuvant-containing liposomes evoked potent antibody responses and shifted the IgG1/IgG2a balance to a IgG2a response, no matter whether DT and poly(I:C) were individually encapsulated or co-encapsulated in the liposomes. These results indicate that the combination of DT and poly(I:C) individually encapsulated liposomes are as efficient as DT and poly(I:C) co-encapsulated liposomes for the modulation of the immune response.

In Chapter 6 studies are reported in which DT loaded and lipid bilayer coated MSNs (LB-MSN-DT) were coated onto pH-sensitive microneedle arrays. Additionally, the antibody response elicited by coated microneedles was compared to that elicited by hollow microneedle-delivered LB-MSN-DT. By using the same preparation method as described for OVA loaded MSNs in Chapter 2, DT was successfully loaded into MSNs followed by fusion of a negatively charged lipid bilayer onto the surface of MSNs. The synthesized nanoparticles showed a high loading capacity of DT of about 20%. The LB-MSN-DT and N-trimethyl chitosan (TMC) were alternately coated onto the pH sensitive surface of the pyridine-modified microneedle arrays by using a layer-by-layer coating approach. SEM and CLSM images demonstrated that LB-MSN-DT were successfully coated onto the microneedle surfaces. It was shown that the cumulative coated amount of nano-encapsulated DT for a 5-layer and 3-layer coating on the microneedle surface of one microneedle array was about 1.9 µg and 1.1 µg, respectively, corresponding to 9.7 µg and 5.7 µg LB-MSN-DT (expressed as the weight of MSNs). A release study in *ex vivo* human skin showed that 0.814 µg and 0.256 µg of the encapsulated DT were released from a 5-layer and 3-layer coated microneedle array, respectively. An *in vivo* study in mice showed that LB-MSN-DT delivered by both coated and hollow microneedles successfully induced DT-specific antibody responses. The nano-encapsulated DT induced stronger antibody responses than DT solution when delivered by hollow microneedles (after 1st boost immunization), but induced only comparable responses as DT solution when delivered by coated microneedles. The results of the research described in this chapter demonstrate that both the encapsulation of antigen and the type of microneedles can affect the immunogenicity of antigen, and that the coated microneedle system may need to be improved in order to obtain optimal immune responses.

In summary, the collective results described in this thesis show that nanoparticulate vaccines can be delivered intradermally by coated and hollow microneedles and evoke antigen-specific immune responses. The choice of both the nanoparticles and the microneedle(s) could have important influences on the immune responses. Microneedle arrays coated with antigen loaded and lipid bilayer fused MSNs could be a promising system for convenient and fast intradermal delivery of protein antigen, although our results indicate that the system needs to be improved in order to obtain optimal immune responses. Moreover, antigen and adjuvant loaded nanoparticles can increase IgG2a (Th1) and CD8+ responses after intradermal delivery by hollow microneedles. This effect depends on the type and the physicochemical characteristics of the nanoparticles, in which smaller size and controlled release properties of antigen and adjuvant were found to correlate with the stronger effect. Finally, the combination of separate antigen loaded and adjuvant loaded nanoparticles may be as efficient as the antigen and adjuvant co-encapsulated nanoparticles for modification of the immune responses following intradermal immunization.

Discussion and prospects

MSN coated microneedle arrays for intradermal delivery of protein antigen
One main goal of the work described in this thesis was to optimize coated microneedles for intradermal delivery of nanoparticulate vaccines. For coated microneedles, one limiting factor is the relatively small coating amount of antigen due to the small surface area of microneedles. In the studies described in this thesis, MSNs with large pores (10 nm in diameter) were synthesized to allow for efficient loading of antigens. Indeed, it was shown that the synthesized MSNs had a high loading capacity of OVA and DT,which was about 20% for both antigens. The high loading capacity of antigens in MSNs together with the strong surface charge of MSNs may synergistically have led to the higher coating amounts of antigen onto the microneedle array surfaces (about 500 ng per layer) as compared to our previous study (about 300 ng per layer), in which plain DT was coated onto the same type of microneedle arrays [18]. Previously, a layer-by-layer coating approach was used for the coating of antigen onto the pH-sensitive microneedle arrays, in which the coating amount of antigen could be tailored by adjusting the number of coating layers [18, 19]. In Chapter 6 it was shown that this multilayer coating method can also be used for the coating of antigen loaded MSNs.

Besides an adequate coating amount of antigen, it is important that the coated antigen can be released fast into the skin. We showed that by using a multiple insertion mode (10 times penetration in 10 s) of the microneedles, the release efficiency of the coated antigen was significantly increased and the required wearing time of the microneedles was significantly decreased. The shorter wearing time of microneedles may help improving the compliance of vaccinees. However, a disadvantage of using the multiple insertion mode is that an expensive applicator needs to be used. If the applicator is put onto the medical market in the future, the scale production may help decreasing the cost per applicator.

The immunization studies in mice showed that DT encapsulated MSNs induced stronger immune responses than DT solution when delivered by hollow microneedles, but only induced comparable responses as DT solution when delivered by coated microneedles. The results of coated microneedles are contradictory to the results reported in a previous study, in which microneedles coated with OVA loaded lipid nanocapsules enhanced immune responses compared to those induced by plain OVA coated microneedles [11]. In that study, the lipid nanocapsules and a hydrolytically degradable poly(β-amino ester) were alternately coated onto microneedles by using a layer-by-layer coating approach. The results showed that the multilayers were successfully released into the skin and completely broke down within 24 h, thereby allowing uptake of the nanocapsules by APCs. A possible reason for the lower responses of the coated microneedles in the study described in Chapter 6 is that the individual LB-MSN-DT nanoparticles cannot escape from the multiple nanoparticle/TMC layer deposited in the skin. As a result, the nanoparticles may not be efficiently taken up by APCs. It would therefore be interesting to study the use of polymers which are easier to degrade (for example, poly(β-amino ester)) or less viscous (for example, TMC with a lower molecular weight).

Hollow microneedle mediated intradermal delivery of nanoparticulate vaccines
In the studies described in this thesis, hollow microneedles are used as a tool to investigate the effect of the physicochemical characteristics of nanoparticulate vaccines on the immune responses. Previously, it has been shown that antigen and immune modulator co-encapsulated nanoparticles were able to enhance IgG2a and CD8^{+} T cell responses after traditional hypodermic needle mediated intradermal vaccination [8, 20, 21]. Our results showed that this

trend remains in hollow microneedle-mediated intradermal vaccination. The results showed that the co-delivery of antigen and adjuvant by using nanoparticles significantly increased IgG2a titers. Co-encapsulation of antigen and adjuvant (poly(I:C) may allow the delivery of antigen and adjuvant in the same antigen presenting cells, which may increase the presentation of antigen to T cells [20, 22]. Furthermore, nanoparticles with a smaller size and slower release of antigen and adjuvant induced stronger IgG2a titers. The smaller size of nanoparticles may enhance the uptake of antigen and adjuvant by antigen presenting cells [9, 23]. These results demonstrate that the quality and type of immune responses can be modified to desired direction by using nanoparticles with appropriate physicochemical properties.

The results described in the thesis further showed that individual encapsulation of antigen and adjuvant is as efficient as co-encapsulation of antigen and adjuvant in liposomes for the induction of higher IgG2a titers, indicating that co-encapsulation of antigen and adjuvant may not be necessary for the use of intradermal delivery. This might help simplifying the work for development of liposomal formulations. The formulations can be made by simply mixing antigen loaded liposomes and adjuvant loaded liposomes. It will be interesting to test whether these findings remain when other types of TLR ligands are used. Overall, the results described in the thesis indicate that the optimal nanoparticles for intradermal use should be encapsulated with antigen and adjuvant (either individually encapsulated or co-encapsulated), have a small particle size (below 200 nm) and a sustained release of antigen and adjuvant.

In the research described in this thesis, it was also shown that co-encapsulation of antigen and adjuvant in 1,2-dioleoyl-3-trimethylammonium-propane chloride (DOTAP)-based cationic liposomes induced potent Th1/CD8$^+$ T cell responses. Furthermore, the liposomes induced the strongest T cell responses among four types of the nanoparticles. Some recent studies also reported that peptide-loaded cationic liposomes were able to induce effective T cell responses for the prevention of tumor growth [24] and clearance of established tumors [25]. These results demonstrate the potential of cationic liposomes for inducing high T-cell responses, which are important for treatment of tumors and combat against intracellular bacteria. In the future, it would be important to test whether the effectiveness of cationic liposome formulations holds true for other tumor models.

Prospects of the use of microneedles for intradermal delivery of nanoparticulate vaccines
In case of hollow microneedles, the antigen and adjuvant loaded nanoparticles are suspended in buffer before the injection and the physicochemical properties of the nanoparticulate vaccines probably do not change during the injection by hollow microneedles. As a result, by using hollow microneedles it is convenient to study the effect of the physicochemical characteristics of nanoparticles on the immune responses. Furthermore, by using hollow microneedles, the influence of injection depth on the immune responses can be easily studied [26]. Instead, in case of coated and dissolvable microneedles, the nanoparticles suspended in buffer are first coated onto or loaded into the microneedles. The nanoparticles are dried during the fabrication of microneedles and released from the microneedles after the penetration of the skin. During this process, it is possible that the properties of nanoparticles and the encapsulated antigen are impacted. For example, the nanoparticles may aggregate and the antigen may lose some activity. Therefore, hollow microneedles may be more suitable for preliminary research, such as screening of nanoparticulate vaccines for intradermal vaccination and study of the effect of physicochemical characteristics of nanoparticles on immune responses. After the screening, the selected nanoparticulate vaccines can be used for the development of coated or dissolvable microneedles.

Although the results in this thesis showed that the coated and hollow microneedles can be used to intradermally deliver the nanoparticulate vaccines and evoke antigen specific immune responses, further research is needed to develop and optimize the two technologies. The interest in combining microneedle and nanoparticulate vaccine technologies will continue to grow with the emergence of new types of nanoparticles and fabrication methods of microneedles. Finally, the largest challenge is to translate the research to products which can finally benefit patients. This will need continuous and joint efforts from academia and the pharmaceutical industry.

References

[1] E. Larraneta, M.T.C. McCrudden, A.J. Courtenay, R.F. Donnelly, Microneedles: a new frontier in nanomedicine delivery, Pharm. Res. 33 (2016) 1055-1073.

[2] K. van der Maaden, W. Jiskoot, J. Bouwstra, Microneedle technologies for (trans)dermal drug and vaccine delivery, J. Control. Release 161 (2012) 645-655.

[3] Y.C. Kim, J.H. Park, M.R. Prausnitz, Microneedles for drug and vaccine delivery, Adv. Drug Deliver. Rev. 64 (2012) 1547-1568.

[4] S. Henry, D.V. McAllister, M.G. Allen, M.R. Prausnitz, Microfabricated microneedles: a novel approach to transdermal drug delivery, J. Pharm. Sci. 87 (1998) 922-925.

[5] T.M. Tuan-Mahmood, M.T.C. McCrudden, B.M. Torrisi, E. McAlister, M.J. Garland, T.R.R. Singh, R.F. Donnelly, Microneedles for intradermal and transdermal drug delivery, Eur. J. Pharm. Sci. 50 (2013) 623-637.

[6] L. Zhao, A. Seth, N. Wibowo, C.X. Zhao, N. Mitter, C.Z. Yu, A.P.J. Middelberg, Nanoparticle vaccines, Vaccine 32 (2014) 327-337.

[7] E.M. Varypataki, A.L. Silva, C. Barnier-Quer, N. Collin, F. Ossendorp, W. Jiskoot, Synthetic long peptide-based vaccine formulations for induction of cell mediated immunity: A comparative study of cationic liposomes and PLGA nanoparticles, J. Control. Release 226 (2016) 98-106.

[8] S.M. Bal, S. Hortensius, Z. Ding, W. Jiskoot, J.A. Bouwstra, Co-encapsulation of antigen and Toll-like receptor ligand in cationic liposomes affects the quality of the immune response in mice after intradermal vaccination, Vaccine 29 (2011) 1045-1052.

[9] N. Benne, J. van Duijn, J. Kuiper, W. Jiskoot, B. Slutter, Orchestrating immune responses: How size, shape and rigidity affect the immunogenicity of particulate vaccines, J. Control. Release 234 (2016) 124-134.

[10] T. Akagi, M. Baba, M. Akashi, Biodegradable nanoparticles as vaccine adjuvants and delivery systems: regulation of immune responses by nanoparticle-based vaccine, in: S. Kunugi, T. Yamaoka (Eds.) Polymers in Nanomedicine, 2012, pp. 31-64.

[11] P.C. DeMuth, J.J. Moon, H. Suh, P.T. Hammond, D.J. Irvine, Releasable layer-by-layer assembly of stabilized lipid nanocapsules on microneedles for enhanced transcutaneous vaccine delivery, ACS Nano 6 (2012) 8041-8051.

[12] M. Zaric, O. Lyubomska, O. Touzelet, C. Poux, S. Al-Zahrani, F. Fay, L. Wallace, D. Terhorst, B. Malissen, S. Henri, U.F. Power, C.J. Scott, R.F. Donnelly, A. Kissenpfennig, Skin dendritic cell targeting via microneedle arrays laden with antigen-encapsulated poly-D,L-lactide-co-glycolide nanoparticles induces efficient antitumor and antiviral immune responses, ACS Nano 7 (2013) 2042-2055.

[13] M. Zaric, O. Lyubomska, C. Poux, M.L. Hanna, M.T. McCrudden, B. Malissen, R.J. Ingram, U.F. Power, C.J. Scott, R.F. Donnelly, A. Kissenpfennig, Dissolving microneedle delivery of nanoparticle-encapsulated antigen elicits efficient cross-priming and Th1 immune responses by murine langerhans cells, J. Invest. Dermatol. 135 (2015) 425-434.

[14] K. Siddhapura, H. Harde, S. Jain, Immunostimulatory effect of tetanus toxoid loaded chitosan nanoparticles following microneedles assisted immunization, Nanomedicine 12 (2016) 213-222.

[15] K. van der Maaden, E.M. Varypataki, S. Romeijn, F. Ossendorp, W. Jiskoot, J. Bouwstra, Ovalbumin-coated pH-sensitive microneedle arrays effectively induce ovalbumin-specific antibody and T-cell responses in mice, Eur. J. Pharm. 88 (2014) 310-315.

[16] K. van der Maaden, H.X. Yu, K. Sliedregt, R. Zwier, R. Leboux, M. Oguri, A. Kros, W. Jiskoot, J.A. Bouwstra, Nanolayered chemical modification of silicon surfaces with ionizable surface groups for pH-triggered protein adsorption and release: application to microneedles, J. Mater. Chem. B 1 (2013) 4466-4477.

[17] K. van der Maaden, S.J. Trietsch, H. Kraan, E.M. Varypataki, S. Romeijn, R. Zwier, H.J. van der Linden, G. Kersten, T. Hankemeier, W. Jiskoot, J. Bouwstra, Novel hollow microneedle technology for depth-controlled microinjection-mediated dermal vaccination: a study with polio vaccine in rats, Pharm. Res. 31 (2014) 1846-1854.
[18] P. Schipper, K. van der Maaden, V. Groeneveld, M. Ruigrok, S. Romeijn, S. Uleman, C. Oomens, G. Kersten, W. Jiskoot, J. Bouwstra, Diphtheria toxoid and N-trimethyl chitosan layer-by-layer coated pH-sensitive microneedles induce potent immune responses upon dermal vaccination in mice, J. Control. Release 262 (2017) 28-36.
[19] K. van der Maaden, E. Sekerdag, P. Schipper, G. Kersten, W. Jiskoot, J. Bouwstra, Layer-by-layer assembly of inactivated poliovirus and N-trimethyl chitosan on pH-sensitive microneedles for dermal vaccination, Langmuir 31 (2015) 8654-8660.
[20] M.A. Boks, S.C.M. Bruijns, M. Ambrosini, H. Kalay, L. van Bloois, G. Storm, T. de Gruijl, Y. van Kooyk, In situ Delivery of Tumor Antigen- and Adjuvant-Loaded Liposomes Boosts Antigen-Specific T-Cell Responses by Human Dermal Dendritic Cells, Journal of Investigative Dermatology, 135 (2015) 2697-2704.
[21] E.M. Varypataki, K. van der Maaden, J. Bouwstra, F. Ossendorp, W. Jiskoot, Cationic liposomes loaded with a synthetic long peptide and poly(I:C): a defined adjuvanted vaccine for induction of antigen-specific T cell cytotoxicity, AAPS J, 17 (2015) 216-226.
[22] O. Schulz, S.S. Diebold, M. Chen, T.I. Naslund, M.A. Nolte, L. Alexopoulou, Y.T. Azuma, R.A. Flavell, P. Liljestrom, C. Reis e Sousa, Toll-like receptor 3 promotes cross-priming to virus-infected cells, Nature, 433 (2005) 887-892.
[23] M.O. Oyewumi, A. Kumar, Z.R. Cui, Nano-microparticles as immune adjuvants: correlating particle sizes and the resultant immune responses, Expert Rev Vaccines, 9 (2010) 1095-1107.
[24] B. Bayyurt, G. Tincer, K. Almacioglu, E. Alpdundar, M. Gursel, I. Gursel, Encapsulation of two different TLR ligands into liposomes confer protective immunity and prevent tumor development, J. Control. Release 247 (2017) 134-144.
[25] E.M. Varypataki, N. Benne, J. Bouwstra, W. Jiskoot, F. Ossendorp, Efficient eradication of established tumors in mice with cationic liposome-based synthetic long-peptide vaccines, Cancer Immunol. Res. 5 (2017) 222-233.
[26] P. Schipper, K. van der Maaden, S. Romeijn, C. Oomens, G. Kersten, W. Jiskoot, J. Bouwstra, Determination of depth-dependent intradermal immunogenicity of adjuvanted inactivated polio vaccine delivered by microinjections via hollow microneedles, Pharm. Res. 33 (2016) 2269-2279.

Nederlandse samenvatting

Inleiding

Gedurende de laatste twee decennia is veel onderzoek verricht naar micronaalden met als voornaamste toepassing intradermale vaccinatie. Dit zijn, zoals de naam al doet vermoeden, naaldachtige structuren met een lengte van minder dan 1 mm. De micronaalden kunnen worden gebruikt om het stratum corneum (de opperhuid), de bovenste laag en de belangrijkste barrière van de huid, effectief te doorboren, waardoor het eenvoudiger is om vaccins via de huid toe te dienen [1, 2]. Aangezien micronaalden zo kort zijn dat ze geen zenuwen en bloedvaten bereiken, is de toediening van micronaalden minimaal invasief en pijnvrij. Dit beperkt de stress voor gevaccineerden en kan zo bijdragen aan een hogere vaccinatiegraad. Bovendien kan intradermale toediening van vaccins door middel van micronaalden de effectiviteit van vaccinatie verbeteren, omdat de huid een hoge concentratie aan antigeen presenterende cellen (APC's) bevat, zoals epidermale Langerhanscellen en dermale dendritische cellen [3].

Verschillende soorten micronaalden zijn ontwikkeld voor de toediening van vaccins. Aanvankelijk werden massieve micronaalden gebruikt om de huid te doorboren, waarna na verwijdering van de micronaalden vaccinformuleringen op de huid werden aangebracht [4]. Een belangrijk nadeel van deze methode is dat slechts een klein deel van het vaccin in de huid terechtkomt, aangezien de diffusie door de aangebrachte gaatjes beperkt is vanwege de kleine diameter daarvan. Om dit probleem te omzeilen worden nu gecoate, oplosbare en holle micronaalden ontwikkeld. Gecoate micronaalden worden gemaakt uit massieve micronaaldenarrays, waarbij het oppervlak van de micronaalden bedekt is met het antigeen (de "werkzame stof" in een vaccin). Nadat de micronaalden in de huid ingebracht zijn, wordt de coating in de huid afgegeven. Oplosbare micronaalden zijn gemaakt van oplosbare polymeren, biologisch afbreekbare polymeren of suikers. Het antigeen wordt in de matrix van micronaalden geladen. Na het inbrengen van micronaalden in de huid begint de matrix op te lossen of af te breken, waardoor het antigeen vrijkomt. Holle micronaalden bevatten een kanaal waardoor de vaccinformulering in de huid kan worden geïnjecteerd. Een overzicht van de bereidingsmethoden voor deze verschillende soorten micronaaldjes is uitgebreid besproken in de literatuur [1-3, 5].

Op nanodeeltjes gebaseerde vaccins (hieronder nanodeeltjes-vaccins genoemd) bevatten nanodeeltjes met een diameter kleiner dan 1000 nm die beladen zijn met antigeen [6]. Nanodeeltjes zijn in staat om het antigeen te beschermen tegen afbraak en de opname van antigeen door APC's te vergroten. Bovendien is het mogelijk door middel van nanodeeltjes het antigeen en adjuvans (een hulpstof ter bevordering van de immuunrespons) gezamenlijk toe te dienen. Dit zou de immuunrespons kunnen verbeteren [7, 8]. Daarnaast kan de immuunrespons worden gemodificeerd of versterkt door de fysisch-chemische eigenschappen van nanodeeltjes te optimaliseren, zoals grootte en oppervlaktelading van de deeltjes alsmede de afgiftekinetiek van antigeen en adjuvans [9, 10]. Verschillende soorten nanodeeltjes zijn onderzocht als antigeen-afgiftesystemen, zoals o.a. polymere nanodeeltjes, liposomen en anorganische nanodeeltjes [6].

Tegenwoordig wordt steeds meer onderzoek verricht naar het gebruik van micronaalden voor intradermale toediening van nanodeeltjes-vaccins. Dit heeft als doel om de voordelen van micronaalden en nanodeeltjes te combineren. Uit een eerdere studie is gebleken dat micronaalden gecoat met antigeen beladen nanodeeltjes bestaande uit lipiden leidden tot een hogere IgG2a respons dan micronaalden met alleen het antigeen [11]. Uit andere studies bleek

dat oplosbare micronaalden beladen met antigeen bevattende PLGA-nanodeeltjes leidde tot hogere Th1 en CD8$^+$ T-celresponsen in vergelijking met een oplossing van vrij antigeen [12, 13]. Tevens bleek dat met holle micronaalden geïnjecteerde tetanustoxoïde beladen chitosan-nanodeeltjes een hogere IgG2a-respons en hogere expressie van Th1-cytokines leidden dan een commercieel tetanustoxoïdevaccin [14]. Uit deze onderzoeken blijkt dat het gebruik van micronaalden voor intradermale toediening van nanodeeltjes-vaccins voordelen kan bieden.

Gebaseerd op deze bevindingen is het doel van het onderzoek beschreven in dit proefschrift om 1) micronaalden te gebruiken en te optimaliseren om intradermaal nanodeeltjes-vaccins toe te dienen en 2) te onderzoeken of de fysisch-chemische eigenschappen van nanodeeltjes-vaccins de immuunrespons tegen het antigeen beïnvloeden na intradermale toediening met micronaalden. In het onderzoek beschreven in dit proefschrift hebben we ons gericht op het gebruik van gecoate en holle micronaalden. Gecoate micronaalden waren gebaseerd op micronaald-arrays gemaakt van silicium waarbij het oppervlakte gemodificeerd was met pyridinegroepen, waardoor de lading van het oppervlakte pH-gevoelig was. Deze micronaalden zijn in staat om negatief geladen antigenen te binden in een zure omgeving en de coating af te geven bij neutrale pH zoals aanwezig in de huid [15, 16]. In het geval van holle micronaalden werden de micronaalden gemaakt uit silica capillairen die geëtst werden met fluorwaterstofzuur [17]. Deze micronaalden kunnen worden gebruikt om vloeibare formuleringen intradermaal in de huid te injecteren. Microscopische afbeeldingen van een micronaaldenarray en een holle micronaald zijn weergegeven in **Fig. 1.**
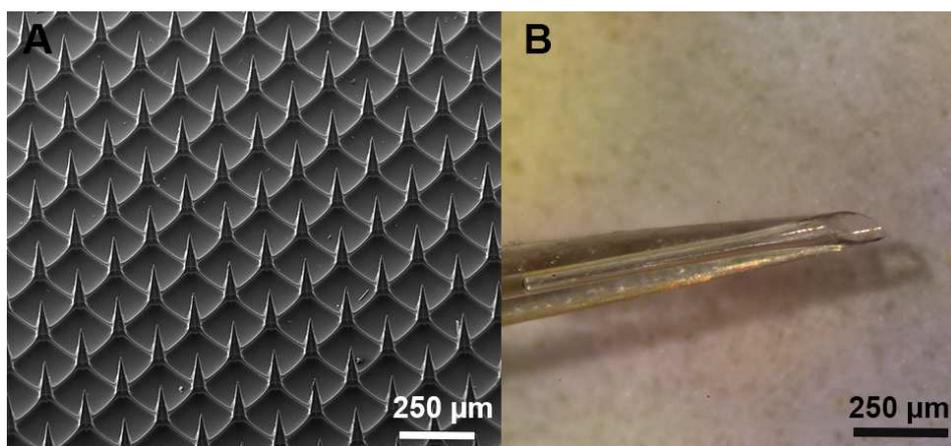
Figuur 1. Microscopische opnamen van micronaalden. A: scanning electronen microscopische afbeelding van een pH-gevoelige micronaaldenarray, B: microscopische opname van een holle micronaald.

Samenvatting van de resultaten

In hoofdstuk 1 wordt een korte inleiding gegeven over het gebruik van micronaalden en nanodeeltjes voor vaccintoediening via de huid.

In hoofdstuk 2 wordt een nieuw type mesoporeuze silica-nanodeeltjes (MSN's) met grote poriën geïntroduceerd. Deze silica-nanodeeltjes werden beladen met ovalbumine (OVA). De maximale beladingscapaciteit was ongeveer 34%. De colloïdale stabiliteit van de MSN's werd verhoogd door het oppervlak van de MSN's te bekleden met een negatief geladen lipidenmembraan (LB-MSN-OVA). Vervolgens werd onderzocht of de MSN's de antigeenopname door dendritische cellen verbeterde. Daartoe werd de opname van LB-MSN-

OVA door dendritische cellen onderzocht en vergeleken met die van een OVA-oplossing. Inderdaad leidde het gebruik van LB-MSN-OVA tot een hogere opname in dendritische cellen dan OVA-oplossing. Vervolgens werden met pyridine gemodificeerde micronaaldenarrays gecoat met LB-MSN-OVA. Het coatingproces vond plaats onder zure omstandigheden (pH 5,8). Het coatingsproces was gebaseerd op de elektrostatische interactie tussen het positief geladen micronaaldenoppervlak en de negatief geladen nanodeeltjes. Uit scanning-elektronenmicroscopie (SEM) en confocale laser-scanningmicroscopie (CLSM) opnamen bleek dat LB-MSN-OVA met succes op het oppervlak van de micronaalden werd gecoat. In totaal kon 1,5 µg OVA in LB-MSN-OVA gecoat worden op één micronaaldenarray. Tenslotte bleek uit afgiftestudies dat de gecoate micronaaldenarrays na penetratie in de menselijke ex-vivo huid de LB-MSN-OVA afgaven.

De studies beschreven in Hoofdstuk 3 zijn uitgevoerd met een ander type nanodeeltje, namelijk poly(melkzuur-co-glycolzuur) (PLGA-)nanodeeltjes. OVA bevattende PLGA-nanodeeltjes werden gemaakt met een positieve of negatieve oppervlaktelading en PLGA-nanodeeltjes die zowel OVA als poly(I:C), een adjuvans, bevatten. Het effect van inkapseling van OVA met of zonder poly(I:C) in PLGA nanodeeltjes op T-celresponsen werd onderzocht. Hiertoe werden de formuleringen met een holle micronaald intradermaal geïnjecteerd in muizen. Er werden verschillende experimenten uitgevoerd. Ten eerste werd onderzocht of OVA bevattende PLGA-nanodeeltjes tot een hogere T-celrespons leidden dan een OVA-oplossing. Het bleek dat OVA bevattende PLGA-nanodeeltjes met een positieve of negatieve oppervlaktelading tot een vergelijkbare verhoging van het aantal OVA-specifieke (niet endogene) $CD8^+$ en $CD4^+$ T-cellen leidden. Het aantal T-cellen was aanzienlijk hoger dan geïnduceerd door een OVA oplossing. Omdat dit een heel positief resultaat was, werd in een tweede stap uitgezocht of OVA bevattende PLGA-nanodeeltjes met en zonder poly(I:C) ook leiden tot een verhoging van endogene T-cellen. Toediening van OVA bevattende PLGA-nanodeeltjes (met een positieve of negatieve oppervlakte lading) en PLGA-nanodeeltjes die zowel OVA als poly (I: C) bevatten leidde tot een verhoging van het aantal endogene OVA-specifieke $CD8^+$ T-cellen. Poly(I:C) in de formulering (hetzij gemengd met OVA-oplossing hetzij met OVA ingebouwd in de PLGA-nanodeeltjes) verhoogde de $CD8^+$ T-celresponsen. Bovendien bleek dat OVA-bevattende PLGA-nanodeeltjes met een positieve oppervlaktelading een sterkere endogene $CD8^+$ T-celrespons opwekten dan OVA bevattende PLGA-nanodeeltjes met een negatieve oppervlakte lading. Ten slotte werd onderzocht of de opgewekte endogene T-celresponsen ook in staat waren de muizen te beschermen tegen een infectie met de intracellulaire bacterie *Listeria monocytogenes*. Het bleek dat OVA en poly(I:C) bevattende PLGA-nanodeeltjes leiden tot een volledige bescherming tegen de bacterie. Samengevat, uit deze studie blijkt dat PLGA-nanodeeltjes uitstekende formuleringen zijn voor de intradermale toediening van een eiwitantigeen, en dat deze formulering resulteert in een beschermende cellulaire immuunrespons.

Uit de resultaten beschreven in hoofdstuk 2 en 3 blijkt dat antigeen bevattende nanodeeltjes de immuunrespons drastisch kunnen verbeteren. Daarom is het interessant om de effectiviteit van verschillen typen OVA bevattende nanodeeltjes met elkaar te vergelijken. Dit onderzoek wordt beschreven in Hoofdstuk 4. In dit hoofdstuk werden verschillende OVA bevattende nanodeeltjes met of zonder adjuvans, poly(I:C), met elkaar vergeleken. Holle micronaalden werden weer gebruikt om de formuleringen intradermaal toe te dienen. OVA en poly(I:C) bevattende negatief geladen PLGA-nanodeeltjes, positief geladen liposomen, negatief geladen MSN's en positief geladen gelatine-nanodeeltjes (GNP's) werden met elkaar vergeleken. De nanodeeltjes verschilden verder in gemiddelde grootte en in afgifteprofiel. PLGA-nanodeeltjes en liposomen hadden een gemiddelde deeltjesgrootte van ongeveer 150 nm.

Tevens was de afgiftesnelheid van OVA en poly(I:C) laag. De deeltjesgrootte van MSN's en GNP's was tussen de 500-700 nm en de afgiftesnelheid van OVA en poly(I:C) was veel sneller. Uit immunisatiestudies in muizen bleek dat OVA bevattende nanodeeltjes en OVA en poly(I:C) bevattende nanodeeltjes in vergelijking met OVA en poly(I:C) in een buffer oplossing tot vergelijkbare IgG- en IgG1-responsen leidden. Echter er was wel een belangrijk verschil in IgG2a-responsen in vergelijking met een OVA / poly(I:C) oplossing. Het type nanodeeltje had invloed op de hoogte van de IgG2a respons: Negatief geladen PLGA-nanodeeltjes en positief geladen liposomen veroorzaakten hogere IgG2a-responsen dan de negatief geladen MSN's en de postief geladen GNP's. Dit geeft aan dat een kleine nanodeeltjesgrootte en/of een langzame afgifte van antigeen en adjuvans leidt tot een hogere IgG2a-respons. Omdat IgG2a vaak gerelateerd is aan cellulaire responsen, werd besloten ook deze te onderzoeken. Het bleek dat OVA en poly(I:C) bevattende positief geladen liposomen de sterkste verhoging van het aantal $CD8^+$ en $CD4^+$ T-cellen teweegbrachten en dus superieur zijn ten opzichte van de andere onderzochte deeltjes. Ook blijkt uit deze studies dat de in eigen huis ontwikkelde holle micronaalden met applicator uitstekend gebruikt kunnen worden voor het screenen van verschillende vaccinformuleringen.

De volgende vraag in het onderzoek was of het cruciaal is om antigen en adjuvans beiden in dezelfde nanodeeltjes te verpakken, of dat ze ieder apart in de nanodeeltjes verpakt kunnen worden met behoud van de immunogeniciteit. De studies om deze vraag te beantwoorden zijn beschreven in hoofdstuk 5. In dit onderzoek werd hetzelfde type positief geladen liposomen gebruikt, waarin DT en poly(I:C) ofwel samen in dezelfde liposomen (DT/poly(I:C)-liposomen) of afzonderlijk in de liposomen (DT-liposomen en poly(I:C)-liposomen) ingebouwd werden. Intradermale vaccinatie werd uitgevoerd met de holle micronaalden met de volgende formuleringen: i) DT in buffer, ii) DT gemengd met poly(I:C) in buffer, iii) DT-liposomen, iv) een mengsel van DT-liposomen en poly(I:C)-liposomen en v) DT/poly(I:C)-liposomen. De antigeen- en adjuvans-bevattende liposomen wekten sterke responsen op, waarbij de IgG2a-respons hoger was in vergelijking met DT in buffer, ongeacht of DT en poly(I:C) individueel of beiden in dezelfde liposomen waren geïncorporeerd. Deze resultaten laten zien dat een intradermaal toegediende formulering met een mengsel van DT-liposomen en poly(I:C)-liposomen even immunogeen is als een formulering met DT/poly(I:C)-liposomen.

In Hoofdstuk 6 worden studies beschreven waarin met een fosfolipidenmembraan omhulde MSN's waarin DT is geïncorporeerd (LB-MSN-DT) zijn gecoat op pH-gevoelige micronaaldenarrays. Met dezelfde bereidingsmethode als beschreven voor OVA in hoofdstuk 2, werd DT geïncorporeerd in MSN's. Vervolgens werd een negatief geladen fosfolipidenmembraan op het oppervlak van de MSN's aangebracht. De nanodeeltjes hadden een hoge beladingscapaciteit van DT, namelijk ongeveer 20%. De negatief geladen LB-MSN-DT nanodeeltjes en het positief geladen N-trimethylchitosan (TMC) werden afwisselend gecoat op het pH-gevoelige oppervlak van de met pyridine gemodificeerde micronaaldenarrays. Uit SEM- en CLSM-afbeeldingen bleek dat de nanodeeltjes met succes op het oppervlak van de micronaalden waren gecoat. De cumulatieve gecoate hoeveelheid DT in LB-MSN-DT voor een 5-laagse en 3-laagse coating was respectievelijk ongeveer 1,9 μg en 1,1 μg DT, overeenkomend met ca. 9,7 μg en 5,7 μg LB-MSN-DT (uitgedrukt als het gewicht van MSN's). Uit een afgiftestudie in de ex vivo menselijke huid bleek dat 0,814 μg en 0,256 μg van de geïncorporeerde DT werd afgegeven aan de huid met respectievelijk een 5-laagse en 3-laagse gecoate micronaaldenarray. Deze gecoate micronaalden arrays werden vervolgens gebruikt voor een intradermale immunisatiestudie. De immuunrespons werd vergeleken met dezelfde dosis LB-MSN-DT toegediend via een holle micronaald. LB-MSN-DT induceerde

sterkere antilichaamresponsen dan een DT-oplossing bij toediening via een holle micronaald, maar induceerde slechts een vergelijkbare respons als een DT-oplossing wanneer toegediend door gecoate micronaalden. De resultaten van het in dit hoofdstuk beschreven onderzoek laten zien dat zowel de incorporatie van het antigeen in een nanodeeltje als de keuze van het type micronaalden de immuunrespons tegen het antigeen kan beïnvloeden, en dat het gecoate micronaaldsysteem mogelijk moet worden verbeterd om een optimale immuunrespons op te wekken.

Samengevat tonen de in dit proefschrift beschreven resultaten aan dat antigenen in nanodeeltjes intradermaal kunnen worden toegediend door gebruikmaking van gecoate en holle micronaalden, waarmee vervolgens antigeen-specifieke antistof- en T-celresponsen opgewekt kunnen worden. De keuze van zowel de nanodeeltjes als de micronaald(en) kan een belangrijke invloed hebben op de effectiviteit van de vaccinatie. Micronaaldenarrays gecoat met antigeen-geladen MSN's zouden een veelbelovend systeem kunnen zijn voor gemakkelijke en snelle intradermale toediening van een eiwit antigeen, hoewel onze resultaten aangeven dat het systeem nog moet worden verbeterd om een optimale immuunrespons te verkrijgen. Bovendien kunnen met antigeen en adjuvans beladen nanodeeltjes IgG2a en vooral CD8$^+$ T-celresponsen verhogen na intradermale toediening door een holle micronaald. Dit effect hangt af van de fysisch-chemische eigenschappen van de nanodeeltjes, waarbij bleek dat de kleinere nanodeeltjes en/of een langzame afgifte van het antigeen en adjuvans uit de deeltjes de respons versterken. Ten slotte kan, wanneer intradermaal toegediend via een holle micronaald, de combinatie van afzonderlijke met antigeen en adjuvans geladen nanodeeltjes even effectief zijn als een formulering met het antigeen en adjuvans samen geïncorporeerd in dezelfde nanodeeltjes.

Appendix I Nederlandse samenvatting

Curriculum Vitae

Guangsheng Du was born at June 14, 1988. After finishing his preschool education in Linyi, China, he started his bachelor study in 2006 at the Pharmacy Institute of Shandong University and obtained his bachelor degree in 2010. After that, he went to the Institute of Pharmaceutical Engineering of Tianjin University and performed his master study under the supervision of Prof. Zhenping Wei. The topic of his master research is "Transcutaneous delivery of water-insoluble drug using D-α-tacopheryl polyethylene glycol 1000 succinate based solid lipid nanoparticles". In the summer of 2013, he obtained his master degree. At the same time, he received his scholarship from the Chinese Scholarship Council (CSC) for PhD study abroad after obtaining the invitation from Prof Joke A. Bouwstra. In September 2013, he started his PhD project at Leiden University under the supervision of Prof. Joke A. Bouwstra and Prof. Wim Jiskoot. His PhD study was focused on intradermal delivery of nanoparticulate vaccines using coated and hollow microneedles, which resulted in this thesis.

List of publications

G.S. Du*, J. Tu*, M.R. Nejadnik, J. Mönkäre, K. van der Maaden, P.H.H. Bomans, N.A.J.M. Sommerdijk, B. Slütter, W. Jiskoot, J.A. Bouwstra, A. Kros. Mesoporous silica nanoparticle-coated microneedle arrays for intradermal antigen delivery. Pharm. Res. 2017,34(8):1693-1706

G.S. Du, R.M. Hathout, M. Nasr, M.R. Nejadnik, J. Tu, R.I. Koning, A.J. Koster, B. Slütter, A. Kros, W. Jiskoot, J.A. Bouwstra, J. Mönkäre. Intradermal vaccination with hollow microneedles: a comparative study of various protein antigen and adjuvant encapsulated nanoparticles. J. Control. Release 2017,266:109-118

G.S. Du*, A.M. de Groot*, J. Mönkäre, A.C.M. Platteel, F. Broere, J.A. Bouwstra, A.J.A.M. Sijts. Hollow microneedle-mediated intradermal delivery of model vaccine antigen-loaded PLGA nanoparticles elicits protective T cell-mediated immunity to an intracellular bacterium. J. Control. Release 2017,266:27-35

G.S. Du, M. Leone, S. Romeijn, G. Kersten, W. Jiskoot, J.A. Bouwstra. Immunogenicity of diphtheria toxoid and poly(I:C) loaded cationic liposomes after hollow microneedle-mediated intradermal injection in mice. Int. J. Pharm. 2018,547:250-257.

G.S. Du, L. Woythe, K. van der Maaden, M. Leone, S. Romeijn, G. Kersten, W. Jiskoot, J.A. Bouwstra, Coated and hollow microneedle-mediated intradermal immunization in mice with diphtheria toxoid loaded mesoporous silica nanoparticles. Pharm. Res. 2018,35:189.

J. Tu, J. Bussmann, **G.S. Du**, Y. Gao, J.A. Bouwstra, A. Kros. Lipid bilayer-coated mesoporous silica nanoparticles carrying bovine hemoglobin towards an erythrocyte mimic. Int. J. Pharm. 2018,543(1-2):169-178.

J. Mönkäre, M. Pontier, E.E.M. van Kampen, **G.S. Du**, M. Leone, S. Romeijn, M.R. Nejadnik, C. O'Mahony, B. Slütter, W. Jiskoot, J.A. Bouwstra. Development of PLGA nanoparticle loaded dissolving microneedles and comparison with hollow microneedles in intradermal vaccine delivery. Eur. J. Pharm. Biopharm.2018,129:111-121.

* Co-first author